

Quantitative Characterization of Pyrene-Labeled Macromolecules in Solution by Global Analysis of Fluorescence Decays

by

Shaohua Chen

A thesis
presented to the University of Waterloo
in fulfillment of the
thesis requirement for the degree of
Doctor of Philosophy
in
Chemistry

Waterloo, Ontario, Canada, 2012

© Shaohua Chen 2012

Author's Declaration

I hereby declare that I am the sole author of this thesis. This is a true copy of the thesis, including any required final revisions, as accepted by my examiners.

I understand that my thesis may be made electronically available to the public.

Abstract

A series of pyrene end-labeled monodisperse poly(ethylene oxide)s (PEO(X)-Py₂ where X represents the number average molecular weight (M_n) of the PEOs and equals 2, 5, 10 and 16.5 K) and one pyrene mono-labeled PEO (PEO(2K)-Py₁) were synthesized and characterized in solution using fluorescence. First, the end-to-end cyclization (EEC) of PEO(X)-Py₂ was investigated in seven organic solvents with viscosities (η) ranging from 0.32 to 1.92 mPa·s. The classical Birks scheme was used to globally fit the pyrene monomer and excimer fluorescence decays. The fraction of pyrenes that did not form excimer (f_{free}) was found to increase with increasing η and M_n . This result was contrary to the assumptions made by Birks' scheme. To account for this, f_{free} was assumed to represent the fraction of PEO chains other than the monolabeled polymer impurities that cannot accomplish EEC. A fluorescence *blob* model (FBM) was applied to handle this assumption in the process of excimer formation for the PEO(X)-Py₂ samples in solution. The radius of a *blob*, R_{blob} , in organic solvents was determined according to the results retrieved from the FBM. To quantitatively account for the existence of pyrene impurity in pyrene-labeled macromolecules, known amounts of PEO(2K)-Py₁ were added into a PEO(2K)-Py₂ solution and the fluorescence decays were fitted globally according to the Birks scheme and "model free" (MF) analysis to verify the validation of the MF analysis. The MF analysis was then applied to determine the amounts of 1-pyrenebutyric acid (PyBA) that had been added to a solution of pyrene end-labeled fourth generation dendritic hybrid (Py₁₆-G4-PS). The results demonstrated that the contribution from unwanted fluorescent species could be isolated and quantitatively accounted for by fitting the fluorescence decays of the pyrene monomer and excimer globally with the MF analysis. Since the PEO(X)-Py₂ samples form hydrophobic pyrene aggregates in aqueous solution, a sequential model (SM) was proposed to characterize the pyrene excimer formation of PEO(X)-Py₂ in water at different polymer concentration (C_p). The capture distance over which the pyrenyl end-groups experience hydrophobic forces in water was determined

by assuming that the end-to-end distances of the PEO(X)-Py₂ samples adopt a Gaussian distribution and that the fraction of pyrenes that are aggregated (f_{E0}) determined by the sequential model corresponds to the fraction of PEO(X)-Py₂ chains whose end-to-end distance is smaller than the hydrophobic capture distance. Since a surfactant can interact with a hydrophobically modified water-soluble polymer in aqueous solution, the interactions taking place between PEO(X)-Py₂ and sodium dodecyl sulfate (SDS) were investigated at a low PEO(X)-Py₂ concentration. The pyrene monomer and excimer fluorescence decays of the PEO(X)-Py₂ and SDS solutions were acquired at various SDS concentrations and globally fitted according to the MF analysis to retrieve the parameters that described the kinetics of pyrene excimer formation. At high SDS concentrations above the critical micelle concentration (CMC), the pyrene end-groups of the short-chain samples (PEO(2K)-Py₂ and PEO(5K)-Py₂) were incorporated inside the same micelle and excimer was formed intramolecularly, while most pyrene groups of the long-chain samples (PEO(10K)-Py₂ and PEO(16.5K)-Py₂) were isolated into different micelles. Lastly, both the rheological properties and fluorescence behavior of a pyrene-labeled hydrophobically-modified alkali-swellaible emulsion (Py-HASE) polymer in basic aqueous solution with SDS were studied. Furthermore, a joint experimental setup that combined a rheometer and a steady-state fluorometer was applied to investigate at the molecular level the effect that a shearing force had on the polymeric network. However, despite the dramatic decrease in solution viscosity with increasing shear rate, no change in the fluorescence spectra was detected, suggesting that changes in the polymeric network that affected the balance of intra- versus intermolecular pyrene associations did not impact the process of excimer formation.

Together the experiments described in this thesis represent the broadest set of examples found in the scientific literature where information on the dynamics and level of association of pyrene-labeled polymers has been retrieved through the quantitative analysis of the fluorescence decays acquired with pyrene-labeled polymers in solution.

Acknowledgements

First and foremost, I would like to express my deepest appreciation to my supervisor Professor Jean Duhamel, who has supported and assisted me in numerous ways throughout my Ph.D. study. This thesis would not have been possible without his support, encouragement and advice. I will never forget his help on my chemistry background when I started my Ph.D. program. I would also like to thank the members of my committee, Dr. Mario Gauthier, Dr. Michael Tam and Dr. Neil McManus, especially Drs. Gauthier and Tam for their advice and helpful discussions regarding my work.

I also wish to acknowledge Professor Mitchell Winnik at the University of Toronto for his suggestions for the second chapter of my thesis and Professor Alex Adronov at McMaster University for supplying the dendrimer sample that I used in the third chapter of my thesis.

I am grateful for the assistance of Alice (Bingqing) Yang, an undergraduate student who helped me with some of the experiments presented in the fifth and sixth chapters of my thesis. A special thank is given to Dr. Howard Siu for his assistance with the rheological experiments. I would like to acknowledge all the Duhamel, Gauthier, and Tam lab members, especially Jamie Yip, Dr. Mark Ingratta, Olivier Nguon, Dr. Firmin Moingeon, Masuduz Zaman, Helen Fan, and Baoliang Peng for their help with my experiments.

I am thankful to the following organizations for their financial support: Ontario Ministry of Training, Colleges and Universities, University of Waterloo and Guelph-Waterloo Centre for Graduate Work in Chemistry and Biochemistry (GWC²).

Finally, I am grateful to my uncle's family in Toronto for their help in my daily life during these years. I would like to express my gratitude to my wife and my parents for all their support, sacrifice, and understanding.

Dedication

To my wife Yudong Wei and my parents for always supporting me.

Table of Contents

Author's Declaration.....	ii
Abstract	iii
Acknowledgements	v
Dedication	vi
Table of Contents	vii
List of Figures	x
List of Tables.....	xvi
List of Schemes	xvii
List of Abbreviations.....	xviii
Chapter 1 Literature Review	1
1.1 Hydrophobically Modified Water-Soluble Polymers (HMWSPs).....	1
1.1.1 Rheological Properties of HMWSPs	5
1.1.2 Interactions between Sodium Dodecyl Sulfate (SDS) and HMWSPs.....	10
1.2 Fluorescence to Study Polymeric Systems.....	12
1.2.1 Pyrene and Pyrene Excimer.....	13
1.2.2 Pyrene-Labeled Polymers and Oligomers	17
1.3 Global Analysis of Pyrene Monomer and Excimer Fluorescence Decays	21
1.3.1 Birks' Scheme.....	24
1.3.2 Fluorescence Blob Model (FBM).....	26
1.3.3 Model Free (MF) Analysis	31
1.3.4 Sequential Model (SM)	34
1.3.5 Summary of Models Used for the Analysis of Fluorescence Decays	35
1.4 Thesis Objectives.....	36
1.5 Thesis Outline.....	38
Chapter 2 Probing End-to-End Cyclization beyond Willemski and Fixman	39
2.1 Overview	39
2.2 Introduction	40
2.3 Theory	43
2.4 Experimental	48
2.5 Results and Discussion.....	54
2.6 Conclusions	78

Chapter 3 Quantifying the Presence of Unwanted Fluorescent Species in the Study of Pyrene-Labeled Macromolecules	80
3.1 Overview	80
3.2 Introduction	80
3.3 Experimental	84
3.4 Results	88
3.5 Discussion	100
3.6 Conclusions	104
Chapter 4 Probing the Hydrophobic Interactions of a Series of Pyrene End-Labeled Poly(ethylene oxide)s in Aqueous Solution Using Time-Resolved Fluorescence	106
4.1 Overview	106
4.2 Introduction	107
4.3 Theory	110
4.4 Experimental	115
4.5 Results and Discussion	118
4.6 Conclusions	140
Chapter 5 Interactions between a Series of Pyrene End-Labeled Poly(ethylene oxide)s and Sodium Dodecyl Sulfate in Aqueous Solution Probed by Fluorescence	142
5.1 Overview	142
5.2 Introduction	143
5.3 Experimental	146
5.4 Results and Discussion	152
5.5 Conclusions	177
Chapter 6 Interactions between Hydrophobically Modified Alkali-Swellable Emulsion Polymers and Surfactant Probed by Fluorescence and Rheology	178
6.1 Overview	178
6.2 Introduction	179
6.3 Experimental	182
6.4 Results and Discussion	189
6.5 Conclusions	207
Chapter 7 Summary and Future Work	209
7.1 Summary of Thesis	209

7.2 Future Work	214
Appendix	217
Chapter 2 Supporting Information.....	217
Chapter 3 Supporting Information.....	247
Chapter 4 Supporting Information.....	267
Chapter 5 Supporting Information.....	271
Chapter 6 Supporting Information.....	279
References	285
Chapter 1	285
Chapter 2	291
Chapter 3	294
Chapter 4	298
Chapter 5	302
Chapter 6	305
Chapter 7	309

List of Figures

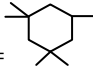
Figure 1.1: (A) Chemical structure of HEUR (with $R' = $ ) and (B) the network formed by the association of the hydrophobic groups of HEUR with themselves and the surface of latex particles. ... 3	3
Figure 1.2: Chemical structures of (A) HASE with $X \sim 50$ mol%, $Y \sim 50$ mol%, $Z \sim 1$ mol% and (B) HMHEC with $R' = H, -(CH_2-CH_2-O)_m-H, R,$ and $-(CH_2-CH_2-O)_m-R$. For both HASE and HMHEC, R represents the hydrophobe..... 4	4
Figure 1.3: Effect of HEUR concentration on polymeric network. Micelle-like clusters are formed at the CMC, followed by the formation of an extended network above C^* . The two photographs show a HEUR solution at low (left) and high (right) polymer concentrations, respectively..... 6	6
Figure 1.4: Viscosity versus shear rate of a 1.0 wt% AT22-3 solution in water and the corresponding hypothetical structure of rosette micelles in the Newtonian (left), shear-thickening (center), and shear-thinning (right) regimes. ¹⁹ 7	7
Figure 1.5: The Jablonsky diagram (top) and the corresponding transitions (bottom) found in the absorption (solid line) and fluorescence emission (dash line) spectra of pyrene in cyclohexane. $[Py] = 2.5 \times 10^{-6}$ M and $\lambda_{ex} = 334$ nm for the emission spectrum. 14	14
Figure 1.6: Steady-state fluorescence spectra of PEO(2K)-Py ₁ (bottom) and PEO(2K)-Py ₂ (top). The two spectra were normalized at 375 nm. $[Py] = 2.5 \times 10^{-6}$ M in acetone, $\lambda_{ex} = 344$ nm, $M_n(\text{PEO}) = 2,000$ g/mol..... 17	17
Figure 1.7: Excimer fluorescence decays of PEO(5K)-Py ₂ in DMF (\square , $[Py] = 2.5 \times 10^{-6}$ M) and in water (\blacksquare , $[Py] = 1.0 \times 10^{-5}$ M). $\lambda_{ex} = 344$ nm, $\lambda_{em} = 510$ nm..... 21	21
Figure 1.8: Timeline and schematic diagrams of the models for global analysis of pyrene monomer and excimer decays. 23	23
Figure 2.1: Chemical structures of the PEO(X)-Py ₂ samples. 49	49
Figure 2.2: Steady-state fluorescence spectra of PEO labeled with pyrene (A) PEO(X)-Py ₂ and PEO(2K)-Py ₁ in acetone with, from top to bottom, $X = 2.0, 5.0, 10.0, 16.5$, PEO(2K)-Py ₁ ; (B) PEO(5K)-Py ₂ , from top to bottom, acetone ($\eta = 0.32$ mPa.s), ACN ($\eta = 0.37$ mPa.s), THF ($\eta = 0.46$ mPa.s), toluene ($\eta = 0.56$ mPa.s), DMF ($\eta = 0.79$ mPa.s), dioxane ($\eta = 1.18$ mPa.s), DMA ($\eta = 1.92$ mPa.s); (C) Scaling relationship for the I_E/I_M ratio with viscosity and chain length for (\blacksquare) acetone, (\square) ACN, (\blacklozenge) THF, (\blacklozenge) toluene, (\bullet) DMF, (\circ) dioxane, (\blacktriangle) DMA. $[Py] = 2.5 \times 10^{-6}$ M, $\lambda_{ex} = 344$ nm..... 56	56

Figure 2.3: Fluorescence decays fitted by Birks' scheme of the pyrene monomer (left; $\lambda_{\text{ex}} = 344$ nm, $\lambda_{\text{em}} = 375$ nm; TPC = 2.04 ns/ch) and excimer (right; $\lambda_{\text{ex}} = 344$ nm, $\lambda_{\text{em}} = 510$ nm; TPC = 2.04 ns/ch) of PEO(2K)-Py ₂ in dioxane. [Py] = 2.5×10^{-6} M, $\chi^2 = 1.01$	60
Figure 2.4: Fluorescence decays fitted by Birks' scheme of the pyrene monomer (left; $\lambda_{\text{ex}} = 344$ nm, $\lambda_{\text{em}} = 375$ nm; TPC = 2.04 ns/ch) and excimer (right; $\lambda_{\text{ex}} = 344$ nm, $\lambda_{\text{em}} = 510$ nm; TPC = 2.04 ns/ch) of PEO(10K)-Py ₂ in dioxane. [Py] = 2.5×10^{-6} M, $\chi^2 = 1.19$	61
Figure 2.5: Scaling behavior of the parameters obtained from the global analysis of the pyrene monomer and excimer experimental fluorescence decays fitted with Equations 2.1 and 2.2, respectively. Symbols are the same as for Figure 2.2C.	63
Figure 2.6: (A) Fraction f_{Mfree} obtained from the global analysis of the monomer and excimer fluorescence decays with Equations 2.1 and 2.2. (◆) PEO(2K)-Py ₂ , (■) PEO(5K)-Py ₂ , (▲) PEO(10K)-Py ₂ , and (●) PEO(16.5K)-Py ₂ . (B) Monomer fluorescence decays of (—) PEO(2K)-Py ₁ and (□) PEO(10K)-Py ₂ in dioxane.	65
Figure 2.7: Fluorescence decays of the pyrene monomer (left; $\lambda_{\text{ex}} = 344$ nm, $\lambda_{\text{em}} = 375$ nm; TPC = 2.04 ns/ch) and excimer (right; $\lambda_{\text{ex}} = 344$ nm, $\lambda_{\text{em}} = 510$ nm; TPC = 2.04 ns/ch) of PEO(10K)-Py ₂ in dioxane fitted with Equations 2.12 and 2.13, respectively. [Py] = 2.5×10^{-6} M, $\chi^2 = 1.06$	68
Figure 2.8: Scaling behavior of the parameters obtained from the global analysis of the pyrene monomer and excimer fluorescence decays of the PEO(X)-Py ₂ samples fitted with Equations 2.3 and 2.4, respectively. (■) PEO(2K)-Py ₂ , (□) PEO(5K)-Py ₂ , (Δ) PEO(10K)-Py ₂ , (×) PEO(16.5K)-Py ₂	70
Figure 2.9: R_{blob} versus $\sqrt{\tau_M / \eta}$ for PEO(5K)-Py ₂ (◇), PEO(10K)-Py ₂ (○), and PEO(16.5K)-Py ₂ (Δ) in the following solvents. From left to right: DMA, dioxane, DMF, toluene, THF, acetonitrile, and acetone.	77
Figure 3.1: Chemical structures of the pyrene-labeled dendrimer hybrid (Py ₁₆ -G4-PS), the mono-(PEO(2K)-Py ₁) and doubly (PEO(2K)-Py ₂) labeled 2K poly(ethylene oxide)s, as well as of 1-pyrenebutyric acid (PyBA).	86
Figure 3.2: Left panel: Fluorescence spectra and decays of PEO(2K)-Py ₂ /PEO(2K)-Py ₁ mixtures in acetone. A) Fluorescence spectra normalized at 375 nm; from top to bottom, $\alpha = 0, 0.15, 0.25, 0.50, 0.70, 0.80$ and 1.00 . B) Monomer fluorescence decays; $\lambda_{\text{em}} = 375$ nm; from bottom to top, $\alpha = 0, 0.15, 0.25, 0.50, 0.70, 0.80$ and 1.00 . C) Excimer fluorescence decays with that acquired for $\alpha = 0.80$ showing a substantial amount of background noise; $\lambda_{\text{em}} = 510$ nm. Right panel: Fluorescence spectra and decays of Py ₁₆ -G4-PS/PyBA mixtures in THF. D) Fluorescence spectra normalized at 375 nm;	

from top to bottom, $\alpha = 0, 0.05, 0.10, 0.15, 0.20, 0.25, 0.35, 0.45, 0.60, 0.70$ and 1.00. E) Monomer fluorescence decays; $\lambda_{em} = 375$ nm; from bottom to top, $\alpha = 0, 0.05, 0.10, 0.15, 0.20, 0.25, 0.35, 0.45, 0.60, 0.70$ and 1.00. F) Excimer fluorescence decays; $\lambda_{em} = 510$ nm, $T = 23$ °C. 89

Figure 3.3: A) Plot of $(I_E / I_M)^{SS}$ (\square), $(I_E / I_M)^{SPC}_{Birks}$ (\bullet), $(I_E / I_M)^{SPC}_{MF}$ (\circ), $(I_E / I_M)^{SPC}_{Birks, f_{free}=0}$ (\blacklozenge), $(I_E / I_M)^{SPC}_{MF, f_{free}=0}$ (\diamond), $\tau_{E, Birks}$ (+), and $\tau_{E, MF}$ (\times) as a function of the molar fraction α . B) Plot of k_1 (\bullet), $\langle k \rangle$ calculated with Equation SI.3.20 (\square), $\langle k \rangle$ calculated with Equation SI.3.21 (\circ), α_{MF} (\diamond), and α_{Birks} (\blacklozenge) as a function of α . $T = 23$ °C. 92

Figure 3.4: A) Plot of $(I_E / I_M)^{SS}$ (\square), $(I_E / I_M)^{SPC}_{MF}$ (\circ), $(I_E / I_M)^{SPC}_{MF, f_{free}=0}$ (\diamond), and $\tau_{E, MF}$ (\times) as a function of the molar fraction α . B) Plot of $\langle k \rangle$ calculated with Equation SI.3.20 (\square), $\langle k \rangle$ calculated with Equation SI.3.21 (\circ), and α_{MF} (\diamond) as a function of α . $T = 23$ °C. 98

Figure 3.5: Simulated $(I_E / I_M)^{SPC}_{Birks}$ ratios of a series of PEOs with $M_n = 2,000, 3,000, 4,000, 5,000, 6,000, 7,000, 8,000, 9,000, 10,000, 12,000, 15,000, 17,500, 20,000, 25,000, 30,000, 35,000, 40,000$ g/mol (from bottom to top) calculated with Equation SI.3.18 and plotted as a function of f_{free} . Inset: Zoom in representation of the top-left corner of Figure 3.5. 103

Figure 4.1: Chemical structure of the PEO(X)-Py₂ samples. n equals 45, 113, 227, and 375 for PEO(X)-Py₂ with $X = 2, 5, 10,$ and 16.5 K, respectively. 116

Figure 4.2: I_E / I_M ratio of PEO(2K)-Py₂ (\square), PEO(5K)-Py₂ (\diamond), PEO(10K)-Py₂ (Δ), and PEO(16.5K)-Py₂ (\circ) as a function of polymer concentration, $\lambda_{ex} = 344$ nm. Solid lines are provided to guide the eye, vertical dashed line indicates $C^F = 4 \times 10^{-5}$ M. 120

Figure 4.3: The natural log-log plot of I_E / I_M ratios at $C_p < C^F$ versus PEO molecular weights. Data obtained in this study (\square) and by Char et al.⁴⁴ (\diamond). 122

Figure 4.4: The excimer fluorescence decays obtained with (A) PEO(5K)-Py₂ at 5×10^{-4} M (\square) and 1.25×10^{-6} M (\diamond) and (B) PEO(2K)-Py₂ (\square), PEO(5K)-Py₂ (\diamond), PEO(10K)-Py₂ (Δ) and PEO(16.5K)-Py₂ (\circ) at 1.25×10^{-6} M. The solid lines are drawn for those decays where no rise time was detected at the beginning of the decays. $\lambda_{ex} = 344$ nm, $\lambda_{em} = 510$ nm. 125

Figure 4.5: SM analysis of the fluorescence decays of the pyrene monomer (left; $\lambda_{ex} = 344$ nm, $\lambda_{em} = 375$ nm) and excimer (right; $\lambda_{ex} = 344$ nm, $\lambda_{em} = 510$ nm) of PEO(5K)-Py₂ in water at $[Py] = 2.5 \times 10^{-6}$ M with a time per channel of 2.04 ns/ch. $\chi^2 = 1.18$ 126

Figure 4.6: Fractions f_{agg}^{SM} (◆), f_{diff}^{SM} (■), and f_{free}^{SM} (▲), as well as the fractions f_{agg} (□), f_{E0} (◇), f_{diff1} (○), and f_{diff2} (△) used to calculate f_{agg}^{SM} , f_{diff}^{SM} and f_{free}^{SM} as a function of C_p obtained with (A) PEO(2K)-Py₂, (B) PEO(5K)-Py₂, (C) PEO(10K)-Py₂, and (D) PEO(16.5K)-Py₂. The vertical dashed lines represent the position of C^F 128

Figure 4.7: Rate constants as a function of C_p , k_{11} (■), and k_{12} (◆) obtained with (A) PEO(2K)-Py₂, and (B) PEO(5K)-Py₂, k_{diff} (■) obtained with (C) PEO(10K)-Py₂, and (D) PEO(16.5K)-Py₂. The dash lines represent the position of C^F 130

Figure 4.8: Plot of k_2 obtained for PEO(2K)-Py₂ (□), PEO(5K)-Py₂ (◇), PEO(10K)-Py₂ (△) and PEO(16.5K)-Py₂ (○) as a function of C_p . The dashed line represents the position of C^F and the horizontal solid line represents the average value of k_2 131

Figure 4.9: (A) molar fractions of f_{agg}^{SM} (◇), f_{diff}^{SM} (□), and f_{free}^{SM} (△) and (B) rate constants of k_{11} (◆) and k_2 (■) as a function of PEO molecular weight..... 133

Figure 4.10: Plot of the ratios $\langle R^2 \rangle_{2K}^{-1.5} / \langle R^2 \rangle_{5K}^{-1.5}$, $\langle R^2 \rangle_{2K}^{-1.5} / \langle R^2 \rangle_{10K}^{-1.5}$, $\langle R^2 \rangle_{2K}^{-1.5} / \langle R^2 \rangle_{16.5K}^{-1.5}$, $\langle R^2 \rangle_{5K}^{-1.5} / \langle R^2 \rangle_{10K}^{-1.5}$, $\langle R^2 \rangle_{5K}^{-1.5} / \langle R^2 \rangle_{16.5K}^{-1.5}$, and $\langle R^2 \rangle_{10K}^{-1.5} / \langle R^2 \rangle_{16.5K}^{-1.5}$ versus the unitless capture radius R_c obtained after normalization by the length of one ethylene oxide unit (=0.439 nm). The $(I_E/I_M)_{5K}/(I_E/I_M)_{10K}$, $(I_E/I_M)_{10K}/(I_E/I_M)_{16.5K}$, and $(I_E/I_M)_{10K}/(I_E/I_M)_{16.5K}$ ratios are given as the square symbols. The $(I_E/I_M)_{2K}/(I_E/I_M)_{5K}$, $(I_E/I_M)_{2K}/(I_E/I_M)_{10K}$, and $(I_E/I_M)_{2K}/(I_E/I_M)_{16.5K}$ ratios are represented by the cross symbols at $R_c = 4.2$ 137

Figure 4.11: The capture distance obtained with f_{E0} (solid symbols) and f_{agg}^{SM} (hollow symbols) versus PEO molecular weights. The errors on the data points are smaller than the symbols..... 140

Figure 5.1: Chemical structure of the PEO(X)-Py₂ samples. n equals 45, 113, 227, and 375 for PEO(X)-Py₂ with $X = 2, 5, 10,$ and 16.5 K, respectively..... 146

Figure 5.2: Isothermal titration curves for titrating a 0.2 M SDS solution into water (◇) and aqueous solutions of 1.25×10^{-6} M PEO(2K)-Py₂ (●), 1.25×10^{-6} M PEO(16.5K)-Py₂ (▲), 6.1×10^{-5} M PEO(16.5K) (■), and 6.1×10^{-5} M PEO(16.5K)-Py₂ (□). $T = 298$ K, $P = 1$ atm. The solid line represents the CMC of SDS in water. 154

Figure 5.3: Plot of EMF versus SDS concentration for (A) water (◆) and 1.25×10^{-6} M PEO(2K)-Py₂ (◇), PEO(5K)-Py₂ (□) and PEO(10K)-Py₂ (△) solutions and (B) water (◆), 1.25×10^{-6} M PEO(10K) (□), 1.0×10^{-4} M PEO(10K) (◇), and 1.0×10^{-4} M PEO(10K)-Py₂ (△) solutions. (C) Plot of solution

conductance versus SDS concentration for water (\blacklozenge), 1.25×10^{-6} M PEO(10K) (\square) solution and 1.0×10^{-4} M PEO(10K) (\diamond) and PEO(10K)-Py ₂ (\triangle) solutions. The vertical line represents the CMC of SDS in water.	157
Figure 5.4: Fluorescence emission spectra of PEO(5K)-Py ₂ with SDS concentrations ranging from (A) 0 to 4 mM and (B) from 4 to 20 mM. All spectra were normalized at 375 nm.	158
Figure 5.5: Plot of $(I_E/I_M)^{SS}$ (bottom panel) and I_1/I_3 (top panel) vs. SDS concentration for PEO(2K)-Py ₂ (square), PEO(5K)-Py ₂ (diamond), PEO(10K)-Py ₂ (triangle) and PEO(16.5K)-Py ₂ (circle). All samples were excited at 344 nm. The vertical lines on the right and left of the plot represent the CMC of SDS in water and $[SDS]_p^{I_E/I_M}$, respectively.	159
Figure 5.6: Fluorescence decays of the pyrene monomer (left; $\lambda_{ex} = 344$ nm, $\lambda_{em} = 375$ nm) and excimer (right; $\lambda_{ex} = 344$ nm, $\lambda_{em} = 510$ nm) of PEO(5K)-Py ₂ with 5×10^{-6} M SDS using a time per channel of 2.04 ns/ch. $\chi^2 = 1.09$. The decays were globally fitted with the MF analysis. [Py] = 2.5×10^{-6} M.	164
Figure 5.7: Fluorescence decays of the pyrene monomer (left; $\lambda_{ex} = 344$ nm, $\lambda_{em} = 375$ nm) and excimer (right; $\lambda_{ex} = 344$ nm, $\lambda_{em} = 510$ nm) of PEO(5K)-Py ₂ with 10 mM SDS using a time per channel of 2.04 ns/ch. $\chi^2 = 1.09$. The decays were globally fitted with the MF analysis. [Py] = 2.5×10^{-6} M.	165
Figure 5.8: Fractions f_{diff} (\diamond), f_{free} (\square), and f_{E0} (\triangle) and $\langle k \rangle$ (\blacklozenge) as a function of SDS concentration for (A) PEO(2K)-Py ₂ , (B) PEO(5K)-Py ₂ , (C) PEO(10K)-Py ₂ , and (D) PEO(16.5K)-Py ₂ . The vertical line represents the CMC of SDS in water.	167
Figure 5.9: The $(I_E/I_M)^{SS}$ ratio (\diamond), $(I_E/I_M)^{SPC}$ ratio (\blacklozenge) and $(I_E/I_M)^{SPC}/(I_E/I_M)^{SS}$ (\square) as a function of SDS concentration for (A) PEO(2K)-Py ₂ , (B) PEO(5K)-Py ₂ , (C) PEO(10K)-Py ₂ and (D) PEO(16.5K)-Py ₂	170
Figure 5.10: Schematic overview of the interactions between SDS and PEO(X)-Py ₂ as a function of SDS concentration.	176
Figure 6.1: Chemical structure of Py-HASE12 with X:Y:Z = 40:59:0.2.	182
Figure 6.2: Experimental setup enabling the acquisition of fluorescence spectra of a Py-HASE solution under shear in the rheometer.	188
Figure 6.3: Fluorescence emission spectra of an 8 g/L Py-HASE12 solution (top) with SDS concentrations ranging from (A) 0 to 3.5 mM and (B) from 3.5 to 50 mM and a 57 g/L Py-HASE12 solution (bottom) with SDS concentrations ranging from (C) 0 to 10 mM and (D) from 10 to 100 mM.	

The solution is a 0.01 M Na₂CO₃ aqueous solution at pH 9. All spectra were normalized at 375 nm.

..... 190

Figure 6.4: Plot of I_E/I_M (bottom panel) and I_1/I_3 (top panel) vs. SDS concentration for Py-HASE12 at 8 g/L (\diamond) and 57 g/L (\square). All samples were excited at 344 nm. 191

Figure 6.5: Fractions f_{diff} (\blacklozenge and \lozenge), f_{free} (\blacksquare and \square), and f_{agg} (\blacktriangle and \triangle) as a function of SDS concentration for Py-HASE12 at polymer concentrations of (A) 8 and (B) 57 g/L. The filled and hollow symbols indicate that the pyrene monomer and excimer decays were globally fitted with the FBM or MF analysis, respectively. 194

Figure 6.6: Steady-shear viscosity as a function of shear rate for Py-HASE12 at 57 g/L with SDS concentrations ranging from (A) 0.1 to 10 mM and (B) 11.1 to 100 mM. 198

Figure 6.7: Values of $\langle n \rangle$ (top panel) and I_E/I_M and η (bottom panel) plotted as a function of SDS concentration for a Py-HASE12 concentration of (A) 8, and (B) 57 g/L. 200

Figure 6.8: Plot of τ_r as a function of SDS concentration for the 57 g/L Py-HASE12 solution. 202

Figure 6.9: Fluorescence emission spectra normalized at 375 nm of 57 g/L Py-HASE12 solution with a SDS concentration of 11.1 mM acquired in a triangular fluorescence cell (\blacksquare) and with shear rates of 0 (—), 0.005 (---), 0.05 (.....), 1 (—), 10 (— —) and 500 (.....) s⁻¹. 204

Figure 6.10: I_E/I_M (filled symbols) and I_1/I_3 (hollow symbols) of 57 g/L Py-HASE12 solution with SDS concentrations of 0.1 (circle), 6.0 (square), 11.1 (diamond) and 17 (triangle) mM. 205

Figure 6.11: Proposed mechanism for the transition of inter- to intramolecular pyrene interaction of PyHASE solution with and without SDS under a shearing force. 207

List of Tables

Table 1.1: Diagrams of the four excited pyrene species often encountered with pyrene-labeled polymers.	20
Table 2.1: PEO molecular weights, PDI, pyrene contents λ_{py} in $\mu\text{mol/g}$ polymer, and the labeling efficiency for the PEO(2K)-Py ₁ and PEO(X)-Py ₂ samples.....	51
Table 4.1: R_c determined by different methods.	139
Table 5.1: ψ obtained in the two plateau regions at low and high SDS concentrations for PEO(2K)-Py ₂ , PEO(5K)-Py ₂ , and PEO(10K)-Py ₂ . For PEO(10K)-Py ₂ , the results are only considered when [SDS] < 6 mM.	172

List of Schemes

Scheme 1.1: Birks' scheme and structures of the excited pyrene monomer and the pyrene excimer.	15
Scheme 1.2: Modified Birks scheme for pyrene end-labeled polymer chains.	24
Scheme 1.3: End-to-end cyclization according to the FBM.	29
Scheme 1.4: Pyrene excimer formation according to the sequential manner.	34
Scheme 2.1: EEC with the capture radius of the excited fluorophore.	40
Scheme 2.2: EEC with the excursion volume of the excited fluorophore.	42
Scheme 2.3: Birks' two-state model for Py excimer formation.	44
Scheme 2.4: End-to-end cyclization according to the Fluorescence Blob Model.	46
Scheme 2.5: Synthesis of 1-pyrenemethyl methyl ether.	50
Scheme 2.6: Dependency of f_{Mfree} as a function of r_{EE}/R_{blob} . Left: $r_{EE}/R_{blob} \ll 1$ and $f_{Mfree} = 0$. Right: $r_{EE}/R_{blob} > 1$ and $f_{Mfree} > 0$.	73
Scheme 3.1: Quenching mechanism between an excited fluorophore F^* and its quencher Q covalently attached onto a macromolecule.	82
Scheme 3.2: Excimer formation between pyrenyl groups covalently attached onto a macromolecule.	83
Scheme 4.1: (A) Intra- (top) and inter- (bottom) molecular excimer formation occurring sequentially via the formation of an intermediate pyrene aggregate. (B) Probability distribution function of end-to-end distances for intramolecular pyrene excimer formation.	111

List of Abbreviations

α	molar fraction of fluorescent impurities
$\dot{\gamma}$	shear rate
ΔH	change in enthalpy
ϕ_M	fluorescence quantum yield of the pyrene monomer
ϕ_E	fluorescence quantum yield of the pyrene excimer
η	viscosity
η_0	zero-shear viscosity
κ	specific conductivity
Λ	equivalent conductivity
λ_{em}	emission wavelength
λ_{ex}	excitation wavelength
λ_{Py}	pyrene content
ν	density of elastically active chains
τ_{E0}	fluorescence lifetime of pyrene excimer
τ_M	fluorescence lifetime of excited pyrene monomer
τ_r	relaxation time of individual polymer chain
τ_{res}	residence time of the hydrophobic groups in a hydrophobic aggregate
ω	angular frequency
ACN	acetonitrile
Agg*	excited pyrene aggregates
AT	associative thickener
C^*	overlap concentration
C_2	saturation concentration
C^F	onset concentration for the transition between intra- and intermolecular pyrene excimer formation of PEO(<i>X</i>)-Py ₂
CAC	critical aggregation concentration
C_m	concentration where free SDS micelles start to form

CMC	critical micelle concentration
C_p	polymer concentration
D	poorly-stacked long-lived pyrene dimers
DMA	<i>N,N</i> -dimethylacetamide
DMF	<i>N,N</i> -dimethylformamide
E_0	well-stacked pyrene dimers
EEC	end-to-end cyclization
EMF	electromotive force
ES^*	short-lived excimer species
F	fluorophore
f_{agg}	molar fraction of aggregated pyrenes in solution
FBM	fluorescence blob model
FDQ	fluorescence dynamic quenching
f_{diff}	molar fraction of pyrenes forming excimer via diffusion in solution
f_{free}	molar fraction of isolated pyrenes in solution
G'	storage modulus
G''	loss modulus
G_0	storage modulus when the angular frequency tends to infinity
GPC	gel permeation chromatography
HASE	hydrophobically-modified alkali-swelling emulsion copolymer
HEUR	hydrophobically-modified ethoxylated urethane polymer
HMHEC	hydrophobically-modified hydroxyethylcellulose
HMWSP	hydrophobically-modified water-soluble polymer
I_1/I_3	ratio of the first to the third peak intensities of the excited pyrene monomer
I_E/I_M	ratio of the excimer to monomer intensities
ITC	isothermal titration calorimetry
IRF	instrument response function
$\langle k \rangle$	average rate constant of excimer formation
k_{-1}	dissociation rate constant of pyrene excimer
k_{-cy}	dissociation rate constant of excimer formed by end-to-end cyclization of a

	pyrene end-labeled polymer
k_1	diffusion-controlled rate constant of pyrene excimer formation
k_{11}	pyrene excimer formed by intramolecular diffusion
k_{12}	pyrene excimer formed by intermolecular diffusion
k_2	pyrene excimer formed by hydrophobic interaction
k_B	Boltzmann constant
k_{blob}	rate constant for excimer formation between one excited and one ground-state pyrene inside a same <i>blob</i>
k_{cy}	cyclization rate constant
$k_e[\text{M}0]$	rate constant of pyrene exchange between <i>blobs</i> times the concentration of <i>blobs</i> that contain zero ground-state pyrene
$k_e[\text{M}1]$	rate constant of pyrene exchange between <i>blobs</i> times the concentration of <i>blobs</i> that contain one ground-state pyrene
$k_{\text{ex}}[\text{blob}]$	rate constant of pyrene exchange between <i>blobs</i> times the <i>blob</i> concentration
k_{rad}	radiative rate constant
l	PEO Kuhn length
MF	model free
M_n	number-average molecular weight
$\langle n \rangle$	average number of pyrenes per blob
n	Number of PEO Kuhn segments
N_{agg}	average number of hydrophobic pendants per aggregate
n_{kq}	number of different populations of fluorophores
N_n	number-average degree of polymerization
n_{Py}	number of pyrene pendants attached onto the pyrene-labeled macromolecules
P_A	peak-to-valley ratio of the pyrene absorption
PDI	polydispersity index
PEO	poly(ethylene oxide)
PEO-Hyd ₂	hydrophobically end-capped monodisperse poly(ethylene oxide)
PEO(<i>X</i>)-Py ₂	pyrene end-labeled PEO with a number-average molecular weight of <i>X</i>
PEO(<i>X</i>)-Py ₁	pyrene mono-labeled PEO with a number-average molecular weight of <i>X</i>

PS	polystyrene
$[\text{Py}]_{\text{loc}}$	local pyrene concentration
Py	pyrene
Py ₁₆ -G4-PS	4 th generation dendron hybrid end-capped with pyrene
P_{yagg}	aggregated pyrenes
PyBA	1-pyrenebutyric acid
PyCH ₂ OH	1-pyrenemethanol
PyCH ₂ OMe	1-pyrenemethyl methyl ether
PNIPAM	poly(<i>N</i> -isopropylacrylamide)
P_{ydiff}	pyrenes forming excimer via diffusion
P_{yfree}	isolated pyrenes
PyMe	1-methylpyrene
P_{ys}^*	pyrene species having a short lifetime
Py-HASE	pyrene-labeled hydrophobically-modified alkali-swelling emulsion polymer
Py-HMWSP	pyrene-labelled hydrophobically-modified water-soluble polymer
Q	quencher
R_{blob}	radius of a <i>blob</i>
R_{c}	capture radius
r_{EE}	end-to-end distance
SI	supporting information
SDS	sodium dodecyl sulfate
SM	sequential model
SPC	single photon counting
SS	steady-state
THF	tetrahydrofuran
TPC	time per channel
TR	time-resolved
V_{coil}	volume of a polymer coil

Chapter 1

Literature Review

This thesis employs fluorescence to characterize hydrophobically modified water-soluble polymers (HMWSPs). Consequently, this chapter provides an introduction on the interesting properties exhibited by their aqueous solutions and a description of the more traditional techniques used to probe these properties. It is then followed by a detailed review of fluorescence topics relevant to this thesis and the advances implemented in the analysis of fluorescence data to study in a quantitative manner the behavior of aqueous solutions of HMWSP by fluorescence. This chapter closes with an overview of the thesis goals and a description of the thesis layout.

1.1 Hydrophobically Modified Water-Soluble Polymers (HMWSPs)

HMWSPs are polymers with a water-soluble polymer backbone onto which small amounts of hydrophobic pendants (<5 mol%) are covalently attached.¹⁻⁶ The low level of hydrophobic modification ensures that these polymers are still soluble in aqueous solution and confer unique properties to HMWSPs that have found many important applications in the industry where they are used as associative thickeners (AT) in paint formulation,⁶ for paper coating,⁷ or as aircraft anti-icing fluids.⁸ Association of the hydrophobic pendants of HMWSPs in water occurs via an entropy driven mechanism.⁹ Above the polymer overlap concentration (C^*), HMWSPs develop into an extended network where aggregates of the hydrophobic pendants enable the intermolecular bridging of HMWSP molecules.^{10,11} The polymer chains are connected with each other via hydrophobic aggregates and their motions are mutually restricted, resulting in a significant increase of the solution viscosity. All HMWSPs consist of a water-soluble polymer bearing more than one hydrophobic group to induce the formation of an extended polymeric network via interpolymeric bridging. Although HMWSPs can be designed in a quasi-infinite number of ways depending on chemical composition

and molecular architecture, three major groups of HMWSPs are most commonly encountered and have been commercially used in industry settings.^{2,12} The first family of HMWSPs consists of the hydrophobically modified ethoxylated urethane (HEUR) polymers having a telechelic architecture. HEUR polymers are generally made of a poly(ethylene oxide) (PEO) backbone, urethane interconnecting units, and two terminal alkyl hydrophobes as represented in Figure 1.1A. The increase in viscosity results from the formation of an interpolymeric network between HEUR molecules where the hydrophobes attached to the chain ends of a given HEUR molecule are bound to the hydrophobes of other polymer chains as well as to any other hydrophobic entities present in solution such as the surface of latex particles (Figure 1.1B).¹³ Indeed HEUR and latex particles are often encountered in paint formulation. The associations formed between the hydrophobes of HEUR and the surface of the latex particles result in the formation of a network where the latex particles act as additional crosslinking points resulting in a viscosity increase.

The second major family of HMWSPs is constituted of hydrophobically modified alkali-swellaible emulsion (HASE) polymers. HASEs are terpolymers composed of equimolar fractions of methacrylic acid and ethyl acrylate and a small molar fraction of a PEO macromonomer terminated at one end with a hydrophobe and connected at the other end to an α -methylstyrene monomer through a urethane linker. The chemical structure of a typical HASE polymer is given in Figure 1.2A. This polymer is produced as a latex dispersion in a slightly acidic aqueous solution. The methacrylic acid monomers of HASE are completely ionized in strongly alkaline solutions. Under these conditions the polymer coils expand due to electrostatic repulsion between the negatively charged methacrylate monomers. This expansion facilitates the formation of an extended polymeric network which promotes intermolecular hydrophobic associations. As such, the HASE solution becomes highly viscous at polymer concentration larger than C^* , the overlap concentration. The third family of HMWSPs is represented by the hydrophobically modified hydroxyethyl celluloses (HMHEC) where

hydrophobic pendants are randomly grafted onto the rigid cellulose backbone. The chemical structure of a HMHEC polymer is shown in Figure 1.2B.

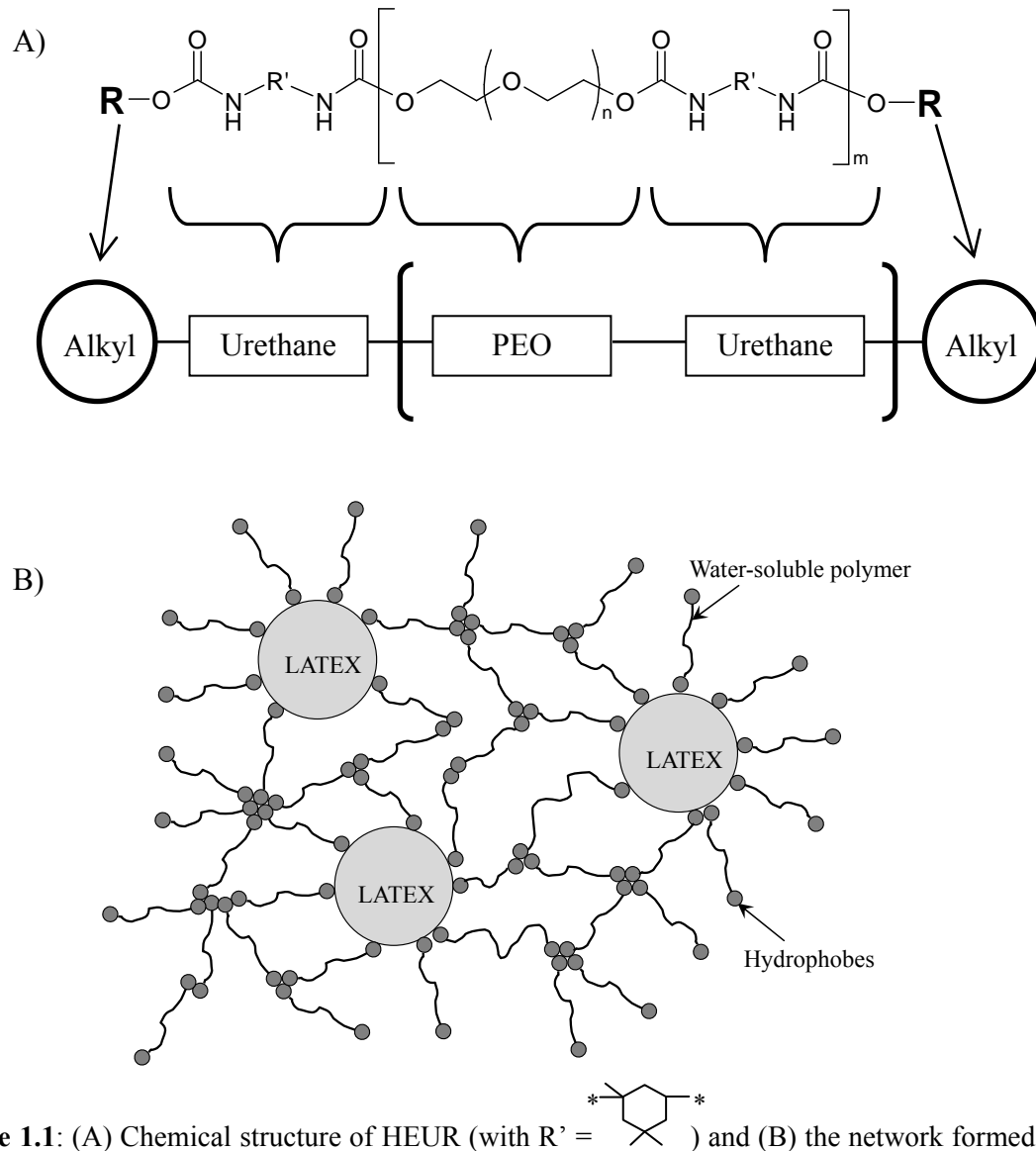
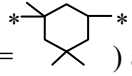


Figure 1.1: (A) Chemical structure of HEUR (with $R' =$ ) and (B) the network formed by the association of the hydrophobic groups of HEUR with themselves and the surface of latex particles.

The HMWSPs belonging to these three families are widely employed as rheology modifiers to obtain a high and stable viscosity in the formulation of paints or coatings.¹⁻⁴ The paints without ATs are usually very “thin”, that is, low in viscosity. Therefore they suffer from several disadvantages like low sag resistance and poor brush or roller loading. The addition of ATs significantly increases the viscosity of paint or coating formulations.⁶ Furthermore, the rheological properties of ATs are altered under shear as they usually exhibit a low and high viscosity at high and low shear rates, respectively. This peculiar behavior facilitates the application of a coating, as the viscosity of a paint prepared with an AT is substantially reduced upon application of a shearing force by a brush, allowing a uniform surface coverage by the paint. When the shearing force is withdrawn, the viscosity of the paint forming a protective film on the surface recovers, which prevents sagging of the paint.⁶ The properties of HMWSPs have been probed by various experimental techniques which include rheology,^{10,11,14} laser light scattering,¹⁵ NMR,¹⁶ isothermal titration calorimetry,^{17,18} and fluorescence.^{19,20}

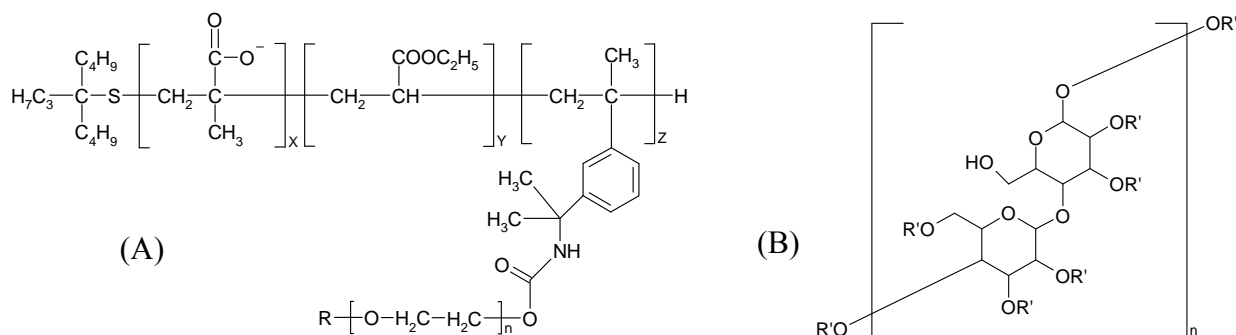


Figure 1.2: Chemical structures of (A) HASE with X ~ 50 mol%, Y ~ 50 mol%, Z ~ 1 mol% and (B) HMHEC with R' = H, $-(\text{CH}_2-\text{CH}_2-\text{O})_m-\text{H}$, R, and $-(\text{CH}_2-\text{CH}_2-\text{O})_m-\text{R}$. For both HASE and HMHEC, R represents the hydrophobe.

1.1.1 Rheological Properties of HMWSPs

In aqueous solutions, the HMWSPs form both inter- and intramolecular polymeric aggregates via hydrophobic interactions between their hydrophobic pendants.⁶ The peculiar rheological behavior of HMWSP solutions results from these intermolecular polymeric associations.²¹ Above C^* , the viscosity of a HMWSP solution is significantly greater than that of the unmodified water-soluble polymer at the same concentration. This viscosity increase can be rationalized by a model proposed by the Winnik research group that describes the structure of a network formed by HEUR polymers. It is illustrated in Figure 1.3.²²⁻²⁴ At very low concentration, the polymer chains are present in solution as dissociated unimers. When the concentration is increased to the critical micelle concentration (CMC), their hydrophobes associate resulting in the formation of well-defined “flower-like” micelles. The concentration of “flower-like” micelles increases with increasing HEUR concentration in a process that decreases the intermicellar distance to a point where two micelles can be bridged by a HEUR polymer. When this happens, the viscosity of the solution increases dramatically. The associated structures become larger with increasing polymer concentration until they eventually fill the entire available volume, at which point, a polymeric gel is formed. The HEUR network can be viewed as a transient network where the chains adopt either a bridge or loop conformation.^{25,26} The balance between bridging and looping chains controls the rheological behavior of the solution when a stress is applied to it such as when the solution is diluted or subjected to shear.

When a HEUR solution is subjected to shear, the solution exhibits a Newtonian behavior (viscosity is independent of shear rate) at low shear rates and shear-thinning (viscosity decrease with shear rate) at higher shear rates. Furthermore, at higher polymer concentration, the solution can undergo shear-thickening (viscosity increase with shear rate) above a certain critical shear rate.^{14,19,27} These complicated rheological behaviors are related to the three-dimensional transient network formed in water, as shown in Figure 1.3. The change of the rheological properties observed at the

macroscopic level is believed to be due to changes in the polymeric network that take place at the molecular level.^{14,19,27}

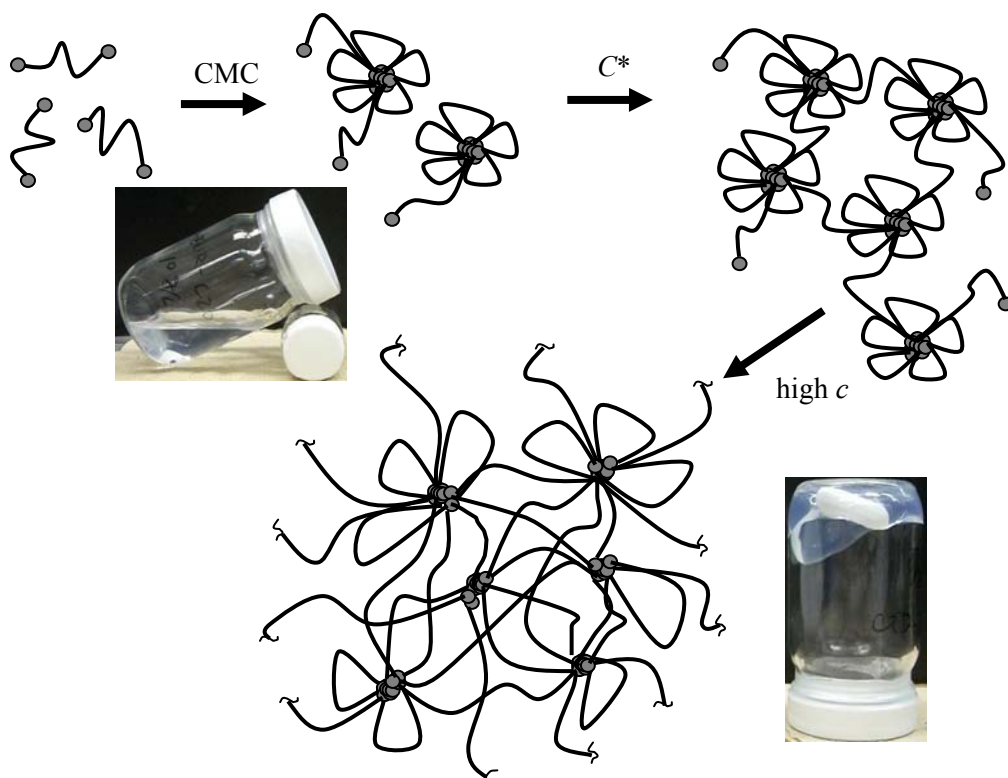


Figure 1.3: Effect of HEUR concentration on polymeric network. Micelle-like clusters are formed at the CMC, followed by the formation of an extended network above C^* . The two photographs show a HEUR solution at low (left) and high (right) polymer concentrations, respectively.

Winnik and co-workers^{14,19} have conducted a systematic study of the viscoelastic properties of a series of HEUR polymers. One typical sample named AT22-3 ($M_n = 51,000$ g/mol, PDI = 1.7) was synthesized by the reaction of PEO ($M_n = 8,200$ g/mol) with isophorone diisocyanate and hexadecanol to provide the $C_{16}H_{33}$ - terminal hydrophobes. In Figure 1.4, the viscosity versus shear rate profile of a 1.0 wt% aqueous solution of AT22-3 shows Newtonian, shear-thickening, and shear-

thinning regions. A hypothetical network structure associated with each region was also proposed by Yekta et al.²² based on the polymeric network shown in Figure 1.3.

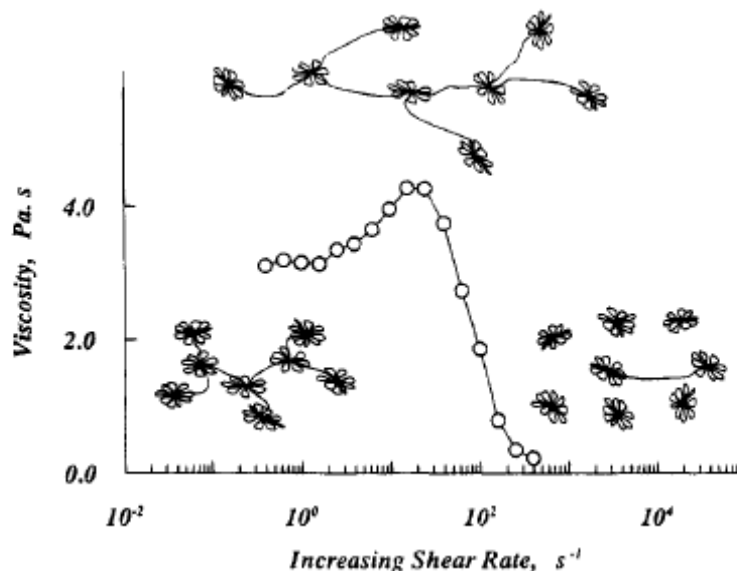


Figure 1.4: Viscosity versus shear rate of a 1.0 wt% AT22-3 solution in water and the corresponding hypothetical structure of rosette micelles in the Newtonian (left), shear-thickening (center), and shear-thinning (right) regimes.¹⁹

At low concentrations, HEUR polymers form flower-like micelles according to a closed association mechanism. These micelles are connected to each other by a secondary association that yields larger structures. The size, shape, and connectivity of the hydrophobic microdomains within these structures are not affected at low shear rates where the solution behaves as a Newtonian liquid. In the shear-thickening region, stretching of the network is accompanied by a change in the conformation of the bridging chains which results in a reorganization of the network structure. For example, the dangling chain ends tend to associate with the hydrophobic junctions via a shear-induced crosslinking mechanism, which increases the number of bridging chains between

neighboring micelles and therefore increases the solution viscosity. Earlier studies have identified three mechanisms through which shear-thickening occurs: shear-induced crosslinking, shear-induced stretching of the bridging chains, and network structure rearrangement.^{14,19,27} The stress experienced by the deformed structure is increased with increasing shear rate and once a critical stress is exceeded, the ends of the bridging chains are pulled out of the hydrophobic junctions, and the network structure is destroyed by fragmentation. The network ends up with a few bridging chains, the micelles are not connected with each other, and the shear-thinning behavior is observed.

The dynamic viscoelastic behavior of HEUR solutions is well handled by the Maxwell model.^{12,25} This result suggests that the transient network formed by the polymer can be described by a single relaxation time (τ_r) which is taken as the residence time of the hydrophobic groups (τ_{res}) in a hydrophobic aggregate.^{25,28} The storage modulus (G') and loss modulus (G'') are given by Equations 1.1 and 1.2, respectively.

$$G' = \frac{G_0 \omega^2 \tau_r^2}{1 + \omega^2 \tau_r^2} \quad (1.1)$$

$$G'' = \frac{G_0 \omega \tau_r}{1 + \omega^2 \tau_r^2} \quad (1.2)$$

G_0 is the storage modulus when the angular frequency (ω) tends to infinity. G_0 is related to the crosslink density of the network ν by Equation 1.3, where k_B is Boltzmann constant and T is the temperature in Kelvin.

$$G_0 = \nu k_B T \quad (1.3)$$

Some of these transitions are also encountered with HASE solutions. When a shearing force is applied to a HASE solution at high concentration, the solution undergoes dramatic shear-thinning accompanied by a reduction in solution viscosity of several orders of magnitude. This shear thinning behavior is usually rationalized by invoking rearrangement of the hydrophobic groups. With little to no shear, the hydrophobic pendants associate in water resulting in the formation of large intermolecular aggregates which hinder the flow of the solution and the solution viscosity is large.²⁹ Application of a shear to the solution disrupts the polymeric network, resulting in the formation of more intramolecular hydrophobic associations which is associated with a dramatic decrease of the solution viscosity.²⁹ However, unlike HEUR solutions, HASE solutions normally do not exhibit a shear-thickening effect. Furthermore, the transient networks formed by HASE do not follow the maxwellian behavior reflecting the more complex viscoelastic behavior exhibited by HASE solutions under shear.²⁹⁻³²

The rheological behavior of HMHEC is more complicated than the other two commercial ATs due to its rigid polymer backbone and comb structure that prevent the formation of long bridging chains.¹² At temperatures below 25 °C, a HMHEC solution exhibits shear thickening at intermediate shear rates but only in a certain range of polymer concentration and the magnitude of shear thickening decreases with increasing temperature.³³ The shear thickening effect encountered with HMHEC solutions was found to be stronger than that of HEUR solutions at 10 °C.³³ Similarly to HASE, the viscoelastic behavior of HMHEC cannot be described by the Maxwell model. Maestro et al.¹² proposed a generalized Maxwell model to describe the transient networks formed by HMHEC. Their model uses a distribution of relaxation times whose origin is described hereafter. Application of a shear onto an HMHEC aqueous solution is believed to generate a stress onto the rigid HMHEC chains which affects the relaxation time of the hydrophobes located inside the hydrophobic junctions. The magnitude of the stress is related to the position of the hydrophobes along the backbone and inside the

intra- and intermolecular hydrophobic junctions. Since HMHEC is hydrophobically modified at random, the hydrophobes are randomly distributed throughout the solution, which results in the distribution of relaxation times.

1.1.2 Interactions between Sodium Dodecyl Sulfate (SDS) and HMWSPs

SDS is an anionic surfactant composed of a hydrophobic tail and an anionic hydrophilic head. In pure water, SDS forms micelles at a critical micelle concentration (CMC) of 8.2 mM and its micelles are made of 62 molecules at 25 °C.³⁴ Adding SDS into the aqueous solution of a HMWSP alters both the microscopic and macroscopic behaviors of the solution. At the macroscopic level, the control achieved on the solution viscosity upon addition of a tensioactive molecule, as was demonstrated for SDS in a number of reports, has resulted in many applications such as in cosmetics and paints, as well as in enhanced oil recovery.^{1,4,5,35} Two models have been proposed to rationalize the change in viscosity of an AT solution upon addition of a surfactant. The first model assumes that the polymeric network is altered by the interactions taking place between the HMWSP and the surfactant which happen to be SDS in a majority of studies.^{17,18,36-40} In the case of HEUR, Annable et al.²⁸ found that at low SDS concentration, the free SDS molecules replace the hydrophobic alkyl groups of HEUR inside the hydrophobic aggregates leading to the formation of mixed micelles constituted of the hydrophobic pendants of HEUR and SDS molecules. The released hydrophobic groups of the polymer are then capable of bridging neighboring mixed micelles in a process that extends the polymeric network and increases the solution viscosity. However, addition of an excess amount of SDS induces the complete disruption of the polymeric network as the hydrophobic pendants are isolated in different SDS micelles. The HEUR polymer chains having lost their connectivity, the HEUR solution becomes very fluid. The interactions taking place between the hydrophobes of a HMWSP and SDS were quantitatively investigated with a pyrene-labeled HASE (Py-HASE)⁴¹ where the hydrophobe was replaced by the hydrophobic chromophore pyrene, whose

behavior could be monitored in solution by fluorescence. It was found that the solution viscosity reached its maximum value when the average number of pyrenyl hydrophobes per micelle ($\langle n \rangle$) equaled 2.0, implying that the large viscosity of the solution was associated with the formation of a most efficient polymeric network. Further addition of SDS resulted in a decrease in solution viscosity, as well as a decreased value of $\langle n \rangle$.⁴¹ The second model considers that the timescale over which the structure of the transient network formed by HMWSP and SDS in water is preserved is controlled by the residence time τ_{res} of a hydrophobic group connected to an elastically active chain in a mixed micelle.^{25,28} In the case of HEUR which exhibits a single τ_r , τ_{res} equals τ_r .^{25,28} Upon addition of SDS, τ_{res} for the hydrophobes of HEUR polymers was found to increase before passing through a maximum and decreasing after a certain SDS concentration.^{28,42} The variations observed with τ_{res} contrasted with the behavior of G_0 which remained constant with SDS concentration. According to Equation 1.3, this result implied that the density of elastically active junctions remained constant.⁴² Together, these trends suggested that the increase in solution viscosity was due not to an increase in the number of elastically active crosslinks as the first model suggested, but rather to a slower rate of dissociation ($k_{-1} = \tau_{\text{res}}^{-1}$) of the hydrophobes from the mixed micelles.⁴² Further addition of SDS shortened the relaxation time and the solution viscosity decreased accordingly.

The interactions between SDS and HEUR are further complicated by the interactions that are known to occur in aqueous solution between SDS and the hydrophilic PEO backbone that constitutes HEUR. The mechanism of SDS binding to PEO has been widely investigated by different techniques such as isothermal titration calorimetry (ITC),⁴³⁻⁴⁵ surface tension,^{46,47} light scattering,⁴⁸ viscosity,⁴⁹ NMR,⁵⁰⁻⁵² and size exclusion chromatography.⁵³ These studies have revealed the existence of several concentrations that define boundaries for the different binding regimes. SDS molecules start to bind onto PEO at the critical aggregation concentration (CAC), which represents the onset concentration for the interactions between SDS and PEO. In the case of SDS and PEO, the CAC has been found to

be independent of polymer concentration.⁴³ The PEO chains become saturated with SDS molecules at the saturation concentration (C_2) and no additional binding between SDS and PEO occurs beyond this concentration. For PEO samples with M_n values larger than 3,350 g/mol, ITC titration curves show distinct exothermic peaks which result from the re-hydration of PEO chain segments as they are expelled from the hydrophobic core of SDS micelles to their surface where they are exposed to the water phase.⁴³ This process reduces the electrostatic repulsion between the SDS micelles and better shields the hydrophobic core of the SDS micelles from the aqueous phase. With excess amounts of SDS, the critical concentration (C_m) is reached which represents the concentration where free SDS micelles start to form. When ITC titration experiments were conducted to characterize the binding between SDS and HEUR, they confirmed the general binding mechanism between SDS and PEO, except that a smaller CAC value was obtained due to the early binding of SDS onto the hydrophobes of HEUR. This effect was further confirmed by potentiometry experiments carried out with a surfactant-sensitive electrode.¹⁸

1.2 Fluorescence to Study Polymeric Systems

Many of the techniques introduced so far are used to probe the behaviour of HMWSP solutions at the macroscopic level. Fluorescence can be used to investigate HMWSPs solutions at the molecular level. Fluorescence describes a photophysical phenomenon whereby absorption of an electromagnetic radiation by a fluorophore at a given wavelength is followed by the emission of light at longer wavelengths.⁵⁴ The extreme sensitivity of photodetectors to fluorescence enables the study of solutions where the fluorophores are present at such low levels that the fluorescence signal being detected reports on isolated fluorophores. This feature of fluorescence has led to its application in numerous fields of chemistry, physics, biology, and nanotechnology, to name but a few. Except for a few examples such as conjugated polymers, most polymers do not fluoresce. Therefore a chromophore needs to be covalently attached onto a polymer chain for the polymer sample to become

fluorescent. In this thesis, pyrene was used as the fluorescent label of choice and the properties of pyrene are described in details hereafter.

1.2.1 Pyrene and Pyrene Excimer

Pyrene is a chromophore which can be excited by irradiation with UV light. The absorption and fluorescence of pyrene can be described by the Jablonsky diagram shown in Figure 1.5 for pyrene in cyclohexane. The absorption spectrum of a pyrene molecule is composed of several absorbance bands where the 0-0 transition peaks representing the excitation of pyrene from the ground-state to the lowest vibrational energy level of the higher electronic energy levels S_1 , S_2 , S_3 , and S_4 can be found at, respectively, 372, 334, 272 and 243 nm for pyrene in cyclohexane. The $S_1 \leftarrow S_0$ band is very weak due to the fact that the transition between the S_0 and S_1 electronic states is symmetry forbidden.⁵⁵⁻⁵⁷ The absence of overlap between the absorption and fluorescence emission spectra of pyrene shown in Figure 1.5 indicates that little energy transfer can occur between an excited and a ground-state pyrene. In many studies, pyrene is excited at the $S_2^0 \leftarrow S_0^0$ transition peak using an excitation wavelength between 334 and 345 nm depending on the pyrene derivative and the solvent being used. Using these wavelengths where pyrene has a larger molar absorption coefficient allows the efficient excitation of pyrene while avoiding the shorter wavelengths of the deep UV where many chemicals absorb. Furthermore, light scattering is strongly reduced when acquiring a fluorescence emission spectrum of pyrene due to the satisfying wavelength separation between the excitation wavelength and the lowest wavelength at which the fluorescence spectrum is being acquired.

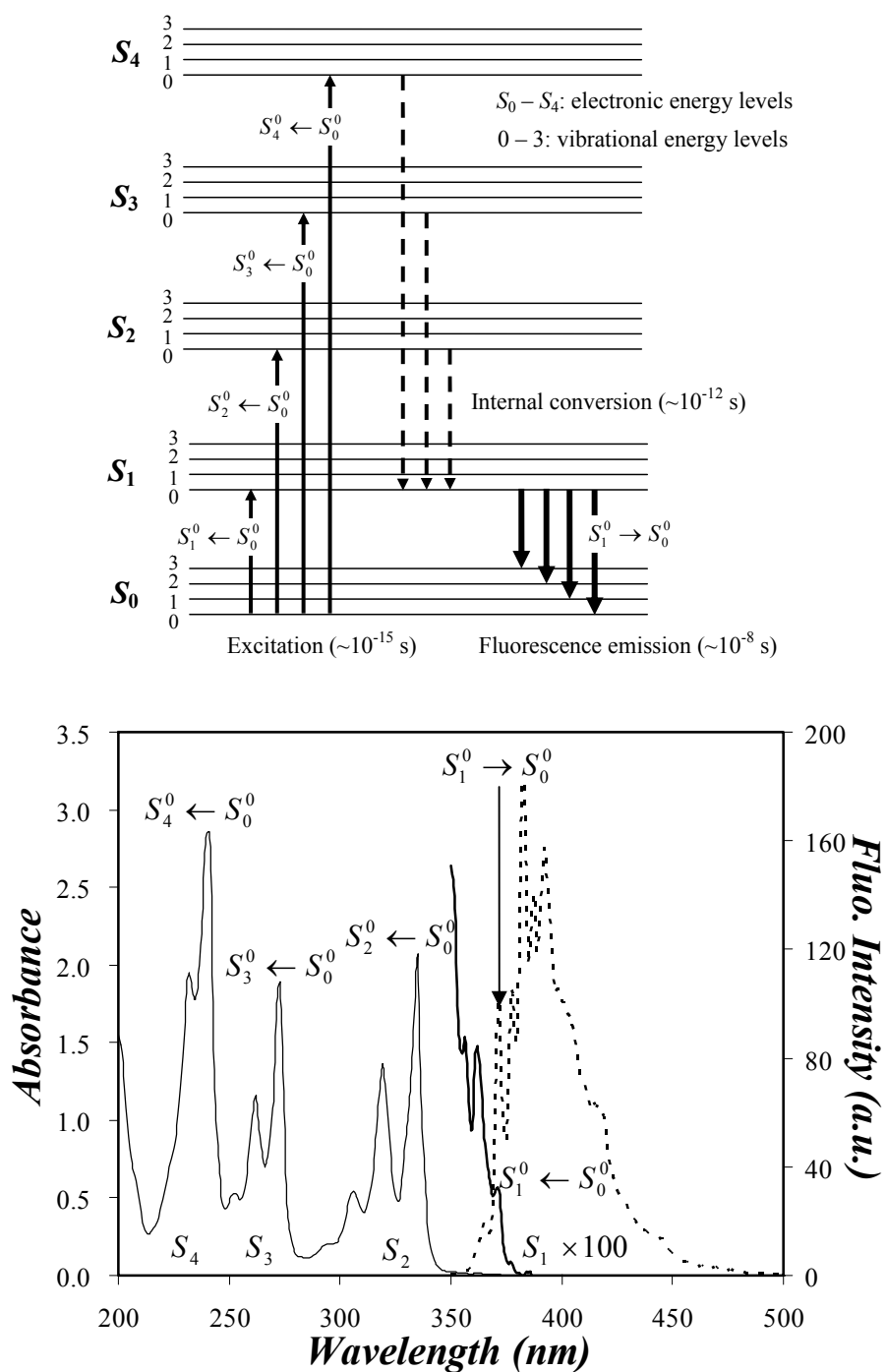
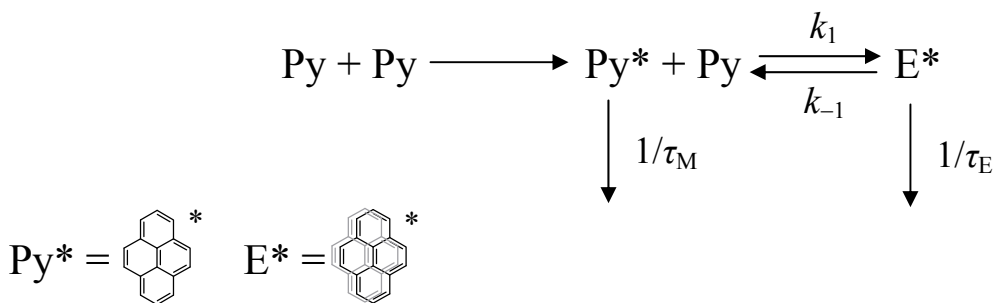


Figure 1.5: The Jablonsky diagram (top) and the corresponding transitions (bottom) found in the absorption (solid line) and fluorescence emission (dash line) spectra of pyrene in cyclohexane. $[\text{Py}] = 2.5 \times 10^{-6}$ M and $\lambda_{\text{ex}} = 334$ nm for the emission spectrum.

The presence of pyrene aggregation in solution can be detected from the absorption spectrum of pyrene. The P_A value is defined as the ratio of the peak-to-valley absorbance of the $S_2^0 \leftarrow S_0^0$ transition peak. In the case of pyrene in cyclohexane (Figure 1.5), the wavelengths corresponding to the peak and valley of the $S_2^0 \leftarrow S_0^0$ absorbance used to obtain the P_A value are 334 and 326 nm, respectively. A P_A value of 3.0 or larger as shown in Figure 1.5 suggests that no pyrene aggregates are present, as is typically found in organic solvents where pyrene is completely soluble. A P_A value smaller than 3.0 indicates the presence of pyrene aggregates, as typically obtained in water with pyrene-labeled HMWSPs (Py-HMWSPs).^{58,59}

Following absorption, an excited pyrene monomer (Py*) can either deactivate itself by returning to the ground-state via fluorescence (Figure 1.5), or associate with a ground-state pyrene (Py) to form an excimer (E*).*⁶⁰ If the association between two pyrene moieties occurs by diffusive encounter, the process of excimer formation can be described by Birks' Scheme given in Scheme 1.1, where τ_M and τ_E are the lifetimes of the excited pyrene monomer and the excimer, respectively, and k_1 and k_{-1} are the rate constants of formation and dissociation, respectively. As deduced from the minimal overlap between the absorption and fluorescence spectra in Figure 1.5, no energy transfer takes place between Py* and Py before the formation of E*.



Scheme 1.1: Birks' scheme and structures of the excited pyrene monomer and the pyrene excimer.

The excited pyrene monomer and the pyrene excimer are two different fluorescent species. Figure 1.6 shows the typical steady-state fluorescence emission spectra of pyrene obtained with a solution of a PEO chain with a 2,000 g/mol number-average molecular weight (M_n) labeled at one (PEO(2K)-Py₁) or both (PEO(2K)-Py₂) ends with pyrene. The excited pyrene monomer emission is characterized by several sharp peaks between 360 nm and 425 nm, whereas the pyrene excimer emission features a broad and structureless peak centered at around 480 nm. No excimer emission can be formed in acetone with PEO(2K)-Py₁. It is experimentally convenient that the wavelength regions where the excited monomer and excimer emit are well separated as demonstrated in Figure 1.6. The extent of excimer formation can be qualitatively quantified by determining the I_E/I_M ratio where I_E and I_M represent the fluorescence intensity of the pyrene excimer and monomer, respectively. I_M and I_E are calculated by integrating the fluorescence spectrum over the wavelengths 372 – 378 nm and 500 – 530 nm, respectively. The wavelength range chosen to calculate I_E , which is slightly shifted from the excimer peak maximum at 480 nm (see Figure 1.6), and that for I_M are selected to minimize any possible interference between the fluorescence spectra of the two fluorescent species.

Information about the polarity of the medium surrounding pyrene can be obtained by further analysis of the steady-state fluorescence spectrum. The ratio of the first (I_1) to the third (I_3) peak has been found to report on the polarity of the microenvironment where pyrene is located. The I_1/I_3 ratio is larger for pyrene in polar solvents such as water (1.67) and relatively lower for pyrene in non-polar solvents like hexane (0.6).⁵⁶ Substitution at the 1-position of the pyrene molecule results in a loss of the sensitivity of pyrene to its local micropolarity.^{59,61} However, the introduction of a heteroatom such as oxygen in the β -position of the pyrene alkyl substituent was found to partially regenerate the response of pyrene to the polarity of its local environment.⁶² Therefore, the I_1/I_3 ratio obtained with polymer samples such as PEO(2K)-Py₁ and PEO(2K)-Py₂ which were end-labeled with 1-

pyrenemethyl ether (Py-CH₂-O-) groups still reports on the polarity of the micro-environment surrounding the pyrene end group.

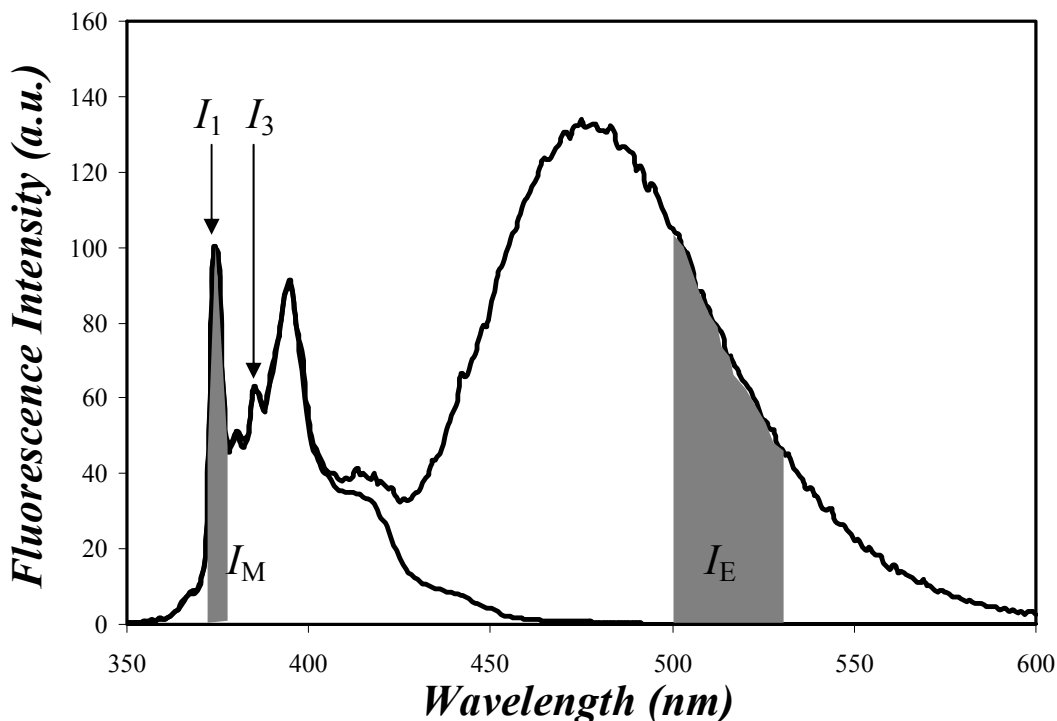


Figure 1.6: Steady-state fluorescence spectra of PEO(2K)-Py₁ (bottom) and PEO(2K)-Py₂ (top). The two spectra were normalized at 375 nm. [Py] = 2.5×10^{-6} M in acetone, $\lambda_{\text{ex}} = 344$ nm, $M_n(\text{PEO}) = 2,000$ g/mol.

1.2.2 Pyrene-Labeled Polymers and Oligomers

The hydrophobic chromophore pyrene has been considered to be “*by far the most frequently used dye in fluorescence studies of labeled polymers*”.⁵⁸ It has been widely used as a fluorescent probe to investigate polymer chain and side-chain dynamics,⁶³⁻⁶⁵ polymer coil-to-globule transitions,⁶⁶ the association between polymers and surfactants,^{41,67-69} and the hydrophobic aggregation of Py-HMWSPs in aqueous solutions where pyrene is used in lieu of the hydrophobe.⁷⁰⁻⁷² For these latter

studies, pyrene can be viewed as the ideal chromophore because it is highly hydrophobic (the solubility of pyrene in water has been reported to be in the range of 0.3-0.7 μM),¹⁹ it has a well-characterized long-lived excited state,⁷⁰ the excited pyrene monomer can associate with a ground-state pyrene to form an excimer,⁶⁰ it has a large molar absorbance coefficient,⁷³ and its emission spectrum is sensitive to its microenvironment.⁵⁶

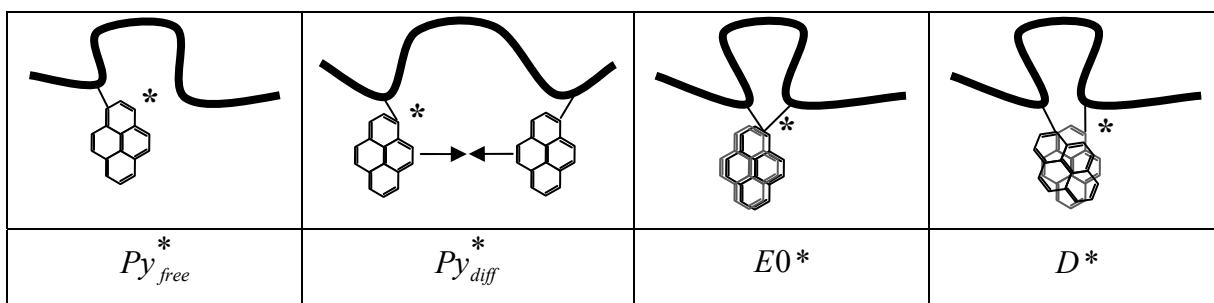
The process of end-to-end cyclization (EEC) of short-chain molecules and long-chain polymers has been characterized by probing the process of excimer formation during the loop formation of the molecular chain labeled at both ends with pyrene. EEC probed by pyrene excimer formation has been found to depend on the stiffness of the molecular backbone, the solvent quality toward the polymer and the solvent viscosity.^{63,74-76} Diffusion-controlled pyrene excimer formation can be viewed as a fluorescence dynamic quenching (FDQ) experiment where an excited pyrene is being quenched upon excimer formation. The theory describing the application of FDQ to investigate EEC was first proposed by Willemski and Fixman in 1974.^{77,78} EEC experiments benefit from using pyrene as it acts as both a chromophore and a quencher during excimer formation. The first experiment where pyrene excimer formation was used to investigate the internal dynamics of oligomers was performed by Zachariasse in 1976 to study the EEC of a series of *n*-alkanes end-labeled with a 1-pyrenemethyl group.⁷⁹ In 1977, Cuniberti and Perico⁸⁰ applied fluorescence spectroscopy to investigate the EEC of a series of pyrene end-labeled PEO constructs (PEO-Py₂) having different chain lengths. The work on the EEC of polymers was refined by Winnik in 1980 who applied the Birks scheme to the analysis of the pyrene monomer and excimer fluorescence decays of a series of pyrene end-labeled polystyrene constructs (PS-Py₂) to retrieve the rate constant of EEC (k_{cy}) quantitatively.⁸¹ Later on, the EEC of other pyrene end-labeled polymers such as polydimethylsiloxane,^{82,83} poly(bisphenol A – diethylene glycol carbonate),⁸⁴ poly(ϵ -caprolactone),⁸⁵ and poly(*N*-isopropylacrylamide) (PNIPAM)⁸⁶ were also characterized. The effect of chain length on

the EEC of short pyrene end-labeled oligomers was studied by Zachariasse and others.^{74,87-90} For long polymer chains, Winnik investigated the effect of chain length on the EEC of a series of PS-Py₂ constructs and found that k_{cy} decreases strongly with increasing polymer chain length (N).⁶³ k_{cy} was experimentally determined⁶³ to scale as $N^{-1.62\pm 0.10}$.

Since pyrene is hydrophobic, it has been used to replace the traditional alkyl hydrophobes of HMWSPs to enable the investigation of Py-HMWSPs by fluorescence. The water-soluble polymer backbones that have been labeled with pyrene include poly(acrylic acid),^{91,92} poly(maleic acid),⁹³ HASE,^{41,67-70} poly(*N,N*-dimethylacrylamide),⁹⁴⁻⁹⁶ PNIPAM,⁸⁶ polyethylenimine,⁹⁷ cellulose,^{72,98} and PEO.^{71,99-102} Interestingly, a number of these studies have established that not all hydrophobic pyrene pendants of a Py-HMWSP are associated in water.^{41,67-70,94-96} Furthermore the pyrene pendants of a Py-HMWSP can be found in different states. In the case of Py-HASE, four possible pyrene excited species are generated upon excitation.^{41,68,70} They are referred to as Py_{free}^* , Py_{diff}^* , $E0^*$, and D^* , as schematically represented in Table 1.1. Py_{free}^* is an excited pyrene that emits with its natural lifetime (τ_M) and never forms an excimer. This species is detected in the monomer decay and it exhibits a mono-exponential decay. Py_{diff}^* is the excited pyrene that forms excimer via diffusional encounter with a ground-state pyrene. Its presence can be probed in both the monomer and excimer decays.^{41,68,70} $E0^*$ represents a pyrene excimer constituted of two properly stacked pyrene moieties having a lifetime τ_{E0} . Its contribution is found in the excimer decay. The restricted geometry experienced by a pyrene moiety attached to a macromolecule implies that not all excimer are formed through the interaction between two properly stacked pyrenes. Some pyrene excimers (D^*) are generated through the direct excitation of poorly stacked pre-associated pyrene molecules. They emit with a lifetime τ_D that is different from τ_{E0} . The sum of the concentrations of the two aggregated

pyrene species $[E0^*]$ and $[D^*]$ yields $[Py_{agg}^*]$, the overall concentration of excited aggregated pyrenes.

Table 1.1: Diagrams of the four excited pyrene species often encountered with pyrene-labeled polymers.



Pyrene can form excimer by the diffusional encounter of an excited and a ground state pyrene or the direct excitation of ground-state pyrene aggregates.^{68,70} A steady-state fluorescence spectrum does not provide any information about the manner by which an excimer is being formed. However, these two processes can be distinguished through analysis of the excimer fluorescence decays. If the excimer is formed by diffusion between two pyrene groups, excimer formation is delayed and a rise time is observed in the excimer decay. On the other hand, excimer formation by direct excitation of ground-state pyrene aggregates is instantaneous and no rise time is detected in the excimer decay. The excimer decays acquired with pyrene end-labeled PEOs (PEO-Py₂) in an organic solvent where pyrene is soluble and in water where pyrene tends to form aggregates are compared in Figure 1.7.

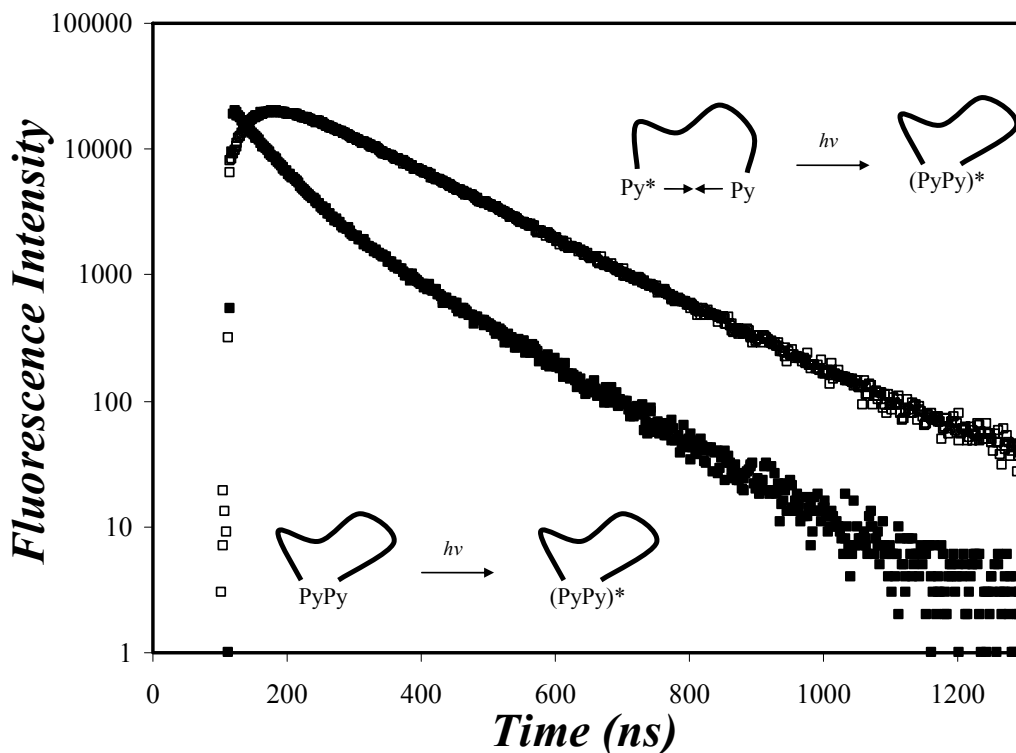


Figure 1.7: Excimer fluorescence decays of PEO(5K)-Py₂ in DMF (□, [Py] = 2.5×10⁻⁶ M) and in water (■, [Py] = 1.0×10⁻⁵ M). $\lambda_{\text{ex}} = 344 \text{ nm}$, $\lambda_{\text{em}} = 510 \text{ nm}$.

1.3 Global Analysis of Pyrene Monomer and Excimer Fluorescence Decays

Compared with other chromophores that do not form complexes upon excitation, the photophysical behavior of pyrene is complicated by pyrene excimer formation. Indeed, the fluorescence decays of the pyrene monomer are usually multiexponential in the case of pyrene-labeled macromolecules and the time scale over which a pyrene excimer is being formed can be estimated by calculating the average decay time of the fluorescence decay. However, such analysis where the pyrene monomer and excimer decays are fitted separately does not provide any quantitative information about the intrinsic properties of the pyrene-labeled polymers, such as the polymer chain

and side-chain dynamics, or the level of hydrophobic association. On the other hand, global analysis of the pyrene monomer and excimer fluorescence decays targets those processes that are probed in both the monomer and excimer decays, such as diffusion-controlled pyrene excimer formation.^{68,70} This procedure enables a more accurate assignment of the different photophysical processes undergone by the pyrene species and results in greater accuracy in the retrieval of the kinetic parameters that are used to describe those processes. Thus, global analysis of the fluorescence decays of the pyrene monomer and excimer provides a reliable and robust method to quantitatively investigate a wide variety of pyrene-labeled macromolecules under a broad range of experimental conditions. The first analysis of the fluorescence decays of the pyrene monomer and excimer was introduced by Birks et al. in 1963 for the excimer formation of molecular pyrene in organic solvents.¹⁰³ It was then modified to describe the EEC of intramolecular pyrene excimer formation of short (*n*-alkanes) and long polymer chains by covalently attaching pyrene onto the opposite ends of the chains by Zachariasse⁷⁹ in 1976 and Winnik⁸¹ in 1980, respectively. Since 1998, the Duhamel laboratory has proposed a series of models^{67,68,102,104,105} which are applicable to globally analyze the pyrene monomer and excimer fluorescence decays obtained with different pyrene-labeled macromolecules under various conditions. These models, starting from Birks' scheme and followed by the fluorescence blob model (FBM), the sequential model (SM), and the "model free" analysis (MF) are schematically depicted in Figure 1.8 according to the year when they were first introduced. These models are briefly described hereafter.

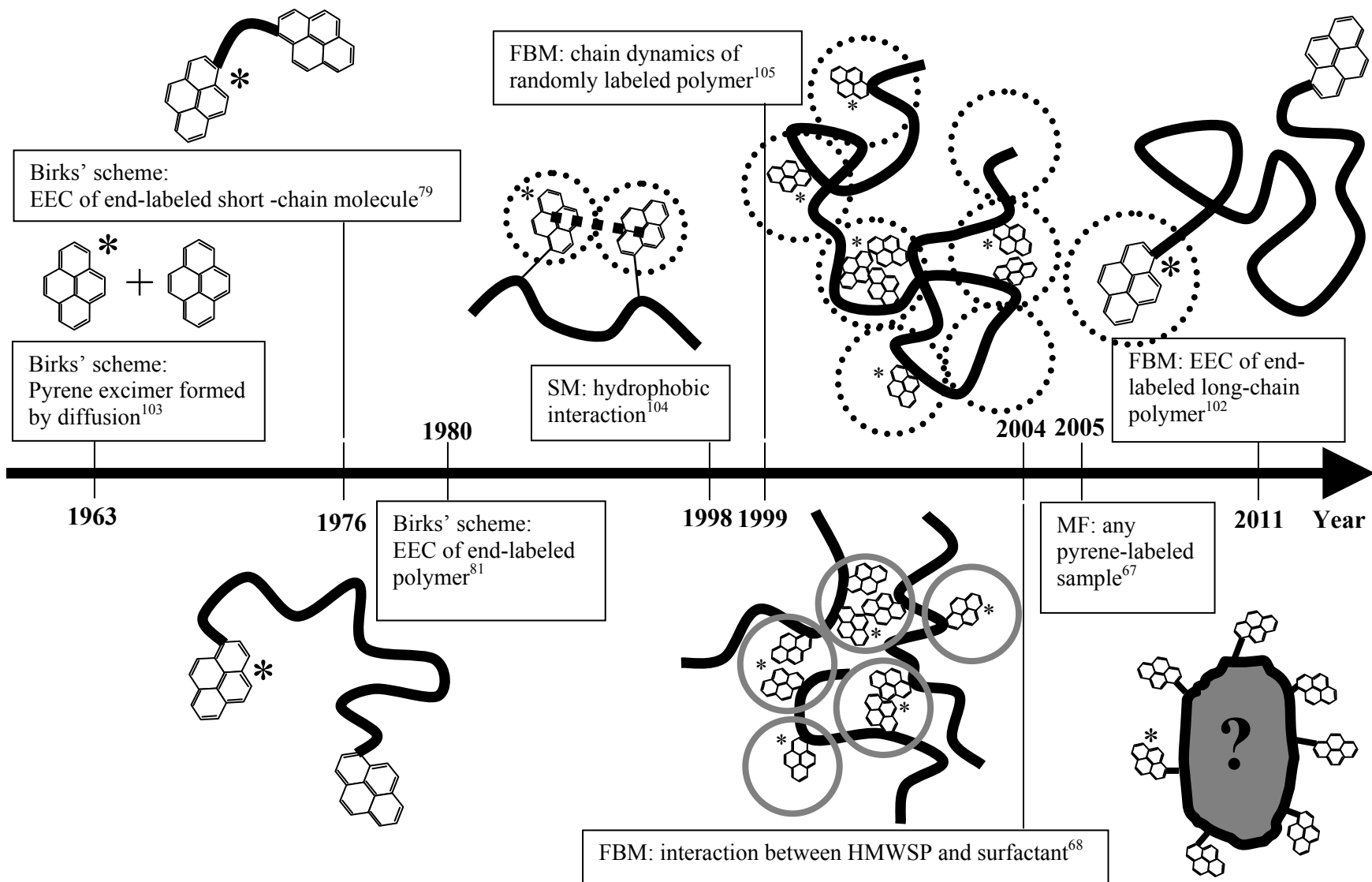
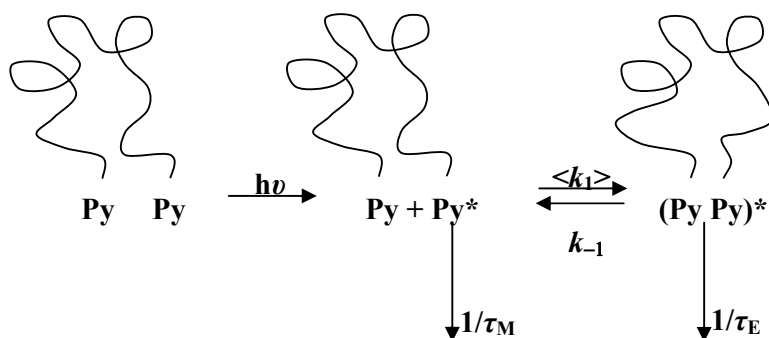


Figure 1.8: Timeline and schematic diagrams of the models for global analysis of pyrene monomer and excimer decays.

1.3.1 Birks' Scheme

Excimer formation between an excited and a ground-state aromatic chromophore like pyrene in solution is well described by Birks' Scheme (Scheme 1.1), first introduced by J. B. Birks in 1963.¹⁰³ When the pyrenes are covalently attached to the chain ends of a polymer with narrow molecular weight distribution, a modified Birks Scheme has been proposed in Scheme 1.2.⁸¹



Scheme 1.2: Modified Birks scheme for pyrene end-labeled polymer chains.

Schemes 1.1 and 1.2 are essentially equivalent, the main difference revolving around the nature of the rate constant of excimer formation being denoted as k_1 and $\langle k_1 \rangle$ in Schemes 1.1 and 1.2, respectively. $\langle k_1 \rangle$ is a pseudo-unimolecular rate constant, which is used to describe the excimer formation that occurs intramolecularly between two pyrenes attached to the end of the polymer. $\langle k_1 \rangle$ can be described by Equation 1.4¹⁰⁶

$$\langle k_1 \rangle = k_1 \times [Py]_{loc} \quad (1.4)$$

where k_1 is the bimolecular encounter rate constant which is the same as k_1 defined in Scheme 1.1. k_1 for molecular pyrene would equal $2 \times RT / (3 \times \eta)$ with R , T , and η being, respectively, the ideal gas constant, the absolute temperature in K, and the solvent viscosity, and $[Py]_{loc}$ represents the effective or local concentration of ground state pyrene in the neighborhood of the excited pyrene. Since the local pyrene concentration $[Py]_{loc}$ within the polymer coil is difficult to estimate experimentally, $\langle k_1 \rangle$ is used to represent the product $k_1 \times [Py]_{loc}$. The I_E/I_M ratio is given by Equation 1.5.¹⁰⁶

$$\frac{I_E}{I_M} = \kappa \frac{\phi_E^o}{\phi_M^o} \tau_M k_1 [Py]_{loc} \quad (1.5)$$

where κ is a constant that depends on the geometry and sensitivity of the spectrofluorometer used, ϕ_M^o and ϕ_E^o are the fluorescence quantum yields of, respectively, the pyrene monomer and excimer, and τ_M is the natural lifetime of the pyrene monomer. Equation 1.4 assumes that there is no dissociation of the pyrene excimer ($k_{-1} = 0$), which is a reasonable assumption for the pyrene excimer at temperatures lower than 35 °C.⁶⁰

The expressions for the time-dependent concentrations of the pyrene monomer and excimer are given in Equations 1.6 and 1.7, respectively.

$$[Py^*] = \frac{[Py_{diff}^*]_0}{\sqrt{(X - Y)^2 + 4\langle k_1 \rangle k_{-1}}} \left((X - \tau_2^{-1}) \times \exp(-t / \tau_1) - (X - \tau_1^{-1}) \times \exp(-t / \tau_2) \right) + [Py_{free}^*]_0 \exp(-t / \tau_M) \quad (1.6)$$

$$[E^*] = \frac{k_1 [Py_{diff}^*]_0}{\sqrt{(X - Y)^2 + 4\langle k_1 \rangle k_{-1}}} (-\exp(-t/\tau_1) + \exp(-t/\tau_2)) \quad (1.7)$$

where $X = \langle k_1 \rangle + \frac{1}{\tau_M}$ and $Y = k_{-1} + \frac{1}{\tau_E}$. $[Py_{diff}^*]_0$ and $[Py_{free}^*]_0$ represent the initial concentrations of those pyrenes that form excimer by diffusion and that never form an excimer, respectively. The expressions for the decay times τ_1 and τ_2 are given in Equations 1.8 and 1.9, respectively.

$$\tau_1^{-1} = \frac{X + Y + \sqrt{(X - Y)^2 + 4\langle k_1 \rangle k_{-1}}}{2} \quad (1.8)$$

$$\tau_2^{-1} = \frac{X + Y - \sqrt{(X - Y)^2 + 4\langle k_1 \rangle k_{-1}}}{2} \quad (1.9)$$

Birks' Scheme is applied when pyrene excimer formation can be described by a single rate constant, such as when pyrene is molecularly dissolved in a homogeneous solution or covalently attached to the ends of a monodisperse polymer. Some limitations to the applicability of Birks' Scheme to the EEC will be presented in Chapter 2 of this thesis.

1.3.2 Fluorescence Blob Model (FBM)

The FBM was first established in 1999 to study the chain dynamics of polymers randomly labeled with pyrene.¹⁰⁵ Since the labeling is random, any two pyrenes along the polymer are separated by different chain lengths so that excimer formation takes place according to a distribution of rate constants. The FBM assumes that an excited pyrene monomer probes a finite

volume inside the polymer coil while it remains excited and this volume has been referred to as a *blob*. The polymer coil is then arbitrarily divided into *blobs* among which the pyrene pendants distribute themselves randomly according to a Poisson distribution. Interestingly, the FBM can also be used when studying the interactions between Py-HMWSP and SDS at high SDS concentrations.⁶⁸ Then the hydrophobic pyrene pendants distribute themselves randomly among the SDS micelles, which become the *blobs* in the analysis. Regardless of the polymeric system being investigated, FBM analysis of the fluorescence decays yields the number of monomers making up a blob (N_{blob}), the average number of pyrenes per *blob* ($\langle n \rangle$), the rate constant (k_{blob}) of excimer formation by diffusive encounter between an excited and a ground-state pyrene located inside a same *blob*, and the product ($k_{ex}[blob]$) of the rate constant describing the exchange of ground-state pyrene between blobs and the local *blob* concentration [*blob*]. By establishing a relationship between these parameters, several results have demonstrated that the FBM provides quantitative information about polymer chain dynamics and the occupancy of mixed micelles by the pyrene hydrophobes of a Py-HMWSP in the presence of SDS micelles. The equations used to fit the monomer and excimer fluorescence decays according to the FBM are given in Equations 1.10 and 1.11, respectively.

$$[Py^*] = [Py_{diff}^*]_0 \exp \left[- \left(A_2 + \frac{1}{\tau_M} \right) t - A_3 (1 - \exp(-A_4 t)) \right] + [Py_{free}^*]_0 \exp(-t / \tau_M) \quad (1.10)$$

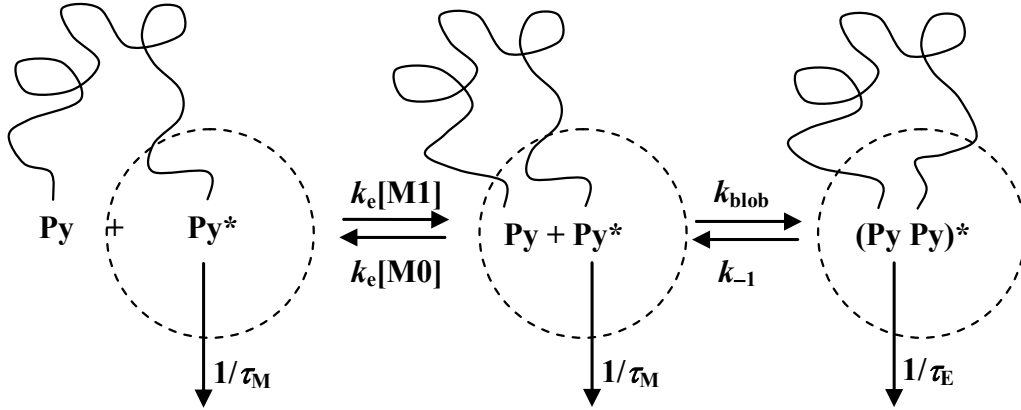
$$\begin{aligned}
[E^*] = & -[Py_{diff}^*]_0 e^{-A_3} \sum_{i=0}^{\infty} \frac{A_3^i}{i!} \frac{A_2 + i A_4}{\frac{1}{\tau_M} - \frac{1}{\tau_{E0}} + A_2 + i A_4} \exp\left(-\left(\frac{1}{\tau_M} + A_2 + i A_4\right)t\right) \\
& + \left([E0^*]_0 + [Py_{diff}^*]_0 e^{-A_3} \sum_{i=0}^{\infty} \frac{A_3^i}{i!} \frac{A_2 + i A_4}{\frac{1}{\tau_M} - \frac{1}{\tau_{E0}} + A_2 + i A_4} \right) e^{-t/\tau_{E0}} \\
& + [D^*]_0 e^{-t/\tau_D}
\end{aligned} \tag{1.11}$$

The parameters A_2 , A_3 , and A_4 used in Equations 1.10 and 1.11 are given in Equation 1.12.

$$\begin{aligned}
A_2 = \langle n \rangle & \frac{k_{blob} k_{ex} [blob]}{k_{blob} + k_{ex} [blob]} & A_3 = \langle n \rangle & \frac{k_{blob}^2}{(k_{blob} + k_{ex} [blob])^2} \\
A_4 = & k_{blob} + k_{ex} [blob]
\end{aligned} \tag{1.12}$$

Work from this laboratory presented in Chapter 3 has demonstrated that the FBM is also applicable to pyrene end-labeled telechelic polymers.¹⁰² As the chain ends are being separated by ever longer distances, a large fraction of the polymer chains can no longer form pyrene excimer intramolecularly, and those pyrenes emit with the same lifetime τ_M as the monolabeled polymer. A pyrene excimer is formed via diffusion only if an excited and a ground-state pyrene are close enough and are located in a sub-volume of the polymer coil called a blob where they form excimer with a rate constant k_{blob} . Ground-state pyrenes can exchange between blobs with a rate constant $k_c[M_1]$ and $k_c[M_0]$, where $[M_0]$ and $[M_1]$ represent the concentrations of blobs that contain zero or one ground-state pyrene, respectively. The kinetic scheme describing the process

of excimer formation for pyrene end-labeled polymers according to the FBM is shown in Scheme 1.3.



Scheme 1.3: End-to-end cyclization according to the FBM.

The mathematical expressions used to fit the fluorescence decays of the pyrene monomer and excimer are given in Equations 1.13 and 1.14, respectively.

$$\begin{aligned}
 [Py^*] = & \frac{[Py_{diff}^*]_o}{4\sqrt{\Delta}k_e([M0]+[M1])} \left(\left[\left((k_e([M0]+[M1]) + \sqrt{\Delta})^2 - k_1^2 \right) f_M(t) \times \exp(-t/\tau_A) \right. \right. \\
 & \left. \left. + \left[k_1^2 - \left((k_e([M0]+[M1]) - \sqrt{\Delta})^2 \right) \right] f_M(t) \times \exp(-t/\tau_B) \right] \right) \\
 & + [Py_{free}^*]_o f_M(t) + [Py_S^*]_o \exp(-t/\tau_S) \tag{1.13}
 \end{aligned}$$

$$[E^*] = \frac{k_1[M_{diff}^*]_o}{4\sqrt{\Delta}k_e([M0]+[M1])} \left(- \frac{(k_1 + k_e[M0])^2 - (k_e[M1] + \sqrt{\Delta})^2}{\frac{1}{\tau_E} - \frac{1}{\tau_M} - \frac{1}{\tau_A}} (f_M(t) \times \exp(-t/\tau_A) - f_E(t)) \right)$$

$$\begin{aligned}
& \left. + \frac{(k_1 + k_e[M0])^2 - (k_e[M1] - \sqrt{\Delta})^2}{\frac{1}{\tau_E} - \frac{1}{\tau_M} - \frac{1}{\tau_B}} (f_M(t) \times \exp(-t/\tau_B) - f_E(t)) \right) \\
& + [E^*]_o \times f_E(t) + [Py_S^*]_o \exp(-t/\tau_S)
\end{aligned} \tag{1.14}$$

where the species Py_S^* with a very short decay time ($\tau_S = 2$ to 4 ns) was usually observed when the pyrene pendants were confined onto a polymer, in a lipid bilayer, or for samples forming little excimer. The parameters Δ , τ_A , and τ_B are given by Equations 1.15 – 1.17.

$$\Delta = [k_1 + k_e([M0] - [M1])]^2 + 4k_e^2[M0][M1] \tag{1.15}$$

$$\tau_A^{-1} = \frac{1}{2} (k_1 + k_e([M0] + [M1]) + \sqrt{\Delta}) \tag{1.16}$$

$$\tau_B^{-1} = \frac{1}{2} (k_1 + k_e([M0] + [M1]) - \sqrt{\Delta}) \tag{1.17}$$

One major difference between Birks' scheme and the FBM is the definition of f_{Mfree} . In Birks' scheme, f_{Mfree} represents the fraction of pyrenes that do not form excimer resulting from the chains that were labeled at one end only. In the case of the FBM, f_{Mfree} represents the fraction of chains where an excited pyrene monomer cannot diffusionally encounter the ground-state pyrene at the opposite chain end because they are separated by too long a chain. Therefore, f_{Mfree} for the FBM is not an intrinsic property of the sample but depends on many factors such as solvent viscosity, the size of the polymer coil in solution, the length of the polymer chain, and the lifetime of the monomer τ_M , to name but a few. It is important to note that both models are applicable and yield consistent results for short polymers end-labeled with pyrene. Under such conditions, the polymer coil occupies a volume that is smaller than that of a *blob* and the excited pyrene

monomer can always find the ground-state pyrene to form an excimer intramolecularly. For such polymers, f_{Mfree} represents the fraction of the monolabeled polymers which act as fluorescent impurities.

1.3.3 Model Free (MF) Analysis

The MF analysis does not make any specific assumptions on the nature of pyrene excimer formation, and theoretically can be applied to any pyrene-labeled macromolecule.^{67,107-109} As mentioned earlier, four excited pyrene species are usually expected to be present when studying a pyrene-labeled macromolecule. Among these excited pyrene species, the excited pyrene monomers that form excimer by diffusion (Py_{diff}^*) are observed in both the monomer and excimer fluorescence decays, and $[Py_{diff}^*]_{(t)}$ can always be approximated by a sum of exponentials as shown in Equation 1.18 where the sum of the pre-exponential factors a_i equals unity ($\sum a_i = 1$).

$$[Py_{diff}^*] = [Py_{diff}^*]_0 \times \sum_{i=1}^n a_i \times \exp(-t / \tau_i) \quad (1.18)$$

Equation 1.18 could then be used to determine the time-dependent concentrations of the pyrene monomer and excimer, as shown in Equations 1.19 and 1.20, respectively.

$$[Py^*] = [Py_{diff}^*]_0 \times \sum_{i=1}^n a_i \times \exp(-t / \tau_i) + [Py_{free}^*]_0 \times \exp(-t / \tau_M) \quad (1.19)$$

$$\begin{aligned}
[E^*] = & -[Py_{diff}^*]_0 \times \sum_{i=1}^n a_i \frac{\frac{1}{\tau_i} - \frac{1}{\tau_M}}{\frac{1}{\tau_i} - \frac{1}{\tau_{E0}}} \exp(-t / \tau_i) \\
& + \left([E0^*]_0 + [Py_{diff}^*]_0 \times \sum_{i=1}^n a_i \frac{\frac{1}{\tau_i} - \frac{1}{\tau_M}}{\frac{1}{\tau_i} - \frac{1}{\tau_{E0}}} \right) \times \exp(-t / \tau_{E0}) \\
& + [D^*]_0 \times \exp(-t / \tau_D)
\end{aligned} \tag{1.20}$$

The pre-exponential factors a_i and decay times τ_i determined by the global analysis of the monomer and excimer decays according to Equations 1.19 and 1.20 can be used to calculate the average rate constant of excimer formation $\langle k \rangle$ using either the number-average rate constant, or the number-average decay time, as shown in Equations 1.21 and 1.22, respectively.

$$\langle k \rangle = \sum_{i=1}^n \frac{a_i}{\tau_i} - \frac{1}{\tau_M} \tag{1.21}$$

$$\langle k \rangle = \left(\sum_{i=1}^n a_i \times \tau_i \right)^{-1} - \frac{1}{\tau_M} \tag{1.22}$$

Global analysis of the monomer and excimer decays also allows the determination of the fractions f_{Mdiff} , f_{Mfree} , f_{Ediff} , f_{EE0} , and f_{ED} of the pyrene species Py_{free}^* , Py_{diff}^* , $E0^*$ and D^* which are given in Equations 1.23 – 1.27 where the subscripts M and E indicate the fractions that are retrieved from the analysis of the pyrene monomer and excimer fluorescence decays, respectively.

$$f_{Mdiff} = \frac{[Py_{diff}^*]_0}{[Py_{diff}^*]_0 + [Py_{free}^*]_0} \quad (1.23)$$

$$f_{Mfree} = \frac{[Py_{free}^*]_0}{[Py_{diff}^*]_0 + [Py_{free}^*]_0} \quad (1.24)$$

$$f_{Ediff} = \frac{[Py_{diff}^*]_0}{[Py_{diff}^*]_0 + [EO^*]_0 + [D^*]_0} \quad (1.25)$$

$$f_{EE0} = \frac{[EO^*]_0}{[Py_{diff}^*]_0 + [EO^*]_0 + [D^*]_0} \quad (1.26)$$

$$f_{ED} = \frac{[ES^*]_0}{[Py_{diff}^*]_0 + [EO^*]_0 + [D^*]_0} \quad (1.27)$$

The fractions obtained from Equations 1.23 – 1.27 can be used to calculate the overall molar fractions of Py_{diff}^* , f_{diff} , Py_{free}^* , f_{free} , EO^* , f_{E0} , D^* , f_D and f_{agg} according to Equations 1.28 – 1.32.

$$f_{diff} = \frac{[Py_{diff}^*]_0}{[Py_{diff}^*]_0 + [Py_{free}^*]_0 + [EO^*]_0 + [D^*]_0} = \left(1 + \frac{f_{Mfree}}{f_{Mdiff}} + \frac{f_{EE0}}{f_{Ediff}} + \frac{f_{ED}}{f_{Ediff}} \right)^{-1} \quad (1.28)$$

$$f_{free} = \frac{[Py_{free}^*]_0}{[Py_{diff}^*]_0 + [Py_{free}^*]_0 + [EO^*]_0 + [D^*]_0} = f_{diff} \times \frac{f_{Mfree}}{f_{Mdiff}} \quad (1.29)$$

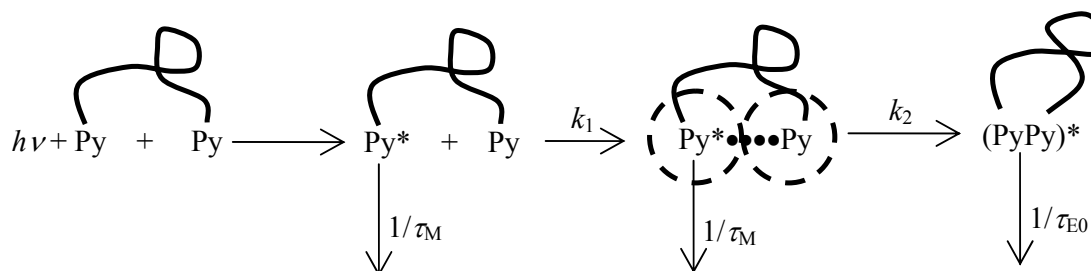
$$f_{E0} = \frac{[EO^*]_0}{[Py_{diff}^*]_0 + [Py_{free}^*]_0 + [EO^*]_0 + [D^*]_0} = f_{diff} \times \frac{f_{EE0}}{f_{Ediff}} \quad (1.30)$$

$$f_D = \frac{[D^*]_0}{[Py_{diff}^*]_0 + [Py_{free}^*]_0 + [EO^*]_0 + [D^*]_0} = f_{diff} \times \frac{f_{ED}}{f_{Ediff}} \quad (1.31)$$

$$f_{agg} = f_{E0} + f_D \quad (1.32)$$

1.3.4 Sequential Model (SM)

The SM was introduced in 1998 to describe the complex kinetics of pyrene excimer formation between pyrenyl groups attached at specific positions on PEO constructs by assuming a two step sequence.¹⁰⁴ The kinetic pathway is described in Scheme 1.4.



Scheme 1.4: Pyrene excimer formation according to the sequential manner.

Since pyrene is hydrophobic, a pyrene group in water is attracted to another pyrene via hydrophobic interactions when their distance is smaller than a capture distance equal to $2 \times R_c$ where R_c represents the capture radius of a pyrene group in water. R_c was found to equal 20 \AA by Char et al.⁹⁹ In the case of a PEO-Py₂ construct,¹⁰⁴ the excited pyrene diffuses randomly in solution until it encounters a ground-state pyrene. This encounter leads to the formation of a pyrene aggregate (Agg^* , shown as $\text{Py}^*\bullet\bullet\bullet\text{Py}$ in Scheme 1.4) which occurs with a rate constant k_1 . Since two pyrenes forming an aggregate are held together via hydrophobic forces, each pyrene is assumed to retain its monomer character and emit with its natural lifetime τ_M . Thereafter, rapid rearrangement of the two pyrenes occurs within the pyrene aggregate with a larger rate constant k_2 to form an excimer which emits with a lifetime τ_{E0} . The dissociation rate constants associated with the two steps have been neglected.¹⁰⁴

Mathematical expressions for the time-dependent concentrations of the pyrene monomer and excimer can be derived based on Scheme 1.4 and they are shown in Equations 1.33 and 1.34, respectively.

$$\begin{aligned}
 [Py^*] = & \left([Agg^*]_o + \frac{k_1}{k_1 - k_2} [Py_{diff}^*]_o \right) \exp \left[- \left(k_2 + \frac{1}{\tau_M} \right) t \right] \\
 & + \frac{k_2}{k_2 - k_1} [Py_{diff}^*]_o \exp \left[- \left(k_1 + \frac{1}{\tau_M} \right) t \right] + [Py_{free}^*]_o \exp(-t / \tau_M)
 \end{aligned} \tag{1.33}$$

$$\begin{aligned}
 [E0^*] = & - \frac{k_2}{k_2 + \frac{1}{\tau_M} - \frac{1}{\tau_E}} \times \left([Agg^*]_o + \frac{k_1}{k_1 - k_2} [Py_{diff}^*]_o \right) \exp \left[- \left(k_2 + \frac{1}{\tau_M} \right) t \right] \\
 & + \frac{k_1 [Py_{diff}^*]_o}{k_1 + \frac{1}{\tau_M} - \frac{1}{\tau_{E0}}} \frac{k_2}{k_1 - k_2} \exp \left[- \left(k_1 + \frac{1}{\tau_M} \right) t \right] \\
 & + \left([E0^*]_o + \frac{k_2 k_1 [Py_{diff}^*]_o}{\left(k_1 + \frac{1}{\tau_M} - \frac{1}{\tau_{E0}} \right) \left(k_2 + \frac{1}{\tau_M} - \frac{1}{\tau_{E0}} \right)} + \frac{k_2 [Agg^*]_o}{k_2 + \frac{1}{\tau_M} - \frac{1}{\tau_{E0}}} \right) \exp(-t / \tau_{E0})
 \end{aligned} \tag{1.34}$$

1.3.5 Summary of Models Used for the Analysis of Fluorescence Decays

Starting with the well-known Birks scheme, this chapter has reviewed many of the models that were introduced by this laboratory to study pyrene-labeled macromolecules in solution. While the family of models that were described enables the quantitative study of a large number of pyrene-labeled macromolecules displaying a vast number of different architectures that

can be linear or dendritic in nature, prior knowledge of the macromolecule behavior in solution remains the key to decide whether a specific model can be applied to a given pyrene-labeled macromolecule. The variety of polymeric systems generated by distinct macromolecules placed under different conditions and characterized by fluorescence in this thesis provides examples on how models can be selected and applied to analyse the fluorescence exhibited by given macromolecules.

1.4 Thesis Objectives

The first objective of this thesis was to quantitatively characterize the process of excimer formation for different Py-HMWSPs under various experimental conditions by applying the analytical procedures introduced in this chapter. The second objective of this thesis was to correlate the information retrieved by fluorescence on the behavior of the Py-HMWSPs at the molecular level with the macroscopic properties of the Py-HMWSP solutions characterized mostly by rheology. The experiments that were implemented to achieve these objectives are presented hereafter.

Over the past four decades, the EEC of a polymer chain has been studied effectively using fluorescence to probe the process of excimer formation with pyrene end-labeled polymers.^{63,76,81-85} All these earlier studies focused on short polymer chains and Birks' scheme was applied to obtain the kinetic parameters that describe EEC and characterize polymer chain flexibility. It was found that k_{cy} decreased significantly with increasing polymer chain length to the point where so little excimer was formed that it could no longer be detected.⁶³ When this happens, the excited pyrene monomer probes a finite volume within its lifetime, which has been referred to as a blob,¹⁰⁵ and that is smaller than the overall volume of the polymer coil.¹⁰² This effect results in a breakdown of

Birks' classic scheme, which then provides parameters that are not physically relevant to the EEC for long polymer chains.¹⁰² One accomplishment of this thesis was to apply the FBM to the analysis of the pyrene monomer and excimer fluorescence decays of a series of PEO-Py₂ constructs having different chain length and retrieve a consistent set of kinetic parameters to describe EEC.¹⁰²

The analysis of many results obtained by fluorescence is affected by the presence of trace amounts of fluorescent impurities in the study of fluorescently labeled macromolecules and yields results that depart significantly from those that would have been obtained with the pure labeled samples. Fluorescence experiments conducted on pyrene-labeled dendrimers constitute a case in point. Noticeable inconsistencies are found in the literature regarding the trends obtained between the I_E/I_M ratio and dendrimer generation number, probably due to the presence of free pyrene impurities.¹¹⁰ The second accomplishment of this thesis was to demonstrate that global analysis applied to the models described earlier can successfully isolate the contribution of these impurities to the fluorescence signal and provide the parameters describing the kinetics of pyrene excimer formation with unmatched accuracy.¹⁰⁹

Although numerous studies about Py-HMWSPs have been published over the years,^{71,72,91-93,97-100} few of them carry out a quantitative analysis of the fluorescence decays which retrieves the parameters describing the kinetics of excimer formation. The third accomplishment of this thesis was to apply the various models developed in the Duhamel laboratory to characterize at the molecular level how pyrene excimer formation takes place for different PEO-Py₂ and Py-HASE constructs in aqueous solution, in the presence or absence of surfactant. Such information should

prove extremely important as it characterizes the behavior of model HMWSPs that are commercially available in a number of industrial applications.

1.5 Thesis Outline

This thesis is composed of seven chapters. Chapter 1 was a literature review of HMWSPs, pyrene fluorescence, and the types of global analyses applied to retrieve the parameters used to describe the behavior of the various pyrene-labeled macromolecules studied in this thesis. Chapter 2 is an in-depth study of EEC for a series of pyrene end-labeled PEOs in organic solvents. Two analyses were applied and the FBM was found to be more robust than Birks' classic scheme. In Chapter 3, the applicability of the MF analysis was confirmed and it was used to explore how pyrene species often found as pyrene fluorescent impurities affect the fluorescence behavior of pyrene-labeled macromolecules. In Chapter 4, the hydrophobic interactions of pyrene end-labeled PEOs in water were investigated quantitatively using the SM. Chapter 5 is a study of the interactions taking place between SDS and pyrene end-labeled PEOs in water using the MF analysis. In Chapter 6, both the rheological and fluorescent properties of Py-HASE in the presence of SDS were studied and correlated. In particular, a joint rheometer/fluorometer setup was employed to monitor the behavior of these solutions at the molecular level by fluorescence as the samples were sheared. Chapter 7 reviews the many conclusions that were reached in this thesis and provides suggestions for future work. Chapters 2 and 3 have already been published as research articles in the *Journal of Physical Chemistry B*.^{102,109}

Chapter 2

Probing End-to-End Cyclization beyond Willemski and Fixman

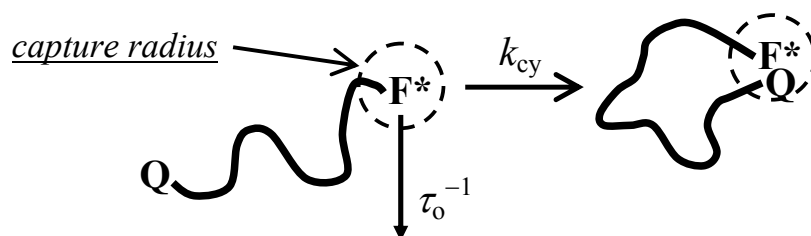
2.1 Overview

A series of poly(ethylene oxide)s labeled at both ends with pyrene (PEO(X)-Py₂ where X represents the number average molecular weight (M_n) of the PEO chains and equals 2, 5, 10 and 16.5 K) was prepared together with one pyrene mono-labeled PEO (PEO(2K)-Py₁). The process of end-to-end cyclization (EEC) was investigated by monitoring intramolecular excimer formation in seven organic solvents with viscosities (η) ranging from 0.32 to 1.92 mPa·s. The steady-state fluorescence spectra showed that excimer formation of PEO(X)-Py₂ decreased strongly with increasing η and M_n . The monomer and excimer time-resolved fluorescence decays were analyzed according to the traditional Birks Scheme. Birks' scheme analysis indicated that the decrease in excimer formation with increasing M_n and η was due partly to a decrease in the rate constant of EEC, but most importantly, to a large increase in the fraction of pyrenes that did not form excimer (f_{Mfree}). This result is in itself incompatible with the Birks scheme analysis which requires that f_{Mfree} be the molar fraction of chains bearing a single pyrene at one chain end; in short, f_{Mfree} does not depend on M_n and η within the framework of the Birks scheme analysis. In turn, this unexpected result agrees with the framework of the Fluorescence Blob Model (FBM) which predicts that quenching takes place inside a *blob*, which is the finite volume probed by an excited chromophore during its lifetime. Increasing M_n and η results in a larger fraction of chains having a conformation where the quencher is located outside the *blob* resulting in an increase in f_{Mfree} . Equations were derived to apply the FBM analysis, originally designed to study randomly

labeled polymers, to the end-labeled PEO(*X*)-Py₂ series. FBM analysis was found to describe satisfyingly the data obtained with the longer PEO(*X*)-Py₂ samples.

2.2 Introduction

End-to-end cyclization experiments (EEC) of polymers have been of interest since the classic theoretical description of the end-to-end cyclization probability of polymer chains by Jacobson and Stockmayer in 1950.¹ Many EEC experiments are conducted by attaching a fluorophore F and a quencher Q at the opposite ends of a polymer chain (Scheme 2.1). In the Willemski-Fixman formulation,^{2,3} the excited fluorophore F* is quenched by Q with a single rate constant k_{cy} when internal chain dynamics bring both into proximity, within a capture volume whose radius is characteristic of the reaction distance of the two groups, typically 1 nm or less.

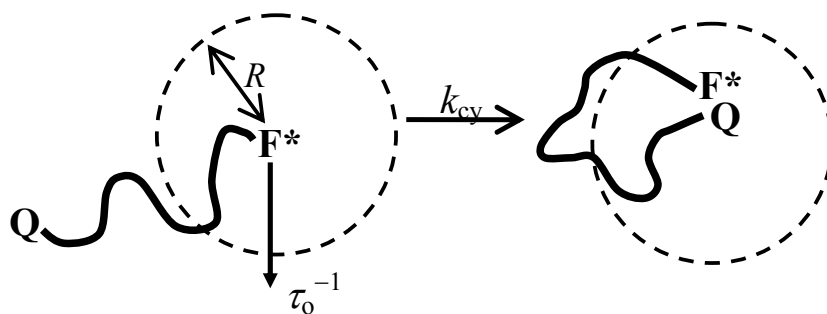


Scheme 2.1: EEC with the capture radius of the excited fluorophore.

Many examples of this type of EEC experiment have been reported.⁴⁻³⁷ When EEC experiments are carried out with short peptides, they are expected to reflect the dynamics of the most basic step encountered in protein folding, namely loop formation.⁴⁻¹⁶ In these fluorescence experiments, quenching of F* by Q (see Scheme 2.1) shortens its fluorescence decay time but maintains the exponential decay profile, and this decay time τ is related to k_{cy} by the expression

$\tau = (\tau_0^{-1} + k_{cy})^{-1}$, where τ_0 is the natural (unquenched) lifetime of F*. Analysis of the fluorescence decays is thus straightforward and yields k_{cy} , a measure of polymer flexibility. This theoretical insight brought to the fore by Willemski and Fixman^{2,3} has been confirmed by numerous experimental studies carried out on a variety of polymer backbones⁴⁻³⁷ which found that k_{cy} decreases with increasing number-average degree of polymerization (N_n) as $N_n^{-\alpha}$ where reported values of α range between 0.9 and 1.9.^{13-20,35}

In these EEC experiments, τ_0 serves as a clock that determines the time for a measurable F*-Q encounter. For long chains or slow relaxation rates, due to chain stiffness or elevated solvent viscosity, only a tiny fraction of the polymer chains in a sample will have their chain ends close enough to interact on the time scale of τ_0 . Most of the excited fluorophores will not react within this time window, and the measured value of τ will be indistinguishable from τ_0 . These ideas are summarized in Scheme 2.2, where we now focus on the radius R that describes the excursion volume sampled by the excited dye F* during its excited state. The volume sampled will be much larger for aromatic ketone³⁴ or anthracene³⁵ phosphorescence ($\tau_0 \approx 100 \mu\text{s}$) than for the fluorescence of dyes like naphthalene^{36,37} or pyrene¹⁷⁻³² ($\tau_0 \approx 50 - 300 \text{ ns}$). For fluorescent dyes and very long polymer chains, the vast majority of chain ends lie outside the excursion volume. Cyclization kinetics becomes difficult to study. Thus most experiments of this sort are carried out on polymers of short and intermediate lengths.



Scheme 2.2: EEC with the excursion volume of the excited fluorophore.

This observation leads to the question how the measured EEC kinetics might change under borderline conditions, where cyclization is being hindered by a long chain or a viscous solvent. If the chain is too long or the solvent is too viscous, a large fraction f_{free} of the excited chromophores will decay to the ground state with a lifetime τ_0 before having undergone an EEC event. EEC will occur only between those chain ends that are located sufficiently close to each other at the time of sample excitation and whose molar fraction equals $(1 - f_{\text{free}})$. As suggested in Scheme 2.2, the magnitude of f_{free} is expected to reflect the chain end distribution of the polymer in solution. It will also be important to distinguish this concept of f_{free} from another source of unquenchable chromophores that arise from imperfect synthesis of the labeled polymers, i.e. the small fraction of polymer chains in the sample that bear no Q.

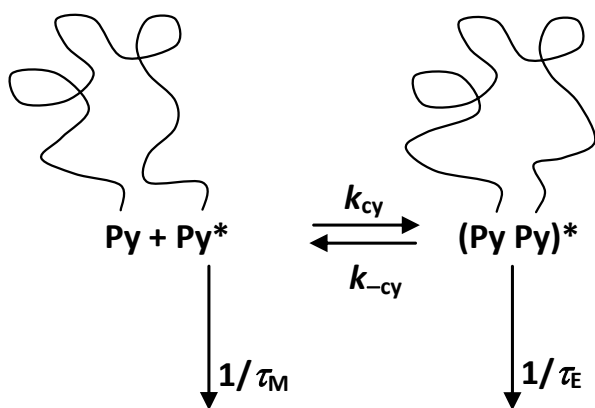
The present study represents an attempt to investigate how f_{free} varies for a series of poly(ethylene oxide) (PEO) samples labeled at both ends with pyrene (Py) under conditions where EEC is hindered by either elevated solvent viscosity and/or sufficiently long polymer chains. Pyrene provides a particular sensitivity for the study of EEC reactions where an excited

pyrene (Py*) interacts with another Py in the ground-state to form an excimer (PyPy)* that has its own distinct emission.¹⁷⁻³² Four monodisperse PEO samples with a number average molecular weight (M_n) value of 2000 (2K), 5000 (5K), 10000 (10K), and 16500 (16.5K) were labeled at both ends with Py groups. The four PEO constructs referred to as PEO(X)-Py₂ where X equals M_n were studied in seven organic solvents with viscosities ranging from 0.32 mPa.s for acetonitrile to 1.92 mPa.s for *N,N*-dimethylacetamide. The process of excimer formation with monodisperse end-labeled polymers is normally well-described by Birks' two-state mechanism,³⁸ where an extra term is added (with fraction f_{free} and pyrene monomer lifetime τ_M) to account for the small fraction of monolabeled polymers that cannot form excimer. However, our experiments lead to the surprising result that the magnitude of f_{free} increases for samples of longer chain length and for individual samples at high solvent viscosity. This strange result indicates that the magnitude of f_{free} is not linked to a fraction of chains missing a Py, but to a more fundamental feature of EEC kinetics when the fraction of cyclizing chains detected in the experiment is small. We were able to understand the nature of the phenomena by analyzing the fluorescence decay data in terms of a fluorescence blob model.

2.3 Theory

The process of excimer formation between two pyrenes covalently attached to both ends of a monodisperse polymer has been found to be well described by Birks' scheme (Scheme 2.3).^{17,38} Excimer formation between an excited monomer and a ground-state monomer is described by the first-order rate constant k_{cy} which depends among other factors on polymer chain length, solvent viscosity, and solvent quality toward the polymer.^{17,38} Dissociation of the excimer occurs with the rate constant $k_{-\text{cy}}$. Excimer dissociation is usually found to be rather slow

compared to the emission rate constant of the excimer τ_E^{-1} , taken as the inverse of the excimer lifetime.³⁸ The lifetime of the pyrene monomer τ_M can be obtained with a model compound which can be the pyrene derivative used to label the polymer, or even more accurately, by using a polymer bearing a single pyrene unit.



Scheme 2.3: Birks' two-state model for Py excimer formation.

Integration of the differential equations describing the kinetics depicted in Scheme 2.3 yields Equations 2.1 and 2.2 for the time-dependent concentrations of the pyrene monomer and excimer, respectively.^{17,38}

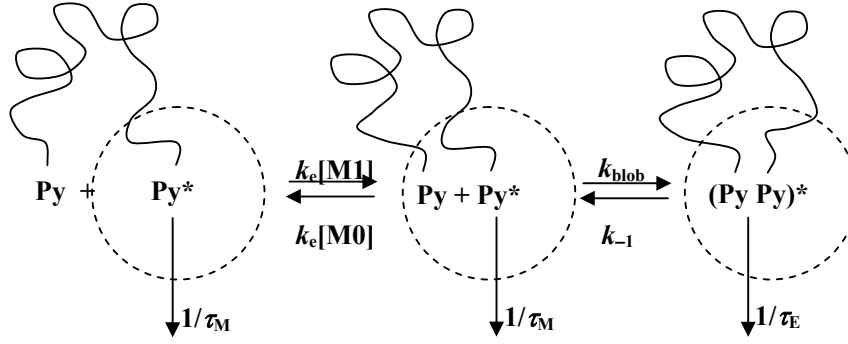
$$\begin{aligned}
 [Py^*] = & \frac{[Py_{diff}^*]_o}{\sqrt{(X - Y)^2 + 4k_{cy}k_{-cy}}} \left((X - \tau_2^{-1}) \times \exp(-t/\tau_1) - (X - \tau_1^{-1}) \times \exp(-t/\tau_2) \right) \\
 & + [Py_{free}^*]_o \exp(-t/\tau_M) + [Py_S^*]_o \exp(-t/\tau_S)
 \end{aligned} \tag{2.1}$$

$$[E^*] = \frac{k_{cy} [Py_{diff}^*]_o}{\sqrt{(X - Y)^2 + 4k_{cy} k_{-cy}}} (-\exp(-t/\tau_1) + \exp(-t/\tau_2)) + [Py_s^*]_o \exp(-t/\tau_s) \quad (2.2)$$

In Equations 2.1 and 2.2, X equals $k_{cy} + \tau_M^{-1}$, Y equals $k_{-cy} + \tau_E^{-1}$, the expressions for the decay times τ_1 and τ_2 are given in Equations SI.2.3 and SI.2.4 in the Supporting Information (SI), and $[Py_{diff}^*]_o$ and $[Py_{free}^*]_o$ represent the initial concentrations of pyrenes that form excimer by diffusion or do not form excimer because they are attached onto monolabeled chains, respectively.

These equations also have a term for a component of very short decay time (2 – 4 ns), denoted Py_s^* not explicitly incorporated into the Birks mechanism. The species Py_s^* is encountered occasionally at wavelengths where the excimer is measured when excimer formation occurs in restricted geometries such as when the pyrene pendants are confined onto a polymer^{29,30} or in a lipid bilayer.³⁹ In the present study, Py_s^* was observed for solutions of PEO(X)-Py₂ constructs prepared with longer chains and for samples in more viscous solvents.

Interestingly, our analysis of the monomer and excimer fluorescence decays with the above set of equations never yielded a complete set of satisfactory parameters despite the numerous theoretical adjustments made to Birks' scheme (see the Supporting Information). In particular, the fraction of unquenched pyrenes ($f_{Mfree} = [Py_{free}^*]_o / ([Py_{free}^*]_o + [Py_{diff}^*]_o)$) was found to increase with increasing polymer chain length and solvent viscosity, regardless of the model used. To account for this observation which is not predicted by Birks' scheme, the Fluorescence Blob Model (FBM) was introduced (Scheme 2.4).^{40,41}



Scheme 2.4: End-to-end cyclization according to the Fluorescence Blob Model.

The FBM assumes that while excited, a chromophore probes a finite volume referred to as a *blob*. Excimer will form with a rate constant k_{blob} only if a ground-state pyrene manages to be in a *blob* together with an excited pyrene. Ground-state pyrenes can move in and out of the *blob* with a rate constant $k_e[\text{M1}]$ and $k_e[\text{M0}]$, respectively, where $[\text{M0}]$ and $[\text{M1}]$ are the concentrations of *blobs* that contain zero or one ground-state pyrene, respectively, and k_e is the rate constant representing the exchange of ground-state pyrenes between *blobs*. Assuming that $k_{-1} \ll \frac{1}{\tau_E}$ (i.e. no excimer dissociation),³⁸ in the Supporting Information, Equations 2.3 and 2.4 were derived that describe the time-dependent concentration of the pyrene monomer and excimer, respectively.

$$\begin{aligned}
 [Py^*] = & \frac{[Py_{diff}^*]_o}{4\sqrt{\Delta}k_e([\text{M0}] + [\text{M1}])} \left(\left[\left((k_e([\text{M0}] + [\text{M1}] + \sqrt{\Delta})^2 - k_{blob}^2) \right] f_M(t) \times \exp(-t/\tau_A) \right. \right. \\
 & \left. \left. + \left[k_{blob}^2 - \left((k_e([\text{M0}] + [\text{M1}] - \sqrt{\Delta})^2 \right) \right] f_M(t) \times \exp(-t/\tau_B) \right) \right) \\
 & + [Py_{free}^*]_o f_M(t) + [Py_S^*]_o \exp(-t/\tau_S)
 \end{aligned} \tag{2.3}$$

$$\begin{aligned}
[E^*] = & \frac{k_{blob}[Py_{diff}^*]_o}{4\sqrt{\Delta}k_e([M0]+[M1])} \left(- \frac{(k_{blob} + k_e[M0])^2 - (k_e[M1] + \sqrt{\Delta})^2}{\frac{1}{\tau_E} - \frac{1}{\tau_M} - \frac{1}{\tau_A}} (f_M(t) \times \exp(-t/\tau_A) - f_E(t)) \right. \\
& \left. + \frac{(k_{blob} + k_e[M0])^2 - (k_e[M1] - \sqrt{\Delta})^2}{\frac{1}{\tau_E} - \frac{1}{\tau_M} - \frac{1}{\tau_B}} (f_M(t) \times \exp(-t/\tau_B) - f_E(t)) \right) \\
& + [E^*]_o \times f_E(t) + [Py_S^*]_o \exp(-t/\tau_S) \tag{2.4}
\end{aligned}$$

The expressions of the parameters Δ , τ_A , and τ_B are given hereafter. The expressions of $f_M(t)$ and $f_E(t)$ are given in Equations 2.8 and 2.9.

$$\Delta = [k_{blob} + k_e([M0] - [M1])]^2 + 4k_e^2[M0][M1] \tag{2.5}$$

$$\tau_A^{-1} = \frac{1}{2} (k_{blob} + k_e([M0] + [M1]) + \sqrt{\Delta}) \tag{2.6}$$

$$\tau_B^{-1} = \frac{1}{2} (k_{blob} + k_e([M0] + [M1]) - \sqrt{\Delta}) \tag{2.7}$$

$$f_M(t) = \alpha \times \exp(-t/\tau_{M1}) + (1 - \alpha) \times \exp(-t/\tau_M) \quad \text{with } 0 < \alpha < 1 \tag{2.8}$$

$$f_E(t) = \exp(-t/\tau_E) \tag{2.9}$$

The functions $f_M(t)$ and $f_E(t)$ describe the natural decay of the pyrene monomer and excimer, respectively. $f_M(t)$ was found to depart from the monoexponential form typically expected for small molecules in solution, certainly due to residual interactions between pyrene

and the PEO backbone. A second decay time τ_{M1} was introduced in Equation 2.8. The main difference between Equation 2.1 obtained with Birks' scheme and Equation 2.3 obtained from the FBM resides in the definition of f_{Mfree} . In the case of Birks' scheme, f_{Mfree} represents the fraction of pyrenes that do not form excimer resulting from PEO chains labeled at one end only. Consequently, f_{Mfree} describes the labeled PEO sample and should not be affected by the viscosity of the solvent or τ_M . In the case of the FBM, f_{Mfree} represents the fraction of chains where the ground-state pyrene is so far from the excited pyrene that it cannot form excimer. As a result, any effect that facilitates the search of the polymer coil by the excited pyrene located at the chain end, such as a lower solvent viscosity, a shorter chain, or a longer monomer lifetime τ_M , is expected to result in a smaller f_{Mfree} fraction.

If the pyrene monomer decays exponentially, Equations 2.3 and 2.4 based on the FBM are both sums of four exponentials. Equations 2.1 and 2.2 based on Birks' scheme are sums of four and three exponentials, respectively. The kinetic parameters used in the FBM are k_{blob} , $k_e[M1]$, $k_e[M0]$, and τ_E , whereas Birks' scheme uses the parameters k_{cy} , k_{-cy} , and τ_E , implying that the FBM uses one additional parameter. Here, however, we fix τ_E in the FBM analysis. Consequently, global analysis of the monomer and excimer fluorescence decays with the sets of Equations 2.1 and 2.2, and 2.3 and 2.4 with τ_E fixed, uses the same number of adjustable parameters.

2.4 Experimental

Materials: Distilled in glass *N,N*-dimethylformamide (DMF), tetrahydrofuran (THF), acetone, dioxane and HPLC grade methanol (MeOH) were purchased from Caledon Laboratories (Georgetown, ON). HPLC grade acetonitrile (ACN) and ethanol (EtOH) were obtained from

Fischer Scientific (FairLawn, NJ). EMD Science (Gibbstown, NJ) and Sigma-Aldrich (Oakville, ON) supplied HPLC grade toluene and *N,N*-dimethylacetamide (DMA), respectively. All solvents were used as received. The poly(ethylene oxide) ($M_n = 2K, 5K, 10K$ and $16.5K$) and poly(ethylene oxide) methyl ether ($M_n = 2K$) samples were purchased from Polymer Source (Montreal, QC). 1-Pyrenemethanol (98%) and 1-methylpyrene (97%) were purchased from Aldrich.

Synthesis of the mono- and doubly-labeled PEO: The synthesis of the PEO(2K)-Py₁ sample is described in the Supporting Information. The same synthetic procedure was used to prepare all PEO(*X*)-Py₂ samples. The structure of PEO(*X*)-Py₂ is shown in Figure 2.1. The functionality of the synthesized PEO(*X*)-Py₂ determined by UV-Vis absorption measurements was greater than 1.89 ensuring that most chain ends were capped by a pyrenyl pendant.

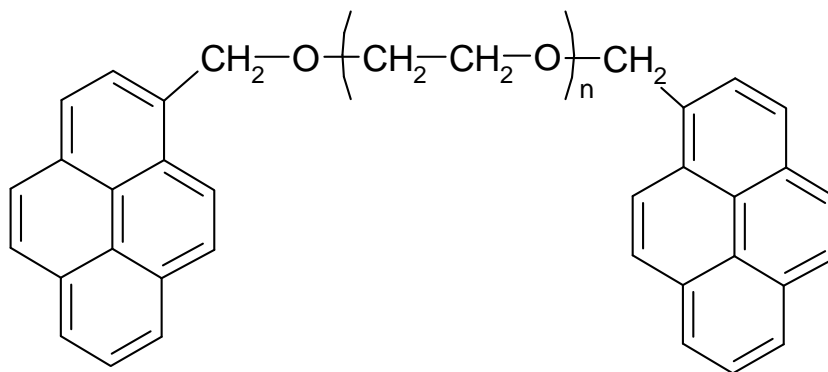
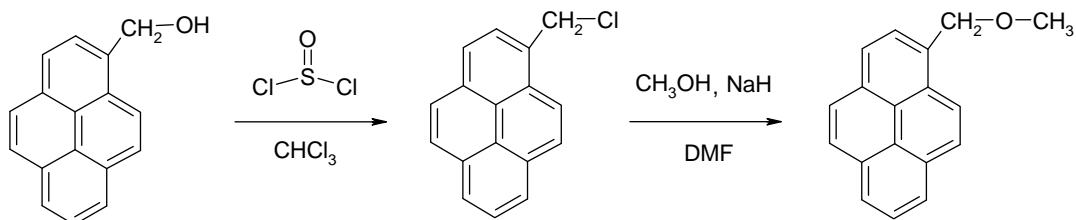


Figure 2.1: Chemical structure of the PEO(*X*)-Py₂ samples.

The number-average molecular weight, polydispersity index (PDI), and pyrene content of the pyrene-labeled PEO samples are given in Table 2.1.

Synthesis of 1-pyrenemethyl methyl ether (PyCH₂OMe): The synthesis of PyCH₂OMe was carried out according to Scheme 2.5. A detailed description of the synthesis is given in the Appendix.



Scheme 2.5: Synthesis of 1-pyrenemethyl methyl ether.

Absorption measurements: Absorption spectra were acquired on a Cary 100 UV-Vis spectrophotometer with a UV cell having a 1 cm path length.

Pyrene content determination: The pyrene content (λ_{py}) of the labeled PEOs was determined by measuring the absorption (Abs) of a DMF solution of known mass concentration of the labeled polymer [$Poly$] expressed in g.L^{-1} . The pyrene content was obtained directly from the quantity $Abs/([Poly] \times \epsilon_{\text{py}})$ where ϵ_{py} is the molar absorption coefficient of 1-pyrenemethanol in DMF ($\epsilon_{\text{py}} = 38900 \text{ M}^{-1}.\text{cm}^{-1}$ at 344 nm). We note that the molar absorption coefficient of 1-pyrenemethanol is the same as that of PyCH₂OMe in DMF ($\epsilon_{\text{py}} = 39000 \text{ M}^{-1}.\text{cm}^{-1}$ at 344 nm).

Table 2.1: PEO molecular weights, PDI, pyrene contents λ_{py} in $\mu\text{mol/g}$ polymer, and the labeling efficiency for the PEO(2K)-Py₁ and PEO(X)-Py₂ samples.

Sample	M_n (PEO) ^a (g/mol)	PDI ^a	λ_{py} ^b ($\mu\text{mol/g}$)	Number of labeled ends ^c (no. of ends)
PEO(2K)-Py ₁	2000	1.05	446	0.99 (1)
PEO(2K)-Py ₂	2000	1.10	800	1.93 (2)
PEO(5K)-Py ₂	5000	1.08	350	1.89 (2)
PEO(10K)-Py ₂	10000	1.05	184	1.92 (2)
PEO(16.5K)-Py ₂	16500	1.05	113	1.91 (2)

^a Information supplied by Polymer Source.

^b Measured by UV-Vis absorption.

^c Number of labeled ends = $\lambda_{py} \times M_n / (1 - \lambda_{py} \times M_{py})$ where $M_{py} = 215 \text{ g.mol}^{-1}$ for pyrene-CH₂-.

Intrinsic viscosity measurements: The intrinsic viscosity of the PEO sample with a molecular weight of 10000 g.mol^{-1} was determined in the seven organic solvents used in the fluorescence experiments. An Ubbelohde viscometer was used with a water bath to maintain the temperature at $25 \pm 0.1 \text{ }^\circ\text{C}$. Four polymer concentrations ranging from 4.5 to 10 g.L^{-1} were used to obtain the intrinsic viscosity in each solvent. Plotting the reduced viscosity of the polymer solution as a function of polymer concentration yielded a straight line whose intercept was taken as the intrinsic viscosity $[\eta]$.

Steady-state fluorescence measurements: The steady-state fluorescence spectra were acquired on a PTI fluorometer equipped with an Ushio UXL-75Xe Xenon arc lamp and PTI 814 photomultiplier detection system. All spectra were acquired with the right angle geometry. After degassing for 30 min under a gentle flow of N₂ to remove oxygen, the solutions were excited at a wavelength of 344 nm, and the emission spectrum was acquired from 350 to 600 nm. For each

PEO(*X*)-Py₂ sample, the fluorescence intensity of the monomer (I_M) was calculated by integrating the fluorescence spectrum from 372 to 378 nm. The fluorescence intensity of the excimer (I_E) was determined by normalizing the fluorescence spectrum of the monolabeled PEO(2K)-Py₁ sample to that of PEO(*X*)-Py₂ at the first monomer peak (~ 375 nm), subtracting the normalized spectrum of PEO(2K)-Py₁ from that of PEO(*X*)-Py₂ and integrating the result of that subtraction from 500 to 530 nm. This procedure ensured that no residual monomer fluorescence that might have leaked into the excimer emission would contribute to the calculation of the I_E/I_M ratio.

Time-resolved fluorescence measurements: All polymer solutions for time-resolved fluorescence measurements were prepared following the same protocol as for the steady-state fluorescence experiments. The instrumentation used in the time-resolved fluorescence measurements has been described earlier.³¹

Analysis of the fluorescence decays: The analysis of the monomer and excimer decays was done globally using, respectively, Equations 2.1 and 2.2 for Birks' scheme and Equations 2.3 and 2.4 for the FBM. The two sets of equations were convoluted with the instrument response function. The parameters were optimized using the Marquardt-Levenberg algorithm to obtain the best χ^2 .⁴² A light scattering correction was applied to the analysis of the fluorescence decays to account for the presence of residual light scattering. An additional parameter was added to account for the background noise that became somewhat important when studying PEO(*X*)-Py₂ constructs prepared with the longer PEO chains or in high viscosity solvents. The fits were considered good when the χ^2 was less than 1.30 and the residuals and autocorrelation of the residuals were randomly distributed around zero.

A special note must be made that in these global analyses of the pyrene monomer and excimer fluorescence decays, the parameters k_{cy} , k_{-cy} , and τ_E for Equations 2.1 and 2.2 were fitted directly. Similarly, k_{blob} , $k_c[M0]$, $k_c[M1]$, and τ_E in Equations 2.3 and 2.4 were fitted directly. This represents a departure from the usual analysis of fluorescence decays with a sum of exponentials, where the various rate constants describing the kinetics of excimer formation are derived from the decay times and pre-exponential factors retrieved from the analysis. Directly fitting the parameters gives control to the experimentalist on whether a given parameter should be allowed to float or be fixed.

Determination of the natural lifetime τ_M of the pyrene label: τ_M was estimated by comparing the lifetime of several pyrene derivatives, namely the lifetime of 1-methylpyrene (PyMe), 1-pyrenemethanol (PyCH₂OH), 1-pyrenemethyl methyl ether (PyCH₂OMe), and PEO(2K)-Py₁ in several organic solvents. The lifetimes of the pyrene derivatives are reported in Table SI.2.1. PEO(2K)-Py₁ yields slightly bi-exponential decays with more than 92% of the pre-exponential weight obtained for the long decaytime τ_{M2} which was attributed to τ_M . The existence of a second decaytime for PEO(2K)-Py₁ is attributed to interactions taking place between the polymer backbone and the pyrene label. Comparison of the τ_M values obtained for PEO(2K)-Py₁ and the lifetime of PyCH₂OMe shows that within experimental error, these values are identical, differing by less than 1.0 %. On the other hand, the lifetimes of PyCH₂OH and PyMe are, on average, 7 % and 30 % smaller than τ_M , respectively. Except for the lifetime obtained in THF, a good agreement is observed between the τ_M values found in this work for PyMe and those reported by others in a recent publication.³⁰ However, the different τ_M values found for PyCH₂OH and PyMe

with respect to PEO(2K)-Py₁ suggest that these two pyrene derivatives are not appropriate model compounds to estimate τ_M for the PEO(X)-Py₂ samples.

2.5 Results and Discussion

All pyrene labeled PEO samples were studied in seven organic solvents that were chosen to cover a range of viscosities from 0.32 to 1.92 mPa·s while maintaining a similar solvent quality toward PEO. The solvent quality toward PEO was estimated by measuring the intrinsic viscosity of a monodisperse PEO sample ($M_n = 10000$; PDI = 1.05) in the seven organic solvents listed in Table SI.2.2. The intrinsic viscosity did not depend much on solvent taking an average value of $22.1 \pm 0.4 \text{ mL}\cdot\text{g}^{-1}$. These values are quite reasonable when compared to those reported earlier for a similar PEO sample ($M_n = 9600$; PDI = 1.10) in tetrahydrofuran, toluene, *N,N*-dimethylformamide, and dioxane and found to equal $21.7 \pm 0.8 \text{ mL}\cdot\text{g}^{-1}$.²¹ The similar intrinsic viscosity values obtained for PEO in seven different organic solvents suggests that the PEO chain adopts similar dimensions in terms of end-to-end distance or radius of gyration in these different solvents.

Analysis of the steady-state fluorescence spectra: The steady-state fluorescence spectra of the PEO(X)-Py₂ and PEO(2K)-Py₁ samples were acquired with a pyrene concentration of $2.5 \times 10^{-6} \text{ M}$ in the same organic solvents as those used in Table SI.2.2. The fluorescence spectra were also acquired with a concentration of $1.2 \times 10^{-6} \text{ M}$. The excellent overlap observed for the fluorescence spectra obtained at the two concentrations ensured that the solutions were dilute enough for excimer formation to occur intramolecularly. The fluorescence spectra normalized at 375 nm for the PEO(X)-Py₂ series in acetone are shown in Figure 2.2A. As the PEO chain length increases, the emission at 480 nm typical of the excimer decreases, reflecting the decrease in the number of

EEC events. A viscous solvent also hinders excimer formation, as can be seen in Figure 2.2B, where excimer fluorescence decreases strongly with increasing solvent viscosity. Some changes are observed in the features of the monomer fluorescence where the intensity of the third peak increases with respect to the intensity of the first peak as the solvent becomes less polar. The effect is particularly obvious in toluene, which is the least polar solvent used in this study (see dashed trace in Figure 2.2B). This effect reflects the sensitivity of the first peak located at ~ 375 nm in the fluorescence spectrum to solvent polarity and is the result of a symmetry forbidden transition.⁴³⁻⁴⁷ Although the substitution of pyrene in the 1-position by a methyl or longer alkyl chain breaks the symmetry of pyrene, lowers the solvent sensitivity of the I_1/I_3 ratio and shortens the unquenched fluorescence lifetime of the pyrene derivative, the introduction of a β -oxygen in an alkyl pyrene substituent at the 1 position (as in 1-alkoxymethyl-pyrene) helps to resymmetrize the pyrene molecular orbitals.⁴⁸ As a consequence, the solvent sensitivity of the I_1/I_3 ratio is amplified and the lifetime is longer compared to that of 1-alkylpyrenes (see Table SI.2.1).

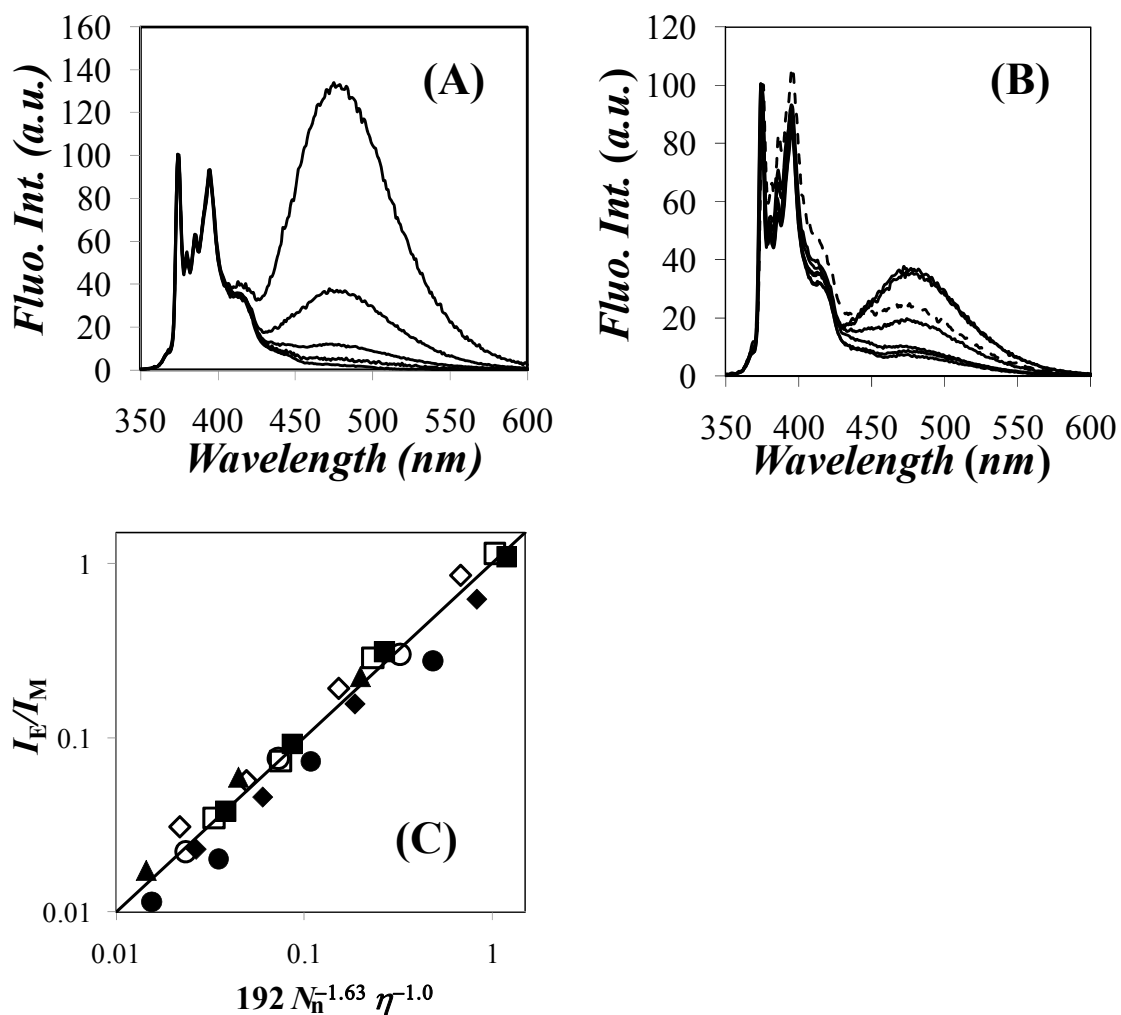


Figure 2.2: Steady-state fluorescence spectra of PEO labeled with pyrene (A) PEO(*X*)-Py₂ and PEO(2K)-Py₁ in acetone with, from top to bottom, *X* = 2.0, 5.0, 10.0, 16.5, PEO(2K)-Py₁; (B) PEO(5K)-Py₂, from top to bottom, acetone ($\eta = 0.32$ mPa.s), ACN ($\eta = 0.37$ mPa.s), THF ($\eta = 0.46$ mPa.s), toluene ($\eta = 0.56$ mPa.s), DMF ($\eta = 0.79$ mPa.s), dioxane ($\eta = 1.18$ mPa.s), DMA ($\eta = 1.92$ mPa.s); (C) Scaling relationship for the I_E/I_M ratio with viscosity and chain length for (■) acetone, (□) ACN, (◆) THF, (◇) toluene, (●) DMF, (○) dioxane, (▲) DMA. $[\text{Py}] = 2.5 \times 10^{-6}$ M, $\lambda_{\text{ex}} = 344$ nm.

Since the first peak is typically taken to represent the monomer fluorescence intensity, the sensitivity of the symmetry forbidden transition to solvent polarity suggests that care must be applied when using the pyrene fluorescence spectra to compare the process of excimer formation in different solvents. Nevertheless, Figure 2.2B indicates that the monomer fluorescence spectra overlap relatively well in all solvents except toluene so that if this effect plays a part, it will at most affect the results obtained in toluene only. The reduction in excimer formation with increasing polymer chain length and solvent viscosity observed in Figures 2.2A and 2.2B was summarized by determining the ratio of the fluorescence intensity of the excimer over that of the monomer, namely the I_E/I_M ratio. The I_E/I_M ratio was calculated for all PEO(*X*)-Py₂ samples in all solvents and is plotted in Figure 2.2C where it was found to scale as $\eta^{-1.0} \times N_n^{-1.6}$. Despite the possible effect of solvent polarity on the I_E/I_M ratio, the scaling relationship found for the I_E/I_M ratio in Figure 2.2C is in excellent agreement with what is theoretically expected³³ and experimentally found^{13-21,35} as shown hereafter.

The steady-state fluorescence spectra shown in Figures 2.2A and 2.2B differ from those reported³⁰ for a 9500 g.mol⁻¹ PEO end-labeled with a 1-pyrenemethylene oxide derivative (PEO(9.5K)-Py₂) having supposedly the same chemical structure as the PEO(*X*)-Py₂ samples prepared for the present study. In particular, the features of the pyrene monomer fluorescence of PEO(9.5K)-Py₂ were quite different from those shown in Figure 2.2B, but similar to those expected of a 1-pyrenebutyl derivative (see fluorescence spectra given in references 17, 21, 24-29, 31, and 49). This leads us to suspect that the PEO(9.5K)-Py₂ sample described in reference 30 was labeled with a 1-pyrenebutyl derivative. Since a 1-pyrenebutyl derivative in organic solvents has been shown to have a fluorescence lifetime that is about 70 ns shorter than that of a 1-

pyrenemethyl derivative,⁴⁹ conclusions drawn in reference 30 from the analysis of the fluorescence decays acquired with PEO(9.5K)-Py₂ must be treated cautiously.

Cuniberti and Perico have suggested that at room temperature where the dissociation rate constant (k_{-cy}) is negligible, the I_E/I_M ratio is given by Equation 2.10 and is proportional to k_{cy} , itself equal to $k_1 \times [Py]_{loc}$ where k_1 is the diffusion-controlled rate constant of excimer formation and $[Py]_{loc}$ is the local concentration of pyrenes inside the polymer coil.³³

$$\frac{I_E}{I_M} = \kappa \frac{\phi_E^o}{\phi_M^o} \tau_M k_1 [Py]_{loc} \quad (2.10)$$

In Equation 2.10, κ is a constant that depends on the geometry and sensitivity of the instrument used, ϕ_M^o and ϕ_E^o are the fluorescence quantum yields of the pyrene monomer and excimer, respectively, and τ_M is the lifetime of the pyrene monomer. The I_E/I_M ratio has been found to scale as $N^{-\alpha}$ for a number of pyrene end-labeled polymers and oligomers where α takes values ranging from 0.9 to 1.9.^{13-20,35} Furthermore, k_1 representing a process controlled by diffusion is expected to be inversely proportional to viscosity,^{21,33} as found experimentally in Figure 2.2C for the I_E/I_M ratio.

Analysis of the fluorescence decays according to Birks' scheme: The excellent agreement observed between theory and experiment for the I_E/I_M ratio suggests that k_{cy} obtained directly from the analysis of the monomer and excimer fluorescence decays of the PEO(X)-Py₂ samples should obey a similar scaling relationship as the one obtained for the I_E/I_M ratio. To this end, the fluorescence decays of the pyrene monomer and excimer were acquired in all organic solvents. They were fitted globally with Equations 2.1 and 2.2. The pre-exponential factors and decay

times retrieved from this analysis are listed in Table SI.2.3A. For the shorter chains and lower viscosity solvents, the fits were excellent with all χ^2 being smaller than 1.20, the residuals and the autocorrelation of the residuals being randomly distributed around zero. A sample decay analysis is shown in Figure 2.3. The monomer and excimer decays are shown on the left and right sides of the figure, respectively.

As the chain length was increased from 2K in Figure 2.3 to 10K in Figure 2.4, the quality of the fits became poorer, in particular for the excimer decay. Excimer formation is strongly reduced according to the $I_E/I_M \sim N^{-1.6}$ relationship found in Figure 2.2C, and the background level in the excimer decay is increased in Figure 2.4. The excimer decay for both PEO(2K)-Py₂ and PEO(10K)-Py₂ exhibit a rise time, but a spike appears at early times in the excimer decay of PEO(10K)-Py₂ only. This spike became prominent as excimer formation was reduced, either due to the use of a high viscosity solvent, a long PEO chain, or both. The existence of this fast decay has been reported previously and has been attributed to the presence of ground-state dimers.^{29,30,39} Nevertheless, it must be acknowledged that in the present study, this spike occurred only when the excimer emission was weak, so that the possibility that it might be due to light scattering or the presence of an impurity, due to a possible post-degradation of pyrene, can not be ruled out. To handle the spike, an additional exponential was added for the analysis of the monomer and excimer fluorescence decays with a decay time (τ_s) fixed to 3.5 ns, as this value has been found in other studies^{29,30,39} (see Equations 2.1 and 2.2, and 2.3 and 2.4).

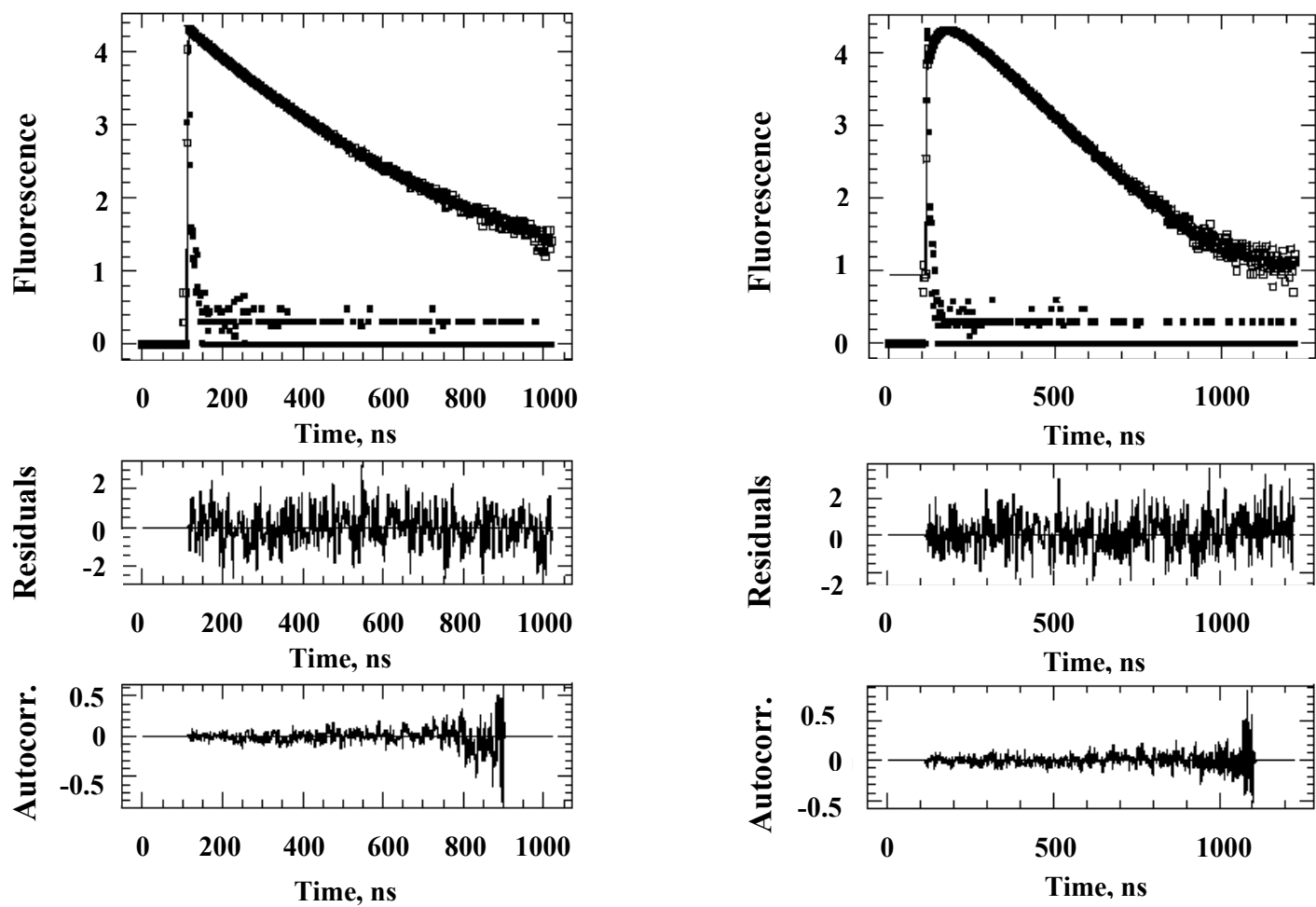


Figure 2.3: Fluorescence decays fitted by Birks' scheme of the pyrene monomer (left; $\lambda_{\text{ex}} = 344 \text{ nm}$, $\lambda_{\text{em}} = 375 \text{ nm}$; TPC = 2.04 ns/ch) and excimer (right; λ_{ex} = 344 nm, $\lambda_{\text{em}} = 510 \text{ nm}$; TPC = 2.04 ns/ch) of PEO(2K)-Py₂ in dioxane. [Py] = $2.5 \times 10^{-6} \text{ M}$, $\chi^2 = 1.01$.

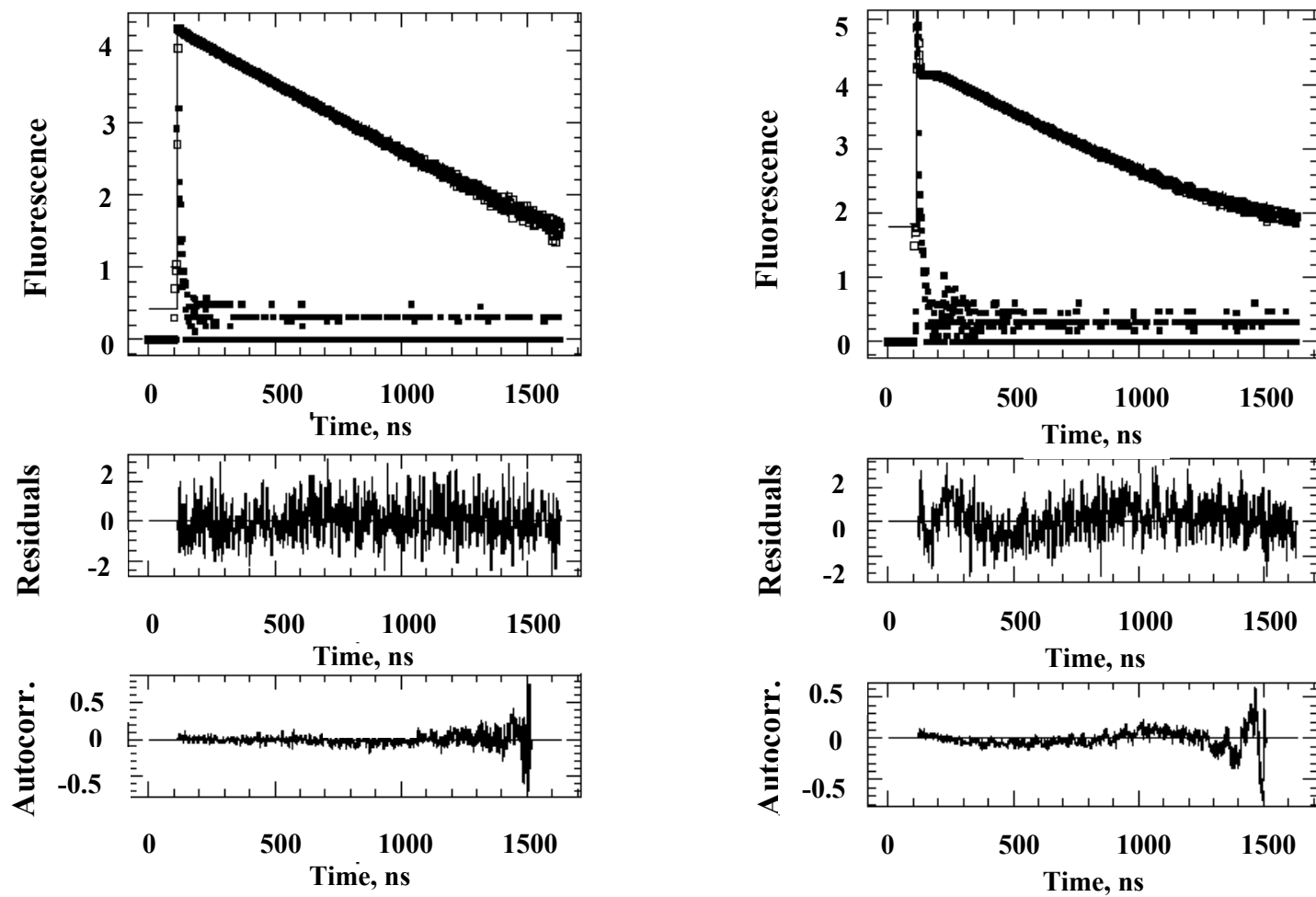


Figure 2.4: Fluorescence decays fitted by Birks' scheme of the pyrene monomer (left; $\lambda_{\text{ex}} = 344$ nm, $\lambda_{\text{em}} = 375$ nm; TPC = 2.04 ns/ch) and excimer (right; $\lambda_{\text{ex}} = 344$ nm, $\lambda_{\text{em}} = 510$ nm; TPC = 2.04 ns/ch) of PEO(10K)-Py₂ in dioxane. [Py] = 2.5×10^{-6} M, $\chi^2 = 1.19$.

The cyclization rate constant, k_{cy} , the dissociation rate constant, k_{-cy} , and the excimer lifetime, τ_E , were determined directly from the global analysis of the monomer and excimer fluorescence decays. Their values are reported in Table SI.2.3B. Since they were found to depend on viscosity (η) and the number average degree of polymerization (N_n), their scaling behavior was determined as a function of η and N_n as shown in Figures 2.5A-C. Equation 2.10 predicts that k_{cy} should scale as η^{-1} and $N_n^{-\alpha}$ where α values have been found to range from 0.9 to 1.9 experimentally.^{13-20,35} For small N_n and η values, k_{cy} was found to scale as $\eta^{-1} \times N_n^{-1.34}$. Although an exponent of -1.34 is consistent with values reported in the literature, it is nevertheless different from that of -1.6 found for the I_E/I_M ratios in Figure 2.2C. Furthermore, for larger N_n and η values, k_{cy} in Figure 2.5A remained constant within experimental error. A similar break point was also observed in the trends for k_{-cy} and τ_E .

Since k_{-cy} and τ_E describe intrinsic properties of the excimer, they are not expected to vary with polymer length as long as the polymer is long enough. Interestingly, the opposite is observed where k_{-cy} and τ_E take constant values of, respectively, $1.8 (\pm 0.5) \times 10^6 \text{ s}^{-1}$ and $48 \pm 1 \text{ ns}$ for small N_n and η values. These values for k_{-cy} and τ_E are quite reasonable for pyrene excimer in organic solvents³⁸ with k_{-cy} being about 10 times smaller than τ_E^{-1} , which supports the notion that the dissociation of the pyrene excimer is negligible at room temperature, as was assumed to derive Equation 2.10. However, k_{-cy} and τ_E were found to increase markedly for larger N_n and η values. Incidentally, this behavior was also observed for a series of pyrene end-labeled monodisperse polystyrenes.³¹ As it turns out, all trends shown in Figures 2.5A – C show a break point that occurs for N_n and η values such that $N_n \times \eta \sim 80 \text{ mPa.s}$.

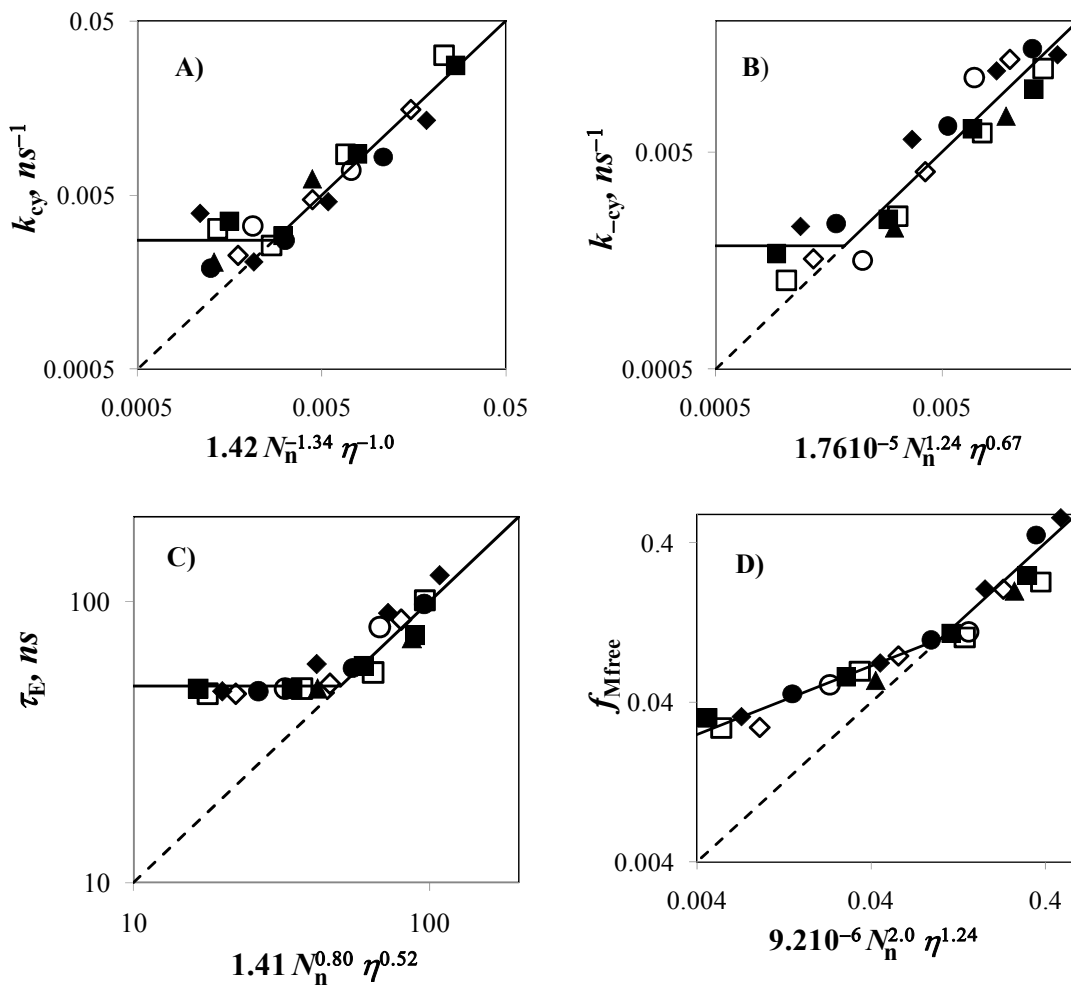


Figure 2.5: Scaling behavior of the parameters obtained from the global analysis of the pyrene monomer and excimer experimental fluorescence decays fitted with Equations 2.1 and 2.2, respectively. Symbols are the same as for Figure 2.2C.

Another parameter which was found to behave unexpectedly is the fraction f_{Mfree} , representing the molar fraction of pyrene monomers that do not form excimer and emit as if they were free in solution. f_{Mfree} equals $[Py_{free}^*]_o / ([Py_{diff}^*]_o + [Py_{free}^*]_o)$ (see Equation 2.1 for the definition of $[Py_{diff}^*]_o$ and $[Py_{free}^*]_o$) and is plotted as a function of viscosity in Figure 2.6. The

fraction f_{Mfree} was never equal to zero as a small amount (less than 5 mol% of the PEO chains) of monolabeled polymer was always present in the samples. Interestingly, f_{Mfree} was found to increase linearly with increasing viscosity, and the increase was more pronounced with increasing polymer chain length. This result was unexpected, since f_{Mfree} is supposedly a measure of the labeling efficiency of the polymer, which depends on neither solvent nor polymer chain length. f_{Mfree} remained relatively small (i.e. < 0.1) for N_n and η values, such that $N_n \times \eta < 80$ mPa.s, but for larger N_n and η values, f_{Mfree} took much larger values as large as 0.85 in dioxane for PEO(10K)-Py₂. In the log-log plot presented in Figure 2.5D, a break point for f_{Mfree} can be observed for $N_n \times \eta > 80$ mPa.s. Recently, a similar increase in f_{Mfree} with increasing viscosity has been observed in our laboratory for a series of pyrene end-labeled monodisperse poly(N-isopropylacrylamide)s (PNIPAM) in mixtures of 1-hexanol and methanol used to modify the solvent viscosity without affecting its quality toward the PNIPAM backbone.⁵⁰ This observation made with both PEO and PNIPAM pyrene end-labeled polymers suggests that the effect shown in Figure 2.6A might be general.

The trends shown in Figures 2.5A – D can be summarized as follows. As long as the chain is short and the solvent is fluid such that $N_n \times \eta < 80$ mPa.s, k_{cy} decreases with increasing chain length and viscosity as $\eta^{-1.0} \times N_n^{-1.34}$, k_{-cy} and τ_E remain constant, and f_{Mfree} is small. In other words, the parameters k_{cy} , k_{-cy} , τ_E , and f_{Mfree} behave as expected in this range of N_n and η values. For N_n and η values resulting in $N_n \times \eta$ being larger than 80 mPa.s, k_{cy} plateaus and k_{-cy} , τ_E , and f_{Mfree} increase with increasing viscosity and chain length. We have demonstrated in SI that these discrepancies are due neither to limitations in the analysis of the fluorescence decays, nor the presence of fluorescent impurities whose emission might overlap that of the pyrene monomer

and/or excimer. Consequently, our results suggest that Birks' scheme does not apply to study the EEC kinetics of long chains in viscous solvents and that an alternative analysis is required under such conditions.

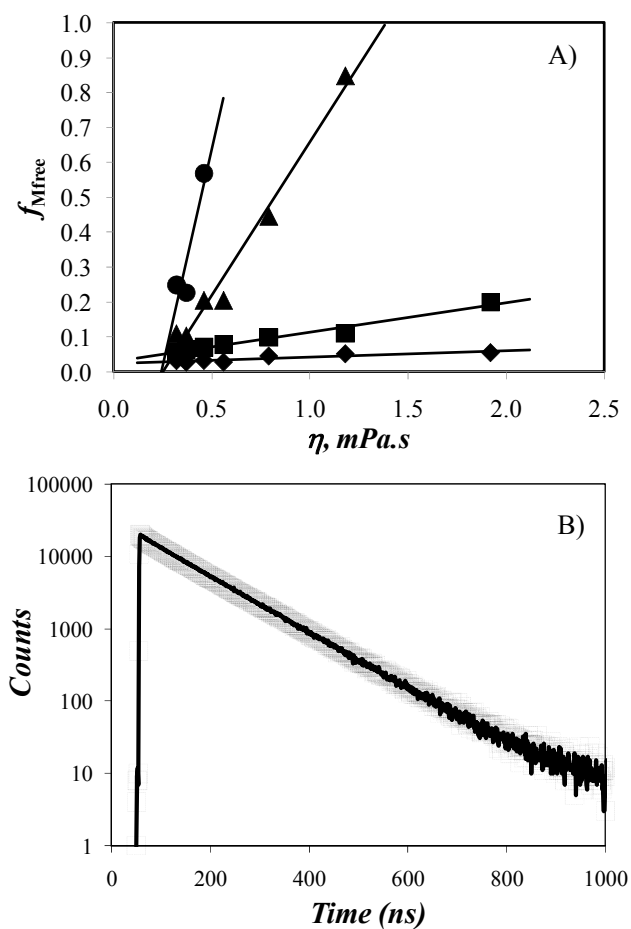


Figure 2.6: (A) Fraction f_{Mfree} obtained from the global analysis of the monomer and excimer fluorescence decays with Equations 2.1 and 2.2. (◆) PEO(2K)-Py₂, (■) PEO(5K)-Py₂, (▲) PEO(10K)-Py₂, and (●) PEO(16.5K)-Py₂. (B) Monomer fluorescence decays of (—) PEO(2K)-Py₁ and (□) PEO(10K)-Py₂ in dioxane.

Fluorescence Blob Model analysis of the fluorescence decays: Excimer formation for PEO(10K)-Py₂ in dioxane represents a case in point for this study. Global analysis of the monomer and excimer decays with Equations 2.1 and 2.2 yields an f_{Mfree} value of ~ 0.85 . Indeed the fluorescence decays of the pyrene monomer acquired for PEO(10K)-Py₂ and PEO(2K)-Py₁ are essentially superimposable in Figure 2.6B, suggesting that no excimer forms. Yet, after the prominent spike found at the early times and characteristic of the Py_S^* species in Equations 2.1 and 2.2, a rise time is observed in the excimer decay of PEO(10K)-Py₂ in Figure 2.4, a clear indication that excimer formation occurs by diffusive encounters between the two ends. Together Figures 2.4 and 2.6B imply that a small fraction ($1 - f_{\text{Mfree}}$) of all excited pyrenes form excimer by diffusion. We postulate that those pyrenes that form excimer by diffusion are close to each other, closer than the overall distribution of end-to-end distances (r_{EE}) suggests. If this is the case, excimer formation for PEO(10K)-Py₂ in dioxane would involve only a small fraction ($1 - f_{\text{Mfree}}$) of all excited pyrenes, namely those pyrene-labeled ends that are located within a distance r_{EE} smaller than a cut-off distance referred to as $r_{\text{EE}}^{\text{blob}}$. The superscript *blob* refers to the subvolume where excimer formation takes place inside the polymer coil.

Interestingly, the concept of localized reactivity inside the polymer coil can be easily handled by using the Fluorescence Blob Model (FBM), originally developed to handle the complex kinetics of excimer formation encountered for polymers randomly labeled with pyrene.^{40,41} According to the FBM, an excited pyrene probes a finite volume called a *blob* while it remains in the excited state. Excimer formation occurs inside a *blob* with a rate constant k_{blob} . Ground-state pyrenes can move inside the *blob* containing an excited pyrene with a rate constant $k_c[\text{M1}]$ where k_c is the exchange rate constant and $[\text{M1}]$ is the local concentration of *blobs* inside

the polymer coil that contain one ground-state pyrene. Ground-state pyrenes exit the *blob* containing one excited pyrene with a rate constant $k_e[M_0]$ where $[M_0]$ is the local concentration of *blobs* that contain no ground-state pyrene. Application of the FBM to end-labeled polymers has been described in the Theory section, and Equations 2.3 and 2.4 were used to fit globally the monomer and excimer decays, respectively. All fits were excellent, even for PEO(*X*)-Py₂ samples prepared with long PEO chains and/or large solvent viscosity, yielding small χ^2 values (< 1.20), randomly distributed residuals and autocorrelation function of the residuals. The parameters retrieved from the fits are listed in Tables SI.2.5. In particular, the poorer fits obtained for the Birks scheme analysis of the fluorescence decays acquired with the longer chains in more viscous solvents are much improved as can be seen by comparing the fits shown in Figure 2.4 and Figure 2.7.

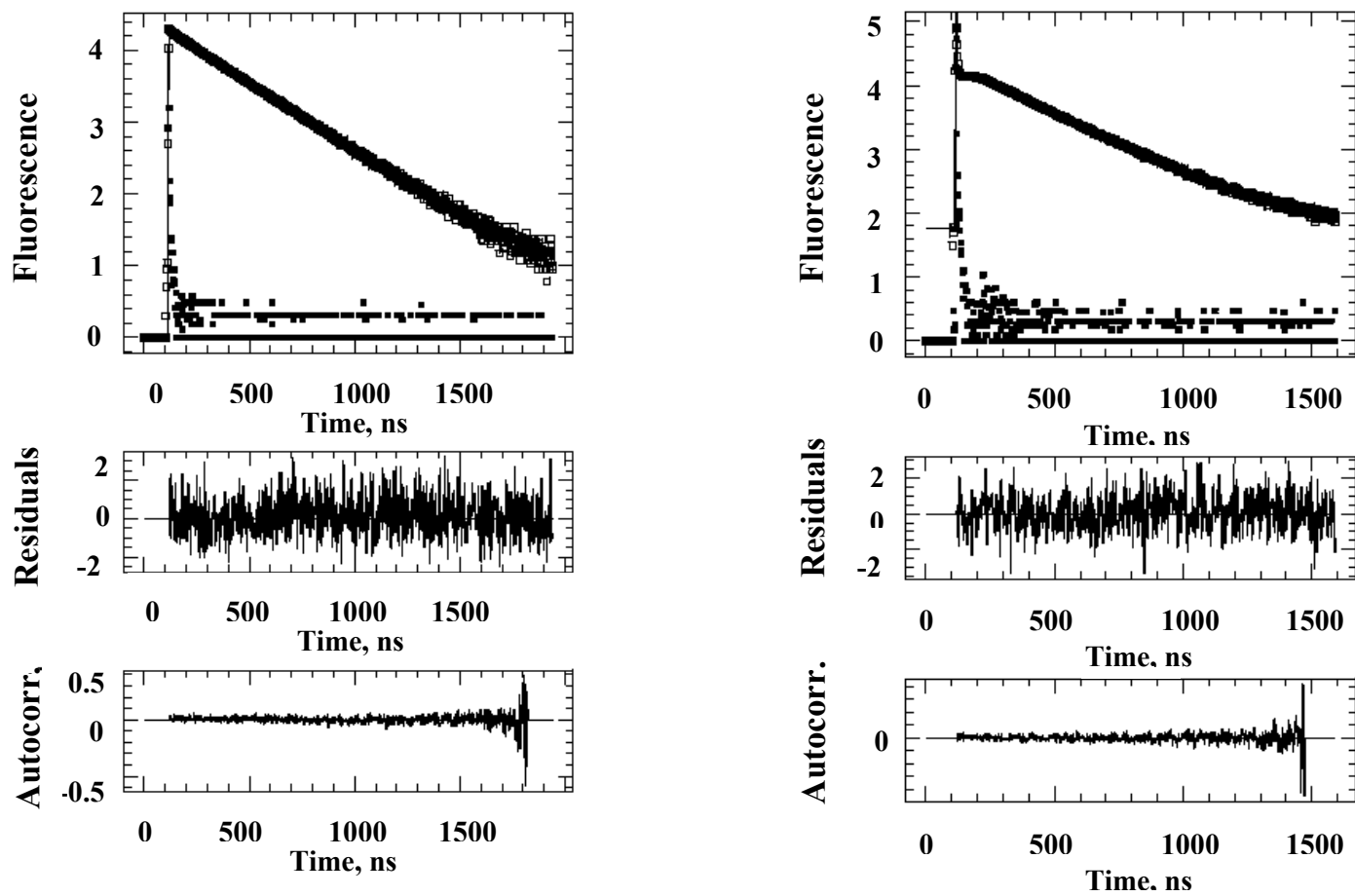


Figure 2.7: Fluorescence decays of the pyrene monomer (left; $\lambda_{\text{ex}} = 344$ nm, $\lambda_{\text{em}} = 375$ nm; TPC = 2.04 ns/ch) and excimer (right; $\lambda_{\text{ex}} = 344$ nm, $\lambda_{\text{em}} = 510$ nm; TPC = 2.04 ns/ch) of PEO(10K)-Py₂ in dioxane fitted with Equations 2.12 and 2.13, respectively. $[\text{Py}] = 2.5 \times 10^{-6}$ M, $\chi^2 = 1.06$.

Figure 2.8 illustrates how k_{blob} , $k_c[\text{M1}]$, $k_c[\text{M0}]$, and f_{P1} ($f_{\text{P1}} = [\text{M1}]/([\text{M1}] + [\text{M0}] + [Py_{\text{free}}^*]_o)$), the molar fraction of pyrenes located in a *blob* containing the excited pyrene and one ground-state pyrene, behave as a function of solvent viscosity and polymer molecular weight. As the viscosity increases or the molecular weight increases, k_{blob} in Figure 2.8A decreases. However, the data show substantial scatter for the PEO constructs with a high molecular weight and solutions with large solvent viscosities. The increased scatter found for k_{blob} reflects the fact that as chain length or solvent viscosity increases, the fraction of pyrenes forming excimer inside a *blob* decreases. This effect explains also why $k_c[\text{M1}]$ decreases and $k_c[\text{M0}]$ increases with increasing η and M_n in Figure 2.8B. As the size of the polymer coil expands with increasing M_n , the local concentration of *blobs* inside the polymer coil containing the ground-state pyrene ($[\text{M1}]$) decreases whereas $[\text{M0}]$ increases. A similar effect is achieved by increasing the solvent viscosity.

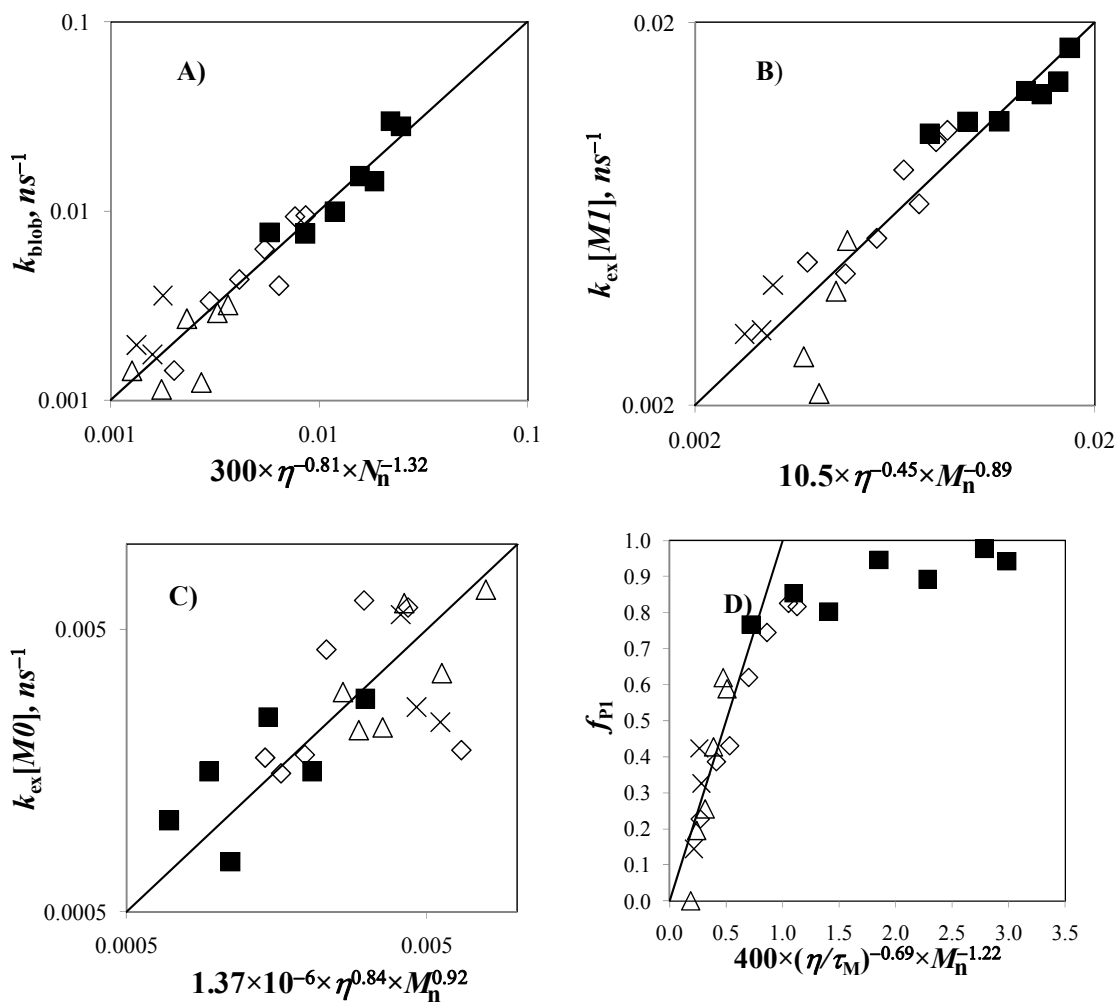


Figure 2.8: Scaling behavior of the parameters obtained from the global analysis of the pyrene monomer and excimer fluorescence decays of the PEO(*X*)-Py₂ samples fitted with Equations 2.3 and 2.4, respectively. (■) PEO(2K)-Py₂, (□) PEO(5K)-Py₂, (△) PEO(10K)-Py₂, (×) PEO(16.5K)-Py₂.

As the solvent viscosity increases, the size of a *blob* decreases and [M1] decreases whereas [M0] increases. It is worth noting that M1 (the *blobs* that contain the ground-state pyrene) and M0 (the *blobs* that contain no ground-state pyrene) provide information about the behavior of the pyrenes that are involved in the process of excimer formation. As the chain length

and solvent viscosity become too large, a substantial fraction of the excited pyrenes are unable to form excimer. These pyrenes are denoted by Py_{free}^* in Equation 2.3, and their contribution increased with increasing η and M_n . When taken into account, one obtains the fractions of *blobs* that contain one ground-state pyrene f_{p1} ($f_{p1} = [M1]/([M1]+[M0]+[Py_{free}])$) which is given in Figure 2.8D. For short chains and low viscosity solvents, f_{p1} is close to 1.0 indicating that both chain ends are located inside a same *blob*. As M_n and η increase, the chance of finding both ends inside a same *blob* decreases to zero for the larger M_n and η values used in this study.

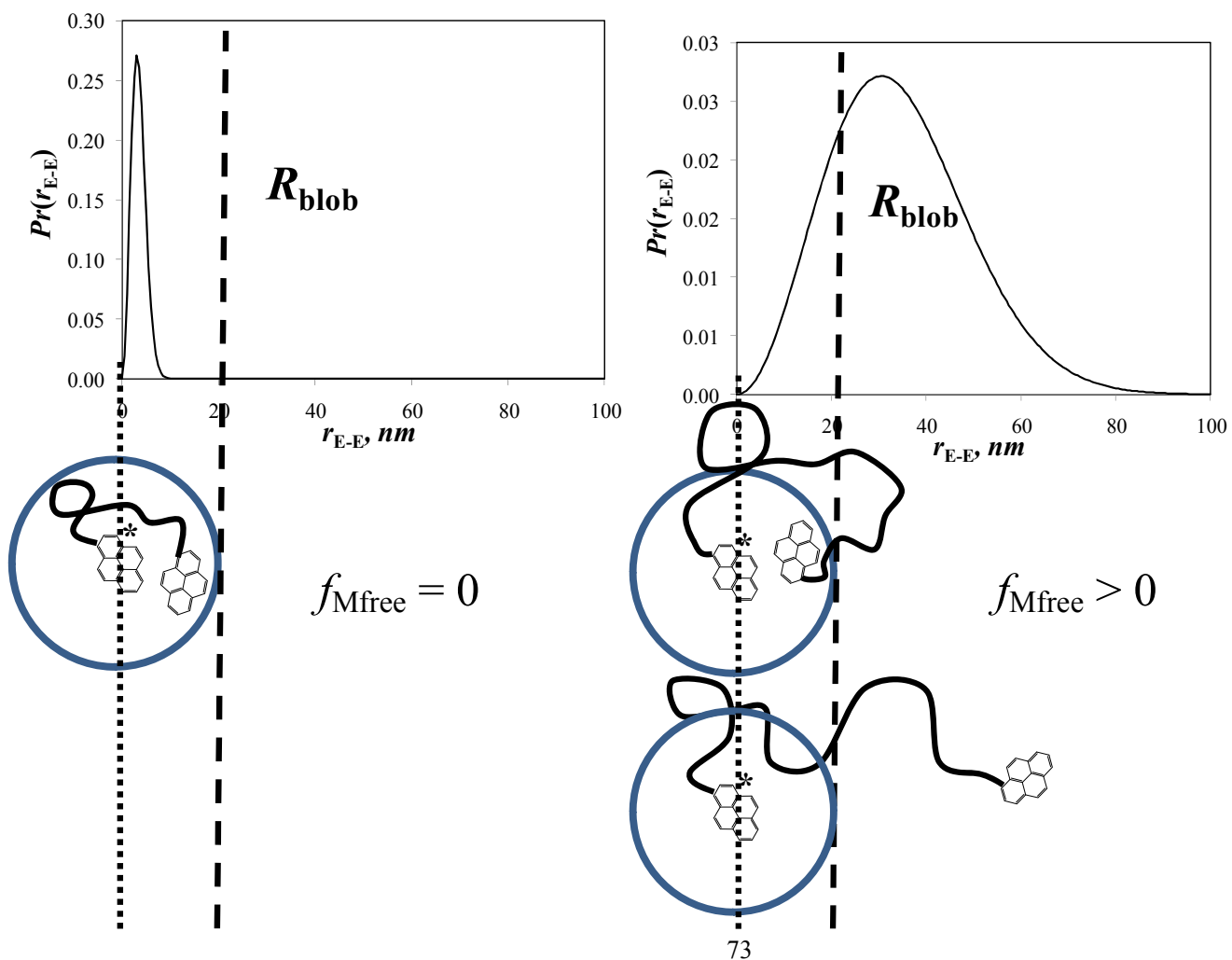
Based on this work, the analysis of the kinetics of excimer formation for pyrene end-labeled polymers yields distinct results for two different sets of sample and solvent conditions. The first set encompasses the PEO(*X*)-Py₂ samples prepared with short chains and low viscosity solvents. Here both pyrene-labeled ends are located in the same *blob*, and the rate constant of excimer formation k_{blob} is recovered with good accuracy and is found to decrease with increasing M_n and η . The second set involves samples with longer chains, where the fraction of *blobs* containing a ground-state pyrene (f_{p1} in Figure 2.8D) is much smaller. Since fewer pyrenes form excimer, k_{blob} is recovered with little accuracy, showing substantial scatter in Figure 2.8A, but seems to remain constant for large M_n and η values with several data points clustering around an average value of $k_{blob} = 1.5 (\pm 0.3) \times 10^6 \text{ s}^{-1}$.

Comparison of the steady-state and time-resolved fluorescence results: The above discussion implies that the kinetics of excimer formation for pyrene end-labeled polymers should fall into two regimes. The first regime encountered for short chains and low viscosity solvents describes excimer formation when both pyrene-labeled ends are located in a same *blob*. In effect, this regime is properly handled by Birks' scheme, as we have shown in Figure 2.5A-D. In this

regime, k_{cy} scales as $N^{-1.34}$ in Figure 2.5A in agreement with earlier studies.^{13-20,35} For longer chains and high viscosity solvents, a fraction of the pyrenes never meet, and these pyrenes do not form excimer. This second regime is not properly handled by Birks' scheme and is more realistically described by the FBM. It is however surprising that those two regimes so clearly identified by the time-resolved fluorescence measurements described in this study seem to go undetected by the steady-state fluorescence measurements shown in Figure 2.2C where no breakpoint between the two regimes is observed. An explanation for this apparent contradiction is provided below.

The above discussion suggests that excimer formation occurs inside a *blob* of radius r_{EE}^{blob} with an excimer rate constant k_{cy}^{blob} that remains the same regardless of polymer chain length, as long as the polymer chain length is such that the polymer coil radius is greater than r_{EE}^{blob} . The rate constants k_{cy} and τ_E^{-1} are expected to retain the values obtained for shorter chains. Those PEO(10K)-Py₂ coils for which r_{EE} is larger than r_{EE}^{blob} do not form excimer and emit in the same manner as the pyrene monomer of PEO(2K)-Py₁. According to these conditions, the fraction f_{Mfree} of pyrene end groups that do not form excimer increases with increasing chain length or viscosity as observed experimentally in Figures 2.5D and 2.8D.

Scheme 2.6: Dependency of f_{Mfree} as a function of $r_{\text{EE}}/R_{\text{blob}}$. Left: $r_{\text{EE}}/R_{\text{blob}} \ll 1$ and $f_{\text{Mfree}} = 0$. Right: $r_{\text{EE}}/R_{\text{blob}} > 1$ and $f_{\text{Mfree}} > 0$.



The concept of a *blob* discussed above is depicted in Scheme 2.6. It is applied to predict the scaling relationship that would exist between the I_E/I_M ratio and N_n . The mathematical derivation shown hereafter assumes that the coil is in a theta solvent and that the chain adopts a Gaussian conformation. According to Scheme 2.6, the experimentally found fraction of polymer coils (f_{P1}) whose pyrene-labeled ends are located inside a *blob* is given by the integral

$$\int_0^{R_{blob}} \left(\beta/\sqrt{\pi}\right)^3 \exp(-\beta^2 r^2) 4\pi r^2 dr \text{ where } \beta^2 = 3/(2nl^2) \text{ with } n \text{ and } l \text{ being the number of Kuhn}$$

segments and Kuhn length, respectively. The I_E/I_M ratio is proportional to the ratio of the integrals

$$\int_0^\infty [E^*]_{(t)} dt / \int_0^\infty [M^*]_{(t)} dt \text{ which is given in Equation 2.11 after integrating Equations 2.1 and 2.2.}$$

This derivation assumes that $f_{P1} = 1 - f_{Mfree}$ and neglects the contribution from the Py_S^* species whose lifetime τ_s equal to 3.5 ns is much shorter than the other decay times involved.

Implicit in the derivation of Equation 2.11 is the fact that as N_n tends to infinity, k_{cy} tends to

$$k_{cy}^{blob} \text{ and } f_{Mfree} \text{ tends to unity. According to Equation 2.11, the limit of } \int_0^\infty [E^*]_{(t)} dt / \int_0^\infty [M^*]_{(t)} dt$$

when n becomes large equals a constant that does not depend on chain length multiplied by $n^{-1.5}$.

$$\frac{\int_0^\infty [E^*]_{(t)} dt}{\int_0^\infty [M^*]_{(t)} dt} = \frac{\frac{k_{cy}(\tau_2 - \tau_1)}{\sqrt{(X-Y)^2 + 4k_{cy}k_{-cy}}} \times (1 - f_{Mfree})}{\frac{(X - \tau_2^{-1})\tau_1 - (X - \tau_1^{-1})\tau_2}{\sqrt{(X-Y)^2 + 4k_{cy}k_{-cy}}} \times (1 - f_{Mfree}) + f_{Mfree} \times \tau_M} \xrightarrow{f_{Mfree} \rightarrow 1} \frac{1}{\tau_M} \frac{k_{cy}^{blob} \times (\tau_2 - \tau_1)}{\sqrt{(X-Y)^2 + 4k_{cy}k_{-cy}}} \times (1 - f_{Mfree}) \xrightarrow{n \rightarrow \infty} \frac{1}{\tau_M} \frac{k_{cy}^{blob} \times (\tau_2 - \tau_1)}{\sqrt{(X-Y)^2 + 4k_{cy}k_{-cy}}} \times \sqrt{\frac{6}{\pi}} \left(\frac{R_{blob}}{l}\right)^3 n^{-3/2} \quad (2.11)$$

Furthermore, $k_{cy}^{blob} \times R_{blob}^3$ is expected to be inversely proportional to viscosity. Since the I_E/I_M ratio is proportional to $\int_0^\infty [E^*]_{(t)} dt / \int_0^\infty [M^*]_{(t)} dt$, Equation 2.11 implies that the I_E/I_M ratio scales as $n^{-1.5} \times \eta^{-1}$ for longer chains, a scaling behavior similar to that expected for shorter chains where Equation 2.10 holds. In other words, the I_E/I_M ratio is not expected to sense the switch that might be occurring when the chain becomes so large that a large fraction of the chain ends are no longer inside the *blob*. Only time-resolved fluorescence experiments can probe the switch depicted in Scheme 2.6, since these experiments yield the actual rate constants describing the process of EEC as well as the fraction f_{P1} of excited chromophores involved in EEC events.

Information about the distribution of end-to-end distances: According to the FBM analysis of the fluorescence decays, the fraction f_{P1} represents the fraction of the chains whose ends are located in the same *blob* and close enough to form excimer. Consequently, f_{P1} is the probability of having the two polymer ends at a distance smaller than R_{blob} , and an expression of f_{P1} can be determined by using the Gaussian distribution of end-to-end distances. Its expression is given by Equation 2.12 where the integral in the denominator equals unity.

$$f_{P1} = \frac{\int_0^{R_{blob}} \left(\frac{\beta}{\sqrt{\pi}} \right)^3 \exp(-\beta^2 r_{EE}^2) 4\pi r_{EE}^2 dr_{EE}}{\int_0^\infty \left(\frac{\beta}{\sqrt{\pi}} \right)^3 \exp(-\beta^2 r_{EE}^2) 4\pi r_{EE}^2 dr_{EE}} \quad (2.12)$$

Equation 2.13 has been derived for the end-to-end distance (r_{EE}) of PEO in water.⁵¹

$$r_{EE} = 0.119 \times \sqrt{M_n} \times 0.707 \text{ nm} \quad (2.13)$$

If the coil dimensions of the short PEO chains in the organic solvents used in this study are similar to that of PEO in water, Equation 2.13 could also be used to determine r_{EE} of PEO in the organic solvents listed in Table SI.2.2. To establish whether this was the case, intrinsic viscosity ($[\eta]$) measurements were conducted for PEO(10K) in the seven organic solvents used in this study. $[\eta]$ was found to remain constant and equal to $22.1 \pm 0.4 \text{ mL.g}^{-1}$ (Table SI.2.2). This $[\eta]$ value happens to be close to that of PEO(10K) in water at 25 °C (23.9 mL.g^{-1}) estimated from the Mark-Houwink-Sakurada parameters $K = 49.9 \times 10^{-3} \text{ mL.g}^{-1}$ and $a = 0.67$.⁵² Comparison of the $[\eta]$ values obtained in water and DMF by using the relationship $[\eta] = 2.0 + 24.0 \times 10^{-3} \times M_n^{0.73}$ for PEO in DMF at 25 °C⁵² indicates that the difference in $[\eta]$ between PEO in water and DMF differs by less than 8.2% for M_n values between 2 K and 16 K, i.e. the range of M_n values used for the PEO(X)-Py₂ samples.

The effect that the pyrene label might have on the coil dimensions of the PEO(X)-Py₂ samples was investigated by measuring $[\eta]$ of PEO(5K)-Py₂ in DMF and comparing the $[\eta]$ value obtained for PEO(5K)-Py₂ with that of PEO(5K). Within experimental error, the $[\eta]$ value obtained for PEO(5K)-Py₂ in DMF ($14.0 \pm 0.2 \text{ mL.g}^{-1}$) matches that obtained for the unlabeled sample ($14.0 \pm 0.2 \text{ mL.g}^{-1}$). The results of these control experiments led us to the conclusion that the polymer coils of the PEO(X)-Py₂ samples must have similar dimensions in the organic solvents listed in Table SI.2.2 and water so that Equation 2.13 could be used to estimate the r_{EE} values of the PEO(X)-Py₂ samples in these organic solvents.

Using the f_{P1} values reported in Figure 2.8D and Equation 2.13 to estimate r_{EE} for the PEO(X)-Py₂ samples, Equation 2.12 could be solved numerically to retrieve R_{blob} . Since the f_{P1} values reported in Figure 2.8D for PEO(2K)-Py₂ are close to unity, the FBM does not apply for this sample. Consequently, R_{blob} was determined for the other PEO(X)-Py₂ samples and it is plotted as a function of $\sqrt{\tau_M / \eta}$ in Figure 2.9. Within experimental error, R_{blob} is found to increase linearly with increasing $\sqrt{\tau_M / \eta}$. Since R_{blob} is expected to be a measure of the distance travelled by an excited

pyrene undergoing Brownian motion, R_{blob} is expected to increase with increasing lifetime and decrease with increasing solvent viscosity as experimentally found in Figure 2.9. To the best of our knowledge, Figure 2.9 represents the first example in the literature where pyrene end-labeled monodisperse polymers have been used to retrieve information on the end-to-end distance distribution of polymers in solution.

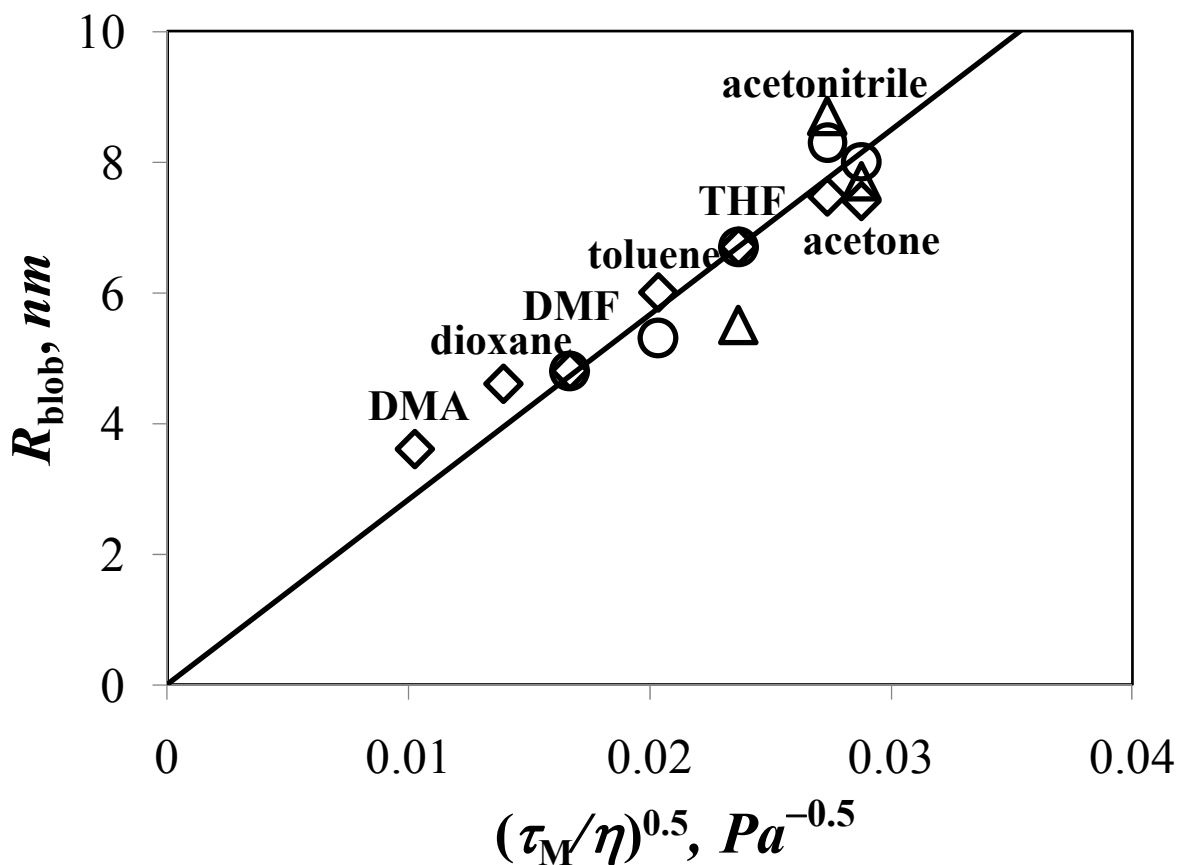


Figure 2.9: R_{blob} versus $\sqrt{\tau_M/\eta}$ for PEO(5K)-Py₂ (\diamond), PEO(10K)-Py₂ (\circ), and PEO(16.5K)-Py₂ (\triangle) in the following solvents. From left to right: DMA, dioxane, DMF, toluene, THF, acetonitrile, and acetone.

2.6 Conclusions

A series of PEO(*X*)-Py₂ samples were synthesized and their monomer and excimer fluorescence decays were acquired in seven organic solvents with viscosities ranging from 0.32 to 1.92 mPa.s. Analysis of the steady-state fluorescence spectra showed that the I_E/I_M ratio scaled as $\eta^{-1.0} \times N_n^{-1.6}$ as theory³³ and other experimental studies predicted.^{13-21,35} However, analysis of the fluorescence decays with Birks' scheme showed a major inconsistency. As polymer chain length and/or solvent viscosity were increased, an increasing fraction of excited pyrenes failed to form excimer. Refinement in the analysis programs coupled with simulations demonstrated that this effect is real. This effect was attributed to the fact that excimer formation occurs in a sub-volume of the polymer coil. Analysis of the fluorescence decays with the FBM yielded a set of parameters which was internally consistent with the assumptions of the FBM.

EEC of pyrene end-labeled monodisperse polymers has been thoroughly studied over the past three decades.²⁻³⁷ It is thus somewhat surprising that the inconsistencies uncovered in this report have been so far unnoticed. One reason for this resides in the nature of the label used to prepared pyrene end-labeled polymers. In many instances, a 1-pyrenebutyl derivative has been used.^{17-21,23-29,31} This end group has a lifetime (τ_M) that is about 70 ns shorter than the 1-pyrenemethyl derivative used in this study.⁴⁹ The longer butyl linker provides enough flexibility to ensure rapid rearrangement of the chain ends of a rigid polymer. For instance, some of us found out that EEC kinetics according to Birks' scheme were not followed when 1-pyrenemethylamine was used to label a series of monodisperse polystyrenes whereas they were when using 1-pyrenebutylamine.³¹ The slow chain end rearrangements experienced with polystyrene that required the use of 1-pyrenebutylamine instead of 1-pyrenemethylamine was not a problem with the more flexible PEO backbone. As M_n and η increase, the long decaytime τ_2 in Equation 2.1 increases and if τ_M is too short such as for the 1-pyrenebutyl derivative, τ_2 matches τ_M before the polymer coil is large enough for the two pyrene-labeled ends to be located in different *blobs*. Using a longer-lived pyrene label such as the 1-

pyrenemethylene derivative employed in the present study enables one to probe the cross-over between the two regimes. We suspect that this effect will require revisiting some of the conclusions which have been reached earlier for pyrene end-labeled polymers. In particular and if more experiments confirm the claims made in the present study, the assumption that the I_E/I_M ratio be readily taken as a sole measure of the rate constant of EEC³³ might no longer be valid, as it also accounts for those pyrenes that cannot form excimer. Most importantly, and since Birks' scheme and the Wilemski-Fixman theoretical framework seem to be better suited to the study of pyrene end-labeled short chains or oligomers, these experiments will establish the universality of the FBM to study the chain dynamics of actual polymers by monitoring the encounters between a fluorophore and a quencher covalently attached to a polymer regardless of their position on the chain, be they randomly distributed along the chain^{31,40,41,49} or at the chain ends (cf. this work) when the polymer coil is larger than the volume of a blob.

Chapter 3

Quantifying the Presence of Unwanted Fluorescent Species in the Study of Pyrene-Labeled Macromolecules

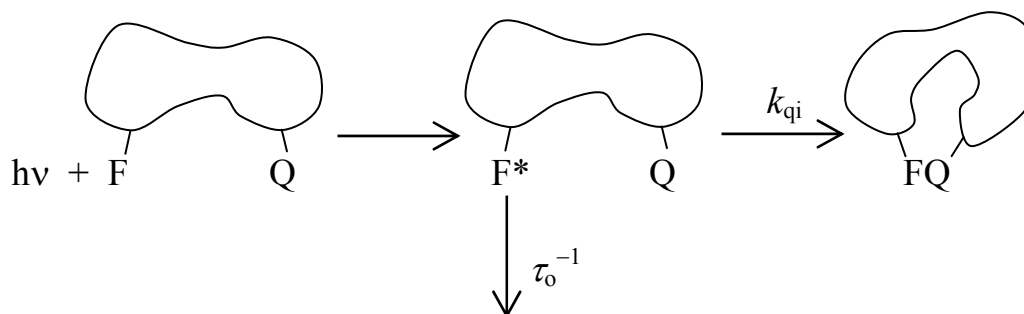
3.1 Overview

In order to mimic the effect that unwanted fluorescent species have on the process of excimer formation between pyrene labels covalently attached onto macromolecules, the steady-state fluorescence spectra and time-resolved fluorescence decays were acquired for mixtures of pyrene mono- and doubly end-labeled 2K poly(ethylene oxide) referred to as PEO(2K)-Py₁ and PEO(2K)-Py₂, respectively, and mixtures of 1-pyrenebutyric acid (PyBA) and a 4th generation dendron end-capped with pyrene (Py₁₆-G4-PS). Monolabeled polymers like PEO(2K)-Py₁ and unattached fluorescent labels like PyBA are amongst the most typical fluorescent impurities that are encountered in the study of fluorescently labeled macromolecules. Our fluorescence experiments revealed that the addition of minute amounts of PEO(2K)-Py₁ or PyBA to, respectively, PEO(2K)-Py₂ or Py₁₆-G4-PS solutions induced a dramatic reduction of the ratio of the fluorescence intensity of the pyrene excimer to that of the pyrene monomer, namely the I_E/I_M ratio. Although the extreme sensitivity of fluorescence in general and the I_E/I_M ratio in particular to the presence of fluorescent impurities is a great concern, it is nevertheless reassuring that this effect can be quantitatively accounted for by analyzing the fluorescence decays of the pyrene monomer and excimer globally, according to a protocol which is described in detail in this study. The experiments presented herein demonstrate the importance of studying fluorescently labeled macromolecules that are of the highest purity when probing the rapid internal dynamics of a macromolecule by fluorescence.

3.2 Introduction

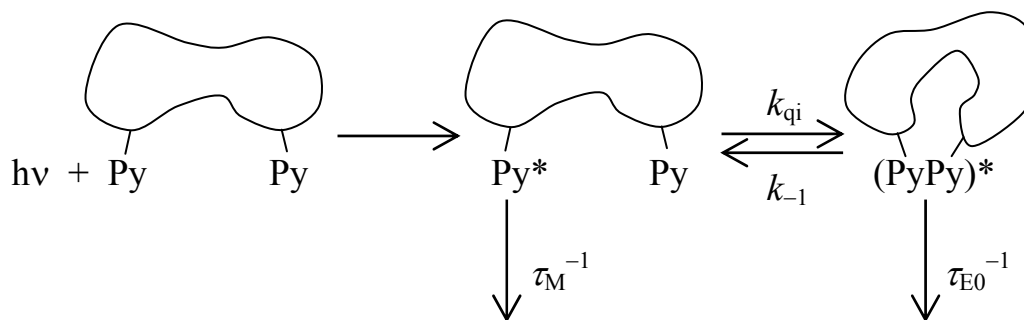
Fluorescence dynamic quenching (FDQ) is a well-known phenomenon which has been applied in a variety of ways to estimate the rate constants for rapid processes taking place in

biological or synthetic macromolecules and their supramolecular assemblies.¹ FDQ works by exciting a fluorophore which then undergoes diffusional motion, collides with a quencher and loses its excess energy (Scheme 3.1). In its simplest form, the rate at which the excited fluorophore loses its energy can be described by a single rate constant k_q which is typically determined by analyzing the fluorescence decay of the quenched fluorophore with a single decay time $\tau = (\tau_0^{-1} + k_q)^{-1}$ where τ_0 is the natural lifetime of the fluorophore. More complicated situations involve a number n_{kq} of different populations of fluorophores P_i ($0 < i < n_{kq} - 1$) which are being quenched dynamically with n_{kq} different rate constants k_{qi} . Each population of fluorophore P_i decays with a single exponential whose decay time τ_i equals $(\tau_0^{-1} + k_{qi})^{-1}$. The fluorescence decay becomes a sum of exponentials whose pre-exponential factors reflect the molar fractions f_{Pi} of the fluorophore species P_i and whose decay times τ_i yield the rate constants k_{qi} . In turn, the rate constant k_{qi} provides information on the environment of the fluorophore population P_i , whether P_i is accessible to or protected from the solvent, is located in a rigid or fluid environment, whereas f_{Pi} describes the molar fractions of fluorophores P_i which are in the environment defined by k_{qi} . The combination of parameters f_{Pi} and k_{qi} provides a complete description of the distribution of fluorophores and the properties of their local environment, information that is used to understand the complex behavior of macromolecules and their assemblies.¹ Important applications of these aspects of FDQ experiments include the determination of the aggregation number of surfactant micelles and a measure of their internal dynamics,²⁻⁴ the quantitative description of long range polymer chain dynamics,⁵ or finding the fraction f_a of fluorophores accessible to a quencher in a protective quenching experiment.^{6,7}



Scheme 3.1: Quenching mechanism between an excited fluorophore F^* and its quencher Q covalently attached onto a macromolecule.

While FDQ experiments have proved extremely successful in the characterization of fluorescently labeled biological and synthetic macromolecules, they are limited in practice by the ability of the software used to analyze the fluorescence decays to retrieve the decay times τ_1 and the fractions f_{p_i} of the fluorophore population. However, recent studies suggest that the analysis of fluorescence decays to retrieve information on complex FDQ processes is dramatically enhanced if the product of an $F^* - Q$ encounter emits with its own fluorescence as is the case with pyrene excimer formation (Scheme 3.2).⁸⁻¹¹ Upon irradiation with UV light, an excited pyrene monomer can either fluoresce with a lifetime τ_M or form an excimer with one or several rate constants which are equivalent to k_{qi} in Scheme 3.1. The excimer can fluoresce with a lifetime τ_{E0} or dissociate with a rate constant k_{-1} which, for temperatures lower than 35 °C, can be considered to be negligible.⁸⁻¹¹ In turn, information on the (f_{p_i}, k_{q_i}) parameters is incorporated, not only in the pyrene monomer fluorescence decay but also in the pyrene excimer fluorescence decay and the pairs of (f_{p_i}, k_{q_i}) parameters are retrieved from the analysis of the pyrene monomer and excimer fluorescence decays. Experiments based on Scheme 3.2 have been instrumental in the study of the internal dynamics of pyrene end-labeled monodisperse polymers,¹²⁻²⁸ dendrimers,²⁹⁻³⁹ and telomers with specific chain lengths.⁴⁰⁻⁴²



Scheme 3.2: Excimer formation between pyrenyl groups covalently attached onto a macromolecule.

The global analysis of coupled fluorescence decays, introduced some twenty years ago,⁴³⁻⁴⁵ has been applied to develop families of programs where both decay times and pre-exponential factors are optimized as a function of the parameters f_{pi} , k_{qi} , and τ_{E0} according to the Fluorescence Blob Model,⁴⁶⁻⁵⁶ the Birks scheme,^{56,57} or the Model Free analysis.^{47,58,59} To date, this type of analysis has been applied successfully to determine the level of association of pyrene-labeled hydrophobically modified water-soluble polymers (HMWSPs),⁴⁶⁻⁵⁰ the molar absorbance coefficient of pyrene aggregates in water,⁵⁰ the critical micelle concentration of pyrene-labeled Gemini surfactants,⁵⁹ and to study the internal dynamics of linear and branched macromolecules,⁵²⁻⁵⁸ the phase-separation of pyrene-labeled lipids⁵¹ and the breakdown of Birks' scheme analysis used to describe the end-to-end cyclization of a series of pyrene end-capped monodisperse poly(ethylene oxide)s.⁵⁷

Beside the ability of this type of analysis to provide a solid description of the process of pyrene excimer formation under a wide variety of experimental conditions,⁴⁶⁻⁵⁹ some reports also suggest that it retrieves with remarkable accuracy the fraction $f_{free} = f_{p0}$ of pyrene monomers that are unable to encounter a ground-state pyrene to form an excimer and for which $k_{q0} = 0 \text{ s}^{-1}$.⁵⁷⁻⁵⁹ These pyrenes that do not form excimer behave as if they were free in solution. For this reason, they are referred to as Py_{free} in this study and they emit with the natural lifetime of the pyrene monomer τ_M . Unfortunately, the Py_{free} species covalently attached onto a macromolecule are usually

indistinguishable from the pyrene derivative used in the labeling reaction which might not have been properly removed from the fluorescently labeled macromolecule. These pyrene species act as fluorescent impurities that corrupt the fluorescence response of the labeled macromolecule. Consequently, the ability to determine f_{free} reliably for pyrene-labeled macromolecules would be an invaluable analytical tool for the quantitative description of the process of pyrene excimer formation. Furthermore it would enable the experimentalist to gauge the extent by which the presence of Py_{free} might affect the analysis of the fluorescence data.

In order to assess the extent to which this type of analysis can determine f_{free} reliably, solutions of pyrene-labeled macromolecules were contaminated with known amounts of a pyrene monomer species. Their fluorescence decays were analyzed globally and the fraction f_{free} retrieved from the analysis was compared to that expected from the amount of a pyrene monomer species purposely added to the solution. The two pyrene-labeled macromolecules considered for this study were a 2K poly(ethylene oxide) (PEO(2K)-Py₂) and a 4th generation dendrimer hybrid (Py₁₆-G4-PS) whose ends were capped with pyrene. The solutions of PEO(2K)-Py₂ and Py₁₆-G4-PS were tainted by adding a sample of PEO(2K) labeled at one end with pyrene (PEO(2K)-Py₁) and 1-pyrenebutyric acid (PyBA), respectively. Monolabeled chains such as PEO(2K)-Py₁ or unattached labels such as PyBA are fluorescent impurities that are typically encountered in these types of experiments. This study describes how the global analysis of the pyrene monomer and excimer fluorescence decays handles the presence of pyrene monomer species in samples of pyrene-labeled macromolecules.

3.3 Experimental

Materials: The syntheses of the pyrene-labeled dendrimer hybrid (Py₁₆-G4-PS) and PEO(2K) (PEO(2K)-Py₂ and PEO(2K)-Py₁), whose structures are shown in Figure 3.1, have been described in two earlier publications.^{57,60} The PEO(2K)-Py₂ and Py₁₆-G4-PS are free of unattached pyrene derivatives as determined by Gel Permeation Chromatography in Figures SI.3.5 and SI.3.6. Solutions of pyrene-labeled dendrimer and poly(ethylene oxide) were prepared with, respectively, distilled in

glass tetrahydrofuran (THF) or acetone which were purchased from Caledon and used as received. 1-Pyrenebutyric acid (PyBA, 97%) was purchased from Aldrich.

Absorbance measurements: Absorption spectra were acquired on a Cary 100 UV-Vis spectrophotometer with a UV cell having a 1 cm path length. All PEO(2K)-Py₂/PEO(2K)-Py₁ mixtures used in the fluorescence experiments had an absorbance smaller than 0.3, equivalent to a pyrene concentration smaller than $7 \times 10^{-6} \text{ mol.L}^{-1}$. These concentrations were low enough to ensure that excimer formation occurred only intramolecularly as diluting the solution concentration by half resulted in a fluorescence spectrum that overlapped perfectly that of the more concentrated solution. All Py₁₆-G4-PS/PyBA solutions had an absorbance of 0.1.

Steady-state fluorescence measurements: All steady-state fluorescence spectra were acquired on a Photon Technology International (PTI) fluorometer equipped with a PTI 814 photomultiplier detection system and an Ushio UXL-75Xe xenon arc lamp as the light source. The sample solutions were degassed under a gentle flow of nitrogen for at least 30 minutes and all spectra were obtained using a quartz cuvette with the right-angle configuration. The samples were excited at a wavelength of 344 nm and all emission spectra were normalized at 375 nm. The fluorescence intensities of the monomer (I_M) and of the excimer (I_E) were estimated by taking the integrals under the fluorescence spectra from 372 to 378 nm for the pyrene monomer, and from 500 to 530 nm for the pyrene excimer, respectively. A superscript of "SS" was used for the ratio of I_E over I_M (I_E/I_M)^{SS} to indicate that the fluorescence intensities were obtained by steady-state fluorescence.

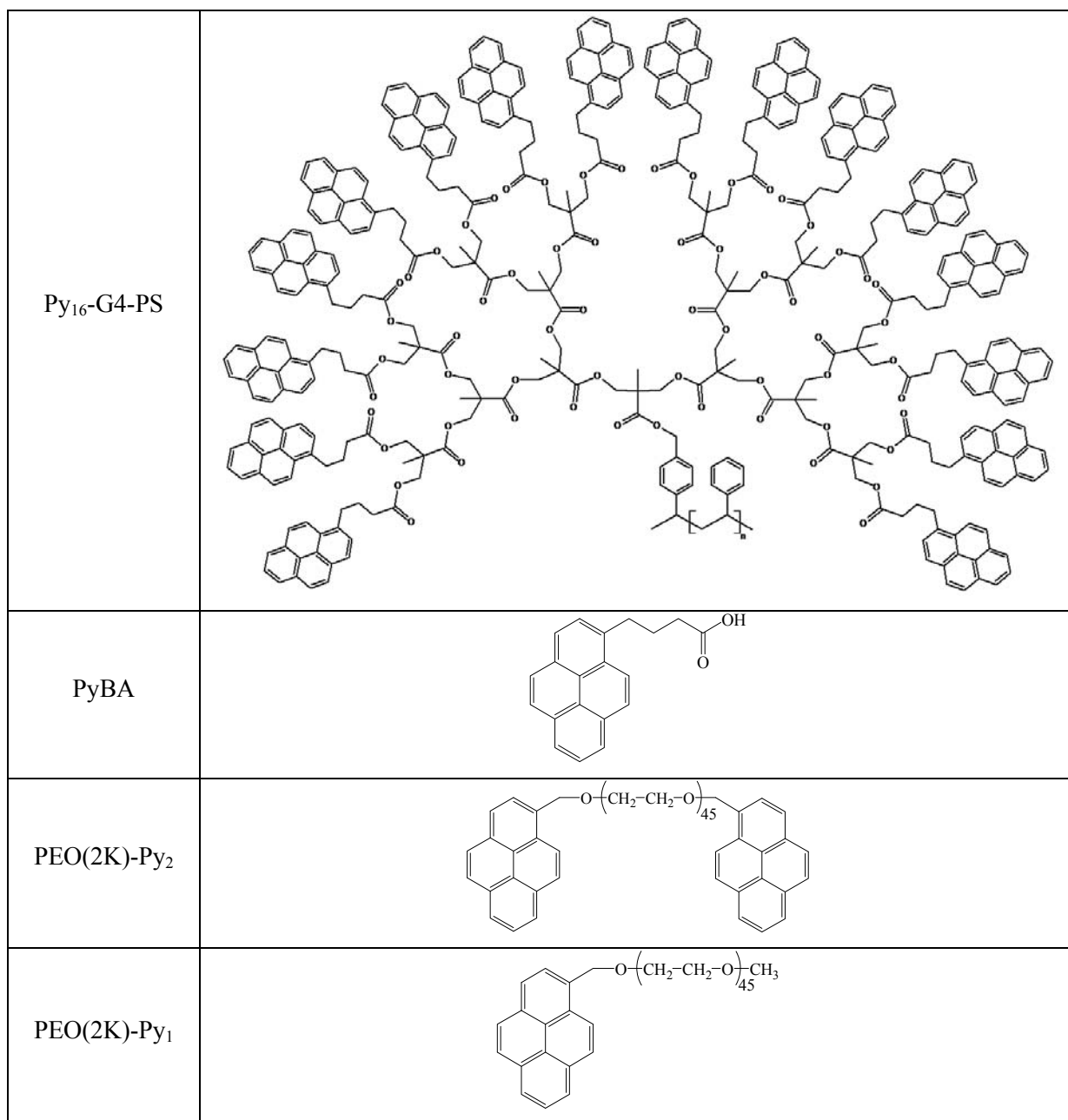


Figure 3.1: Chemical structures of the pyrene-labeled dendrimer hybrid (Py₁₆-G4-PS), the mono- (PEO(2K)-Py₁) and doubly (PEO(2K)-Py₂) labeled 2K poly(ethylene oxide)s, as well as of 1-pyrenebutyric acid (PyBA).

Time-resolved fluorescence measurements: The fluorescence decay curves of the degassed samples were obtained by the time-correlated single-photon counting technique (TC-SPC) on an IBH time-

resolved fluorometer using the right-angle geometry. The excitation source was an IBH 340 nm LED used with a 500 kHz repetition rate. Fluorescence decays were acquired over 1024 channels ensuring a minimum of 20,000 counts at their maximum. The excitation wavelength was 344 nm, and the fluorescence from the pyrene monomer and excimer was monitored at 375 and 510 nm, respectively. To block potential light scattering leaking through the detection system, filters were used with cutoff wavelengths of 370 and 495 nm to obtain the fluorescence decays of the pyrene monomer and excimer, respectively. A time per channel of 2.04 ns/ch and 0.118 ns/ch was used for the Py₂-PEO(2K)/Py₁-PEO(2K) and the Py₁₆-G4-PS/PyBA mixtures, respectively. The shorter time per channel was employed to capture the short decay times observed with the dendrimer solutions.⁵⁸ For all the decays obtained by the PEO(2K)-Py₂/PEO(2K)-Py₁ mixtures, reference decays of degassed solutions of PPO [2,5-diphenyloxazole] in cyclohexane ($\tau = 1.42$ ns) for the pyrene monomer and BBOT [2,5-bis(5-*tert*-butyl-2-benzoxazolyl)thiophene] in ethanol ($\tau = 1.47$ ns) for the pyrene excimer were used to obtain the instrument response function (IRF) via the MIMIC method⁶¹ needed for the analyses of the monomer and excimer decays, respectively. In the case of the dendrimer solution, a Ludox solution was employed to acquire the IRF.

Analysis of the fluorescence decays: The monomer and excimer decays of the PEO(2K)-Py₂/PEO(2K)-Py₁ mixtures in acetone were analyzed globally with Birks' scheme (Equations SI.3.1 and SI.3.2 in the Supporting Information) and MF analysis (Equations SI.3.5 and SI.3.6). A complete derivation of the equations used to fit the fluorescence decays and the physical quantities used in this study has been provided in the Supporting Information. The lifetime τ_M in Equations SI.3.1, SI.3.2, SI.3.5, and SI.3.6 was set to equal 265 ns in the analysis of the decays, as it matches the natural lifetime of PEO(2K)-Py₁ in acetone.⁵⁷ No short lifetime τ_{ES} was needed to fit the decays of the PEO samples. The monomer and excimer decays of the Py₁₆-G4-PS/PyBA mixtures in THF were analyzed globally with Equations SI.3.5 and SI.3.6, respectively, as Birks' scheme does not apply to the complex kinetics of excimer formation exhibited by Py₁₆-G4-PS.⁵⁸ The lifetime τ_M in Equations SI.3.5 and SI.3.6 and τ_{ES} in Equation SI.3.6 were set to equal, respectively, 210 ns and 4 ns in the analysis.

The lifetime τ_M of 210 ns for the pyrene monomer was found from the analysis of the monoexponential fluorescence decay of PyBA in THF. The lifetime τ_{ES} was estimated by letting it float in a first analysis of the fluorescence decays. It was found to fluctuate around a value of 4 ns. It was then fixed to this value in the final analysis reported in this study. The lifetime of 4 ns matches the lifetime value found for other short-lived pyrene dimers.^{24,51,57,62} The analysis was carried out with the Marquardt-Levenberg algorithm⁶³ to obtain the optimized pre-exponential factors and decay times. The fits were good with χ^2 being smaller than 1.30, and residuals and autocorrelation of the residuals randomly distributed around zero.

3.4 Results

The fluorescence spectra and decays of the PEO(2K)-Py₂/PEO(2K)-Py₁ mixtures were acquired for different molar fractions α of the PEO(2K)-Py₁ solution prepared with a pyrene concentration of 3.0×10^{-6} mol.L⁻¹, half that of the PEO(2K)-Py₂ solution for which the pyrene concentration equals 6.0×10^{-6} mol.L⁻¹. Both concentrations are low enough to prevent intermolecular excimer formation. In effect, α which is equal to $[\text{PEO(2K)-Py}_1]/([\text{PEO(2K)-Py}_1] + [\text{PEO(2K)-Py}_2])$ represents the molar fraction of PEO(2K)-Py₁ molecules in the PEO(2K)-Py₂/ PEO(2K)-Py₁ mixture. In other words, α represents the molar fraction of impurity in the mixture assuming that all macromolecules are fully labeled. The spectra are shown in Figure 3.2A. Based on the definition of α , a PEO(2K)-Py₂/PEO(2K)-Py₁ mixture with an α value of 0.15 would have been prepared by mixing a volume fraction $100 \times [1 + (\alpha/(1-\alpha)) \times (6.0 \times 10^{-6} \text{ mol.L}^{-1}/3.0 \times 10^{-6} \text{ mol.L}^{-1})]^{-1} = 74$ vol% of the PEO(2K)-Py₂ solution with 26 vol% of the PEO(2K)-Py₁ solution. Well defined peaks were observed in the wavelength range 370 – 400 nm, characteristic of the pyrene monomer, whereas the usual excimer emission was found as a broad, structureless emission centered around 480 nm. As more PEO(2K)-Py₁ is added to the PEO(2K)-Py₂ solution, the excimer emission at 480 nm decreases in Figure 3.2A and the contribution of the 265 ns decay time characteristic of PEO(2K)-Py₁ increases in Figure 3.2B. Residual contribution of the 265 ns decay time is clearly visible in the fluorescence

decay of pure PEO(2K)-Py₂ indicating the presence of trace amounts of monolabeled polymer in that sample.

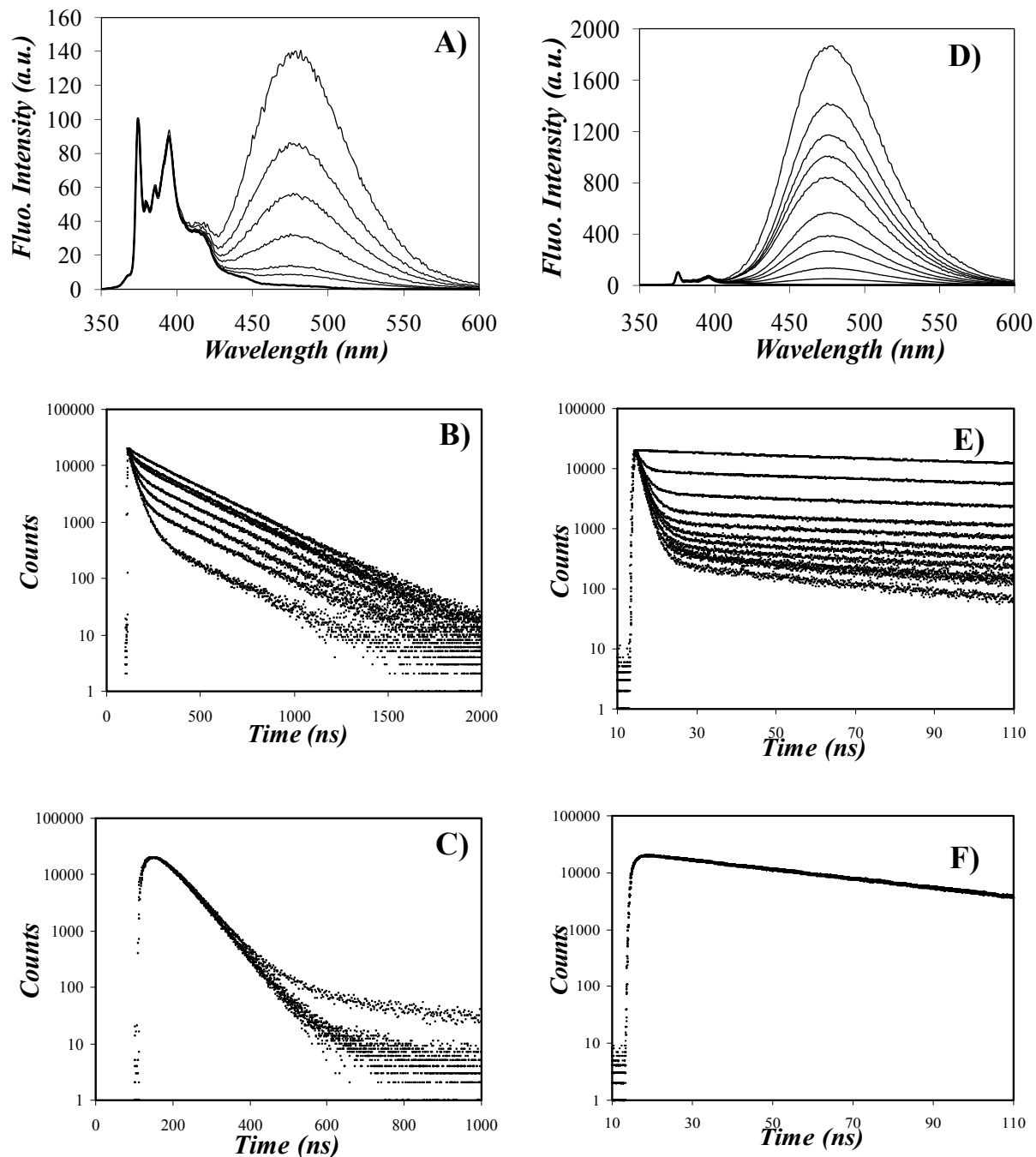


Figure 3.2: Left panel: Fluorescence spectra and decays of PEO(2K)-Py₂/PEO(2K)-Py₁ mixtures in acetone. A) Fluorescence spectra normalized at 375 nm; from top to bottom, $\alpha = 0, 0.15, 0.25, 0.50$,

0.70, 0.80 and 1.00. B) Monomer fluorescence decays; $\lambda_{em} = 375$ nm; from bottom to top, $\alpha = 0, 0.15, 0.25, 0.50, 0.70, 0.80$ and 1.00. C) Excimer fluorescence decays with that acquired for $\alpha = 0.80$ showing a substantial amount of background noise; $\lambda_{em} = 510$ nm. Right panel: Fluorescence spectra and decays of Py₁₆-G4-PS/PyBA mixtures in THF. D) Fluorescence spectra normalized at 375 nm; from top to bottom, $\alpha = 0, 0.05, 0.10, 0.15, 0.20, 0.25, 0.35, 0.45, 0.60, 0.70$ and 1.00. E) Monomer fluorescence decays; $\lambda_{em} = 375$ nm; from bottom to top, $\alpha = 0, 0.05, 0.10, 0.15, 0.20, 0.25, 0.35, 0.45, 0.60, 0.70$ and 1.00. F) Excimer fluorescence decays; $\lambda_{em} = 510$ nm, T = 23 °C.

All excimer fluorescence decays overlapped regardless of PEO(2K)-Py₁ content in Figure 3.2C, as expected, since the pyrene excimer is generated solely by PEO(2K)-Py₂. The mixtures prepared with 80% of monolabeled polymer solution emitted little at 510 nm, where the excimer decays were acquired and the excimer fluorescence decay exhibited more background noise (Figure 3.2C).

Similar trends were observed in Figure 3.2D where the fluorescence spectra of the Py₁₆-G4-PS/PyBA mixtures were obtained for different molar fractions α of the PyBA solution. The Py₁₆-G4-PS and PyBA solutions had a concentration of 2.5×10^{-6} mol.L⁻¹. The high local pyrene concentration found in the dendritic hybrid resulted in efficient excimer formation with a strong excimer emission at 480 nm relative to the weak fluorescence of the pyrene monomer in the 370 – 400 nm range. As more PyBA was added, the contribution of the long monoexponential decay of PyBA increased in Figure 3.2E. However, since the excimer is formed intramolecularly by the pyrene-labeled dendrons, the excimer fluorescence decays overlapped perfectly in Figure 3.2F, regardless of the quantity of PyBA added to the Py₁₆-G4-PS solution.

The fluorescence spectra shown in Figure 3.2A were used to calculate the $(I_E/I_M)^{SS}$ ratios of the PEO(2K)-Py₂/PEO(2K)-Py₁ mixtures which are plotted as a function of α in Figure 3.3A (hollow squares). Similar trends were obtained for the PEO(2K)-Py₂/PEO(2K)-Py₁ mixtures in

toluene and THF. Those results can be seen in Figures SI.3.3 and SI.3.4 in the Supporting Information. As expected from Figure 3.2A, $(I_E/I_M)^{SS}$ decreases continuously with increasing α values. The $(I_E/I_M)^{SS}$ values are relative since they depend on the specific fluorometer used, its settings, and the procedure applied to determine the fluorescence intensities $(I_M)^{SS}$ and $(I_E)^{SS}$. The $(I_E/I_M)^{SS}$ values in Figure 3.3A were normalized to compare them with the $(I_E/I_M)^{SPC}$ ratios determined from the parameters derived from the fluorescence decay analysis and by applying Equations SI.3.18 and SI.3.19 in the Supporting Information.

As typically done with pyrene end-labeled monodisperse polymers,¹²⁻²⁸ Birks' scheme was used to fit globally the monomer and excimer fluorescence decays shown in Figures 3.2B and 3.2C using Equations SI.3.1 and SI.3.2.^{56,57} All fits were excellent with residuals and autocorrelation of the residuals randomly distributed around zero, resulting in all χ^2 being smaller than 1.20. The parameters retrieved from the analysis have been listed in Table SI.3.1 in the Supporting Information. In all polymer mixtures, the excimer lifetime was found to equal 48 ± 2 ns, in good agreement with the τ_{E0} value expected for pyrene excimer in organic solvents.^{8,56,57} Regardless of mixture composition, the rate constant of excimer formation k_1 remained constant with α (Figure 3.3B), taking an average value of $3.0 (\pm 0.2) \times 10^7 \text{ s}^{-1}$. The constancy of k_1 with α is expected since the intramolecular excimer formation of PEO(2K)-Py₂ is independent of the presence of PEO(2K)-Py₁ in the mixtures. In the absence of PEO(2K)-Py₁ (i.e. for $\alpha = 0$), the analysis yields a molar fraction of pyrenes that do not form excimer, namely the f_{Mfree} value, of 0.034 which reflects a residual amount of monolabeled PEO(2K)-Py₁ impurity in the PEO(2K)-Py₂ sample. Not surprisingly, f_{Mfree} increases when increasing amounts of monolabeled sample are added to the solution (see Table SI.3.1A).

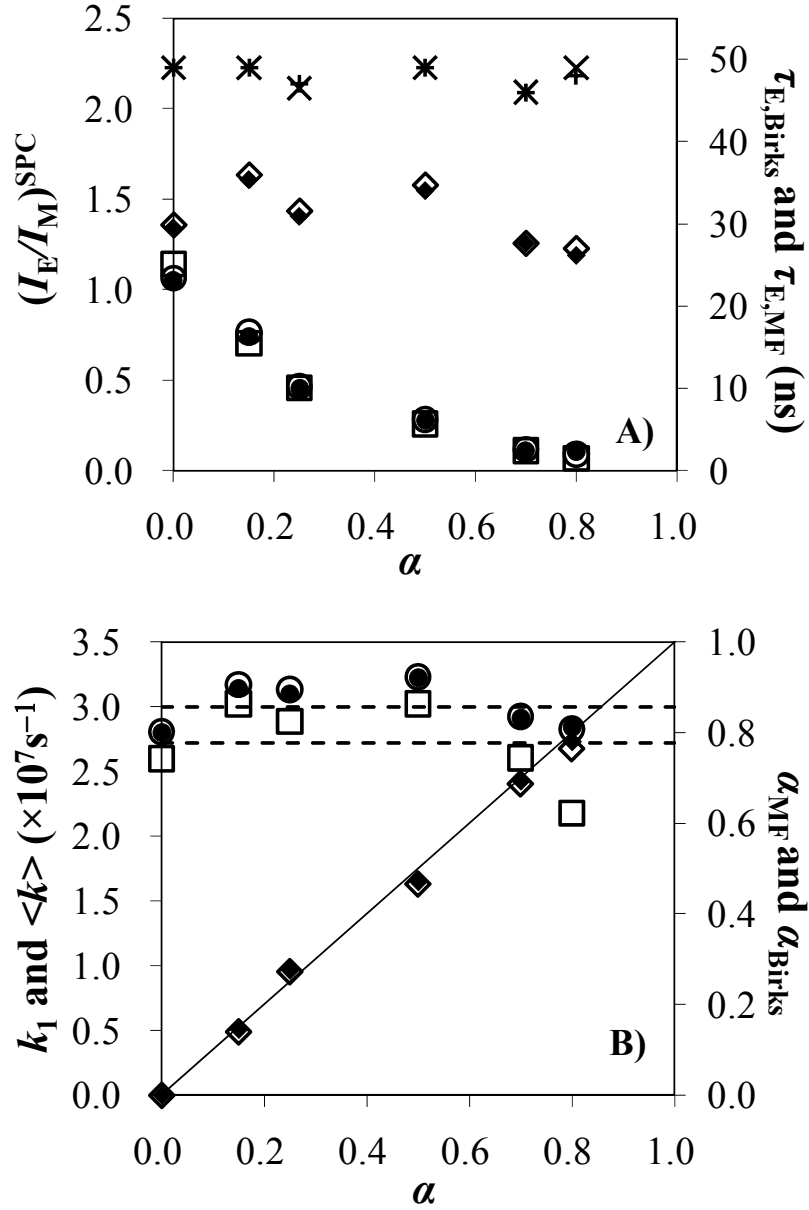


Figure 3.3: A) Plot of $(I_E/I_M)^{SS}$ (\square), $(I_E/I_M)^{SPC}_{Birks}$ (\bullet), $(I_E/I_M)^{SPC}_{MF}$ (\circ), $(I_E/I_M)^{SPC}_{Birks,ffree=0}$ (\blacklozenge), $(I_E/I_M)^{SPC}_{MF,ffree=0}$ (\diamond), $\tau_{E,Birks}$ ($+$), and $\tau_{E,MF}$ (\times) as a function of the molar fraction α . B) Plot of k_1 (\bullet), $\langle k \rangle$ calculated with Equation SI.3.20 (\square), $\langle k \rangle$ calculated with Equation SI.3.21 (\circ), α_{MF} (\diamond), and α_{Birks} (\blacklozenge) as a function of α . T = 23 °C.

The $(I_E / I_M)_{Birks}^{SPC}$ ratio corresponding to the I_E/I_M ratio obtained by using the parameters retrieved by analyzing the monomer and excimer fluorescence decays with Birks' scheme was calculated according to Equation SI.3.18 and is plotted as a function of α (Figure 3.3A). As more monolabeled polymer is added to the solution, $(I_E / I_M)_{Birks}^{SPC}$ decreases. The $(I_E / I_M)_{Birks}^{SPC}$ values overlapped perfectly those obtained for $(I_E / I_M)^{SS}$ indicating that $(I_E / I_M)_{Birks}^{SPC}$ and $(I_E / I_M)^{SS}$ are in effect equivalent, the only difference being that $(I_E / I_M)_{Birks}^{SPC}$ is an absolute value whereas $(I_E / I_M)^{SS}$ is not. The $(I_E / I_M)_{Birks, f_{free}=0}^{SPC}$ ratio expected if no monolabeled polymer is present in the solution was calculated by setting in Equation SI.3.18 the molar fraction of pyrenes forming excimer by diffusion, namely f_{Mdiff} , and f_{Mfree} equal to one and zero, respectively. Within experimental error, $(I_E / I_M)_{Birks, f_{free}=0}^{SPC}$ remained constant as a function of α and equal to 1.4 ± 0.2 in Figure 3.3A as expected, since the $(I_E / I_M)_{Birks, f_{free}=0}^{SPC}$ ratio describes the amount of excimer formed intramolecularly by Py₂-PEO(2K) and it is independent of the PEO(2K)-Py₁ content. It is also worth noting that $(I_E / I_M)_{Birks}^{SPC} = 1.05$ for $\alpha = 0$ is about 40% smaller than $(I_E / I_M)_{Birks, f_{free}=0}^{SPC}$ due to the presence of $f_{Mfree} = 0.034$ of PEO(2K)-Py₁ in the PEO(2K)-Py₂ sample. This represents a rather large drop in the value of the I_E/I_M ratio for the presence of a minute amount (3.4 mol%) of fluorescent impurity (PEO(2K)-Py₁). This impurity is not expected to be free unattached pyrene label as gel permeation chromatography (GPC) of the PEO(2K)-Py₂ sample conducted with a fluorescence detector indicates that it is free of low molecular weight fluorescent impurities.

The MF analysis was then applied to fit globally the monomer and excimer fluorescence decays using, respectively, Equations SI.3.5 and SI.3.6 with $n = 2$. No ES^* species could be detected and their contribution was set to zero in the analysis. The fits were excellent resulting in χ^2 smaller than 1.20 and residuals and autocorrelation of the residuals randomly distributed around zero. An example of the fit of the monomer and excimer decays for the sample with $\alpha = 0.25$ can be found in

Figure SI.3.1 in the Supporting Information. The parameters retrieved from the MF analysis have been listed in Table SI.3.2 in the Supporting Information. Only residual association between ground-state pyrene monomers could be detected amounting to a molar fraction f_{E0} of 0.04 ± 0.02 . The excimer lifetime was found to equal 48 ± 2 ns, which is consistent with the τ_{E0} value obtained by the Birks scheme analysis (Figure 3.3A). Moreover, the molar fractions of PEO(2K)-Py₁ in solution, f_{Mfree} , listed in Tables SI.3.1A and SI.3.2A are identical whether they are obtained directly from Birks' scheme or MF analysis, indicating that both analyses are self-consistent.

The parameters obtained by fitting the monomer and excimer fluorescence decays with the MF analysis and listed in Table SI.3.2 were used to calculate the $(I_E/I_M)_{MF}^{SPC}$ ratio based on Equation SI.3.19. $(I_E/I_M)_{MF}^{SPC}$ is plotted as a function of α in Figure 3.3A. The agreement observed between the ratios $(I_E/I_M)^{SS}$, $(I_E/I_M)_{Birks}^{SPC}$, and $(I_E/I_M)_{MF}^{SPC}$ is excellent, thus confirming their equivalence. The $(I_E/I_M)_{MF, f_{free}=0}^{SPC}$ ratio expected if no monolabeled polymer is present in the solution was calculated by setting in Equation SI.3.19 f_{Mdiff} and f_{Mfree} equal to one and zero, respectively. $(I_E/I_M)_{MF, f_{free}=0}^{SPC}$ remained constant and equal to 1.4 ± 0.2 as a function of α in Figure 3.3A. Within experimental error, $(I_E/I_M)_{Birks, f_{free}=0}^{SPC}$ and $(I_E/I_M)_{MF, f_{free}=0}^{SPC}$ are identical. The average rate constant $\langle k \rangle$ that provides information about the time scale over which excimer is formed by Py₂-PEO(2K) was calculated according to Equations SI.3.20 and SI.3.21. $\langle k \rangle$ was plotted as a function of α in Figure 3.3B and found to remain constant within experimental error and equal to $2.7 (\pm 0.3) \times 10^7 \text{ s}^{-1}$ and $3.0 (\pm 0.2) \times 10^7 \text{ s}^{-1}$, respectively. The value of $\langle k \rangle$ obtained with Equation SI.3.21 from the MF parameters was found to match the cyclization rate constant k_1 obtained by the Birks scheme (Figure 3.3A) and found to equal $3.0 (\pm 0.2) \times 10^7 \text{ s}^{-1}$ after averaging over all the PEO(2K)-Py₂/PEO(2K)-Py₁ mixtures. It suggests that Equation SI.3.21 might be a better approximation to determine the average rate constant of excimer formation $\langle k \rangle$.

Most importantly, the equivalence that is expected to exist between the ratio I_E/I_M and $\langle k \rangle$ for the MF or k_1 for Birks' scheme was found to hold between $\langle k \rangle$, k_1 , $(I_E/I_M)_{MF, f_{free}=0}^{SPC}$, and $(I_E/I_M)_{Birks, f_{free}=0}^{SPC}$. This equivalence was not obeyed for $(I_E/I_M)^{SS}$, $(I_E/I_M)_{Birks}^{SPC}$, and $(I_E/I_M)_{MF}^{SPC}$ since those ratios include the contribution of the monolabeled polymer. Finally, the molar fraction of the monolabeled polymer solution used to prepare the mixture (α_{Birks} or α_{MF}) could be back-calculated from the molar fraction f_{free} and f_{free}^0 ($f_{free}^0 = f_{free}$ when $\alpha = 0$) found with Birks' scheme or by the MF analysis of the fluorescence decays, respectively, according to Equation 3.1.

$$\alpha_{MF} = \alpha_{Birks} = \frac{n_{Py} \times (f_{free} - f_{free}^0)}{n_{Py} \times (f_{free} - f_{free}^0) + 1 - f_{free}} \quad (3.1)$$

In Equation 3.1, n_{Py} is the number of pyrene pendants attached onto the pyrene-labeled macromolecule, i.e. $n_{Py} = 2$ and 16 for PEO(2K)-Py₂ and Py₁₆-G4-PS, respectively. The α_{Birks} and α_{MF} values obtained by applying Equation 3.1 were plotted as a function of α in Figure 3.3B for the PEO(2K)-Py₂/PEO(2K)-Py₁ mixtures. The agreement observed between α_{Birks} , α_{MF} , and α is remarkable, indicating that global analysis of the monomer and excimer fluorescence decays faithfully reports on the molar fraction of PEO(2K)-Py₁ that is present in the PEO(2K)-Py₂/PEO(2K)-Py₁ mixtures regardless of the model used to fit the process of excimer formation. The same analysis was repeated with the fluorescence decays shown in Figures 3.2E and 3.2F for the Py₁₆-G4-PS/PyBA mixtures to probe further the robustness of these global analyses.

The monomer and excimer decays of the Py₁₆-G4-PS/PyBA mixtures were fitted globally with Equations SI.3.5 and SI.3.6, respectively. Three decay times (τ_i , $i = 1-3$) were needed in both equations to handle the excimer formation by diffusion of the pyrenes attached onto the dendrimer chain ends. Two of these decay times are very small, smaller than 3 ns, suggesting that the excimer is

formed by a very rapid process. To deal with the free PyBA that does not form excimer, an extra exponential was added to the expression of the monomer decay in Equation SI.3.5 with a fixed lifetime of 210 ns corresponding to that of PyBA in THF. For all solutions, an additional exponential with a decay time of 4 ns was required to fit the excimer decays. The 4 ns decay time accounts for a short-lived excimer species (ES^*) which is due, either to the self-quenching of some improperly stacked pyrenes or residual pyrene degradation.^{24,51,57,62} All fits obtained from the global analysis of the monomer and excimer decays with the MF were good, resulting in χ^2 smaller than 1.30 and residuals and autocorrelation of the residuals randomly distributed around zero (see Figure SI.3.2 in the Supporting Information for the sample with $\alpha = 0.15$). The parameters retrieved from the analysis are listed in Table SI.3.3. As shown in Table SI.3.3C, the fraction of aggregated pyrenes given by f_{agg} ($= f_{E0} + f_{ES} < 0.20$) is small for all solutions, suggesting that most of the excimer is formed by the diffusive encounter between an excited and a ground-state pyrene. The excimer lifetime was found to equal 53 ± 1 ns, close to the 48 ± 2 ns lifetime found for PEO(2K)-Py₂, and agrees with the τ_{E0} values found in other organic solvents.^{8,56,57} The fractions of the four excited pyrene species (f_{diff} , f_{free} , f_{E0} , and f_{ES}) were obtained using Equations SI.3.12 – SI.3.15. The fraction of free PyBA (f_{free}) in Table SI.3.3C increased with the amounts of PyBA added to the dendrimer solution, as expected.

The ratio $(I_E/I_M)_{MF}^{SPC}$ was calculated according to Equation SI.3.19 and plotted as a function of the molar fraction α in Figure 3.4A. For the Py₁₆-G4-PS/PyBA mixtures, α equals $[\text{PyBA}]/([\text{PyBA}] + [\text{Py}_{16}\text{-G4-PS}])$ assuming that all pyrenes in the Py₁₆-G4-PS solutions are covalently attached onto the dendrons. The $(I_E/I_M)_{MF}^{SPC}$ trends obtained from the global analysis of the monomer and excimer fluorescence decays match perfectly the $(I_E/I_M)^{SS}$ trends calculated from the steady-state fluorescence spectra. The $(I_E/I_M)_{MF, f_{free}=0}^{SPC}$ ratio that would be expected if no free pyrene was present in the solution was calculated by setting f_{Mdiff} and f_{Mfree} equal to one and zero, respectively. The $(I_E/I_M)_{MF, f_{free}=0}^{SPC}$ ratio remained constant as a function of α in Figure 3.4A and

equal to 30 ± 2 , about 21 times larger than for PEO(2K)-Py₂ reflecting the shorter average distance separating every two pyrenes attached onto the dendritic hybrid. The constancy of $(I_E/I_M)_{MF, f_{free}=0}^{SPC}$ is expected since it characterizes the amount of excimer formed by Py₁₆-G4-PS and it is independent of the PyBA content. $(I_E/I_M)_{MF, f_{free}=0}^{SPC}$ for $\alpha = 0$ is 20% larger than $(I_E/I_M)_{MF}^{SPC}(\alpha = 0)$ due to the non-negligible molar fraction of unattached pyrene labels ($f_{free} = 0.003$) present in the Py₁₆-G4-PS sample. The 20% drop in the I_E/I_M ratio due to the presence of a mere 0.3 mol% fluorescent impurity in the form of PyBA in the Py₁₆-G4-PS sample is a testimony to the outstanding sensitivity of fluorescence. It is worth pointing out that the presence of 0.3 mol% of unattached PyBA which is so easily detected in the pyrene monomer fluorescence decays shown in Figure 3.2E goes absolutely undetected in the GPC analysis of the Py₁₆-G4-PS sample carried out with a fluorescence detector (Figure SI.3.6) which fails to indicate the presence of low molecular weight fluorescent impurities.

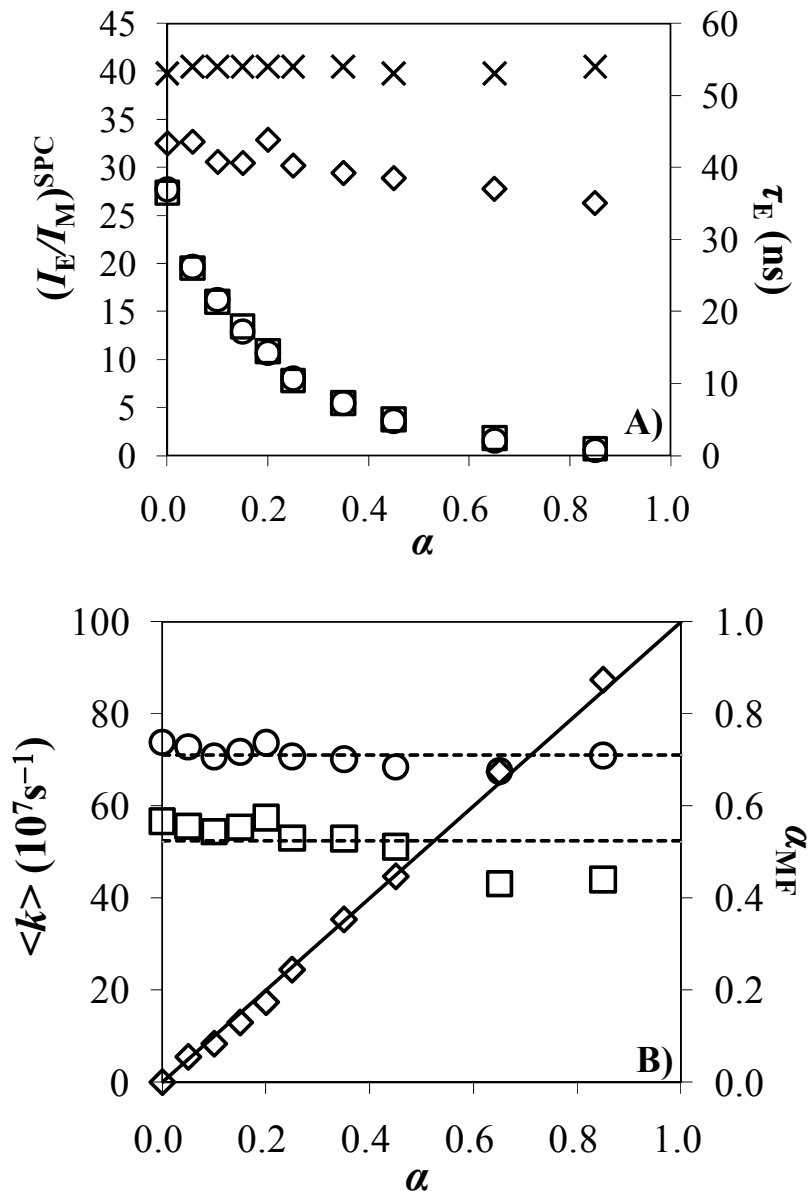


Figure 3.4: A) Plot of $(I_E/I_M)^{SS}$ (□), $(I_E/I_M)_{MF}^{SPC}$ (○), $(I_E/I_M)_{MF, free=0}^{SPC}$ (◇), and $\tau_{E, MF}$ (×) as a function of the molar fraction α . B) Plot of $\langle k \rangle$ calculated with Equation SI.3.20 (□), $\langle k \rangle$ calculated with Equation SI.3.21 (○), and α_{MF} (◇) as a function of α . T = 23 °C.

The average rate constant $\langle k \rangle$ calculated according to Equations SI.3.20 or SI.3.21 provides information about the time scale over which excimer is formed by Py₁₆-G4-PS. On the one hand,

when $\langle k \rangle$ obtained with Equation SI.3.20 was plotted as a function of α in Figure 3.4B, it remained constant within experimental error for PyBA mole fractions smaller than 50% and equal to $5.5 (\pm 0.2) \times 10^8 \text{ s}^{-1}$ (see the lower horizontal line in Figure 3.4B). On the other hand, Equation SI.3.21 yielded $\langle k \rangle$ values that remained constant with α and equal to $7.1 (\pm 0.2) \times 10^8 \text{ s}^{-1}$ in Figure 3.4B. The improved constancy obtained for $\langle k \rangle$ by using Equation SI.3.21 suggests that this equation might be more appropriate than Equation SI.3.20. It must also be pointed out that Equation SI.3.21 is equivalent to that used in the Birks scheme to retrieve the rate constant k_1 of excimer formation.⁸ If Equation SI.3.21 is applied, $\langle k \rangle$ for Py₁₆-G4-PS is 24 times larger than $\langle k \rangle$ for PEO(2K)-Py₂, in agreement with the 21 fold enhancement in $(I_E/I_M)_{MF, f_{free}=0}^{SPC}$ observed between the two pyrene-labeled constructs. As was also found with the PEO(2K)-Py₂ study, the similar trends that are expected between the ratio I_E/I_M and $\langle k \rangle$ are indeed observed between $\langle k \rangle$ and $(I_E/I_M)_{MF, f_{free}=0}^{SPC}$. Different trends are obtained between $\langle k \rangle$ and $(I_E/I_M)^{SS}$ or $(I_E/I_M)^{SPC}$ since those I_E/I_M ratios include the contribution of free PyBA. At high PyBA concentrations ($\alpha > 50\%$), $\langle k \rangle$ obtained with Equation SI.3.20 and $(I_E/I_M)_{MF, f_{free}=0}^{SPC}$ deviate somewhat from their value obtained for smaller α , probably due to the significant contribution of free pyrene in this range of α values. Under these circumstances, the curvature at the start of the monomer decays which accounts for excimer formation through a rapid diffusional process is too small to be fitted accurately (Figure 3.2E). Furthermore, the process of pyrene excimer formation taking place in Py₁₆-G4-PS is much more complicated than that for PEO(2K)-Py₂ necessitating three decay times instead of the two needed for PEO(2K)-Py₂. Two out of the three decay times are also extremely small being within 3 ns. The molar fraction of the PyBA solution used to prepare the mixture (α_{MF}) could be back-calculated according to Equation 3.1 from the fractions f_{free} and f_{free}^o found by the MF analysis of the

fluorescence decays. It is plotted as a function of α in Figure 3.4B. As in Figure 3.3B for PEO(2K)-Py₂, the agreement observed between α_{MF} and α is excellent.

To ensure that these results were not solvent-dependent, the solution of PEO(2K)-Py₂/PEO(2K)-Py₁ mixtures in toluene and THF were prepared, their pyrene monomer and excimer fluorescence decays were acquired and fitted according to the MF analysis and Birks' scheme. The results of these experiments are shown in Figure SI.3.3 and SI.3.4 in the Supporting Information. The trends obtained are identical to those shown in Figure 3.3 for the PEO(2K)-Py₂/PEO(2K)-Py₁ mixtures in acetone demonstrating the trends shown in the present study are not a function of solvent.

3.5 Discussion

Although the ability of the global analyses presented in this report to retrieve quantitatively the molar fraction of a pyrene monomer species, be it PyBA or PEO(2K)-Py₁, present in a sample is quite remarkable, the key advantage of these analyses resides in their ability to predict what the absolute I_E/I_M ratio should be if there were no pyrene monomer species present in the sample. In turn, this feature can be used to guide the experimentalist to assess the effect that the presence of a fluorescent impurity has on the fluorescence data being analyzed and whether the pyrene-labeled macromolecule needs to undergo further purification. In one particular example, this feature was fully taken advantage of to determine that the $(I_E/I_M)^{SS}$ ratio of the Py₁₆-G4 dendron was 4 fold smaller than expected because it contained a mere 3 mol% of unattached pyrene label, PyBA in this case.⁵⁸ Setting f_{free} equal to zero in Equation SI.3.19 resulted in a $(I_E/I_M)_{MF, f_{free}=0}^{SPC}$ ratio that was 4-fold larger than $(I_E/I_M)_{MF}^{SPC}$. Another round of purification removed the unattached PyBA and the $(I_E/I_M)^{SS}$ and $(I_E/I_M)_{MF}^{SPC}$ ratios increased 4-fold to their expected value.⁵⁸

The dependency of the $(I_E/I_M)^{SS}$ ratio on f_{free} is illustrated in Figure 3.5 where $(I_E/I_M)^{SPC}$ is plotted as a function of f_{free} for different rate constants of excimer formation. The trends shown in Figure 3.5 were simulated by assuming that the process of excimer formation for a series of PEO-Py₂

constructs of different chain lengths is well described by Birks' scheme. Using $k_{-1} = 1.85 \times 10^6 \text{ s}^{-1}$, $\tau_E = 48 \text{ ns}$, $\tau_M = 265 \text{ ns}$, and the scaling relationship $k_1 = 5.7 \times 10^{12} \times M_n^{-1.6} \text{ s}^{-1}$ which yields experimentally relevant values for PEO-Py₂ in acetone,⁵⁷ Equation SI.3.18 could be applied to find how the $(I_E/I_M)_{Birks}^{SPC}$ ratio varies as a function of f_{free} . The $(I_E/I_M)_{Birks}^{SPC}$ ratios normalized to their values at $f_{free} = 0$ show a clear trend in Figure 3.5. The $(I_E/I_M)_{Birks}^{SPC}$ ratio depends more strongly on f_{free} for larger rate constants of excimer formation. For PEO(2K)-Py₂ with $k_1 = 3 \times 10^7 \text{ s}^{-1}$, an f_{free} value of 0.004 (0.4 mol% unattached pyrene) is sufficient to decrease $(I_E/I_M)_{Birks}^{SPC}$ by 10%. Based on Figure 3.5, 4 mol% unattached pyrene or PEO(2K)-Py₁ would decrease $(I_E/I_M)_{Birks}^{SPC}$ by 25% as experimentally observed in Figure 3.3A where the presence of 3.4 mol% of monolabeled PEO impurity decreases the I_E/I_M ratio from 1.40 for $(I_E/I_M)_{ffree=0}^{SPC}$ to 1.05 for $(I_E/I_M)^{SPC}$. On the other hand, 4 mol% of unattached pyrene (i.e. a much larger f_{free} value of 0.04) is necessary to decrease $(I_E/I_M)_{Birks}^{SPC}$ by 10% for PEO(10K)-Py₂ for which $k_1 = 2.3 \times 10^6 \text{ s}^{-1}$. In the case of PEO(0.28K)-Py₂ with a k_1 value of $7.1 \times 10^8 \text{ s}^{-1}$ similar to that of Py₁₆-G4-PS, 0.06 mol% free pyrene is enough to reduce $(I_E/I_M)_{Birks}^{SPC}$ by 10%, whereas 0.3 mol% of unattached pyrene would reduce $(I_E/I_M)_{Birks}^{SPC}$ by 30%. This decrease is important as was found experimentally for Py₁₆-G4-PS for which $(I_E/I_M)_{MF}^{SPC}$ was found to be 20% smaller than expected due to the presence of 0.3 mol% of unattached 1-pyrenebutiric acid. The discrepancy between the two values (30% for the simulation versus 20% for the experiments) is due to the different kinetic schemes that are applied to compare the data shown in Figure 3.5 and simulated with Birks' scheme, and the fluorescence decays of Py₁₆-G4-PS which were analyzed with the MF. These last examples illustrate the extreme purity that is required to obtain reliable $(I_E/I_M)^{SS}$ ratio for pyrene-labeled macromolecules that form excimer on a fast time scale, as typically found for pyrene-labeled dendrimers. It certainly rationalizes the origin of the unexpected

trends often reported in studies of pyrene-labeled dendrimers, as has been suggested in a recent publication.⁵⁸

Indeed, pyrene-labeled dendrimers have been prepared in a number of instances.²⁹⁻³⁹ However, the majority of studies are not interested in using the excimer formation process to study the internal dynamics of the dendrimers, but rather the process of energy or electron transfer from the dendrimer periphery to its core. Consequently, little information about the $(I_E/I_M)^{SS}$ ratio or $\langle k \rangle$ is available for those pyrene-labeled dendrimers. But in the few rare instances where these parameters are reported, they often disagree. For instance, calculating the $(I_E/I_M)^{SS}$ ratio from the reported fluorescence spectra of pyrene-labeled polyester dendrimers indicates that it increases by a modest 50% when the generation number increases from 1 to 2 while the rate constant of excimer formation increases by a massive 7-fold.³⁸ In the case of pyrene-labeled poly(amidoamine) dendrimers, the $(I_E/I_M)^{SS}$ ratio increases by 66% when the generation number increases from 2 to 3 while $\langle \tau \rangle$ for the pyrene monomer increases from 35 ns to 65 ns, an implausible result which implies that $\langle k \rangle$ determined with Equation SI.3.20 would decrease.³⁹ These observations contradict a tenant of pyrene excimer formation, namely that the rate constant of excimer formation and the I_E/I_M ratio should vary in a similar manner, as this and other studies demonstrate.^{47,58,59} These inconsistencies are certainly due to the presence of pyrene fluorescent impurities that have not been taken into account in the analysis.

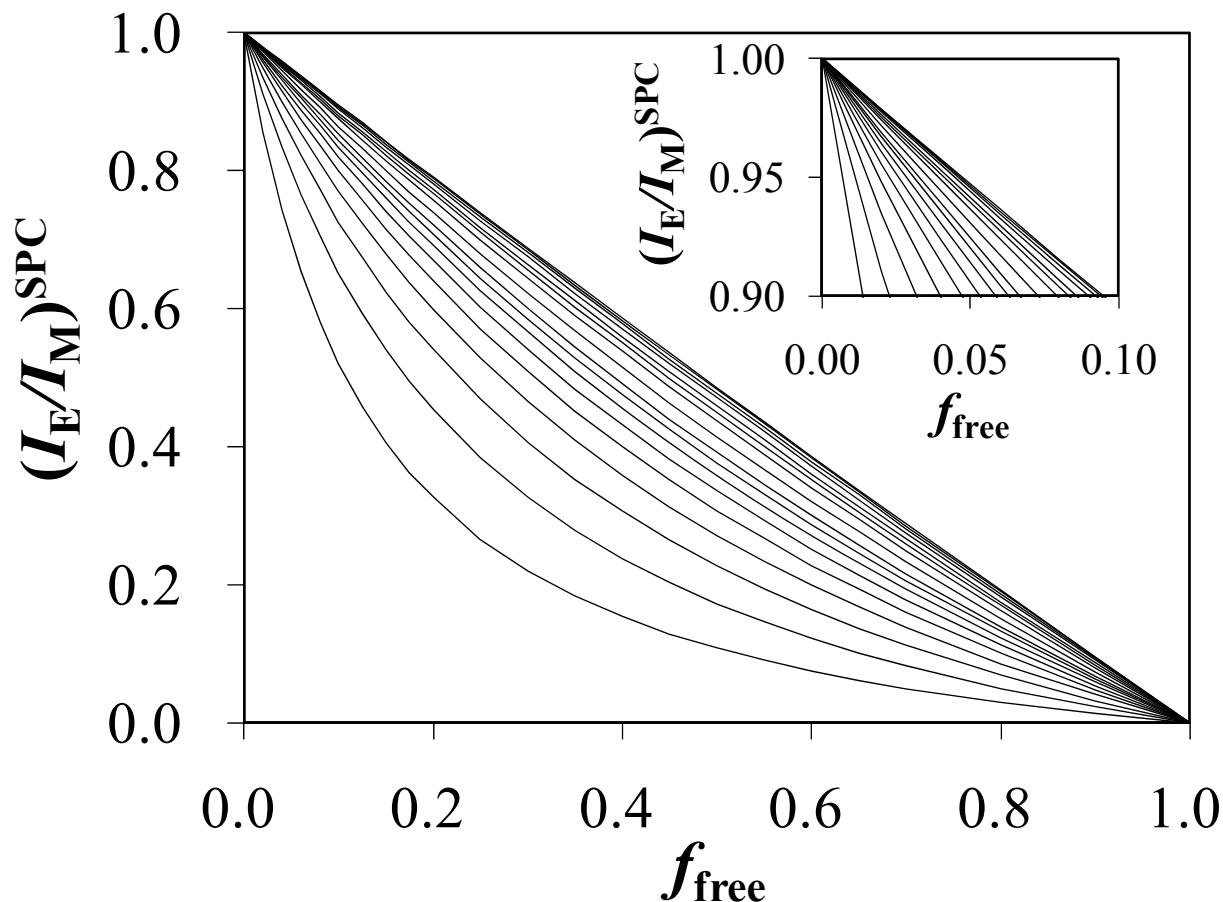


Figure 3.5: Simulated $(I_E / I_M)_{Birks}^{SPC}$ ratios of a series of PEOs with $M_n = 2,000, 3,000, 4,000, 5,000, 6,000, 7,000, 8,000, 9,000, 10,000, 12,000, 15,000, 17,500, 20,000, 25,000, 30,000, 35,000, 40,000$ g/mol (from bottom to top) calculated with Equation SI.3.18 and plotted as a function of f_{free} . Inset: Zoom in representation of the top-left corner of Figure 3.5.

Since all research laboratories dealing with pyrene-labeled macromolecules use the $(I_E/I_M)^{SS}$ ratio as the main analytical tool to characterize the efficiency of a macromolecule at forming excimer,⁹⁻¹¹ the present study highlights in a quantitative manner the importance of ensuring and characterizing the spectral purity of a fluorescently labeled macromolecule to determine the $(I_E/I_M)^{SS}$ ratio. On the one hand, these conclusions might come as a disappointment as they illustrate the extreme sensitivity of fluorescence to the presence of minute quantities of fluorescent impurities

typically found when dealing with fluorescently labeled macromolecules. On the other hand, this study represents a formidable advance forward in the investigation of fluorescently labeled macromolecules in several ways. First, the analyses presented herein take full advantage of the fact that excimer formation is being probed both in the monomer and excimer decays, so that the contribution of any emission not associated with excimer formation in the monomer decay can be determined with unmatched accuracy. As this study demonstrates, this aspect of the analysis is particularly useful to determine f_{free} . In cases where fluorophore and quencher are different and do not form a fluorescent species upon encounter as shown in Scheme 3.1, the analysis is weaker as it relies on the fit of the fluorophore decay only which is limited by the number of exponentials that can be used in the optimization program, usually no more than 3 for closely spaced decay times.¹ Second, the parameters obtained from the global analysis of the monomer and excimer decays can be rearranged to yield an absolute $(I_E/I_M)^{\text{SPC}}$ ratio as we have shown in Equations SI.3.18 and SI.3.19. Third, these parameters can be used to obtain the $(I_E/I_M)_{f_{\text{free}}=0}^{\text{SPC}}$ ratio which yields the value of the $(I_E/I_M)^{\text{SPC}}$ ratio free of fluorescent impurity, i.e. the parameter which is actually sought after by experimentalists. All in all, the experiments compiled in this study are expected to further enhance the use of pyrene excimer formation as being an appealing and reliable approach to study the internal dynamics of macromolecules.

3.6 Conclusions

The experiments presented in this study have illustrated the extreme sensitivity of fluorescence in general and the I_E/I_M ratio in particular to unwanted fluorescent impurities that are inherently present in a solution of pyrene-labeled macromolecules. The magnitude of these effects was demonstrated with two pyrene-labeled macromolecules, namely a 4th generation dendritic hybrid (Py₁₆-G4-PS) and a monodisperse poly(ethylene oxide) chain (PEO(2K)-Py₂) end-labeled with 16 and 2 pyrenes, respectively. In both cases, minute amounts of pyrene monomer species, 0.32 mol% of PyBA for Py₁₆-G4-PS and 3 mol% of PEO(2K)-Py₁ for PEO(2K)-Py₂, were found to decrease the

$(I_E/I_M)^{\text{SPC}}$ ratio, and by implication the $(I_E/I_M)^{\text{SS}}$ ratio, by 20% and 40%, respectively. Although the rather large fluctuations in the I_E/I_M ratios associated with the presence of rather minute quantities of pyrene monomer species are somewhat distressing, the ability of the global analyses presented in this report at, first, accounting quantitatively for this corrupted emission and, second, retrieving the information pertaining to excimer formation in the pyrene-labeled macromolecule, is reassuring. It is hoped that this work expands the advantages associated with the use of pyrene excimer formation to study the behavior of macromolecules in solution by fluorescence.

Chapter 4

Probing the Hydrophobic Interactions of a Series of Pyrene End-Labeled Poly(ethylene oxide)s in Aqueous Solution Using Time-Resolved Fluorescence

4.1 Overview

The hydrophobic association of a series of poly(ethylene oxide)s covalently labeled at both ends with pyrene (PEO(X)-Py₂ where X represents the number average molecular weight (M_n) of the PEO chains equal to 2, 5, 10, and 16.5 K) in aqueous solutions was investigated at different polymer concentrations (C_p) using steady-state and time-resolved fluorescence measurements. Phase separation was observed with PEO(2K)-Py₂ and PEO(5K)-Py₂ samples at high C_p . The steady-state fluorescence spectra showed that the ratios of excimer-to-monomer fluorescence intensities (I_E/I_M) of all PEO samples remained constant when C_p was below 4×10^{-5} M and decreased dramatically with increasing PEO chain length due to a decrease in intramolecular pyrene excimer formation. The I_E/I_M ratio in this regime was found to scale as $M_n^{-2.3 \pm 0.2}$. For $C_p > 4 \times 10^{-5}$ M, pyrene excimer is formed by both intra- and intermolecular interactions and the I_E/I_M ratio increases linearly with increasing C_p except for PEO(2K)-Py₂ which undergoes phase separation. The decays obtained at various polymer concentrations were fitted according to a “Sequential Model” (SM) which assumes that the pyrene excimer is formed in a sequential manner. The molar fractions of all excited pyrene species and the rate constants for pyrene excimer formation were determined from the global analysis of the monomer and excimer fluorescence decays. The fraction of pyrenes that formed excimer from ground-state pyrene aggregates (f_{E0}) was found to increase with C_p in the regime where the pyrene excimer is formed both intra- and intermolecularly and decrease with M_n in the regime where the pyrene excimer is formed only intramolecularly. The fraction of pyrene pendants subject to

hydrophobic interactions were used to determine the hydrophobic capture radius (R_c) of pyrene in water from the distribution of PEO end-to-end distances. R_c was found to equal 2.2 ± 0.2 nm using f_{E0} .

4.2 Introduction

Hydrophobically end-capped monodisperse poly(ethylene oxide)s (PEO) are often used as model polymers to understand the behavior of an important family of commercial associative thickeners, namely the hydrophobically modified ethoxylated urethanes (HEUR) polymers.¹ HEUR polymers are composed of short PEO segments linked via urethane interconnecting units and end-terminated by alkyl hydrophobes.² Numerous reports suggest that HEURs undergo end-to-end hydrophobic association to form “flower-like” micelles in water at low polymer concentration.³⁻⁸ Increasing the HEUR concentration results in a significant increase of the HEUR solution viscosity due to the formation of a polymeric network where the hydrophobes form micelles which are bridged intermolecularly by the polymer chains.^{9,10} Application of a shear to a concentrated HEUR solution results in a dramatic decrease in solution viscosity due to the disruption of the polymeric network.^{5,10-12} Thanks to their interesting rheological properties, HEURs have found numerous industrial applications, such as in paint formulation, paper coating, enhanced oil recovery, and antifreeze formulations.¹³⁻¹⁵

By replacing the hydrophobes of associative thickeners with the hydrophobic chromophore pyrene, the ability of pyrene to form an excimer can be employed to characterize polymer chain dynamics in solution and the level of association of the hydrophobic pyrene pendants in aqueous solution. The fluorescence behavior of many hydrophobically modified water-soluble polymers bearing a pyrene group (Py-HMWSP) has been investigated in aqueous solutions. The water-soluble backbones that have been labelled with pyrene and studied by fluorescence include poly(acrylic acid),¹⁶⁻¹⁸ poly(maleic acid),¹⁹ a terpolymer of methacrylic acid, ethyl acrylate, and a macromonomer terminated at one end with pyrene and at the other end with methyl styrene,²⁰⁻²⁴ poly(*N,N*-

dimethylacrylamide),²⁵⁻²⁷ poly(*N*-isopropylacrylamide),²⁸⁻³⁰ polyethylenimine,³¹ hydroxyethylcellulose,^{32,33} and PEO.³⁴⁻⁴⁵

The fluorescence properties of Py-HMWSPs in water are quite different from those observed in organic solvents. In the case of hydrophobically modified alkali swellable emulsion polymers randomly labeled with pyrene moieties (Py-HASE),²⁴ pyrene excimer formation takes place primarily via diffusive encounters between pyrene pendants in organic solvents, where the pyrene pendants are well-solvated and not pre-associated. On the contrary, aggregates of hydrophobic pyrenes form in aqueous solution and pyrene excimer is mostly generated through direct excitation of ground-state pyrene aggregates. These effects are well known in the field and have been widely communicated.¹⁶⁻⁴⁵

While the existence of pyrene association in water is straightforward to demonstrate by a variety of spectroscopic properties, more quantitative information about the hydrophobic association of pyrene pendants is much more challenging to obtain. Of particular interest is the fraction of hydrophobes that are associated or the time scale over which these associations take place. These parameters describe the behavior of the Py-HMWSPs at the molecular level, providing knowledge that can be used to rationalize the peculiar viscoelastic properties observed at the macroscopic level for solutions of HMWSPs like HEURs and HASEs. Theoretically, such quantitative information can be obtained through careful analysis of the fluorescence decays of the pyrene monomer and excimer. In practice, very few analyses of this kind have been carried out due to the complex nature of the fluorescence decays obtained with aqueous solutions of Py-HMWSPs where pyrene aggregates are present.

Although the hydrophobic interactions between pyrene hydrophobes were investigated for a series of pyrene end-labeled PEOs around twenty years ago by Char et al.⁴⁵ using steady-state fluorescence, quantitative information on the actual level of pyrene association was obtained for the first time by using time-resolved fluorescence in 1998.³⁹ Whereas steady-state fluorescence measurements cannot distinguish whether the pyrene excimer is formed by diffusional encounters or direct excitation of pyrene aggregates, the difference between the two phenomena can be directly

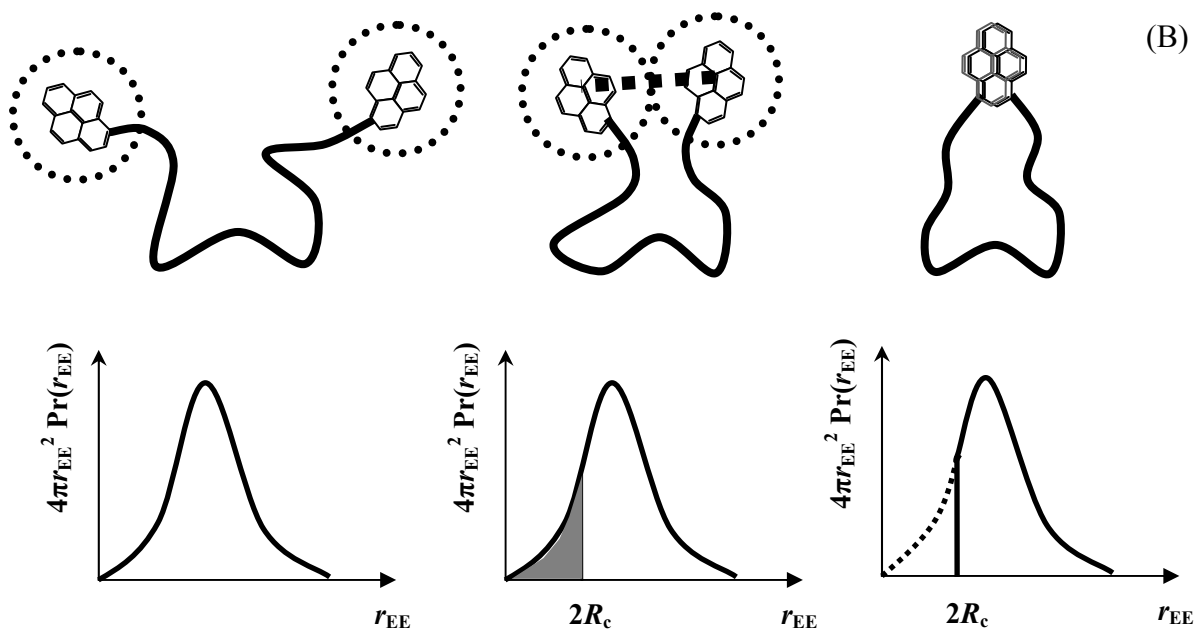
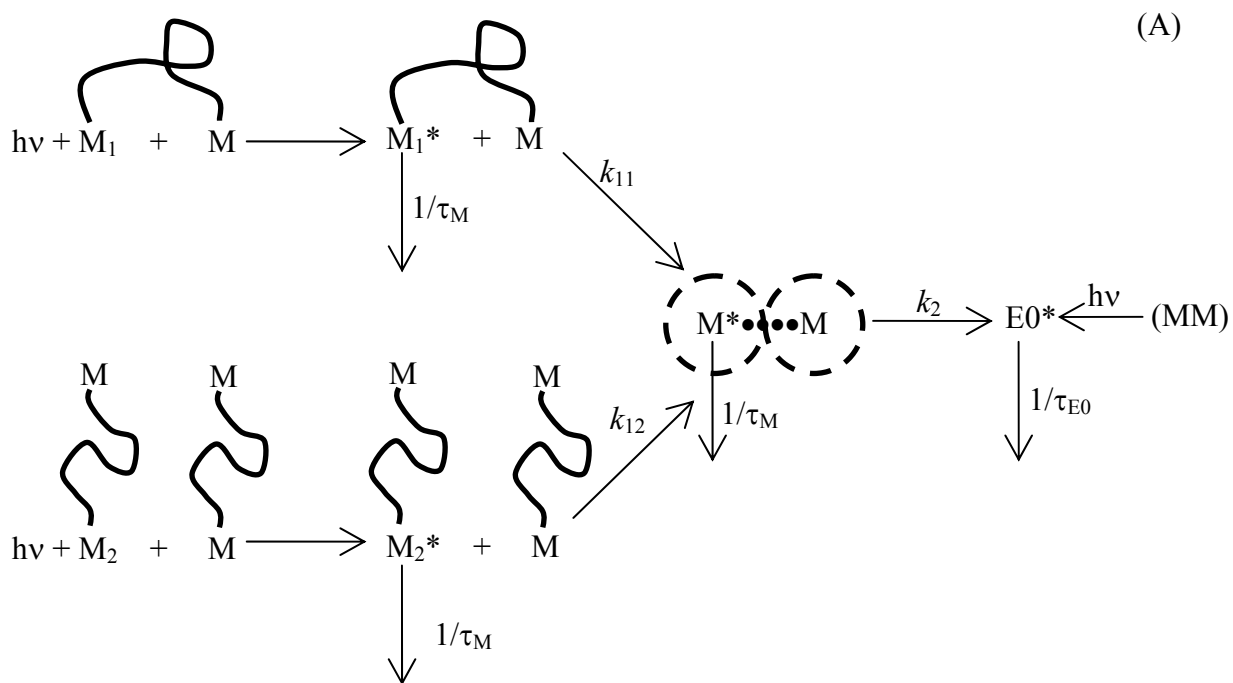
observed by acquiring pyrene excimer fluorescence decays. If the excimer is formed by diffusion between two pyrene groups, excimer formation is delayed and a rise time is observed in the excimer decay. Further analysis of the fluorescence decays provides quantitative information on the kinetics of pyrene excimer formation, from which the molar fraction of aggregated pyrenes can be retrieved. In turn, these parameters are extremely useful to describe the viscoelastic behavior of solutions of Py-HMWSPs. According to the method proposed by Char et al.,⁴⁵ pyrene excimer formation in water occurs in a sequential manner. The two pyrene end-groups are first brought into proximity via diffusion, followed by a rapid process dominated by hydrophobic interaction to form an excimer. Under such circumstances, the kinetics of excimer formation are more complicated than those encountered for diffusion-controlled end-to-end cyclization because the rate of excimer formation is dominated by a combination of a slow diffusive process and a fast process driven by hydrophobic interactions. Therefore, the relationship between the cyclization rate constant (k_{cy}) and the number-average degree of polymerization (N_n) predicted by Willemski and Fixman^{46,47} does not hold when hydrophobic interactions are present.

This report describes how quantitative information about the level of pyrene association and the dynamic processes involved in these associations can be retrieved through the analysis of the fluorescence decays acquired with four pyrene end-labeled PEOs, referred to as PEO(X)-Py₂ where X represents the number average molecular weight (M_n) expressed in kg.mol⁻¹ and equals 2K, 5K, 10K, and 16.5K. These experiments and analyses were conducted over a range of polymer concentrations where pyrene excimer formation took place solely intramolecularly at low polymer concentration and a combination of intra- and intermolecular processes at larger polymer concentrations. Not only do the results obtained in this study fit nicely within the bulk of knowledge already available on pyrene end-labeled PEOs, but this study is also the first example in the literature where the steps leading to excimer formation for PEO(X)-Py₂ samples are probed in a direct manner by time-resolved fluorescence as a function of PEO chain length and PEO(X)-Py₂ concentration.

4.3 Theory

The sequential model was introduced in 1998 to account for the complex kinetics of pyrene excimer formation of pyrene-labeled PEO constructs in water.³⁹ It was applied to dilute aqueous solutions of PEO-Py₂ samples where excimer formation took place only intramolecularly.³⁹ The present study extends the applicability of the original kinetic scheme to conditions where excimer formation occurs both intra- and intermolecularly. These two pathways for excimer formation are described in Scheme 4.1.

According to Scheme 4.1A, the excited pyrene monomers M_1^* and M_2^* encounter a ground-state monomer M to form a pyrene aggregate $M^* \bullet \bullet \bullet M$ (Agg*) intra- and intermolecularly with a rate constant k_{11} and k_{12} , respectively. The two pyrenes forming an aggregate are held together via hydrophobic forces, so that each pyrene is assumed to retain its monomer character and emit with its natural lifetime τ_M . Rapid rearrangement of the two units forming a pyrene aggregate with a rate constant k_2 as well as the direct excitation of preassociated ground-state pyrene dimers (MM) result in the formation of an excimer ($E0^*$) that fluoresces with a lifetime τ_{E0} .



Scheme 4.1: (A) Intra- (top) and inter- (bottom) molecular excimer formation occurring sequentially via the formation of an intermediate pyrene aggregate. (B) Probability distribution function of end-to-end distances for intramolecular pyrene excimer formation.

The differential equations that describe the kinetics involving the species M_1^* , M_2^* , Agg^* , and $E0^*$ introduced in Scheme 4.1A are listed in Equations 4.1 – 4.4.

$$\frac{d[M_1^*]}{dt} = -\left(k_{11} + \frac{1}{\tau_M}\right)[M_1^*] \quad (4.1)$$

$$\frac{d[M_2^*]}{dt} = -\left(k_{12} + \frac{1}{\tau_M}\right)[M_2^*] \quad (4.2)$$

$$\frac{d[Agg^*]}{dt} = k_{11}[M_1^*] + k_{12}[M_2^*] - \left(k_2 + \frac{1}{\tau_M}\right)[Agg^*] \quad (4.3)$$

$$\frac{d[E0^*]}{dt} = k_2[Agg^*] - \frac{1}{\tau_{E0}}[E0^*] \quad (4.4)$$

Integration of Equations 4.1 and 4.2 is trivial and yields the expressions of $[M_1^*]$ and $[M_2^*]$. These expressions are used in Equation 4.3 to determine $[Agg^*]$. Summing $[M_1^*] + [M_2^*] + [Agg^*]$ yields the behaviour of the pyrene monomer given by Equation 4.5.

$$\begin{aligned} [Py^*] = & \left([Agg^*]_o - \frac{k_{11}}{k_2 - k_{11}} [M_1^*]_o - \frac{k_{12}}{k_2 - k_{12}} [M_2^*]_o \right) \exp\left[-\left(k_2 + \frac{1}{\tau_M}\right)t\right] \\ & + \frac{k_2}{k_2 - k_{11}} [M_1^*]_o \exp\left[-\left(k_{11} + \frac{1}{\tau_M}\right)t\right] + \frac{k_2}{k_2 - k_{12}} [M_2^*]_o \exp\left[-\left(k_{12} + \frac{1}{\tau_M}\right)t\right] \end{aligned} \quad (4.5)$$

The expression of $[Agg^*]$ is applied to integrate Equation 4.4 which yields the expression of $[E0^*]$ given in Equation 4.6.

$$\begin{aligned}
[E0^*] = & -\frac{k_2}{k_2 + \frac{1}{\tau_M} - \frac{1}{\tau_{E0}}} \times \left([Agg^*]_o - \frac{k_{11}}{k_2 - k_{11}} [M_1^*]_o - \frac{k_{12}}{k_2 - k_{12}} [M_2^*]_o \right) \exp \left[-\left(k_2 + \frac{1}{\tau_M} \right) t \right] \\
& + \frac{k_{11} [M_1^*]_o}{k_{11} + \frac{1}{\tau_M} - \frac{1}{\tau_{E0}}} \frac{k_2}{k_{11} - k_2} \exp \left[-\left(k_{11} + \frac{1}{\tau_M} \right) t \right] + \frac{k_{12} [M_2^*]_o}{k_{12} + \frac{1}{\tau_M} - \frac{1}{\tau_{E0}}} \frac{k_2}{k_{12} - k_2} \exp \left[-\left(k_{12} + \frac{1}{\tau_M} \right) t \right] \\
& + \left([E0^*]_o + \frac{k_2 k_{11} [M_1^*]_o}{\left(k_{11} + \frac{1}{\tau_M} - \frac{1}{\tau_{E0}} \right) \left(k_2 + \frac{1}{\tau_M} - \frac{1}{\tau_{E0}} \right)} + \frac{k_2 k_{12} [M_2^*]_o}{\left(k_{12} + \frac{1}{\tau_M} - \frac{1}{\tau_{E0}} \right) \left(k_2 + \frac{1}{\tau_M} - \frac{1}{\tau_{E0}} \right)} + \frac{k_2 [Agg^*]_o}{k_2 + \frac{1}{\tau_M} - \frac{1}{\tau_{E0}}} \right) \\
& \exp(-t/\tau_{E0}) \tag{4.6}
\end{aligned}$$

Global analysis of the monomer and excimer fluorescence decays using Equations 4.5 and 4.6 allows the determination of the fractions f_{M1diff} , f_{M2diff} , f_{Mfree} , f_{Magg} , f_{E1diff} , f_{E2diff} , f_{EE0} , and f_{Eagg} , which are given in Equations 4.7 – 4.14.

$$f_{M1diff} = \frac{[Py_{M1diff}^*]_{(t=0)}}{[Py_{M1diff}^*]_{(t=0)} + [Py_{M2diff}^*]_{(t=0)} + [Py_{Magg}^*]_{(t=0)} + [Py_{Mfree}^*]_{(t=0)}} \tag{4.7}$$

$$f_{M2diff} = \frac{[Py_{M2diff}^*]_{(t=0)}}{[Py_{M1diff}^*]_{(t=0)} + [Py_{M2diff}^*]_{(t=0)} + [Py_{Magg}^*]_{(t=0)} + [Py_{Mfree}^*]_{(t=0)}} \tag{4.8}$$

$$f_{Magg} = \frac{[Py_{Magg}^*]_{(t=0)}}{[Py_{M1diff}^*]_{(t=0)} + [Py_{M2diff}^*]_{(t=0)} + [Py_{Magg}^*]_{(t=0)} + [Py_{Mfree}^*]_{(t=0)}} \tag{4.9}$$

$$f_{Mfree} = \frac{[Py_{Mfree}^*]_{(t=0)}}{[Py_{M1diff}^*]_{(t=0)} + [Py_{M2diff}^*]_{(t=0)} + [Py_{Magg}^*]_{(t=0)} + [Py_{Mfree}^*]_{(t=0)}} \quad (4.10)$$

$$f_{E1diff} = \frac{[Py_{E1diff}^*]_{(t=0)}}{[Py_{E1diff}^*]_{(t=0)} + [Py_{E2diff}^*]_{(t=0)} + [Py_{Eagg}^*]_{(t=0)} + [Py_{EE0}^*]_{(t=0)}} \quad (4.11)$$

$$f_{E2diff} = \frac{[Py_{E2diff}^*]_{(t=0)}}{[Py_{E1diff}^*]_{(t=0)} + [Py_{E2diff}^*]_{(t=0)} + [Py_{Eagg}^*]_{(t=0)} + [Py_{EE0}^*]_{(t=0)}} \quad (4.12)$$

$$f_{Eagg} = \frac{[Py_{Eagg}^*]_{(t=0)}}{[Py_{E1diff}^*]_{(t=0)} + [Py_{E2diff}^*]_{(t=0)} + [Py_{Eagg}^*]_{(t=0)} + [Py_{EE0}^*]_{(t=0)}} \quad (4.13)$$

$$f_{EE} = \frac{[Py_{EE0}^*]_{(t=0)}}{[Py_{E1diff}^*]_{(t=0)} + [Py_{E2diff}^*]_{(t=0)} + [Py_{Eagg}^*]_{(t=0)} + [Py_{EE0}^*]_{(t=0)}} \quad (4.14)$$

The fractions obtained from Equations 4.7 – 4.14 can be used to calculate the contributions of f_{diff1} , f_{diff2} , f_{free} , f_{agg} , and f_{E0} according to Equations 4.15 – 4.19.

$$f_{diff1} = \frac{[Py_{diff1}^*]_{(t=0)}}{[Py_{diff1}^*]_{(t=0)} + [Py_{free}^*]_{(t=0)} + [Py_{agg}^*]_{(t=0)} + [Py_{E0}^*]_{(t=0)}} = \left(1 + \frac{f_{Magg}}{f_{M1diff}} + \frac{f_{Mfree}}{f_{M1diff}} + \frac{f_{EE0}}{f_{E1diff}} \right)^{-1} \quad (4.15)$$

$$f_{diff2} = \frac{[Py_{diff2}^*]_{(t=0)}}{[Py_{diff1}^*]_{(t=0)} + [Py_{diff2}^*]_{(t=0)} + [Py_{agg}^*]_{(t=0)} + [Py_{E0}^*]_{(t=0)}} = \left(1 + \frac{f_{Magg}}{f_{M2diff}} + \frac{f_{M1diff}}{f_{M2diff}} + \frac{f_{EE0}}{f_{E2diff}} \right)^{-1}$$

$$= \left(\frac{f_{E2diff}}{f_{E2diff}} + \frac{f_{Eagg}}{f_{E2diff}} + \frac{f_{E1diff}}{f_{E2diff}} + \frac{f_{EE0}}{f_{E2diff}} \right)^{-1} = f_{E2diff} \quad (4.16)$$

$$f_{free} = \frac{[Py_{free}^*]_{(t=0)}}{[Py_{diff1}^*]_{(t=0)} + [Py_{free}^*]_{(t=0)} + [Py_{agg}^*]_{(t=0)} + [Py_{E0}^*]_{(t=0)}} = f_{diff} \times \frac{f_{Mfree}}{f_{Mdiff1}} \quad (4.17)$$

$$f_{agg} = \frac{[Py_{agg}^*]_{(t=0)}}{[Py_{diff1}^*]_{(t=0)} + [Py_{free}^*]_{(t=0)} + [Py_{agg}^*]_{(t=0)} + [Py_{E0}^*]_{(t=0)}} = f_{diff} \times \frac{f_{Magg}}{f_{Mdiff1}} = f_{diff} \times \frac{f_{Eagg}}{f_{Ediff1}} \quad (4.18)$$

$$f_E = \frac{[Py_{E0}^*]_{(t=0)}}{[Py_{diff1}^*]_{(t=0)} + [Py_{free}^*]_{(t=0)} + [Py_{agg}^*]_{(t=0)} + [Py_{E0}^*]_{(t=0)}} = f_{diff} \times \frac{f_{EE0}}{f_{Ediff1}} \quad (4.19)$$

The overall fractions of aggregated pyrene, f_{agg}^{SM} , diffusional pyrene, f_{diff}^{SM} , and isolated pyrene, f_{free}^{SM} of PEO(X)-Py₂ in water can be obtained according to Equations 4.20 – 4.22. The superscript “SM” indicates that the fractions were obtained using the sequential model.

$$f_{agg}^{SM} = f_{agg} + f_{E0} \quad (4.20)$$

$$f_{diff}^{SM} = f_{diff1} + f_{diff2} \quad (4.21)$$

$$f_{free}^{SM} = f_{free} \quad (4.22)$$

4.4 Experimental

Materials: The synthesis of the PEO(X)-Py₂ samples was described elsewhere.⁴⁸ The general chemical structure of the polymers is shown in Figure 4.1. UV-Vis measurements, carried out elsewhere, suggest that all PEO chains were fully end-capped with a pyrene group.⁴⁸ Milli-Q water which was deionized using Millipore Milli-RO 10 Plus and Milli-Q UF Plus (Bedford, MA) systems was used to prepare all aqueous solutions.

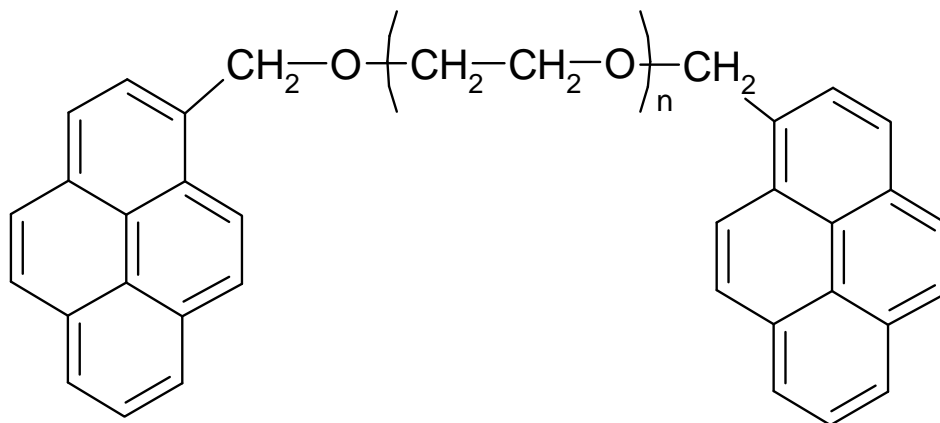


Figure 4.1: Chemical structure of the PEO(X)-Py₂ samples. n equals 45, 113, 227, and 375 for PEO(X)-Py₂ with $X = 2, 5, 10,$ and 16.5 K, respectively.

Steady-state fluorescence measurements: The steady-state fluorescence measurements were performed using a Photon Technology International (PTI) fluorometer with a continuous Ushio UXL-75Xe xenon arc lamp as the light source and a PTI 814 photomultiplier detection system. To avoid the inner filter effect⁴⁹ when acquiring the fluorescence spectra, a triangular cell purchased from Hellma was used for front-face geometry measurements when the absorbance of the solution was greater than 0.1 OD. Below this concentration, a square cell was used to acquire the fluorescence spectra with the right-angle geometry. All PEO(X)-Py₂ samples were excited at a wavelength of 344 nm. The fluorescence intensity of the monomer (I_M) was determined by integrating the fluorescence spectra from 372 to 378 nm. To avoid the residual monomer fluorescence that might have leaked into the excimer emission and would contribute to the I_E/I_M ratio, the fluorescence intensity of the excimer (I_E) was determined by normalizing the fluorescence spectrum acquired with a dilute (2.5×10^{-6} M) aqueous solution of a pyrene monolabeled PEO sample having a molecular weight of 2,000 g/mol (PEO(2K)-Py₁) to that of PEO(X)-Py₂ at the first monomer peak (~ 375 nm), subtracting the normalized spectrum of PEO(2K)-Py₁ from that of PEO(X)-Py₂ and integrating the resulting spectrum

from 500 to 530 nm. Details about the synthesis and characterization of PEO(2K)-Py₁ have been published elsewhere.⁴⁸

Time-resolved fluorescence measurements: The fluorescence decays were acquired by the time-correlated single-photon counting technique (TC-SPC) on an IBH time-resolved fluorometer using a front-face or a right-angle geometry depending on the sample absorption. The excitation source was an IBH 340 nm LED used with a 500 kHz repetition rate. All fluorescence decays were acquired over 1024 channels while ensuring a minimum of 20,000 counts at their maximum. All solutions were excited at 344 nm, and the emission wavelength of the pyrene monomer and excimer were set at 375 and 510 nm, respectively. To reduce potential scattered light, cutoff filters of 370 and 495 nm were used to obtain the fluorescence decays of the pyrene monomer and excimer, respectively. A time per channel of 2.04 ns/ch was used for the acquisition of the monomer and excimer decays of all solutions. For the analyses of the decays, reference decays of degassed solutions of PPO [2,5-diphenyloxazole] in cyclohexane ($\tau = 1.42$ ns) for the pyrene monomer and BBOT [2,5-bis(5-*tert*-butyl-2-benzoxazolyl)thiophene] in ethanol ($\tau = 1.47$ ns) for the pyrene excimer were used to obtain the instrument response function (IRF) via the MIMIC method.⁵⁰

Analysis of the fluorescence decays: To determine τ_M , the fluorescence decay of a dilute (2.5×10^{-6} M) aqueous solution of PEO(2K)-Py₁ was fitted biexponentially. The largest decay time obtained with a pre-exponential weight of 92% was attributed to τ_M . It was found to equal 154 ns and was fixed in the analysis of all fluorescence decays. The global analysis of the decays with Equations 4.5 and 4.6 was carried out with the Marquardt-Levenberg algorithm⁵¹ to obtain the optimized pre-exponential factors and decay times. The fits were considered good with χ^2 being smaller than 1.30, and residuals and autocorrelation of the residuals randomly distributed around zero.

4.5 Results and Discussion

Steady-state fluorescence spectra:

The fluorescence spectra of PEO(*X*)-Py₂ in water were acquired at different PEO(*X*)-Py₂ concentrations. The ratio of the fluorescence intensities of the pyrene excimer over that of the monomer, I_E/I_M , was plotted in Figure 4.2 as a function of PEO(*X*)-Py₂ concentration (C_p) expressed in mol/L using a log-log scale. The data shown in Figure 4.2 can be divided into two regimes where the I_E/I_M ratio of all PEO(*X*)-Py₂ samples remains constant for C_p below 4×10^{-5} M, and increases linearly with polymer concentration for PEO(5K)-Py₂, PEO(10K)-Py₂, and PEO(16.5K)-Py₂ for C_p above 4×10^{-5} M. Char et al.⁴⁴ reported a similar behavior using pyrene end-labeled monodisperse PEOs having weight-average molecular weights of 4800, 9200, and 11200 g/mol. The onset concentration indicating the transition between the two regimes for the PEO(*X*)-Py₂ samples is shown by the dashed line in Figure 4.2 at $C_p = 4 \times 10^{-5}$ M, the same concentration obtained by Char et al.⁴⁴ Here we will refer to this as the critical concentration obtained by fluorescence as C^f . The plateau regime where the I_E/I_M ratio is constant reflects intramolecular pyrene excimer formation while the regime of increasing I_E/I_M ratio observed above C^f for the PEO(*X*)-Py₂ samples other than PEO(2K)-Py₂ results from a mixture of intra- and intermolecular excimer formation.⁴⁴ Interestingly, the I_E/I_M ratio obtained with PEO(2K)-Py₂ does not show any break point and remains constant over the entire range of C_p values presented in Figure 4.2. Furthermore, I_E/I_M obtained with PEO(5K)-Py₂ plateaus when C_p is greater than 5×10^{-4} M.

These effects are due to phase separation of the PEO(2K)-Py₂ and PEO(5K)-Py₂ samples in water, as has been reported earlier.⁴⁴ At high C_p , phase separation could be visually observed. When a 1 g/L solution of PEO(2K)-Py₂ (~ 0.4 mM) was prepared, the sample was not soluble in water and precipitated as a yellow insoluble liquid at the bottom of the solution vial. When phase separation occurred, the sample formed large particles which were insoluble in water and stayed in the polymer-rich layer at the bottom of the cell, suggesting that the solution was saturated in the upper aqueous

layer that is probed by the steady-state fluorometer. Therefore the actual concentration of sample dissolved in water remained constant and no change was observed in the I_E/I_M ratio with increasing C_P . However, it is clear that in this concentration regime, C_P for the entire solution is larger than the polymer concentration in the water saturated portion of the solution that is probed by our fluorescence experiments.

The purpose of this study was to analyze the fluorescence decays of excited pyrene monomer and excimer to obtain quantitative information about the kinetics of pyrene excimer formation. Since these measurements take about 1/2 hour to perform, the stability of the PEO(*X*)-Py₂ solutions needed to be verified over time to ensure that they would remain homogeneous during acquisition of the fluorescence spectra and decays. This was done by monitoring the absorption and fluorescence intensity of PEO(*X*)-Py₂ solutions using the UV-Vis spectrophotometer and steady-state fluorometer, respectively. The absorption and fluorescence spectra overlapped when acquired at different times if the solution did not precipitate over time. It was found that no precipitation occurred when C_P was smaller than 2×10^{-5} M and 2×10^{-4} M for PEO(2K)-Py₂ and PEO(5K)-Py₂, respectively. Above these concentrations, the fluorescence intensity of PEO(2K)-Py₂ and PEO(5K)-Py₂ decreased over time. Therefore, the I_E/I_M ratios and fluorescence decays obtained with PEO(2K)-Py₂ and PEO(5K)-Py₂ for polymer concentrations larger than 2×10^{-5} M and 2×10^{-4} M were not considered in the analysis of the results. In the whole range of C_P given in Figure 4.2 for PEO(10K)-Py₂ and PEO(16.5K)-Py₂, no phase separation was detected. Phase separation is a result of hydrophobic interaction between the pyrene groups.⁴⁴ This attraction is stronger for the shorter PEO chains and at larger C_P .

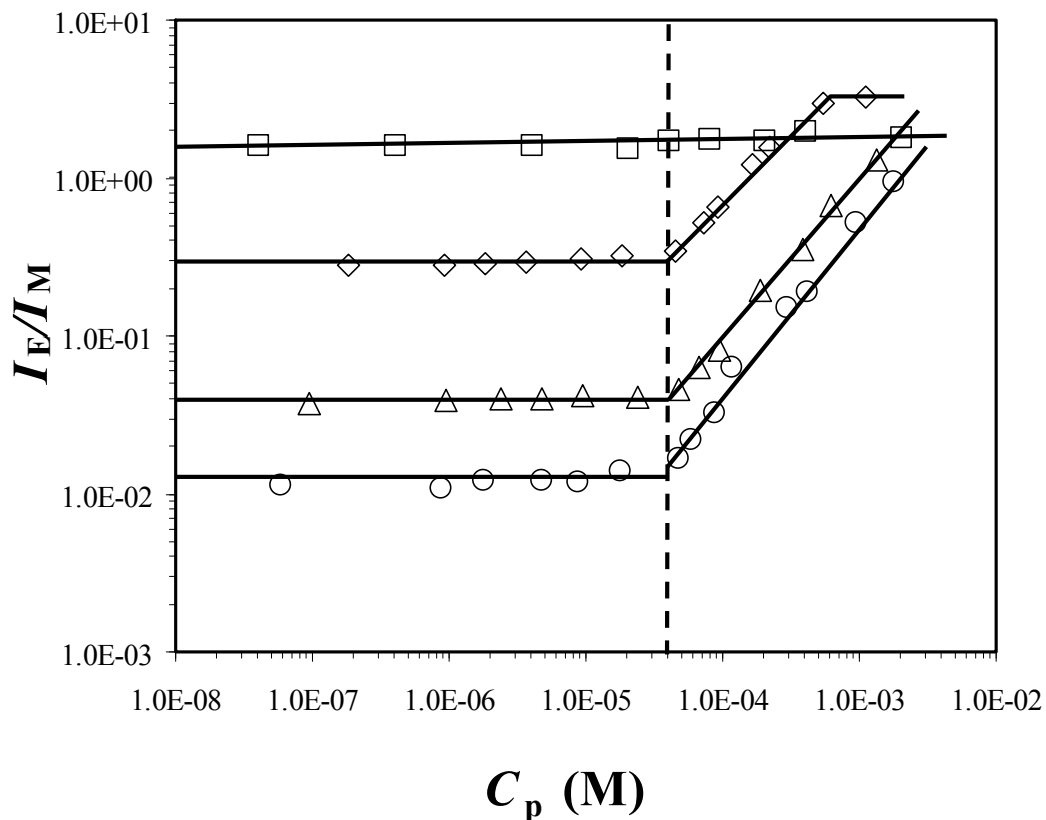


Figure 4.2: I_E/I_M ratio of PEO(2K)-Py₂ (\square), PEO(5K)-Py₂ (\diamond), PEO(10K)-Py₂ (\triangle), and PEO(16.5K)-Py₂ (\circ) as a function of polymer concentration, $\lambda_{\text{ex}}=344$ nm. Solid lines are provided to guide the eye, vertical dashed line indicates $C^F = 4 \times 10^{-5}$ M.

When C_p is less than C^F , I_E/I_M is independent of polymer concentration for all PEO(X)-Py₂ samples, suggesting that each polymer chain is isolated in solution and pyrene excimer formation occurs intramolecularly and depends solely on the local pyrene concentration inside the polymer coil instead of the overall pyrene concentration of the solution.⁵² To investigate how the I_E/I_M ratio varied with the chain length of the PEO(X)-Py₂ samples, the values taken by the I_E/I_M ratio in the plateau regime were averaged over all polymer concentrations smaller than C^F and graphed in Figure 4.3 as a function of the number-average molecular weight (M_n) of the samples as a log-log plot. A straight line

was obtained with a slope of -2.3 ± 0.1 . A log-log plot of the I_E/I_M ratios versus the molecular weight of the sample studied by Char et al.⁴⁴ yields a straight line with an identical slope of -2.3 ± 0.2 . Differences in the absolute I_E/I_M ratios between this study and Char's result from differences in the analysis of the fluorescence spectra. The trends shown in Figure 4.3 indicate that the I_E/I_M ratio scales as $M_n^{-2.3 \pm 0.2}$ for PEO(*X*)-Py₂ in water. This scaling law, however, disagrees with that obtained for the PEO(*X*)-Py₂ samples in organic solvents where pyrene and PEO are soluble and pyrene excimer is formed by diffusive encounters between the two pyrene end groups.⁴⁸ In organic solvents, the I_E/I_M ratio was found to scale as $\eta^{-1} \times N_n^{-1.6}$, where N_n is the number-average degree of polymerization and is proportional to the molecular weight of PEO.⁴⁸ This scaling relationship agrees with theoretical work conducted by Wilemski and Fixman^{46,47} but is no longer valid for PEO(*X*)-Py₂ in aqueous solutions where pyrene aggregates.

When C_p is larger than C^F , the I_E/I_M ratio of PEO(*X*)-Py₂ increases linearly with increasing polymer concentration as pyrene excimer formation occurs intra- and intermolecularly in this concentration regime. The slopes of the straight lines equal 0.97 ± 0.01 , 0.99 ± 0.03 and 1.00 ± 0.03 for PEO(5K)-Py₂, PEO(10K)-Py₂, and PEO(16.5K)-Py₂, respectively. The data obtained with PEO(5K)-Py₂ at concentrations larger than 2×10^{-4} M were not used to obtain the slopes due to the phase separation that occurs with some of the samples. A linear increase in I_E/I_M with C_p is usually attributed to intermolecular pyrene excimer formation via diffusional encounters.^{53,54}

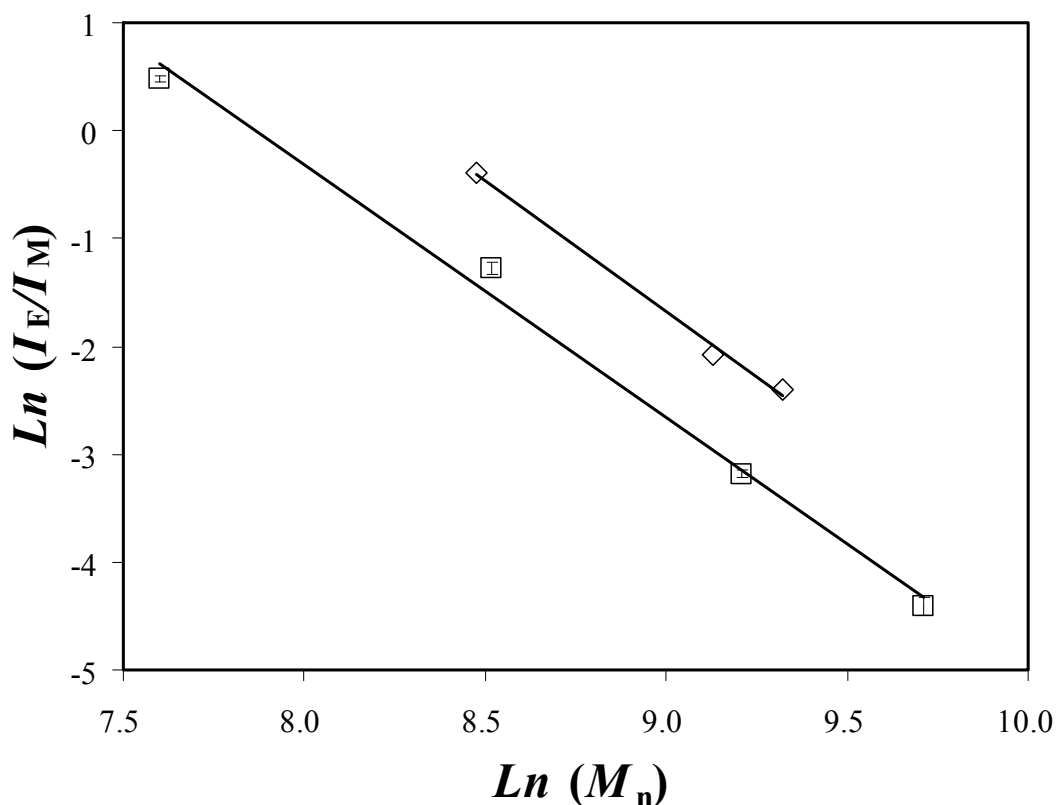


Figure 4.3: The natural log-log plot of I_E/I_M ratios at $C_P < C^F$ versus PEO molecular weights. Data obtained in this study (□) and by Char et al.⁴⁴ (◇).

Another interesting result from the data in Figure 4.2 also observed by Char et al.⁴⁴ is that the break point occurs at $C^F = 4 \times 10^{-5}$ M for all PEO(X)-Py₂ samples regardless of their molecular weight. At concentrations beyond the break point the polymer chains interact with other polymer chains, resulting in intermolecular excimer formation. C^F would thus be expected to mark the boundary between the dilute and the semi-dilute regime, typically described by C^* , the overlap concentration. C^* is taken as the inverse of the intrinsic viscosity ($[\eta]$).^{52,55} $[\eta]$ for unmodified PEO in water can be estimated from the Mark-Houwink-Sakurada parameters $K = 49.9 \times 10^{-3}$ mL.g⁻¹ and $a = 0.67$.⁵⁶ Therefore, C^* is determined to equal 1.33×10^{-2} , 4.19×10^{-3} and 1.81×10^{-3} M for PEO(5K), PEO(10K) and PEO(16.5K), respectively. Not only does C^* change more than 7-fold between PEO(5K) and

PEO(16.5K), but it is also 45 – 330 times larger than $C^F = 4 \times 10^{-5}$ M. That C^F be so much smaller than C^* can be easily understood by noting that C^* and C^F represent static and dynamic descriptions of the polymer solutions, respectively. Indeed, the fact that two polymer coils are not overlapping at concentrations $C_p < C^*$ does not imply that the polymer coils are completely isolated from one another. Brownian motions allow them to diffuse in solution and encounter each other, leading to intermolecular excimer formation for concentrations $C_p > C^F$. The independence of C^F on molecular weight indicates that C^F depends on pyrene concentration rather than chain length. C^F is simply the pyrene concentration describing the boundary between two regimes, whether C_p is smaller or larger than C^F corresponding to regimes where pyrene excimer formation occurs intra- or intermolecularly.

Analysis of the fluorescence decays:

The pyrene monomer and excimer fluorescence decays of PEO(*X*)-Py₂ in water at various polymer concentrations were acquired and globally fitted according to the sequential model (SM). The programs used to fit the decays obtained under various conditions are slightly different due to the complicated kinetics of pyrene excimer formation encountered in this study. When C_p is smaller than C^F , the pyrene excimer is formed intramolecularly via hydrophobic interactions between two pyrene pendants with a rate constant k_2 , diffusional encounters with a rate constant k_{11} , and direct excitation of ground-state pyrene dimers. At C_p larger than C^F , intermolecular pyrene excimer formation is accounted for with the rate constant k_{12} . However, it should be noted that k_{12} must be smaller than k_{11} . As k_{11} decreases dramatically with increasing polymer chain length, k_{11} becomes very small for PEO(10K)-Py₂ and too small to be obtained for PEO(16.5K)-Py₂, to the point where k_{11} becomes comparable to k_{12} . Therefore, only one rate constant (k_{diff}) was used to represent the pyrenes forming excimer via diffusion for PEO(10K)-Py₂ and PEO(16.5K)-Py₂ solutions at $C_p > C^F$. Below C^F , the fraction of pyrenes that cannot form excimer, f_{free} , is not equal to zero due to the presence of PEO chains monolabeled with pyrene that act as fluorescent impurities for the shorter chains⁵⁷ and pyrene groups which are too far from each other to form an excimer for the longer chains,⁴⁸ or a combination of both effects. Above C^F , f_{free} for PEO(5K)-Py₂ was set to equal zero and f_{free} obtained for PEO(10K)-

Py₂ and PEO(16.5K)-Py₂ took small values close to zero as expected in this polymer concentration regime where excimer is formed intermolecularly.

The fluorescence decays could not be fitted globally since the excimer decays showed no rise time. The absence of a rise time was observed under two conditions. First, the excimer decay of PEO(2K)-Py₂ and PEO(5K)-Py₂ showed no rise time at concentrations larger than 4×10^{-5} and 5×10^{-4} M, respectively. These concentrations lay in the regime where the solutions undergo phase separation. The excimer decays obtained for the two largest concentrations of PEO(5K)-Py₂ in Figure 4.2 do not show a rise time at the early times of the excimer decays, suggesting that the kinetics between the excited monomer and excimer are no longer coupled. Figure 4.4A shows the excimer decays of PEO(5K)-Py₂ acquired at concentrations of 5×10^{-4} M and 1.25×10^{-6} M. No rise time was observed with the solution at the higher polymer concentration. The plateau observed for the I_E/I_M ratios at $C_p > 5 \times 10^{-4}$ M for PEO(5K)-Py₂ in Figure 4.2 and the lack of rise time in the excimer decays is certainly a consequence of the phase separation undergone by these solutions at higher C_p . Second, PEO(16.5K)-Py₂ solutions at C_p below 6×10^{-5} M form little excimer. The excimer decays obtained for all the PEO(*X*)-Py₂ samples at a pyrene concentration of 2.5×10^{-6} M are shown in Figure 4.4B. Compared with the other three samples the excimer decay obtained with PEO(16.5K)-Py₂ shows no rise time, indicating that the monomer and excimer decays acquired with this solution cannot be fitted globally.

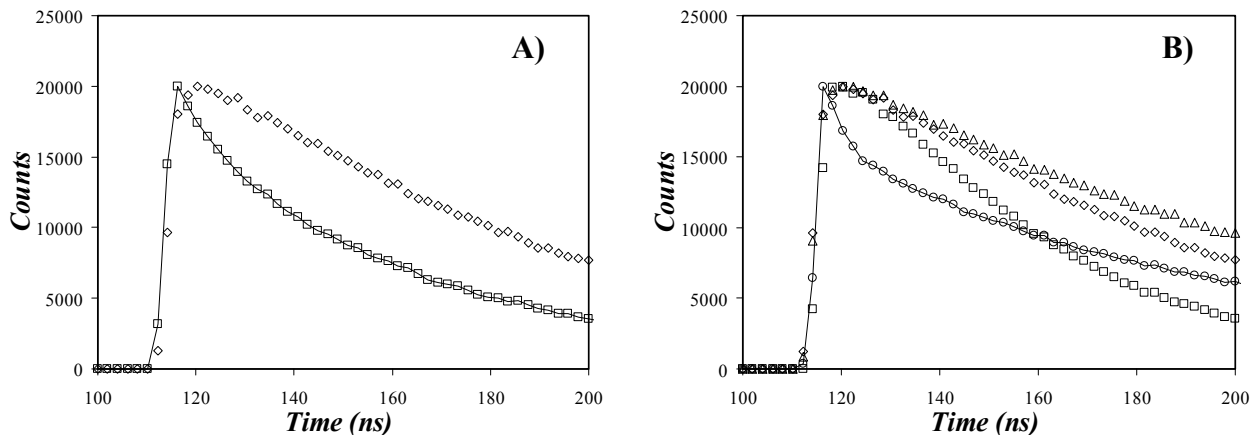


Figure 4.4: The excimer fluorescence decays obtained with (A) PEO(5K)-Py₂ at 5×10^{-4} M (\square) and 1.25×10^{-6} M (\diamond) and (B) PEO(2K)-Py₂ (\square), PEO(5K)-Py₂ (\diamond), PEO(10K)-Py₂ (\triangle) and PEO(16.5K)-Py₂ (\circ) at 1.25×10^{-6} M. The solid lines are drawn for those decays where no rise time was detected at the beginning of the decays. $\lambda_{\text{ex}} = 344$ nm, $\lambda_{\text{em}} = 510$ nm.

All the other decays were successfully fitted by the SM yielding χ^2 smaller than 1.30, and residuals and autocorrelation of the residuals randomly distributed around zero. An example of the fits is shown in Figure 4.5, obtained by analyzing the pyrene monomer and excimer fluorescence decays of PEO(5K)-Py₂ at $[\text{Py}] = 2.5 \times 10^{-6}$ M. The small excimer rise time suggests that excimer formation occurs on a fast time scale, as was observed by Lee and Duhamel for another series of pyrene-labeled PEOs whose fluorescence decays were analyzed with the SM.³⁹ The differences in rise times obtained for the excimer decays acquired in water and those acquired in organic solvents^{39,44,48} reflect differences in the kinetics of excimer formation.

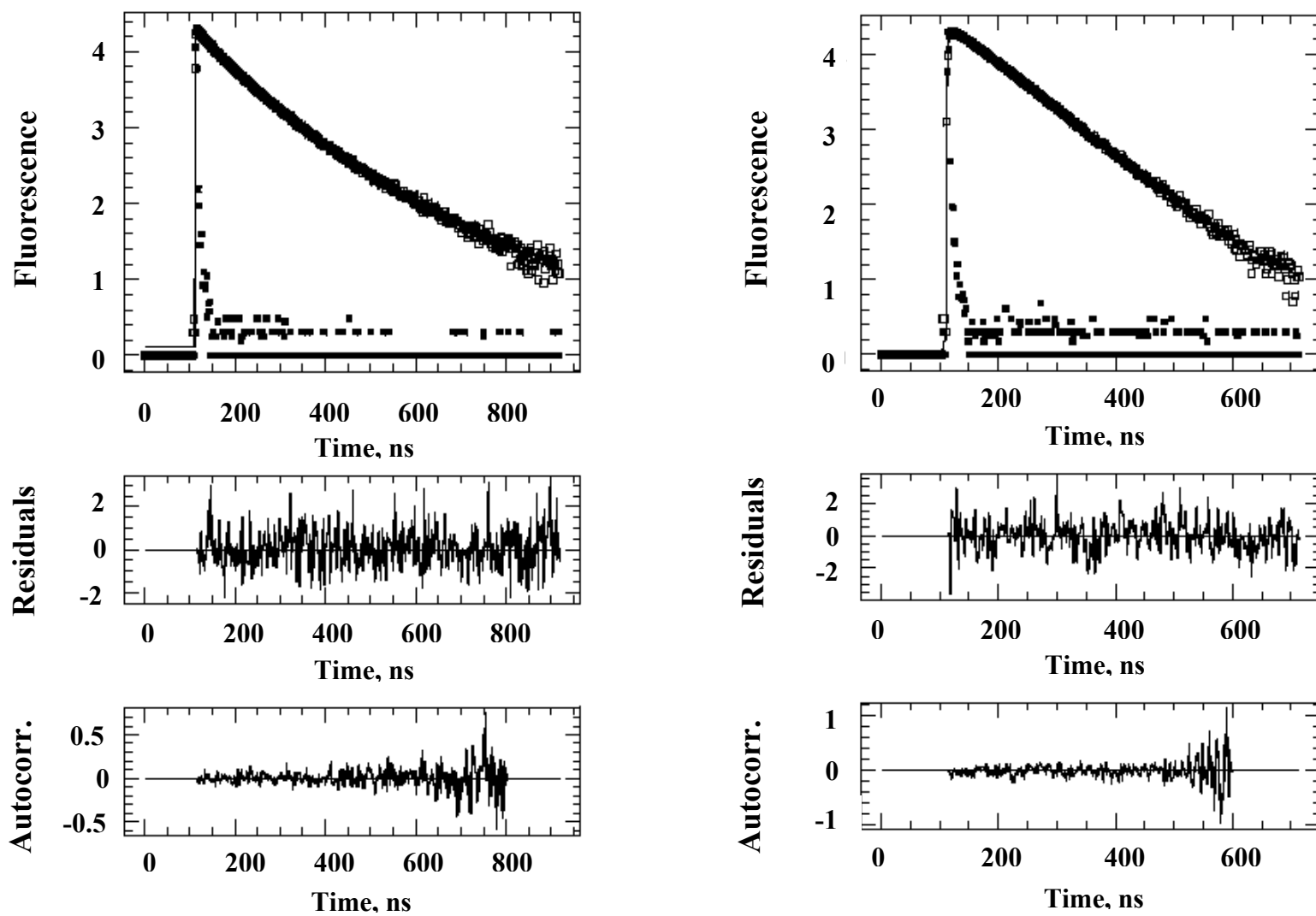


Figure 4.5: SM analysis of the fluorescence decays of the pyrene monomer (left; $\lambda_{\text{ex}} = 344 \text{ nm}$, $\lambda_{\text{em}} = 375 \text{ nm}$) and excimer (right; $\lambda_{\text{ex}} = 344 \text{ nm}$, $\lambda_{\text{em}} = 510 \text{ nm}$) of PEO(5K)-Py₂ in water at $[\text{Py}] = 2.5 \times 10^{-6} \text{ M}$ with a time per channel of 2.04 ns/ch. $\chi^2 = 1.18$.

The parameters retrieved from the SM analysis of the fluorescence decays are listed in Table SI.4.1 of the Supporting Information (SI). Using Equations 4.15 – 4.22, the molar fractions of pyrenes associating via hydrophobic interactions (f_{agg}^{SM}), forming excimer by diffusion (f_{diff}^{SM}), and being excited without forming excimer (f_{free}^{SM}) were determined and are listed in Table SI.4.2. These fractions were plotted as a function of C_p for each PEO(*X*)-Py₂ sample in Figure 4.6. The fractions f_{E0} , f_{agg} , f_{diff1} , and f_{diff2} used to calculate f_{agg}^{SM} , f_{diff}^{SM} , and f_{free}^{SM} were also plotted in Figure 4.6. For PEO(2K)-Py₂, Figure 4.6A shows that most pyrene groups are aggregated ($f_{agg}^{SM} = 0.97$) at low C_p . All the fractions remained constant in the dilute regime, where excimer is formed intramolecularly. Figure 4.6B shows that f_{agg}^{SM} for PEO(5K)-Py₂ in the dilute regime is lower than f_{agg}^{SM} for PEO(2K)-Py₂ and more pyrene excimer is formed by intramolecular diffusion. When C_p is increased above C^F , f_{agg}^{SM} increases and f_{diff}^{SM} decreases indicating that as more PEO(5K)-Py₂ sample is being added to the solution, the pyrene groups form more intermolecular hydrophobic aggregates and consequently more excimer is formed by direct excitation of pyrene aggregates rather than by diffusive encounters. Excimer formation occurs mostly intramolecularly as f_{diff1} represents the main contribution to f_{diff}^{SM} , while f_{diff2} remains small and constant as a function of C_p . For PEO(10K)-Py₂, Figure 4.6C shows that f_{agg}^{SM} is very small in the dilute regime with about 10% of the pyrene groups being associated. In fact, 90% of the pyrene pendants are not associated. Furthermore, around 70% of the excited pyrenes form excimer by diffusive encounter with a ground-state pyrene located at the opposite PEO chain end. At first glance, this result is a little surprising since it seems to disagree with the hydrophobic nature of pyrene. However it agrees with an earlier study by the Winnik group, which showed that only 7% of the pyrene end-groups were pre-associated in water for pyrene end-labeled monodisperse PEO having a molecular weight of 8000.⁴⁰ The rather weak associative character of this PEO(*X*)-Py₂ constructs is unexpected when it is compared to the strong associative behavior of commercial HEURs bearing

alkyl hydrophobes which are known to form rosette micelles in water at very low polymer concentration.

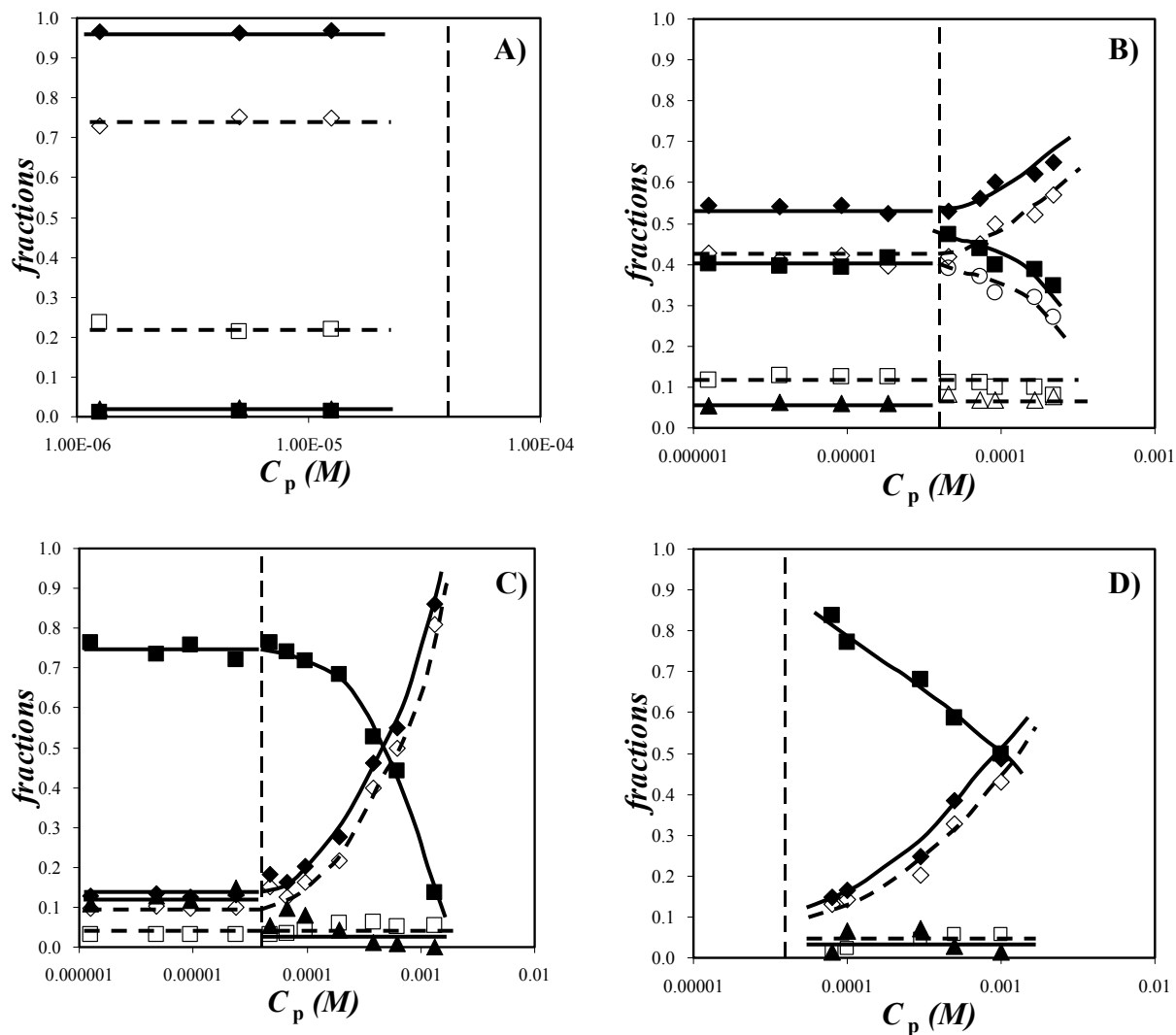


Figure 4.6: Fractions f_{agg}^{SM} (\blacklozenge), f_{diff}^{SM} (\blacksquare), and f_{free}^{SM} (\blacktriangle), as well as the fractions f_{agg} (\square), f_{E0} (\diamond), f_{diff1} (\circ), and f_{diff2} (\triangle) used to calculate f_{agg}^{SM} , f_{diff}^{SM} and f_{free}^{SM} as a function of C_p obtained with (A) PEO(2K)-Py₂, (B) PEO(5K)-Py₂, (C) PEO(10K)-Py₂, and (D) PEO(16.5K)-Py₂. The vertical dashed lines represent the position of C^F .

The weak associative character of the PEO(*X*)-Py₂ samples leads to two conclusions. First, the small fraction f_{agg}^{SM} is probably due to interactions taking place between the pyrene groups and the PEO chain, which reduces the drive of the pyrene groups to associate in water. Second, the hydrophobicity of pyrene is dramatically decreased after its covalent attachment onto the hydrophilic long PEO chains. When $C_p > C^F$, f_{agg}^{SM} increases and f_{diff}^{SM} decreases for PEO(10K)-Py₂ and PEO(16.5K)-Py₂ due to the formation of intermolecular pyrene aggregates. This behavior is similar to that observed with PEO(5K)-Py₂. At the largest C_p , f_{free}^{SM} decreases to around zero as all pyrene species are contributing to excimer formation. PEO(16.5K)-Py₂ shows a trend similar to that of PEO(10K)-Py₂ at higher C_p in Figure 4.6D. As mentioned earlier, the absence of a rise time for the excimer decays acquired in the dilute regime (i.e. with $C_p < 4 \times 10^{-5}$ M) prevents the global analysis of the decays of PEO(16.5K)-Py₂ (see Figure 4.4B).

The rate constants obtained for intramolecular (k_{11}) and intermolecular (k_{12}) excimer formation by diffusion for PEO(2K)-Py₂ and PEO(5K)-Py₂, and for diffusive excimer formation (k_{diff}) for PEO(10K)-Py₂ and PEO(16.5K)-Py₂, as well as for excimer formation between two pyrenes inside the capture distance (k_2) were obtained from the global analysis of the fluorescence decays with Equations 4.5 and 4.6. They are plotted as a function of C_p in Figures 4.7 and 4.8. For PEO(2K)-Py₂ and PEO(5K)-Py₂, k_{12} was set to equal zero for $C_p < C^F$ because no excimer can be formed by intermolecular diffusion at low concentration. As more polymer was added to the solution, the fits required a non-zero k_{12} and the recovered k_{12} increased with increasing concentration for PEO(5K)-Py₂. The k_{11} values obtained for PEO(2K)-Py₂ and PEO(5K)-Py₂ are larger than the rate constant of cyclization (k_{cy}) obtained for these samples in *N,N*-dimethylformamide (DMF),⁴⁸ which has a viscosity (0.79 mPa.s at 25 °C) similar to that of water (0.89 mPa.s at 25 °C).⁵⁸ If pyrene in water interacts with a section of the PEO chain, a smaller part of the chain would remain free to constitute the polymer coil, reducing its overall dimension, thus increasing the local pyrene concentration and k_{11} . Since the rate constant of intermolecular pyrene excimer formation k_{12} cannot be larger than k_{11} ,

only one rate constant representing pyrene excimer formation by diffusion (k_{diff}) was applied to PEO(10K)-Py₂ and PEO(16.5K)-Py₂ because their k_{11} value is known to be much smaller than that of the samples with shorter PEO chain length.⁴⁸ Figures 4.7C and 4.7D show that k_{diff} of PEO(10K)-Py₂ and PEO(16.5K)-Py₂ increases with C_p for $C_p > C^F$ as expected when intermolecular excimer formation takes place.

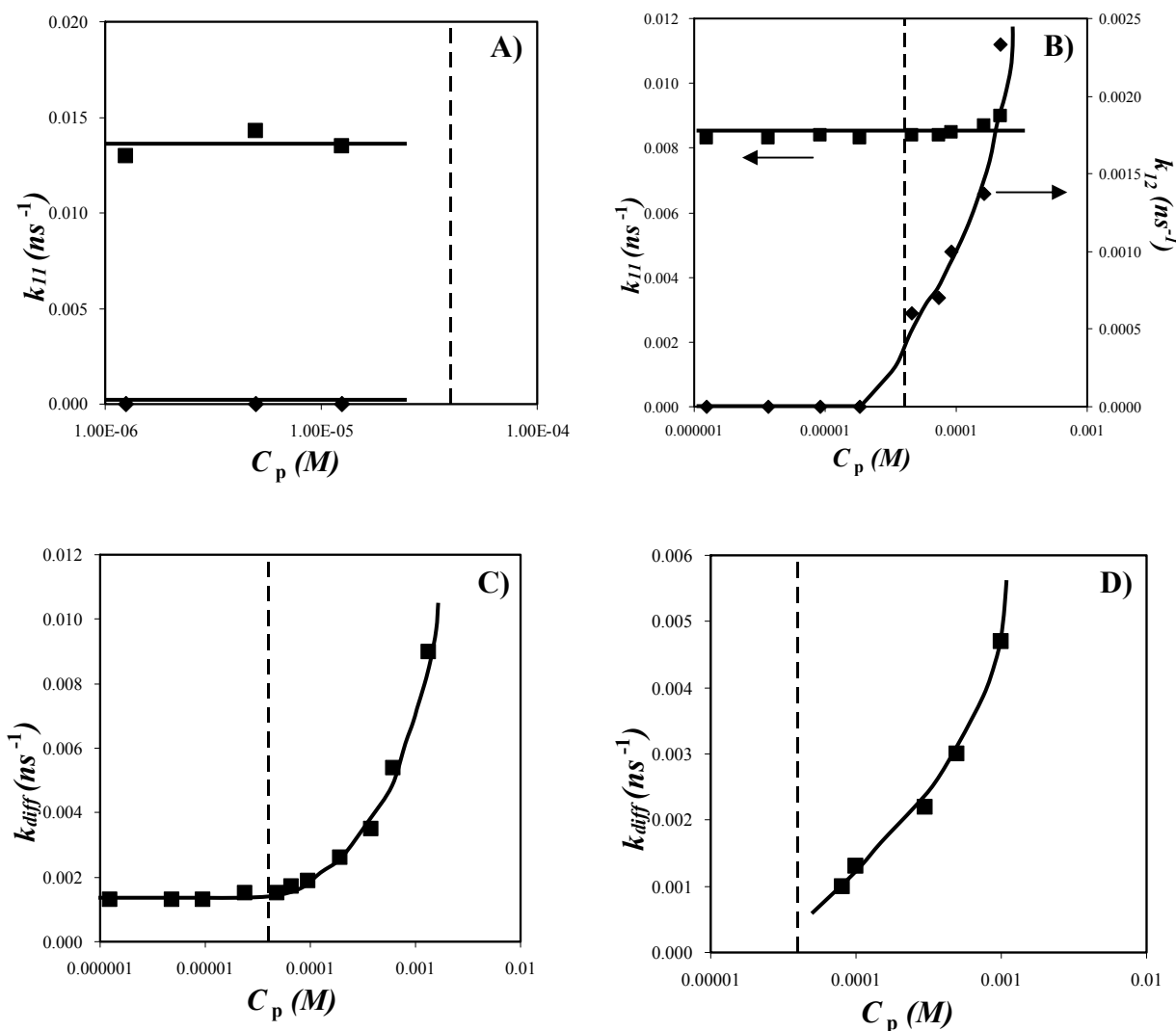


Figure 4.7: Rate constants as a function of C_p , k_{11} (■), and k_{12} (◆) obtained with (A) PEO(2K)-Py₂, and (B) PEO(5K)-Py₂, k_{diff} (■) obtained with (C) PEO(10K)-Py₂, and (D) PEO(16.5K)-Py₂. The dash lines represent the position of C^F .

The rate constant describing pyrene excimer formation through hydrophobic interactions, k_2 , was found to be independent of PEO chain length and C_P , as shown in Figure 4.8. This result is expected from the definition of k_2 which represents an intrinsic property of pyrene in water reflecting the rapid re-arrangement of two pyrene groups within their capture volume. After averaging, k_2 was found to equal $7.3(\pm 0.5) \times 10^7 \text{ s}^{-1}$, which is three times smaller than the k_2 value of $2.3(\pm 0.5) \times 10^8 \text{ s}^{-1}$ found by Lee and Duhamel,³⁹ probably because the hydrophobic attraction induced by the pyrenebutyric linker used in the latter study was stronger than for the pyrenemethyl linker used in this study.

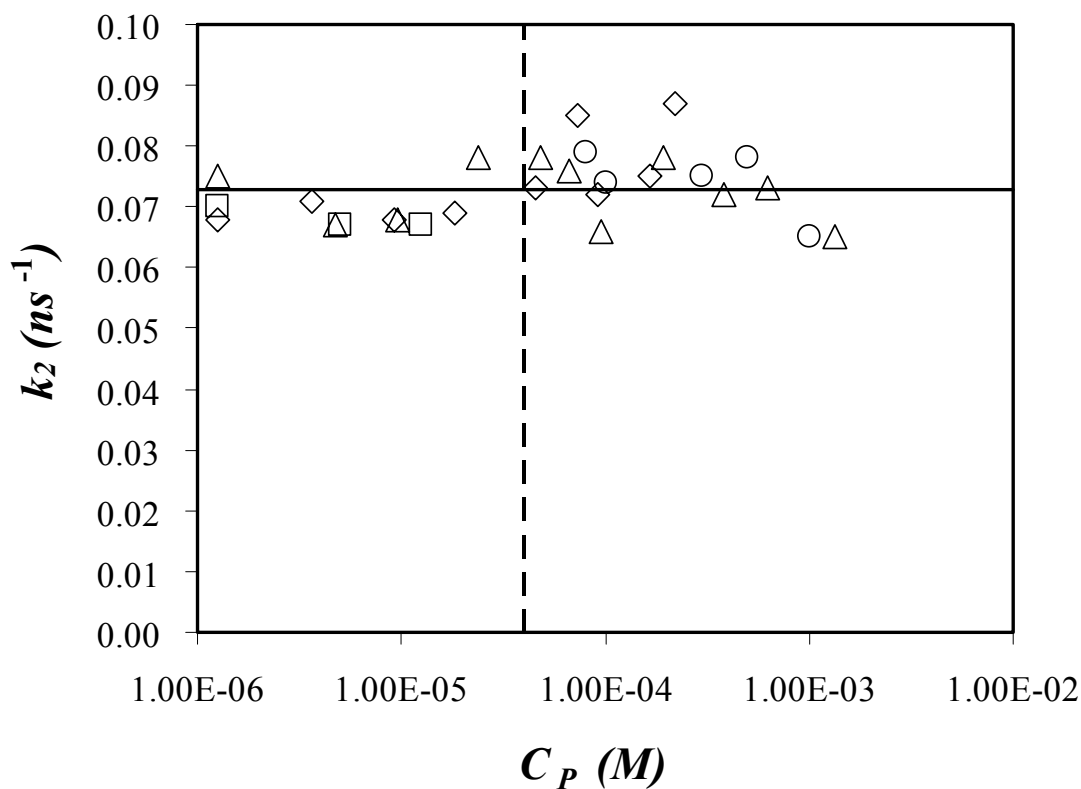


Figure 4.8: Plot of k_2 obtained for PEO(2K)-Py₂ (\square), PEO(5K)-Py₂ (\diamond), PEO(10K)-Py₂ (Δ) and PEO(16.5K)-Py₂ (\circ) as a function of C_P . The dashed line represents the position of C^F and the horizontal solid line represents the average value of k_2 .

The fractions f_{agg}^{SM} , f_{diff}^{SM} , and f_{free}^{SM} obtained for PEO(2K)-Py₂, PEO(5K)-Py₂, and PEO(10K)-Py₂ for $C_p < C^F$ were averaged and plotted as a function of PEO molecular weight in Figure 4.9A. f_{agg}^{SM} decreases dramatically with increasing PEO chain length, reflecting the stronger hydrophobic interaction experienced by the shorter polymers. The rate constants k_{11} and k_2 averaged for $C_p < C^F$ were also plotted as a function of PEO molecular weight in Figure 4.9B. k_{11} decreases significantly with increasing molecular weight as $M_n^{-\alpha}$ with α found to equal 1.4 ± 0.5 , in agreement with the reported values of α ranging from 0.9 to 1.9 for the diffusion-controlled end-to-end cyclization of linear chains without rapid capture process.^{48,59-67} k_2 remained constant and significantly larger than k_{11} for the three samples because k_2 characterizes the behavior of pyrene inside the capture volume, which is a characteristic feature of pyrene and does not change with chain length, while k_{11} represents pyrene motions inside the volume of the polymer coil (V_{coil}) that is outside the capture volume, and this volume increases with the pyrene chain length. Another important observation is that according to the fractions obtained for PEO(10K)-Py₂ for $C_p < C^F$, this sample should behave in water in a manner similar to in organic solvents since most of the excimer is formed by diffusion. However, the excimer decay in water (see Figure 4.4B) does not exhibit the pronounced rise time observed in organic solvents.⁴⁸ This behavior is due to the large k_2 values which are at least 60 times larger than k_{diff} . Although f_{agg}^{SM} is much smaller than f_{diff}^{SM} , the rapid excimer formation within the capture distance results in a less apparent rise time in the excimer decay.

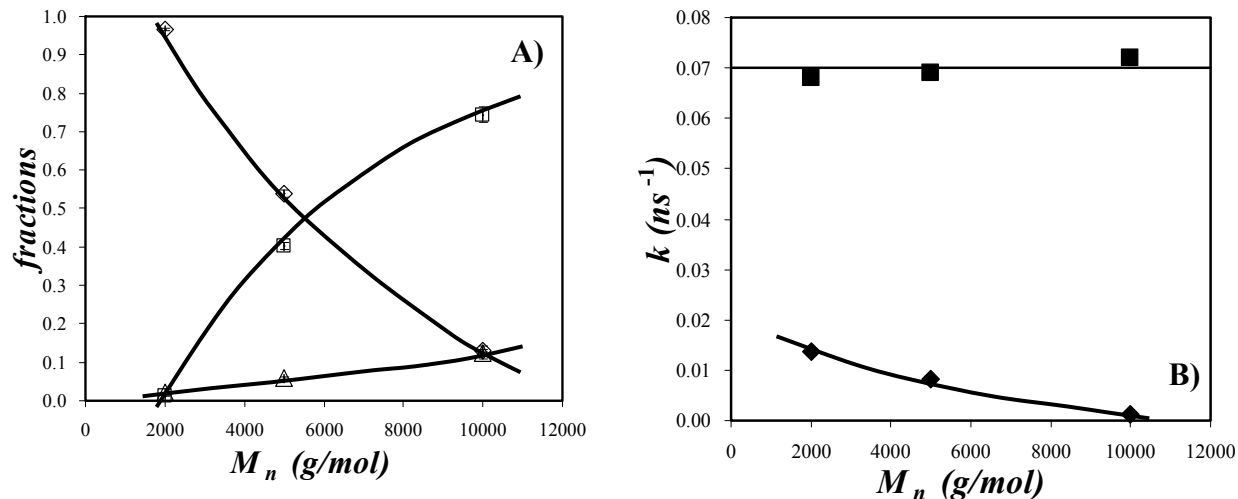


Figure 4.9: (A) molar fractions of f_{agg}^{SM} (\diamond), f_{diff}^{SM} (\square), and f_{free}^{SM} (\triangle) and (B) rate constants of k_{11} (\diamond) and k_2 (\blacksquare) as a function of PEO molecular weight.

Determination of the capture radius (R_c):

The behavior of PEO(X)-Py₂ in the dilute regime ($C_p < C^F$) reflects the process of intramolecular excimer formation. In this regime, the kinetics of pyrene excimer formation are controlled by the end-to-end cyclization (EEC) of a single polymer chain that brings the pyrene end-groups within the capture radius where excimer formation is induced by strong hydrophobic interaction. The intrinsic hydrophobicity of pyrene affects the EEC of the PEO(X)-Py₂ constructs in water compared to organic solvents. Char et al.⁴⁵ first introduced a “capture process” to handle these hydrophobic interactions and estimated experimentally that the capture radius of a pyrene group in water equals ~ 2.0 nm based on an analysis of the I_E/I_M ratios obtained by steady-state fluorescence. In the present study, R_c of the pyrene pendants attached onto the PEO(X)-Py₂ constructs was first determined according to Char’s method using the steady-state fluorescence data and then from the fraction of pyrene groups that are subject to hydrophobic interactions (f_{E0}) obtained directly from the analysis of the fluorescence decays using the SM. In turn, f_{E0} is related to the probability of finding the two ends of the polymer coil within the capture volume defined as a sphere of radius R_c .

The probability of having the two pyrene end-groups separated by a given end-to-end distance (r_{EE}) is given by Equation 4.23 by assuming that the polymer coil adopts a Gaussian conformation in solution.

$$\Pr(r_{EE}) = \left(\frac{m}{\pi}\right)^{3/2} \exp(-mr_{EE}^2) \quad (4.23)$$

The parameter m in Equation 4.23 equals $3/(2 \times N_n)$ with N_n being the number-average degree of polymerization of PEO.⁴⁵

In Scheme 4.1B, the polymer segments distribute themselves in a three dimensional space according to a random walk. However, once the distance between the two chain ends is less than the capture distance $2 \times R_c$, the pyrene end-groups come into contact quasi-instantaneously to generate a ground-state pyrene dimer yielding a zero end-to-end distance. Upon excitation, these ground-state pyrene aggregates form excimer instantaneously and the molar fraction of this excited pyrene species can be described by f_{E0} . Therefore, f_{E0} is given by Equation 4.24 which includes all polymer conformations where the end-to-end distance is smaller than $2 \times R_c$ according to Scheme 4.1B.

$$f_{E0} = \int_0^{2R_c} 4\pi r_{EE}^2 \Pr(r_{EE}) dr_{EE} \quad (4.24)$$

For the pyrene end-groups separated by a distance larger than $2 \times R_c$, the distribution of polymer chain ends is not affected by hydrophobic interactions and the pyrene end-groups diffuse randomly in solution within the polymer coil. The mean-square end-to-end distance $\langle R^2 \rangle$ can be expressed by Equation 4.25.

$$\langle R^2 \rangle = (1 - f_{E0}) \int_{2R_c}^{\infty} 4\pi r_{EE}^4 \Pr(r_{EE}) dr_{EE} \quad (4.25)$$

According to Equations 4.23 – 4.25, Char et al.⁴⁵ derived the expressions of f_{E0} and $\langle R^2 \rangle$ which are functions of R_c and are given in Equations 4.26 and 4.27, respectively.

$$f_{E0} = 4\pi \left(\frac{m}{\pi}\right)^{3/2} \left[-\frac{R_c}{m} \exp(-4mR_c^2) + \frac{\sqrt{\pi/m}}{4m} \operatorname{erf}(2R_c\sqrt{m}) \right] \quad (4.26)$$

$$\langle R^2 \rangle = (1 - f_{E0}) 4\pi \left(\frac{m}{\pi}\right)^{3/2} \left[\frac{R_c \left(4R_c^2 + \frac{3}{2m}\right)}{m} \exp(-4mR_c^2) + \frac{3\sqrt{\pi/m}}{8m^2} \operatorname{erfc}(2R_c\sqrt{m}) \right] \quad (4.27)$$

R_c in Equations 4.26 and 4.27 was normalized by the length of an ethylene oxide repeating segment which Char et al. approximated to equal 0.439 nm. m in Equations 4.26 and 4.27 equals $3/(2 \times N_n)$. For a Gaussian chain without capture distance ($R_c = 0$), the normalization applied to R_c implies that $\langle R^2 \rangle$ in Equation 4.27 equals N_n , namely a unitless end-to-end distance due to the normalization of R_c .

Numerous reports predict that I_E/I_M scales as $\langle R^2 \rangle^{-\alpha}$, with α ranging from 0.9 to 1.9.^{48,59–67} The exponent α was fixed to equal 1.5 by Char et al.⁴⁵ who determined R_c using the I_E/I_M ratios of different PEO(X)-Py₂ constructs in mixtures of water and methanol having different methanol contents.⁴⁵ Char et al. found an R_c value of 2.0 nm in water by comparing the ratios $(I_E/I_M)_1/(I_E/I_M)_2$ of the I_E/I_M ratios of polymer samples 1 and 2 obtained by the ratios $\langle R^2 \rangle_1^{-1.5} / \langle R^2 \rangle_2^{-1.5}$ that were determined with Equation 4.27. The ratios $\langle R^2 \rangle_1^{-1.5} / \langle R^2 \rangle_2^{-1.5}$, namely the ratios

$\langle R^2 \rangle_{2K}^{-1.5} / \langle R^2 \rangle_{5K}^{-1.5}$, $\langle R^2 \rangle_{2K}^{-1.5} / \langle R^2 \rangle_{10K}^{-1.5}$, $\langle R^2 \rangle_{2K}^{-1.5} / \langle R^2 \rangle_{16.5K}^{-1.5}$,
 $\langle R^2 \rangle_{5K}^{-1.5} / \langle R^2 \rangle_{10K}^{-1.5}$, $\langle R^2 \rangle_{5K}^{-1.5} / \langle R^2 \rangle_{16.5K}^{-1.5}$, and $\langle R^2 \rangle_{10K}^{-1.5} / \langle R^2 \rangle_{16.5K}^{-1.5}$, were plotted as a
function of R_c in Figure 4.10. An R_c value of $4.2 \times 0.439 \text{ nm} = 1.9(\pm 0.2) \text{ nm}$ (the square symbols) best
matched the trends shown in Figure 4.10 for the $(I_E/I_M)_{5K}/(I_E/I_M)_{10K}$, $(I_E/I_M)_{10K}/(I_E/I_M)_{16.5K}$, and
 $(I_E/I_M)_{10K}/(I_E/I_M)_{16.5K}$ ratios obtained experimentally. This R_c value is in good agreement with $R_c = \sim 2.0$
nm found by Char et al.⁴⁵ However, Figure 4.10 showed that the $\langle R^2 \rangle_{2K}^{-1.5} / \langle R^2 \rangle_{5K}^{-1.5}$,
 $\langle R^2 \rangle_{2K}^{-1.5} / \langle R^2 \rangle_{10K}^{-1.5}$, and $\langle R^2 \rangle_{2K}^{-1.5} / \langle R^2 \rangle_{16.5K}^{-1.5}$ ratios obtained at a unitless R_c of 4.2 were
significantly overestimated compared to the $(I_E/I_M)_{2K}/(I_E/I_M)_{5K}$, $(I_E/I_M)_{2K}/(I_E/I_M)_{10K}$, $(I_E/I_M)_{2K}/(I_E/I_M)_{16.5K}$
ratios (the cross symbols) obtained experimentally. Pyrene excimers formed by direct excitation of
pyrene aggregates are known to emit less efficiently than those formed from diffusional encounters
between two pyrene moieties.^{23,68,69} Indeed, this effect would be stronger for the PEO(2K)-Py₂
solutions which yielded a fraction f_{agg}^{SM} of approximately 100%. Therefore the I_E/I_M ratio obtained
with the PEO(2K)-Py₂ construct might yield erroneous estimates of R_c , as seems to be the case in
Figure 4.10.

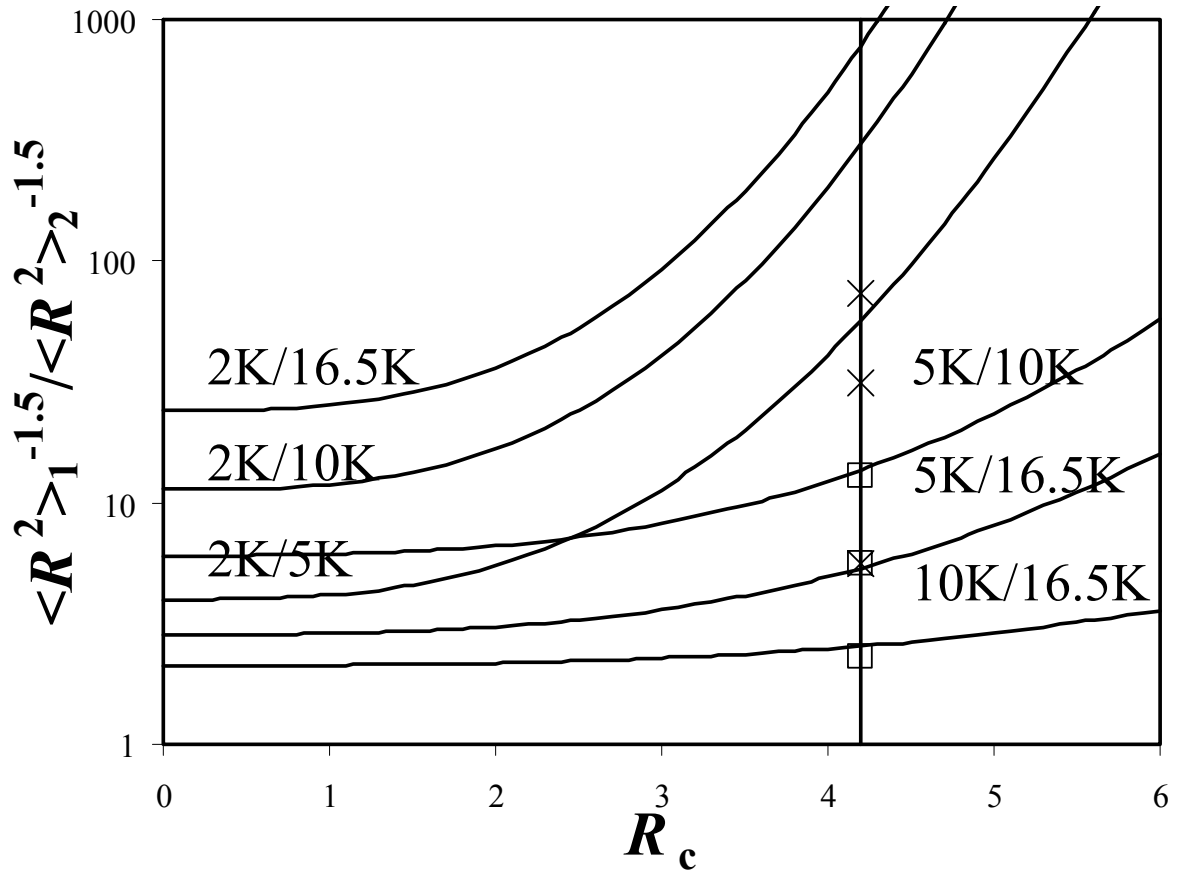


Figure 4.10: Plot of the ratios $\langle R^2 \rangle_{2K}^{-1.5} / \langle R^2 \rangle_{5K}^{-1.5}$, $\langle R^2 \rangle_{2K}^{-1.5} / \langle R^2 \rangle_{10K}^{-1.5}$, $\langle R^2 \rangle_{2K}^{-1.5} / \langle R^2 \rangle_{16.5K}^{-1.5}$, $\langle R^2 \rangle_{5K}^{-1.5} / \langle R^2 \rangle_{10K}^{-1.5}$, $\langle R^2 \rangle_{5K}^{-1.5} / \langle R^2 \rangle_{16.5K}^{-1.5}$, and $\langle R^2 \rangle_{10K}^{-1.5} / \langle R^2 \rangle_{16.5K}^{-1.5}$ versus the unitless capture radius R_c obtained after normalization by the length of one ethylene oxide unit ($=0.439$ nm). The $(I_E/I_M)_{5K}/(I_E/I_M)_{10K}$, $(I_E/I_M)_{10K}/(I_E/I_M)_{16.5K}$, and $(I_E/I_M)_{10K}/(I_E/I_M)_{16.5K}$ ratios are given as the square symbols. The $(I_E/I_M)_{2K}/(I_E/I_M)_{5K}$, $(I_E/I_M)_{2K}/(I_E/I_M)_{10K}$, and $(I_E/I_M)_{2K}/(I_E/I_M)_{16.5K}$ ratios are represented by the cross symbols at $R_c = 4.2$.

A more accurate expression of m in Equation 4.23 is given by $3/(2nl^2)$ with n and l being the number of Kuhn segments and Kuhn length, respectively. For PEO in water, l and n have been determined to equal 0.707 nm and $0.0141M_n$, respectively, where M_n is the number-average molecular

weight of PEO.⁷⁰ Using these values, m was calculated with different PEO(X)-Py₂ samples and used to generate the plot of $(I_E/I_M)_1/(I_E/I_M)_2$ versus R_c . Results similar to the data given in Figure 4.10 were obtained under these conditions yielding an R_c value of 2.1 ± 0.2 nm.

R_c can also be determined from the results obtained by the global analysis of the pyrene monomer and excimer decays based on the SM. Ground-state pyrene aggregates in water lead to the formation of pyrene dimers that produce an excimer instantaneously upon excitation. This species is described as E0* in the theory section. Consequently, the fraction f_{E0} can be viewed as being the probability of having the two polymer ends within the capture distance. Its expression is given by Equation 4.28 where the integral in the denominator equals unity.

$$f_{E0} = \frac{\int_0^{2R_c} \left(\frac{m}{\pi}\right)^{3/2} \exp(-mr_{EE}^2) 4\pi r_{EE}^2 dr_{EE}}{\int_0^{\infty} \left(\frac{m}{\pi}\right)^{3/2} \exp(-mr_{EE}^2) 4\pi r_{EE}^2 dr_{EE}} \quad (4.28)$$

Using Equation 4.28, the capture distance equivalent to $2 \times R_c$ for the pyrene end-groups of PEO(X)-Py₂ was determined from the f_{E0} values listed in Table SI.4.2 and shown in Figure 4.6. The R_c values are plotted in Figure 4.11 as a function of the M_n values of the PEO(X)-Py₂ samples. The capture distance was found to take an average value of 4.4 ± 0.3 nm. Therefore R_c equals 2.2 ± 0.2 nm, which is in agreement with the results obtained by Char et al. using the PEO samples bearing a pyrene butyl hydrophobe and determined by steady-state fluorescence.⁴⁵ The R_c values obtained according to the different methods are summarized in Table 4.1.

It should be noted that when the hydrophobic capture volumes of two pyrenes start to overlap, excimer formation is the result of hydrophobic interactions. Before forming an excimer, two pyrene moieties are within the capture distance, and the fraction of pyrene pendants within the capture radius is given by f_{agg}^{SM} . Therefore, f_{agg}^{SM} might be a better representation of the fraction of pyrene pendants

located inside the capture volume and would then be calculated by replacing f_{E0} in Equation 4.28 by f_{agg}^{SM} . The capture distance calculated from f_{agg}^{SM} was plotted in Figure 4.11 using hollow symbols as a function of the M_n values of the PEO(X)-Py₂ samples. The capture distance calculated with f_{agg}^{SM} was found to decrease with increasing PEO molecular weight. Whether f_{agg}^{SM} or f_{E0} might be better suited to determine R_c remains to be determined. Regardless of the choice and the chosen procedure, the results obtained in Figure 4.10 and Table 4.1 indicate that the R_c value obtained by using the $(I_E/I_M)_1/(I_E/I_M)_2$ ratios or the f_{agg}^{SM} and f_{E0} fractions are relatively close for the PEO(5K)-Py₂ and PEO(10K)-Py₂ constructs.

Table 4.1: R_c determined by different methods.

hydrophobes attached onto PEO chain	methods	R_c (nm)
pyrene butyl	steady-state fluorescence	~2.0 (Ref 45)
pyrene methyl	steady-state fluorescence	1.9±0.2
pyrene methyl	steady-state fluorescence and PEO Kuhn length	2.1±0.2
pyrene methyl	time-resolved fluorescence and PEO Kuhn length	2.2±0.2

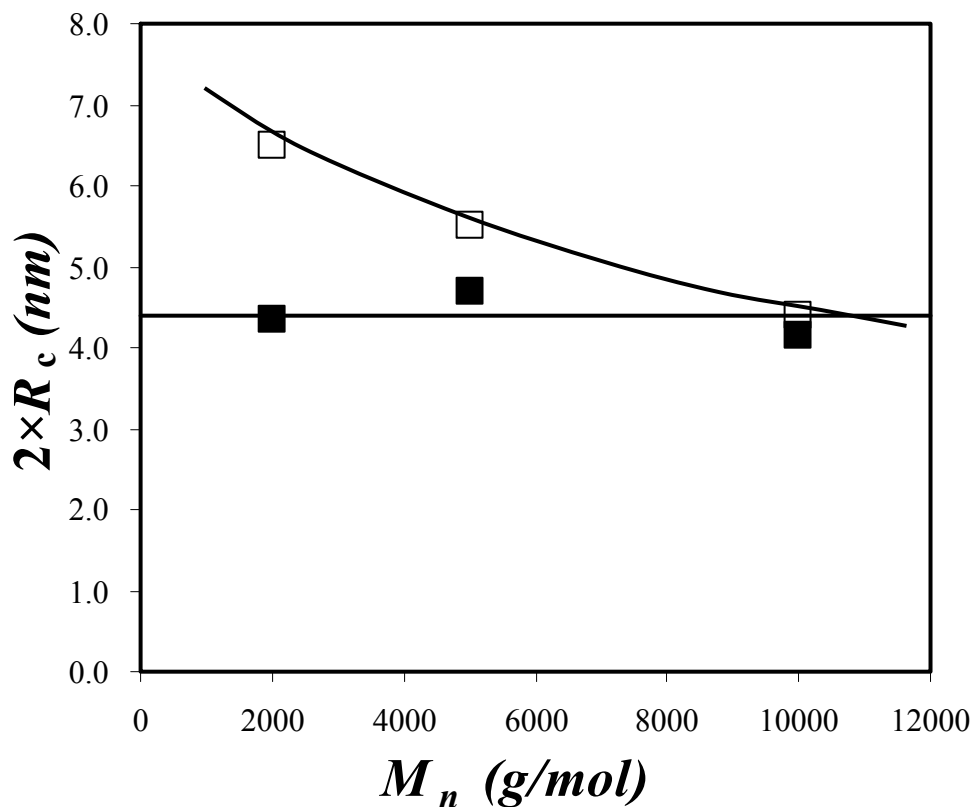


Figure 4.11: The capture distance obtained with f_{E0} (solid symbols) and f_{agg}^{SM} (hollow symbols) versus PEO molecular weights. The errors on the data points are smaller than the symbols.

4.6 Conclusions

The hydrophobic interactions of a series of PEO(*X*)-Py₂ samples have been investigated in aqueous solution using pyrene fluorescence spectra and decays. The samples with shorter PEO chain length exhibited strong hydrophobic interactions which resulted in phase separation of PEO(2K)-Py₂ and PEO(5K)-Py₂ at high polymer concentration. In the dilute regime where the polymer concentration was below 4×10^{-5} M, no change in the fluorescence behavior was observed for all polymer samples regardless of polymer concentration since excimer formation occurs intramolecularly. When the polymer concentration was larger than 4×10^{-5} M, the excimer formed

both intra- and intermolecularly. The concentration when intermolecular excimer formation occurred was the same for all PEO(*X*)-Py₂ constructs regardless of PEO chain length. The complex fluorescence decays were globally fitted according to the SM which assumes that the excimer is formed according to two sequential steps. Two pyrenes located outside a capture volume diffuse randomly, but once they both enter the capture volume, they become subject to hydrophobic interactions and encounter rapidly to form an excimer. Consequently, three rate constants were used to describe the kinetics of excimer formation. The rate constant of intermolecular diffusion in the dilute regime equals zero and increases with increasing C_p for $C_p > C^F$. The rate constant representing intramolecular diffusion is independent of polymer concentration and decreases significantly with increasing polymer chain length. Inside the capture volume, excimers are formed with a rate constant of $7.3(\pm 0.5) \times 10^7 \text{ s}^{-1}$ that is larger than k_{11} or k_{12} , as expected from the strong hydrophobic attraction experienced by the two pyrene pendants. This rate constant is independent of PEO chain length and polymer concentration. According to the concept of capture volume initially introduced by Char et al.,⁴⁵ the capture radius of pyrene in water was determined using the fraction f_{E0} . R_c was found to equal $2.2 \pm 0.2 \text{ nm}$ in agreement with Char et al.'s earlier study that used steady-state fluorescence only.

Chapter 5

Interactions between a Series of Pyrene End-Labeled Poly(ethylene oxide)s and Sodium Dodecyl Sulfate in Aqueous Solution Probed by Fluorescence

5.1 Overview

The interactions between a series of poly(ethylene oxide)s covalently labeled at both ends with pyrene pendants (PEO(X)-Py₂ where X represents the number-average molecular weight of the PEO chains and equals 2, 5, 10, and 16.5 K) and an ionic surfactant, namely sodium dodecyl sulfate (SDS), in aqueous solutions was investigated at a fixed pyrene concentration of 2.5×10^{-6} M, corresponding to polymer concentrations lower than 21 mg/L, and SDS concentrations ranging from 5×10^{-6} M to 0.02 M. The steady-state fluorescence spectra showed that the ratio of excimer-to-monomer emission intensities (the I_E/I_M ratio) of all PEO(X)-Py₂ samples remained constant at low SDS concentrations, then increased, passed through a maximum at the same SDS concentration of 0.004 M before decreasing to a plateau value that is close to zero for PEO(10K)-Py₂ and PEO(16.5K)-Py₂, but never equalled zero for PEO(2K)-Py₂ and PEO(5K)-Py₂. The pyrene end-groups of these two latter samples cannot be located in different micelles due to the short PEO chain spanning the pyrene end-groups and excimer is formed by intramolecular diffusion inside a same SDS micelle. Time-resolved fluorescence decays for the pyrene monomer and excimer of the PEO(X)-Py₂ samples were acquired at various SDS concentrations and globally fitted according to the “Model Free” (MF) analysis over the entire range of SDS concentrations. The molar fractions of the various excited pyrene species and the rate constant of pyrene excimer formation retrieved from the analysis of the fluorescence decays were obtained as a function of SDS concentration. The possibility of SDS interacting with the hydrophilic PEO segments was also investigated by isothermal titration calorimetry, potentiometry with a surfactant-selective electrode, and conductance measurements. Unfortunately, these techniques

proved not to be sensitive enough at the low polymer concentrations used in the fluorescence experiments.

5.2 Introduction

The viscoelastic behavior of an aqueous solution of hydrophobically modified water-soluble polymers (HMWSPs) is significantly altered upon addition of a surfactant. In particular, the viscosity of the solution can be adjusted over a wide viscosity range and this property has been taken advantage of in numerous applications where control of the solution viscosity is required such as in cosmetics and paints, as well as for enhanced oil recovery.¹⁻⁴ Hydrophobically end-capped monodisperse poly(ethylene oxide)s (PEO-Hyd₂) have often been used as model compounds for hydrophobically modified ethoxylated urethanes (HEUR). Consequently, the interactions between PEO-Hyd₂ and anionic surfactants such as sodium dodecyl sulfate (SDS) have been the object of a number of studies.⁵⁻¹² Annable et al.⁷ studied the effect of surfactant addition on the rheological behavior of HEUR in aqueous solution. They found that at low surfactant concentrations, the free surfactant molecules can replace the end groups of HEUR inside the hydrophobic junctions to form mixed micelles. The released end groups can then bridge neighboring mixed micelles, thus extending the polymer network, which induces an increase in the solution viscosity. However, an excess of surfactant completely disrupts the polymer network by solubilizing the hydrophobic end-groups of HEUR into separate surfactant micelles, resulting in a significant drop in viscosity.

SDS is also known to interact with the hydrophilic backbone of PEO. The binding of SDS to PEO has been investigated by various experimental approaches such as isothermal titration calorimetry (ITC),¹³⁻¹⁶ surface tension,^{17,18} viscosity,¹⁹ neutron^{5,19} and laser light²⁰ scattering, NMR,^{16,18,21} fluorescence spectroscopy,²²⁻²⁴ ESR,²⁵ and conductimetry.^{26,27} These studies have revealed the existence of several important concentrations that characterize the boundaries that exist between different binding regimes for PEO and SDS. The onset concentration for the binding of SDS onto PEO is defined as the critical aggregation concentration (CAC). It is independent of PEO

concentration¹³ and has been found to equal 4.3 mM.¹⁴ As the SDS concentration is further increased, a point is reached where the PEO chains are saturated with SDS molecules. This occurs at the saturation concentration (C_2) and no additional binding of SDS onto PEO occurs beyond this concentration. For PEO chains with a molecular weight larger than 3,350 g/mol,¹³ ITC measurements demonstrated that PEO chain segments are expelled from the hydrophobic core of the SDS micelles and become exposed to the water phase. The re-hydrated PEO segments wrap themselves around the surface of the SDS micelles. With excess amounts of SDS, another critical concentration (C_m) is encountered where free SDS micelles begin to form. No interactions between PEO and SDS were observed when the molecular weight of PEO was less than 400 g/mol.¹³

The study of the binding of SDS to HEURs is complicated by the hydrophobic end-groups of HEURs that are preferentially targeted by SDS molecules. Indeed, ITC studies showed that although SDS binds to PEO and HEUR in a similar manner, binding occurs at a smaller CAC for a HEUR solution.^{13,28} This observation was confirmed by potentiometry using a surfactant selective electrode. The smaller CAC reflects the early binding of SDS onto the hydrophobic end-groups of HEUR.⁹ However, binding of SDS to the PEO main chain was not considered when the interactions between SDS and hydrophobically end-capped PEOs were probed by fluorescence spectroscopy⁶ and more recently by ¹³C NMR spectroscopy and small-angle neutron scattering.²⁹

In many studies aiming at characterizing the interactions between HMWSPs and surfactants by fluorescence, pyrene was selected to replace the hydrophobe of HMWSPs (Py-HMWSPs)^{6,30-43} because of its combination of strong hydrophobicity and unique photophysical properties. The fluorescence spectrum of an excited pyrene monomer provides information about the polarity of the microenvironment where pyrene is located.⁴⁴ This is achieved by monitoring the ratio of the first to the third peak, the I_1/I_3 ratio, obtained from the pyrene monomer fluorescence spectrum. This feature can be used effectively to probe whether a hydrophobic pyrene pendant is located inside a surfactant micelle or in aqueous solution.^{30,44} Furthermore, after absorption of a photon, an excited pyrene can interact with a ground-state pyrene to form an excimer⁴⁵ which emits over a range of wavelengths that

is different from the fluorescence spectrum of the excited pyrene monomer. For pyrene-labeled polymers, the ratio of the fluorescence intensities of the pyrene excimer and monomer, the I_E/I_M ratio, can be used to qualitatively describe polymer chain dynamics in organic solvents where pyrene excimer is mainly formed by diffusional encounters between pyrene pendants or the level of hydrophobic association between pyrene pendants of Py-HMWSPs in water.⁴⁶

The interactions between highly diluted pyrene end-labeled PEOs (PEO(*X*)-Py₂) and SDS have been investigated in aqueous solution by several research groups^{6,36,37,41,42} with PEO molecular weights ranging from 7,000 to 20,000 g/mol using steady-state fluorescence. The interactions between PEO(*X*)-Py₂ and SDS were characterized by analyzing the I_1/I_3 and I_E/I_M ratios. However, such an analysis provides information about the pyrene hydrophobes that is qualitative in nature since it does not consider the various states adopted by pyrene in solution. For instance, previous studies on hydrophobically modified alkali swellable emulsion polymers randomly labeled with pyrene moieties (Py-HASE) have shown that although pyrene is an efficient hydrophobe, not all pyrene groups are associated in aqueous solution.³⁰⁻³² In fact, an excited pyrene species can be found under one of three main states whether an excited pyrene is aggregated with other ground-state pyrenes, isolated and unable to form an excimer, or forming an excimer by diffusion.³⁰⁻³² Therefore, the fluorescence behavior of Py-HMWSPs upon addition of SDS must be correlated with the distribution of the pyrene species among these three states. As it turns out, the molar fractions of the different pyrene species found in solution can be determined via global analysis of the pyrene monomer and excimer decays acquired by time-resolved fluorescence measurements.³⁰⁻³²

In an effort to better characterize the complicated interactions taking place between PEO(*X*)-Py₂ and SDS, a series of PEO(*X*)-Py₂ constructs having PEO molecular weights ranging from 2,000 to 16,500 g/mol were prepared. Both steady-state and time-resolved fluorescence were applied to develop a quantitative understanding of how SDS molecules affect pyrene excimer formation of PEO(*X*)-Py₂ at extremely low polymer concentration (< 21 mg/L). The acquired monomer and excimer decays were globally fitted according to a Model Free (MF) analysis which can identify the

different species of excited pyrene present in solution and determine their molar fractions. ITC, potentiometry using a surfactant-selective electrode, and conductimetry were used to probe the interaction between SDS and the PEO hydrophilic backbone. Unfortunately, although the binding taking place between SDS and the hydrophobic PEO ends was detected at higher PEO(*X*)-Py₂ concentrations, these techniques were not sensitive enough to provide any information about whether SDS would bind or not to the PEO backbone in these highly diluted PEO(*X*)-Py₂ solutions. Fluorescence appears to remain the only technique that can reliably probe these interactions under such dilute conditions.

5.3 Experimental

Materials: The detailed synthesis of the PEO(*X*)-Py₂ samples has been described in a recent publication.⁴⁷ The general chemical structure of the polymers is shown in Figure 5.1. The pyrene contents of each sample was determined by UV-vis absorption and indicated that all PEO samples were fully end-capped with pyrene groups.⁴⁷ SDS was purchased from EM Science and used as received. Milli-Q water which was deionized on Millipore Milli-RO 10 Plus and Milli-Q UF Plus (Bedford, MA) systems was used to prepare all aqueous solutions.

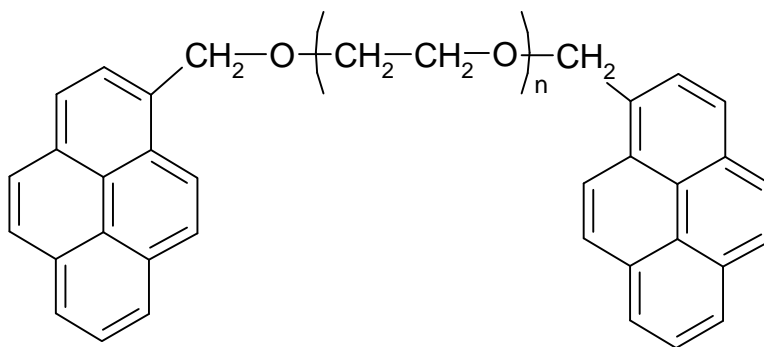


Figure 5.1: Chemical structure of the PEO(*X*)-Py₂ samples. *n* equals 45, 113, 227, and 375 for PEO(*X*)-Py₂ with *X* = 2, 5, 10, and 16.5 K, respectively.

Steady-state fluorescence measurements: Fluorescence emission spectra were acquired via a Photon Technology International LS-100 steady-state fluorometer with a continuous Ushio UXL-75Xe xenon arc lamp as the light source. A fluorescence microcell (3 mm × 3 mm) purchased from Hellma was used with the usual right angle configuration. Emission spectra were acquired by exciting the samples at 344 nm. The fluorescence intensities of the monomer (I_M) and the excimer (I_E) were calculated by taking the integrals under the fluorescence spectra from 372 to 378 nm for the pyrene monomer and from 500 to 530 nm for the pyrene excimer. The superscript "SS" was used for the ratio of I_E over I_M , the $(I_E/I_M)^{SS}$ ratio, to indicate that the fluorescence intensities were obtained by steady-state fluorescence. The I_1/I_3 ratios were determined from the intensity of the first, I_1 , and third, I_3 , peaks in the fluorescence spectrum of the pyrene monomer taken at 374 and 385 nm, respectively.

Time-resolved fluorescence measurements: The fluorescence decay profiles were acquired with the time-correlated single photon counting (TCSPC) technique using an IBH time-resolved fluorometer and an IBH 340 nm LED with a 500 kHz repetition rate as the excitation source. For all PEO(X)-Py₂ solutions, the excitation wavelength was set at 344 nm. The decay curves were obtained by setting the emission wavelength at 374 nm for the monomer and 510 nm for the excimer. To block potential light scattering leaking through the detection system, filters were used with a cutoff at 370 and 495 nm during acquisition of the fluorescence decays for the monomer and excimer, respectively. All fluorescence decays were acquired over 1024 channels, ensuring a minimum of 20,000 counts at their maximum. A time per channel of 2.04 ns/ch was used for the acquisition of the monomer and excimer decays. For all the decay profiles, reference decays of degassed solutions of PPO [2,5-diphenyloxazole] in cyclohexane ($\tau = 1.42$ ns) for the pyrene monomer and BBOT [2,5-bis(5-*tert*-butyl-2-benzoxazolyl)thiophene] in ethanol ($\tau = 1.47$ ns) for the pyrene excimer were used to obtain the instrument response function (IRF) via the MIMIC method.⁴⁸

Analysis of the fluorescence decays: Upon excitation, the excited pyrene species found in all aqueous solutions of PEO(X)-Py₂ and SDS can be divided into three categories referred to as Py_{free}^* , Py_{diff}^* ,

and $E0^*$. Py_{free}^* can be detected in the monomer decay only. It represents the excited pyrenes that emit with the natural lifetime τ_M of pyrene and never form an excimer. Py_{diff}^* refers to the excited pyrenes which form excimer via diffusional encounter with a ground-state pyrene. This process is dynamic and is probed in both the monomer and excimer decays. $E0^*$ represents the pyrene excimer that emits with a lifetime τ_{E0} and can only be detected in the excimer decay. τ_M of pyrene in water and in the presence of SDS micelles ($[SDS] = 50 \text{ mM}$) was determined from the long decay time obtained by using a sum of exponentials to fit the monomer fluorescence decay of an aqueous solution of a 2K PEO chain labeled at a single end with pyrene (PEO(2K)-Py₁)⁴⁷ at a pyrene concentration of $2.5 \times 10^{-6} \text{ mol/L}$. τ_M was found to equal 154 and 157 ns in the absence and presence of SDS, respectively. Therefore, τ_M was fixed in the analysis of the fluorescence decays to equal 155 ns.

The monomer and excimer decays of the PEO(X)-Py₂ samples were globally fitted according to the MF analysis.^{31,49-51} The mathematical expressions used to fit the monomer and excimer fluorescence decays are given by Equations 5.1 and 5.2, respectively.

$$[Py^*]_{(t)} = [Py_{diff}^*]_{(t=0)} \times \sum_{i=1}^n a_i \times \exp(-t/\tau_i) + [Py_{free}^*]_{(t=0)} \times \exp(-t/\tau_M) \quad (5.1)$$

$$[E^*]_{(t)} = -[Py_{diff}^*]_{(t=0)} \times \sum_{i=1}^n a_i \frac{\frac{1}{\tau_i} - \frac{1}{\tau_M}}{\frac{1}{\tau_i} - \frac{1}{\tau_{E0}}} \exp(-t/\tau_i) + \left([E0^*]_{(t=0)} + [Py_{diff}^*]_{(t=0)} \times \sum_{i=1}^n a_i \frac{\frac{1}{\tau_i} - \frac{1}{\tau_M}}{\frac{1}{\tau_i} - \frac{1}{\tau_E}} \right) \times \exp(-t/\tau_{E0}) \quad (5.2)$$

Global analysis of the monomer and excimer decays using Equations 5.1 and 5.2 allows the determination of the fractions f_{Mdiff} , f_{Mfree} , f_{Ediff} and f_{EE0} , which are given in Equations 5.3 – 5.6.

$$f_{Mdiff} = \frac{[Py_{diff}^*]_{(t=0)}}{[Py_{diff}^*]_{(t=0)} + [Py_{free}^*]_{(t=0)}} \quad (5.3)$$

$$f_{Mfree} = \frac{[Py_{free}^*]_{(t=0)}}{[Py_{diff}^*]_{(t=0)} + [Py_{free}^*]_{(t=0)}} \quad (5.4)$$

$$f_{Ediff} = \frac{[Py_{diff}^*]_{(t=0)}}{[Py_{diff}^*]_{(t=0)} + [E0^*]_{(t=0)}} \quad (5.5)$$

$$f_{EE0} = \frac{[E0^*]_{(t=0)}}{[Py_{diff}^*]_{(t=0)} + [E0^*]_{(t=0)}} \quad (5.6)$$

The fractions obtained from Equations 5.3 – 5.6 can be used to calculate the overall contributions of aggregated pyrene, f_{agg} , diffusional pyrene, f_{diff} , and isolated pyrene, f_{free} in an aqueous solution of PEO(X)-Py₂ and SDS according to Equations 5.7 – 5.9.

$$f_{diff} = \frac{[Py_{diff}^*]_{(t=0)}}{[Py_{diff}^*]_{(t=0)} + [Py_{free}^*]_{(t=0)} + [E0^*]_{(t=0)}} = \left(1 + \frac{f_{Mfree}}{f_{Mdiff}} + \frac{f_{EE0}}{f_{Ediff}} \right)^{-1} \quad (5.7)$$

$$f_{free} = \frac{[Py_{free}^*]_{(t=0)}}{[Py_{diff}^*]_{(t=0)} + [Py_{free}^*]_{(t=0)} + [E0^*]_{(t=0)}} = f_{diff} \times \frac{f_{Mfree}}{f_{Mdiff}} \quad (5.8)$$

$$f_{E0} = \frac{[E0^*]_{(t=0)}}{[Py_{diff}^*]_{(t=0)} + [Py_{free}^*]_{(t=0)} + [E0^*]_{(t=0)}} = f_{diff} \times \frac{f_{EE0}}{f_{Ediff}} \quad (5.9)$$

The molar fractions defined in Equations 5.7 – 5.9 can then be used to determine a measure of the fluorescence intensity of the monomer $(I_M)^{SPC}$ and excimer $(I_E)^{SPC}$ according to Equations 5.10 and 5.11 where the functions $[Py^*]_{(t)}$ and $[E^*]_{(t)}$ are given by Equations 5.1 and 5.2, respectively.

$$(I_M)^{SPC} = \int_{t=0}^{\infty} [Py^*]_{(t)} dt \quad (5.10)$$

$$(I_E)^{SPC} = \int_{t=0}^{\infty} [E^*]_{(t)} dt \quad (5.11)$$

Taking the ratio of $(I_E)^{SPC}$ over $(I_M)^{SPC}$ yields the $(I_E/I_M)^{SPC}$ ratio whose expression is given in Equation 5.12

$$\left(\frac{I_E}{I_M} \right)^{SPC} = \frac{-f_{diff} \times \sum_{i=1}^n a_i \frac{\frac{1}{\tau_i} - \frac{1}{\tau_M}}{\frac{1}{\tau_i} - \frac{1}{\tau_{E0}}} \times \tau_i + \left(f_{agg} + f_{diff} \times \sum_{i=1}^n a_i \frac{\frac{1}{\tau_i} - \frac{1}{\tau_M}}{\frac{1}{\tau_i} - \frac{1}{\tau_E}} \right) \times \tau_E}{f_{diff} \times \sum_{i=1}^n a_i \times \tau_i + f_{free} \times \tau_M} \quad (5.12)$$

The rate constant $\langle k \rangle$ can be calculated by considering the average rate constant of excimer formation whose expression is given as a function of the average decay rate constant in Equation 5.13.

$$\langle k \rangle = \sum_{i=1}^n \frac{a_i}{\tau_i} - \frac{1}{\tau_M} \quad (5.13)$$

The MF analysis of the fluorescence decays was conducted globally by applying the Marquardt-Levenberg algorithm⁵² to obtain the optimized pre-exponential factors and decay times. The fits were

considered good when χ^2 was smaller than 1.30 and the residuals and autocorrelation of the residuals were randomly distributed around zero.

In Chapter 4, the fluorescence decays of the pyrene monomer and excimer acquired with aqueous solutions of PEO(*X*)-Py₂ without SDS were globally fitted according to a “sequential model” (SM) to reflect the two steps that are involved during excimer formation. The excited pyrene monomer first diffused into the capture volume occupied by a ground-state pyrene. This diffusive process was accounted for by a rate constant that is much smaller than the one describing the encounter between two pyrenyl units subject to the strong hydrophobic forces at play inside the capture volume. These two steps were successfully isolated by applying the SM to the global analysis of the fluorescence decays. Since the process of pyrene excimer formation inside the capture volume reflected some level of hydrophobic interaction between a ground-state pyrene and an excited pyrene, these pyrenes were considered to be “associated” in Chapter 4. However, the MF analysis does not distinguish between these two sequential processes and f_{diff} obtained in this study represents any excited pyrene that forms an excimer with no distinction being made on whether it is located outside or inside the capture radius. Thus differences between the molar fractions of pyrene species obtained in this and earlier studies are to be expected.

ITC measurements: The enthalpies for the binding of SDS to the PEO(*X*)-Py₂ constructs were determined using a Microcal isothermal titration microcalorimeter with a reference cell and a sample cell having a volume of 1.35 mL. The titration was carried out by injecting 30 times 250 μL of concentrated 0.2 M SDS titrant solution into the sample cell filled with water or PEO(*X*)-Py₂ to titrate the solution. The tip of the syringe served as a stirrer that ensured a continuous mixing efficiency of 307 rpm. The time interval between each injection was set at 2.5 min and each injection was completed within 4 sec. All ITC experiments were conducted at a constant temperature of 25.0 ± 0.1 °C.

Electromotive force (EMF) and conductivity measurements: A Metrohm surfactant membrane electrode selective to SDS monomers and a Metrohm electrode were used for the EMF and conductivity measurements, respectively. The surfactant-selective electrode was used to monitor the

SDS monomer concentration during the binding of SDS to PEO(*X*)-Py₂ by measuring the EMF values relative to a Metrohm bromide ion reference electrode. Conductivity was measured with a conductometer supplied by Metrohm. The titration was conducted by injecting a concentrated 0.8 M SDS titrant solution placed in a 200 mL reservoir into the sample container filled with 50 mL of water or PEO(*X*)-Py₂ titrate solution. Each titration consumed 0.03 mL of SDS solution. Solutions of SDS having concentrations of 0.001, 0.01, 0.1 and 1 mM were used to verify the stability of the instruments and to obtain the reference EMF values. All experiments were conducted at a constant temperature of 25.0 ± 0.1 °C, which was controlled by a VWR water bath.

5.4 Results and Discussion

In this study, the concentration of all PEO(*X*)-Py₂ samples used to conduct the fluorescence measurements was adjusted so that each solution had an identical pyrene concentration of 2.5×10^{-6} M, which corresponds to a polymer concentration of 1.25×10^{-6} M. This extremely low concentration is typically employed to study by fluorescence intramolecular phenomena taking place with pyrene-labeled macromolecules. However, the lowest concentration of 0.1 wt% of the PEO(*X*)-Py₂ samples that was used to perform the ITC, EMF, and conductimetry measurements was still much higher than the concentration used in the fluorescence experiments. Indeed a concentration of 0.1 wt% is equivalent to molar concentrations of 5.0×10^{-4} , 2.0×10^{-4} , 1.0×10^{-4} and 6.1×10^{-5} mol/L for the PEO(*X*)-Py₂ samples having molecular weights of 2, 5, 10, and 16.5 K, respectively. Because SDS is known to interact with PEO and since this binding cannot be probed directly with our PEO(*X*)-Py₂ constructs using fluorescence, ITC, EMF, and conductimetry experiments were conducted to probe the interactions between SDS and the PEO(*X*)-Py₂ molecules.

ITC, EMF and conductimetry experiments:

Figure 5.2 shows the ITC thermograms for the titration of 0.2 M SDS into solutions of 1.25×10^{-6} M PEO(2K)-Py₂, 1.25×10^{-6} M and 6.1×10^{-5} M PEO(16.5K)-Py₂, and 6.1×10^{-5} M PEO(16.5K). The dilution curve of the 0.2 M SDS solution in water is also given as a reference. The

maximum in the SDS dilution profile indicates the critical micelle concentration (CMC) of SDS in water, found to equal 8.4 mM. The titration curves obtained with the 6.1×10^{-5} M PEO(16.5K) and PEO(16.5K)-Py₂ solutions show differences as compared to the SDS dilution curve. For the 6.1×10^{-5} M PEO(16.5K) solution, the titration curve exhibits a CAC of 4.2 mM. The CAC of the 6.1×10^{-5} M PEO(16.5K)-Py₂ solution is much smaller (< 1.0 mM) reflecting that the binding of SDS to the pyrene hydrophobic groups occurs at low SDS concentration, in agreement with the results obtained by Dai et al.^{9,13} The titration curves of both the 6.1×10^{-5} M PEO(16.5K)-Py₂ and PEO(16.5K) solutions display an endothermic process around an SDS concentration of 11.3 mM. The reason for this phenomenon has not yet been confirmed but is suspected to be due to the reorganization of the structure of the polymer/SDS complexes. The titration curves obtained with either the 1.25×10^{-6} M PEO(2K)-Py₂ or PEO(16.5K)-Py₂ solutions overlapped the SDS dilution curve. The lack of CAC, C_2 , and C_m on the titration curves of these dilute solutions provides little evidence that SDS molecules interact with the polymer samples at these low polymer concentrations.

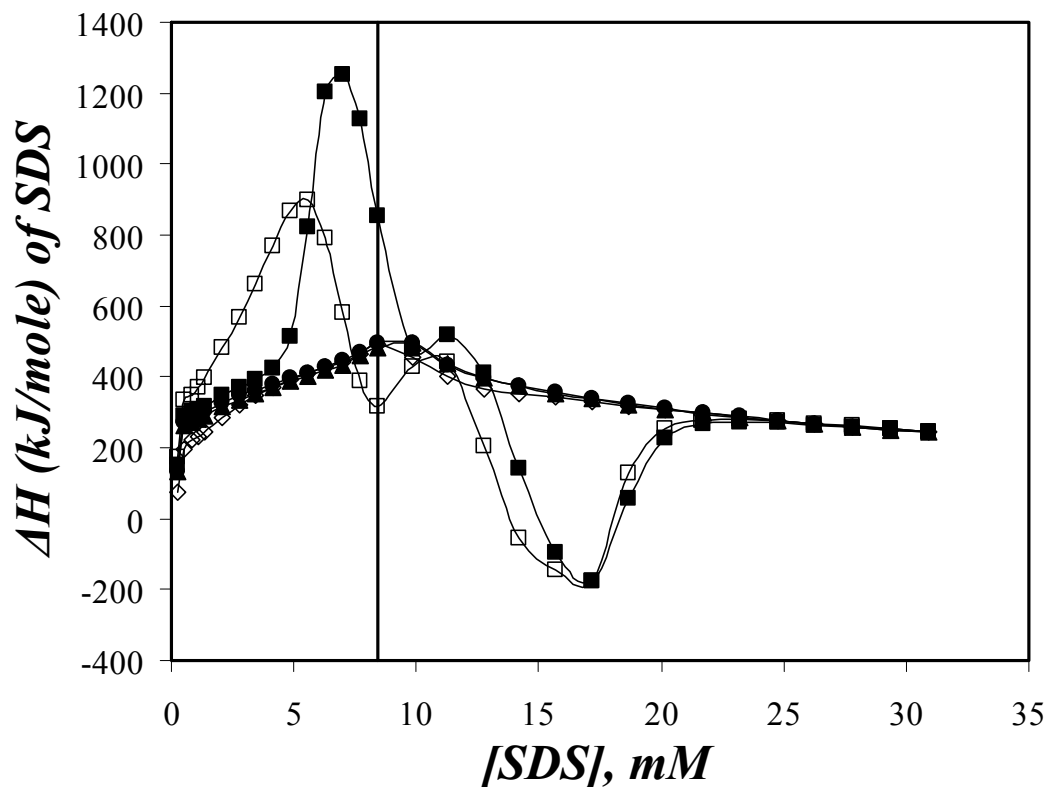


Figure 5.2: Isothermal titration curves for titrating a 0.2 M SDS solution into water (\diamond) and aqueous solutions of 1.25×10^{-6} M PEO(2K)-Py₂ (\bullet), 1.25×10^{-6} M PEO(16.5K)-Py₂ (\blacktriangle), 6.1×10^{-5} M PEO(16.5K) (\blacksquare), and 6.1×10^{-5} M PEO(16.5K)-Py₂ (\square). T = 298 K, P = 1 atm. The solid vertical line represents the CMC of SDS in water.

The EMF of the surfactant-selective electrode is plotted in Figure 5.3A as a function of the total SDS concentration relative to the reference electrode with and without 1.25×10^{-6} M PEO(X)-Py₂. During the titration, the SDS monomer concentration could be determined quantitatively with the surfactant selective membrane electrode and found to be inversely proportional to the measured EMF. Figure 5.3A shows that in the absence of polymer samples, the EMF decreases with increasing SDS concentration before reaching a plateau at higher SDS concentrations. The CMC of SDS in water is given by the concentration of SDS at the transition found to equal 8.2 mM in Figure 5.3A. The EMF profile indicates that when a concentrated SDS solution is titrated into water, the SDS monomer

concentration increases below the CMC due to the decomposition of the SDS micelles into SDS monomers and remains constant above the CMC since in this range of surfactant concentration, the SDS monomer concentration remains constant and equals the CMC. The EMF results acquired with the PEO(*X*)-Py₂ solutions show larger EMF values at the beginning of the titration, which corresponds to lower SDS monomer concentrations due to the binding of SDS to the PEO(*X*)-Py₂ samples at low SDS concentrations. This result agrees with earlier ITC and EMF experiments conducted to study the interactions between SDS and HEUR polymers.⁹ However, both the CAC and C_2 could not be determined from the data presented in Figure 5.3A, suggesting that the interaction between SDS and the PEO backbone of PEO(*X*)-Py₂ cannot be probed at a polymer concentration of 1.25×10^{-6} M. Figure 5.3B shows the EMF values obtained with water, a 1.0×10^{-4} M PEO(10K)-Py₂ solution and PEO(10K) solutions at concentrations of 1.25×10^{-6} M and 1.0×10^{-4} M. The 1.0×10^{-4} M PEO(10K) and PEO(10K)-Py₂ solutions yield trends that are quite different from those obtained with water or the 1.25×10^{-6} M PEO(10K) solution. The overlap of the EMF profiles obtained in pure water and with the 1.25×10^{-6} M PEO(10K) solution suggests that binding between SDS and PEO cannot be detected at such a low polymer concentration.

The conductivity of the solutions at different SDS concentrations was acquired simultaneously with the EMF values and the results were plotted in Figure 5.3C as a function of SDS concentration. At SDS concentrations below the CMC, the main contributions to the specific conductivity (κ) of the solution is due to free dodecyl sulfate anions and sodium cations. κ can be obtained from the SDS concentration and the equivalent conductivity (Λ) which is related to the charge and mobility of the free ions. Above the CMC, the solution conductivity increases more slowly with increasing SDS concentration than below the CMC. Besides the free ions in solution, the charged micelles also contribute to κ of the solution but as they have a smaller Λ due to their lower mobility than the free ions, the conductivity of the solution is smaller than would be expected if all SDS ions were present as unimers. Therefore, the conductivity increases linearly with SDS

concentration with two different slopes for the conductivities measured at concentrations below and above the CMC. The CMC is determined at the break point of the lines. As shown in Figure 5.3C, the results obtained with water and the 1.25×10^{-6} M PEO(10K) solution yield the same CMC with a value of 8.2 mM. For the 1.0×10^{-4} M PEO(10K) and PEO(10K)-Py₂ solutions, the CMC of SDS is altered due to the binding taking place between SDS and the PEO chain. However, this interaction cannot be detected by monitoring the solution conductance at low polymer concentration.

Haldar et al.⁴¹ have investigated the interaction between SDS and a pyrene end-labeled PEO sample having a molecular weight of 9,500 g/mol. Similar effects were observed in their study. Very small enthalpy changes were detected using ITC at a polymer concentration of 2.5×10^{-6} M (0.003 wt%) – the concentration used for their fluorescence measurements. The binding taking place between SDS and PEO was then successfully detected when the polymer concentration was increased to 0.008 wt%. This observation and the results obtained in the current study suggest that, either the binding of SDS to PEO cannot be probed under these conditions because solutions having such low polymer concentrations are beyond the detection capability of ITC, EMF, and conductivity measurements, or no binding of SDS to the PEO backbone occurs at extremely low polymer concentrations because the interaction between SDS and PEO is concentration-dependent. This effect will be further discussed in the following section.

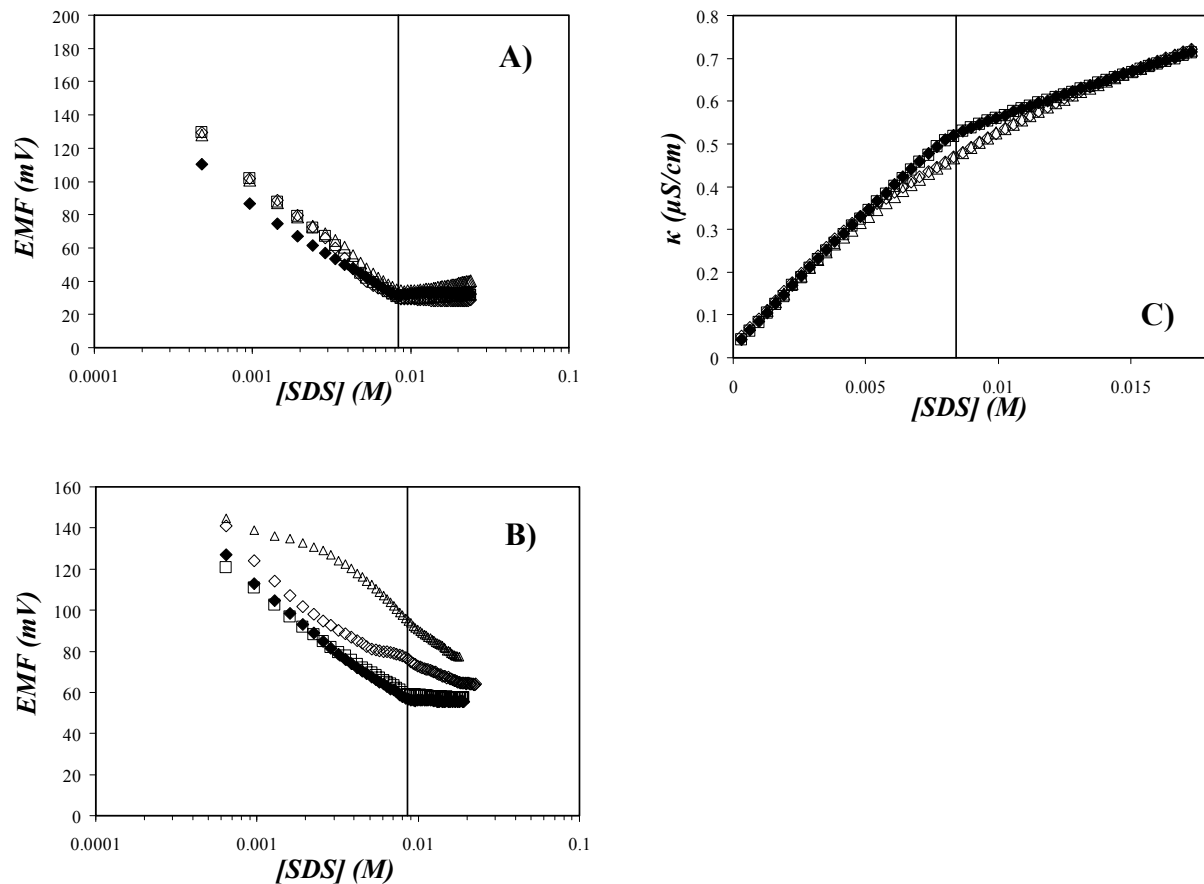


Figure 5.3: Plot of EMF versus SDS concentration for (A) water (\blacklozenge) and 1.25×10^{-6} M PEO(2K)-Py₂ (\diamond), PEO(5K)-Py₂ (\square) and PEO(10K)-Py₂ (\triangle) solutions and (B) water (\blacklozenge), 1.25×10^{-6} M PEO(10K) (\square), 1.0×10^{-4} M PEO(10K) (\diamond), and 1.0×10^{-4} M PEO(10K)-Py₂ (\triangle) solutions. (C) Plot of solution conductance versus SDS concentration for water (\blacklozenge), 1.25×10^{-6} M PEO(10K) (\square) solution and 1.0×10^{-4} M PEO(10K) (\diamond) and PEO(10K)-Py₂ (\triangle) solutions. The vertical line represents the CMC of SDS in water.

Steady-state fluorescence experiments:

All fluorescence experiments with the PEO(X)-Py₂ samples were carried out with a pyrene concentration of 2.5×10^{-6} M. At this concentration, the pyrene excimer is formed intramolecularly and the fraction of aggregated pyrene species decreases significantly with increasing PEO chain

length.⁵³ The addition of SDS to the polymer solution altered the fluorescence spectra of all PEO(*X*)-Py₂ samples, demonstrating that the SDS molecules interact with the pyrene end-groups. The trends observed with all PEO(*X*)-Py₂ samples are similar. The fluorescence spectra obtained with PEO(5K)-Py₂ were normalized at 374 nm and are shown in Figure 5.4 for different SDS concentrations. Figure 5.4A and 5.4B show that the excimer intensity increases for SDS concentrations increasing from 0 to 4 mM and decreases for SDS concentrations increasing from 4 mM to 20 mM. A difference was observed at high SDS concentration between the shorter and the longer PEO samples, where excimer emission is always present for PEO(2K)-Py₂ and PEO(5K)-Py₂, while almost no excimer was detected for the PEO(10K)-Py₂ and PEO(16.5K)-Py₂ samples.

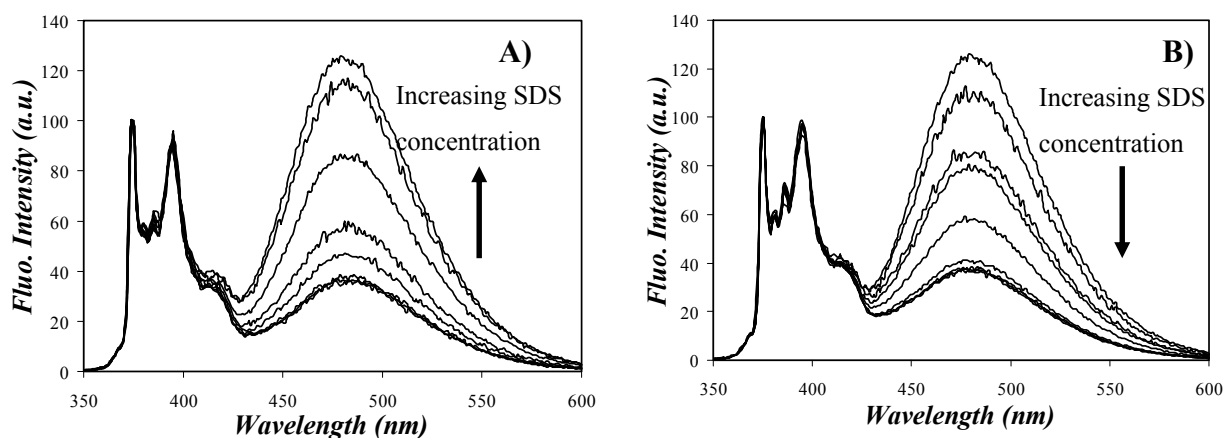


Figure 5.4: Fluorescence emission spectra of PEO(5K)-Py₂ with SDS concentrations ranging from (A) 0 to 4 mM and (B) from 4 to 20 mM. All spectra were normalized at 375 nm.

Figure 5.5 shows the trends of the $(I_E/I_M)^{SS}$ and I_1/I_3 ratios obtained for all PEO(*X*)-Py₂ samples as a function of SDS concentration. The intensity of the third peak (I_3) of the pyrene monomer emission in Figure 5.4A and 5.4B increases with respect to the first peak (I_1) at intermediate SDS concentrations ($2 \text{ mM} < [\text{SDS}] < 6 \text{ mM}$) but remains constant at a value that is either lower or

higher at higher and lower SDS concentrations, respectively. This behavior is captured in the top panel of Figure 5.5.

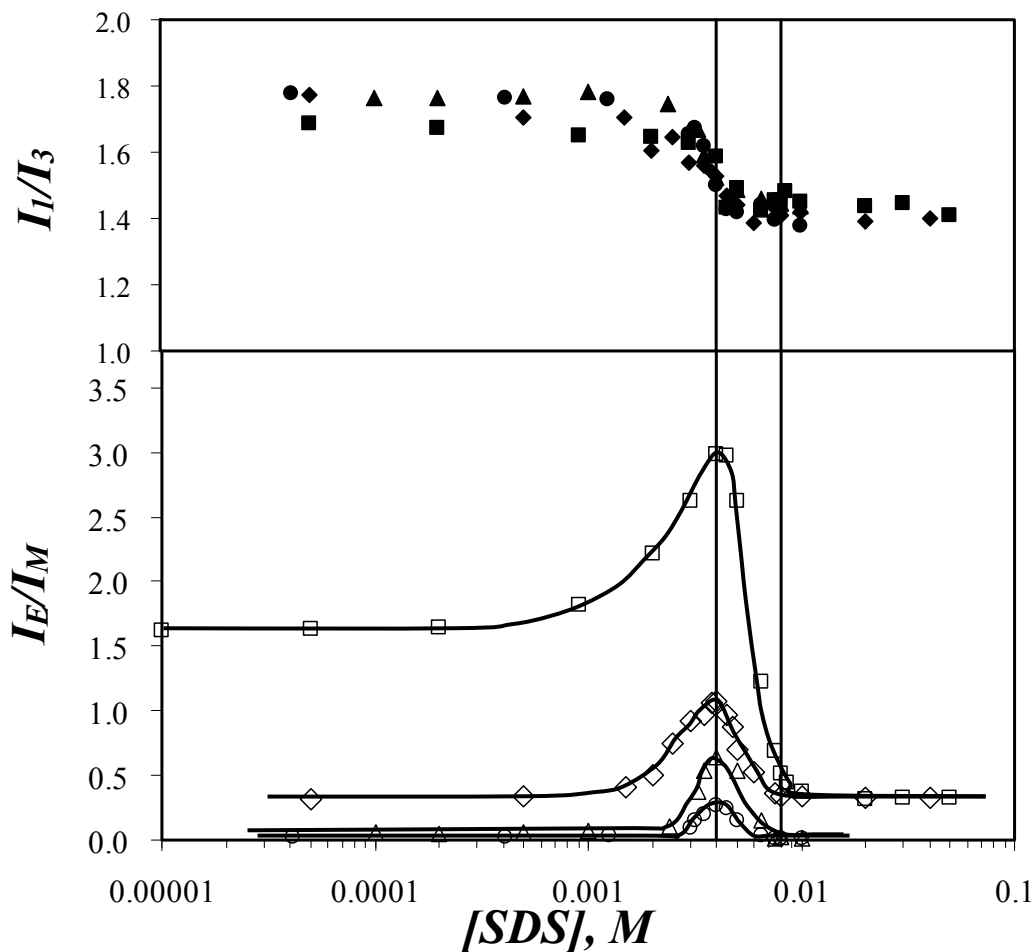


Figure 5.5: Plot of $(I_E/I_M)^{SS}$ (bottom panel) and I_1/I_3 (top panel) vs. SDS concentration for PEO(2K)-Py₂ (square), PEO(5K)-Py₂ (diamond), PEO(10K)-Py₂ (triangle) and PEO(16.5K)-Py₂ (circle). All samples were excited at 344 nm. The vertical lines on the right and left of the plot represent the CMC of SDS in water and $[SDS]_p^{I_E/I_M}$, respectively.

The change in I_1/I_3 indicates that the pyrene pendants experience a more apolar environment as SDS is added to the solution.^{30,44} How the change in the polarity of the medium surrounding the pyrene units affects the process of excimer formation can be inferred by monitoring the $(I_E/I_M)^{SS}$ ratio. The $(I_E/I_M)^{SS}$ ratio describes qualitatively the efficiency of pyrene excimer formation and its behavior is shown in the bottom panel of Figure 5.5 as a function of SDS concentration. At very low SDS concentrations, $(I_E/I_M)^{SS}$ remains constant for each PEO(X)-Py₂ sample. The $(I_E/I_M)^{SS}$ ratio decreases dramatically with polymer molecular weight due to a decrease in the concentration of pyrene aggregates present in solution with increasing PEO chain length.⁵³ At low SDS concentrations, the $(I_E/I_M)^{SS}$ ratio of all PEO(X)-Py₂ samples increases with increasing SDS concentration and peaks at 4 mM ($[SDS]_p^{I_E/I_M} = 4$ mM). This effect is typical of the interactions of SDS with a Py-HMWSP such as Py-HASE,^{30-33,54} or other PEO(X)-Py₂ samples.^{6,36,37,41,42} In the case of Py-HASE and other Py-HMWSPs, this result could be rationalized by invoking the low fluorescence quantum yield of the pyrene excimer formed via the direct excitation of a pyrene aggregate.³³⁻³⁵ $(I_E/I_M)^{SS}$ was found to increase as SDS targeted the pyrene aggregates to form mixed micelles. The alkyl tails of the SDS molecules bound to the pyrene aggregates reduce the strength of the pyrene-pyrene interactions, which enabled the pyrene groups to form excimer by diffusion with a higher fluorescence quantum yield around 4.5 times larger than that of the excimer generated by the direct excitation of a pyrene aggregate in the case of Py-HASE.³³ However, this rationale cannot be invoked in the case of the PEO(X)-Py₂ constructs where X equals 10K and 16.5K. Aqueous solutions prepared with 1.25×10^{-6} M of PEO(10K)-Py₂ and PEO(16.5K)-Py₂ formed hardly any pyrene aggregates in aqueous solution,⁵³ yet $(I_E/I_M)^{SS}$ was still found to increase with increasing SDS concentration. Similarly, a 2.5×10^{-6} M solution of a PEO(2K) chain labeled at a single end with pyrene (PEO(2K)-Py₁), that did not form pyrene aggregates, also exhibited an increase in $(I_E/I_M)^{SS}$ with increasing SDS concentration.³⁰ For the PEO(2K)-Py₁ construct that cannot form intramolecular pyrene excimer, the increase in $(I_E/I_M)^{SS}$ is certainly due to intermolecular pyrene excimer formation that is being

promoted upon addition of SDS. Therefore, the increase in $(I_E/I_M)^{SS}$ observed in Figure 5.5 results from a combination of both the low fluorescence quantum yield of the pyrene excimer formed by direct excitation of a pyrene aggregate and intermolecular pyrene excimer formation induced by the presence of SDS which brings together different polymer chains. After $(I_E/I_M)^{SS}$ peaks at $[SDS]_p^{I_E/I_M}$, further addition of SDS results in a decrease of $(I_E/I_M)^{SS}$ due to the distribution of the pyrene pendants into different mixed micelles which hinders the diffusional encounters between pyrene groups located in different micelles. I_1/I_3 remains constant at 1.43 ± 0.02 for SDS concentrations larger than $[SDS]_p^{I_E/I_M}$ indicating that the pyrene groups are located in the hydrophobic interior of the mixed micelles. Since all pyrene groups are properly solvated inside the SDS micelles, the drop in $(I_E/I_M)^{SS}$ past $[SDS]_p^{I_E/I_M}$ can be attributed to the decrease in the average number of pyrenes per mixed micelle in this range of SDS concentration.^{30,54} For SDS concentrations larger than the CMC of SDS in water (~ 8 mM), the $(I_E/I_M)^{SS}$ ratio of all PEO(*X*)-Py₂ samples plateaus. However, the $(I_E/I_M)^{SS}$ ratios of PEO(2K)-Py₂ and PEO(5K)-Py₂ plateau at a larger value than those of PEO(10K)-Py₂ and PEO(16.5K)-Py₂ with the $(I_E/I_M)^{SS}$ ratios of the latter taking values close to zero. This observation is a result of the PEO(2K)-Py₂ and PEO(5K)-Py₂ being too short to allow the SDS micelles to separate the two pyrene end-groups into two different SDS micelles. Consequently, pyrene excimer is formed intramolecularly by diffusional encounter inside a same SDS micelle. However, the PEO chains of PEO(10K)-Py₂ and PEO(16.5K)-Py₂ being longer allow the pyrene groups to be isolated in different SDS micelles in a process that prevents any pyrene excimer formation. This effect will be further discussed later.

Time-resolved fluorescence experiments:

The monomer and excimer fluorescence decays of PEO(*X*)-Py₂ were acquired at different SDS concentrations. The decays were fitted globally with the MF analysis except for PEO(16.5K)-Py₂ at low SDS concentration. As discussed in a previous study, the fact that the excimer decays acquired with PEO(16.5K)-Py₂ at $[Py] = 2.5 \times 10^{-6}$ M in pure water did not exhibit a rise time

prevented the global analysis of the monomer and excimer fluorescence decays.⁵³ Since the monomer and excimer fluorescence decays of PEO(16.5K)-Py₂ acquired at low SDS concentration were identical to those acquired without SDS, they could not be fitted globally either. Only when sufficient SDS was added to the solutions ([SDS] > 3 mM) did a risetime appear in the excimer fluorescence decays and the global analysis of the decays could be conducted.

As mentioned in the experimental section, the natural lifetime of pyrene, τ_M , set to equal 155 ns in the analysis of the fluorescence decays with Equations 5.1 and 5.2 was determined by fitting the monomer decays of PEO(2K)-Py₁ in the presence and absence of SDS. While the τ_M value of 155 ns proved to yield reasonable fits for most PEO(*X*)-Py₂ solutions, rather poor fits were obtained for the PEO(10K)-Py₂ and PEO(16.5K)-Py₂ samples at SDS concentration larger than 8 mM. For these two samples at SDS concentrations greater than 8 mM, a biexponential fit of the monomer decays yielded decay times of 162 ns and 165 ns, substantially larger than 155 ns. Consequently, τ_M was set equal to 165 ns in the global analysis of the monomer and excimer fluorescence decays acquired with these PEO(*X*)-Py₂ constructs at high SDS concentration. This lengthening of the lifetime observed for PEO(10K)-Py₂ and PEO(16.5K)-Py₂ might be a consequence of the re-hydration of the PEO segments that rearrange themselves at the surface of the SDS micelles in a process that hinders the diffusion of oxygen into the micelles and results in longer-lived excited pyrenes.

The analysis of the fluorescence decays was also complicated by the appearance of a spike in the excimer fluorescence decays acquired with solutions that did not form much excimer such as the PEO(10K)-Py₂ and PEO(16.5K)-Py₂ samples at SDS concentrations greater than 8 mM. Such a spike has been observed earlier and has been attributed to the presence of ground-state pyrene dimers.^{47,55} However, in this study the spike is unlikely due to ground-state dimers because no spike was observed (see Figure 5.6) with all PEO(*X*)-Py₂ samples in aqueous solution, where pyrene is known to form ground-state aggregates.⁵³ On the contrary, the spike was only observed when the pyrene monomers were located in SDS micelles, where excimer should occur via diffusion. Therefore, the

spike in the excimer decay is presumably due to the presence of a small amount of pyrene degradation products or pyrene impurities which emit with a short lifetime. Analysis of the fluorescence decays was started 1-5 channels after the instrument response function (IRF) maximum so that the spike was not included in the analysis of the fluorescence decays. As noted in an earlier publication,⁴⁷ the spike is observed only under conditions where little excimer fluorescence is detected in the steady-state fluorescence spectra.

The fits of the decays were good with all χ^2 smaller than 1.30, and residuals and autocorrelation functions of the residuals randomly distributed around zero. Examples of the fit for PEO(5K)-Py₂ at low and high SDS concentrations are shown in Figures 5.6 and 5.7, respectively. The decay times, pre-exponential factors a_i , and fractions f_{Mdiff} , f_{Mfree} , f_{Ediff} , and f_{EE0} retrieved from the analysis are listed in Table SI.5.1 of the Supporting Information (SI). The fractions were used to determine the molar fractions of aggregated pyrenes (f_{E0}), pyrenes forming excimer by diffusional encounter (f_{diff}), isolated pyrenes that do not form excimer (f_{free}) according to Equations 5.7 – 5.13, while the average rate constant of excimer formation ($\langle k \rangle$) was determined using Equation 5.14. The fractions f_{diff} , f_{free} , and f_{E0} and the rate constant $\langle k \rangle$ are listed in Table SI.5.2 and plotted as a function of SDS concentration in Figure 5.8A-D.

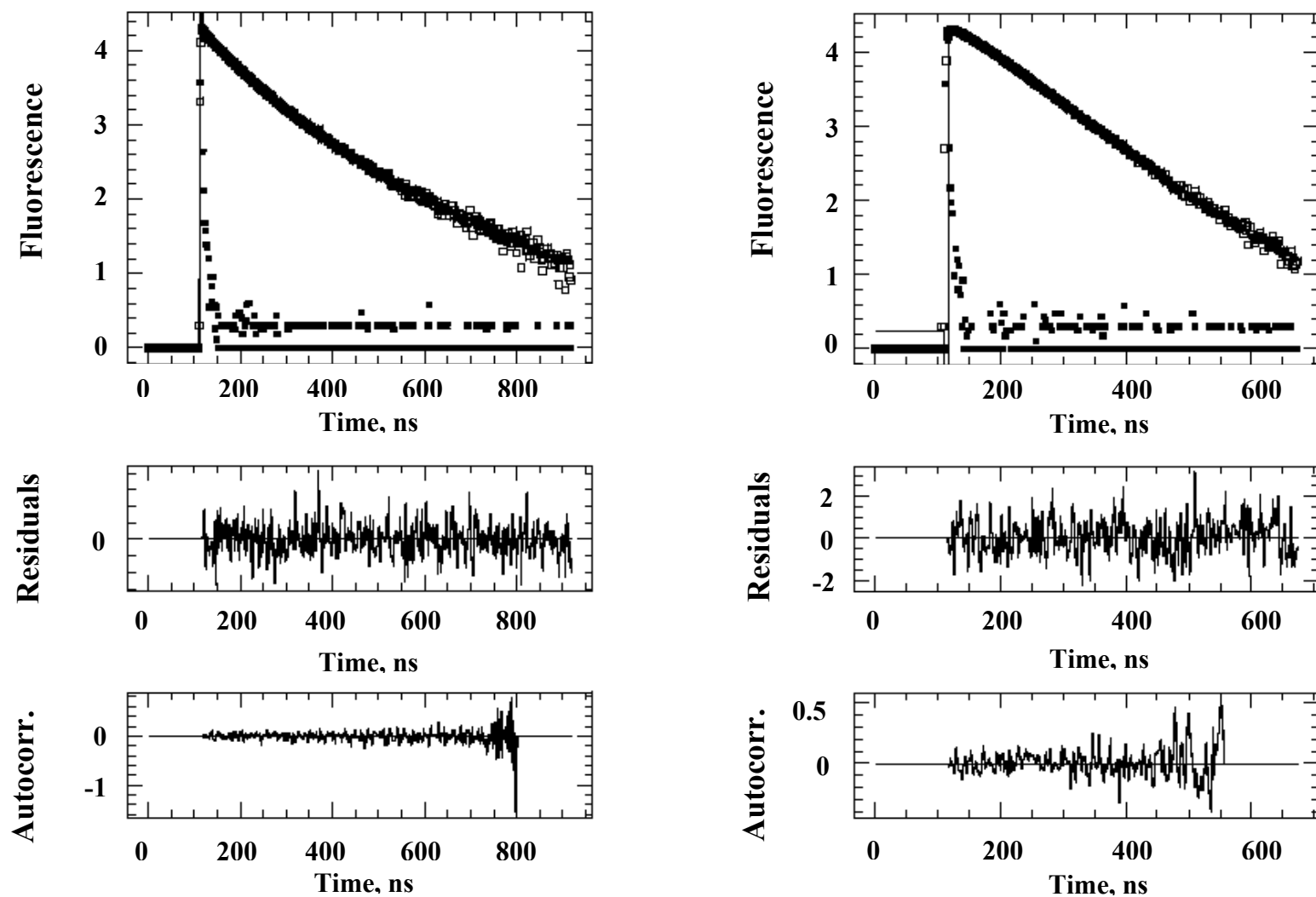


Figure 5.6: Fluorescence decays of the pyrene monomer (left; $\lambda_{\text{ex}} = 344 \text{ nm}$, $\lambda_{\text{em}} = 375 \text{ nm}$) and excimer (right; $\lambda_{\text{ex}} = 344 \text{ nm}$, $\lambda_{\text{em}} = 510 \text{ nm}$) of PEO(5K)-Py₂ with $5 \times 10^{-6} \text{ M}$ SDS using a time per channel of 2.04 ns/ch. $\chi^2 = 1.09$. The decays were globally fitted with the MF analysis. [Py] = $2.5 \times 10^{-6} \text{ M}$.

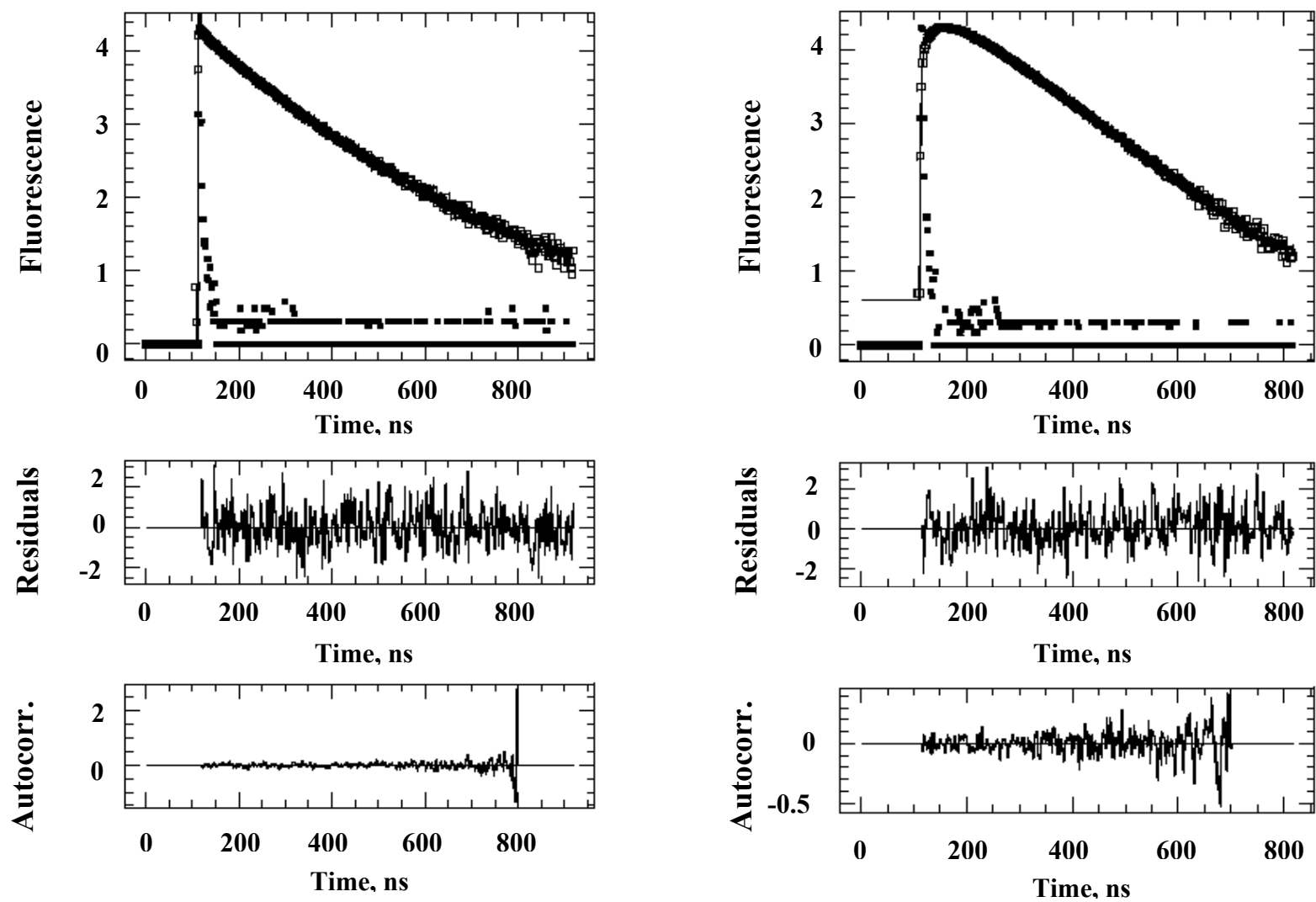


Figure 5.7: Fluorescence decays of the pyrene monomer (left; $\lambda_{\text{ex}} = 344$ nm, $\lambda_{\text{em}} = 375$ nm) and excimer (right; $\lambda_{\text{ex}} = 344$ nm, $\lambda_{\text{em}} = 510$ nm) of PEO(5K)-Py₂ with 10 mM SDS using a time per channel of 2.04 ns/ch. $\chi^2 = 1.09$. The decays were globally fitted with the MF analysis. [Py] = 2.5×10^{-6} M.

At low SDS concentrations, Figure 5.8 shows that in water most of the pyrene pendants are associated for PEO(2K)-Py₂ and the molar fraction f_{E0} decreases from 0.69 ± 0.05 to 0.44 ± 0.01 , and further to 0.16 ± 0.01 for PEO(X)-Py₂ samples having an M_n of 2K, 5K, and 10K, respectively. For each sample, the addition of a sufficient amount of SDS to the solution results in a drop of f_{E0} suggesting that SDS is disrupting the pyrene aggregates. At high SDS concentrations, f_{E0} decreases to around 0.05 for all PEO(X)-Py₂ samples, confirming the disappearance of the pyrene aggregates for high SDS concentrations. However, f_{E0} remains larger than zero at high SDS concentration suggesting that some residual pyrene aggregation is still present in the SDS micelles as has been found previously with Py-HASE.^{30,54} Figure 5.8 also indicates that at low SDS concentrations, not all pyrene excimer is formed by direct excitation of the pyrene aggregates, and that some pyrene excimer is generated by diffusive encounters between an excited and a ground-state pyrene.⁵³ The fraction of pyrenes forming excimer via diffusion, f_{diff} , at low SDS concentrations is found to equal 0.25 ± 0.04 , 0.50 ± 0.01 and 0.71 ± 0.02 for PEO molecular weights of 2K, 5K, and 10K, respectively. With an increase in SDS concentration, f_{diff} increases for PEO(2K)-Py₂ and PEO(5K)-Py₂ until it reaches a maximum value at the CMC of SDS in water above which it remains constant. However for PEO(10K)-Py₂ and PEO(16.5K)-Py₂, f_{diff} decreases after passing through a maximum at an SDS concentration of 5 mM ($[SDS]_p^{diff} = 5$ mM). At this concentration, most pyrene groups are incorporated into mixed micelles as indicated by the I_1/I_3 ratio shown in Figure 5.5 and pyrene excimer is formed by diffusion. The molar fraction f_{diff} at $[SDS]_p^{diff}$ of both PEO(10K)-Py₂ and PEO(16.5K)-Py₂ was found to equal ~ 0.80 . Increasing the SDS concentration past $[SDS]_p^{diff}$ results in a drop in f_{diff} as the pyrene pendants distribute themselves into different micelles in a process that decreases the I_E/I_M ratio. At SDS concentrations higher than the CMC of SDS in water, PEO(10K)-Py₂ and PEO(16.5K)-Py₂ form little excimer.

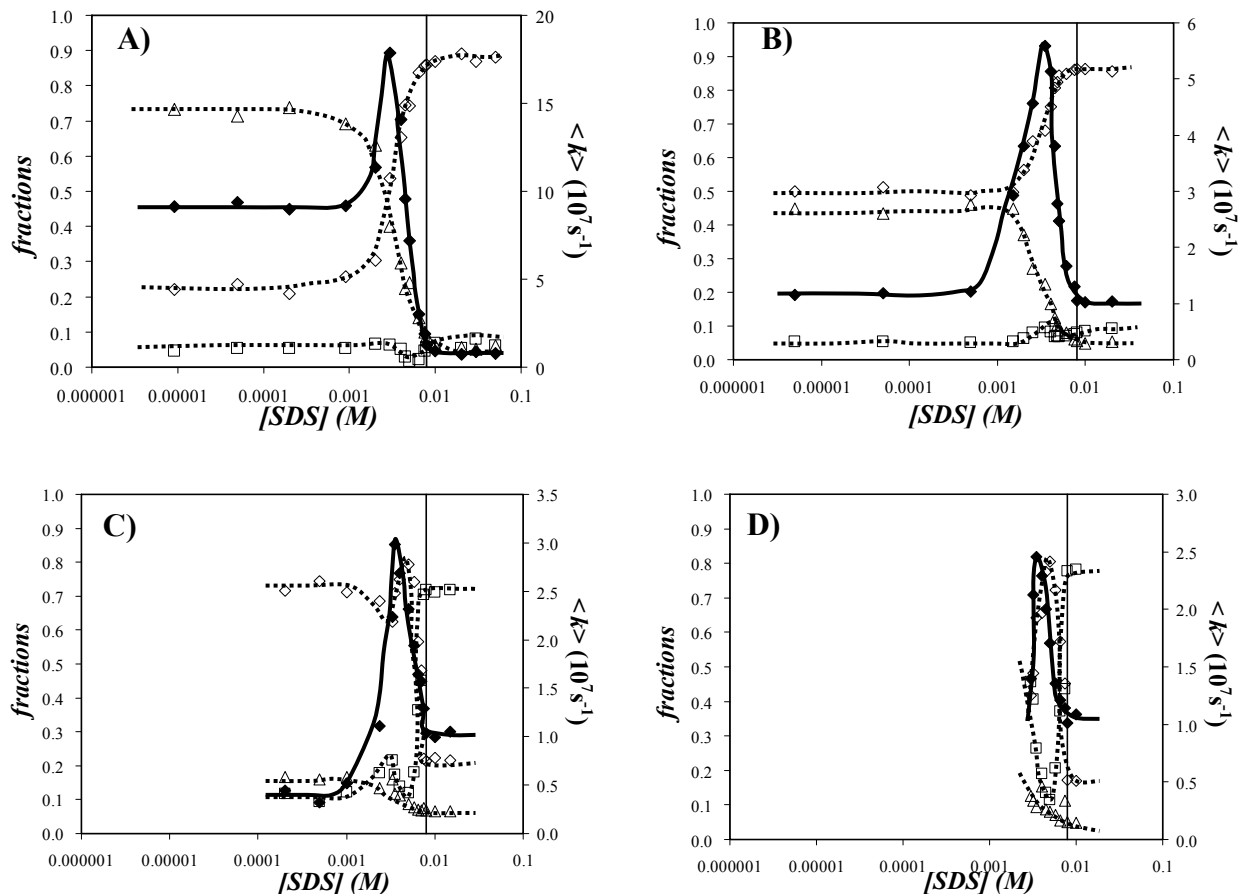


Figure 5.8: Fractions f_{diff} (\diamond), f_{free} (\square), and f_{EO} (\triangle) and $\langle k \rangle$ (\blacklozenge) as a function of SDS concentration for (A) PEO(2K)-Py₂, (B) PEO(5K)-Py₂, (C) PEO(10K)-Py₂, and (D) PEO(16.5K)-Py₂. The vertical line represents the CMC of SDS in water.

At low SDS concentrations the fraction of pyrenes that do not form excimer, f_{free} , is found to equal 0.05 ± 0.01 , 0.05 ± 0.01 and 0.13 ± 0.02 for PEO molecular weights of 2K, 5K, and 10K, respectively. These non-zero f_{free} values result from the presence of pyrene mono-labeled PEO that act as fluorescent impurities for the shorter chains⁵¹ and pyrene groups which are too far to interact with each other for the longer chains,⁴⁷ or a combination of both effects. For PEO(2K)-Py₂ and PEO(5K)-Py₂, f_{free} remains small over the entire range of SDS concentrations within experimental error. PEO(10K)-Py₂ shows a trend that is similar to those obtained with the PEO(2K)-Py₂ and PEO(5K)-

Py₂ samples before $[\text{SDS}]_p^{I_E/I_M}$. Increasing the SDS concentration past $[\text{SDS}]_p^{f_{\text{diff}}}$ for PEO(10K)-Py₂ and PEO(16.5K)-Py₂ results in a dramatic increase of f_{free} as more pyrene groups are isolated in different SDS micelles. After the CMC, f_{free} retains a high value because almost all pyrene pendants are separated in different SDS micelles. In the study of the interactions taking place between Py-HASE and SDS,^{30,54} f_{free} was found to peak at intermediate SDS concentrations below $[\text{SDS}]_p^{I_E/I_M}$ due to the release of free pyrene pendants from the hydrophobic pyrene junctions upon addition of SDS. This observation was confirmed by surface tension measurements.³⁰ However, this effect was not observed in this study because for the short-chain samples, the pyrene end-groups are subject to strong intramolecular hydrophobic interaction⁵³ and they cannot be released into the aqueous phase to behave as a free pyrene. On the other hand f_{E0} is small for the long-chain samples, indicating that most pyrene end-groups are not associated. Under these conditions, the addition of SDS brings the pyrene pendants together instead of releasing more free pyrene groups into the solution as it happens with Py-HASE.

The average rate constants of pyrene excimer formation $\langle k \rangle$ were calculated for the PEO(X)-Py₂ samples according to Equation 5.14 and plotted as a function of SDS concentrations in Figure 5.8. At low SDS concentrations where SDS has little effect on the fluorescence behavior of PEO(X)-Py₂, $\langle k \rangle$ decreases significantly with increasing polymer chain length as the pyrene end-groups are held at a greater distance from each other.⁵³ Further addition of SDS results in an increase of $\langle k \rangle$ due to two effects. First, SDS melts the pyrene aggregates of the short PEO(X)-Py₂ constructs to allow more pyrene excimer to be formed by diffusion. This process is accompanied by a decrease in f_{agg} and an increase in f_{diff} as shown in Figures 5.8A and 5.8B. Second, adding SDS is expected to bring pyrene groups of different chains into the same micelle so that intra- and intermolecular pyrene excimer formation takes place by diffusional encounter between many pyrene units located in a same micelle which results in a larger $\langle k \rangle$. This effect is more predominant with the long-chain PEO(X)-Py₂ constructs which do not form a large amount of pyrene aggregates at low polymer concentration.

After passing through a maximum at an SDS concentration ($[\text{SDS}]_p^{<k>}$), $<k>$ decreases and plateaus at the CMC of SDS in water. The decrease in $<k>$ is due to the separation of the pyrene pendants into different SDS micelles. Interestingly, for SDS concentrations larger than the CMC, $<k>$ takes a constant value of $9.6(\pm 1.1) \times 10^{-6} \text{ s}^{-1}$ for all PEO(X)-Py₂ samples, suggesting that it represents the rate constant for pyrene excimer formation that occurs intramolecularly inside an SDS micelle and that it is independent of the polymer chain length. Although $(I_E/I_M)^{\text{SS}}$ of the long-chain samples takes a value that is close to zero and a large fraction f_{free} is obtained in Figures 5.8C and 5.8D, there still remains a small fraction f_{diff} of pyrene pendants that form excimer intramolecularly inside SDS micelles for PEO(10K)-Py₂ and PEO(16.5K)-Py₂. These constructs form excimer with the same rate constant $<k>$ as the PEO(2K)-Py₂ and PEO(5K)-Py₂ samples.

Self-quenching of the pyrene excimer formed by pyrene aggregates

The effect of self-quenching of the pyrene excimer formed by direct excitation of pyrene aggregates has been investigated previously using different Py-HMWSPs.³²⁻³⁵ In the case of Py-HASE, the quantum yield of a pyrene excimer formed in a pyrene aggregate of Py-HASE in aqueous solution was found to be around 4.5 times smaller than that of the excimer formed inside an SDS micelle.³³ However, the pyrene aggregates formed with Py-HASE were not well characterized as compared to those obtained with PEO(X)-Py₂ because the number of pyrenes per pyrene aggregate of a Py-HASE sample is unknown since the pyrene pendants are incorporated randomly along the Py-HASE backbone. By comparison, PEO(X)-Py₂ has been shown in Chapter 4 to form pyrene excimer intramolecularly at a polymer concentration of $1.25 \times 10^{-6} \text{ M}$, which suggests that under these conditions a pyrene aggregate is composed of two ground-state pyrene pendants only.

The $(I_E/I_M)^{\text{SPC}}$ ratios for the PEO(X)-Py₂ samples were calculated at various SDS concentrations from the parameters retrieved from the global analysis of the monomer and excimer fluorescence decays according to Equation 5.12. $(I_E/I_M)^{\text{SPC}}$, $(I_E/I_M)^{\text{SS}}$, and the ratio $(I_E/I_M)^{\text{SPC}}/(I_E/I_M)^{\text{SS}}$ were plotted in Figure 5.9 as a function of SDS concentration. The difference between $(I_E/I_M)^{\text{SPC}}$ and

$(I_E/I_M)^{SS}$ is that the former ratio is an absolute value while the latter ratio is not. Consequently, the $(I_E/I_M)^{SPC}$ and $(I_E/I_M)^{SS}$ ratios can only be compared on a relative scale and this is achieved by considering the ratio $(I_E/I_M)^{SPC}/(I_E/I_M)^{SS}$. Figure 5.9 exhibits trends that are similar to those found for Py-HASE.

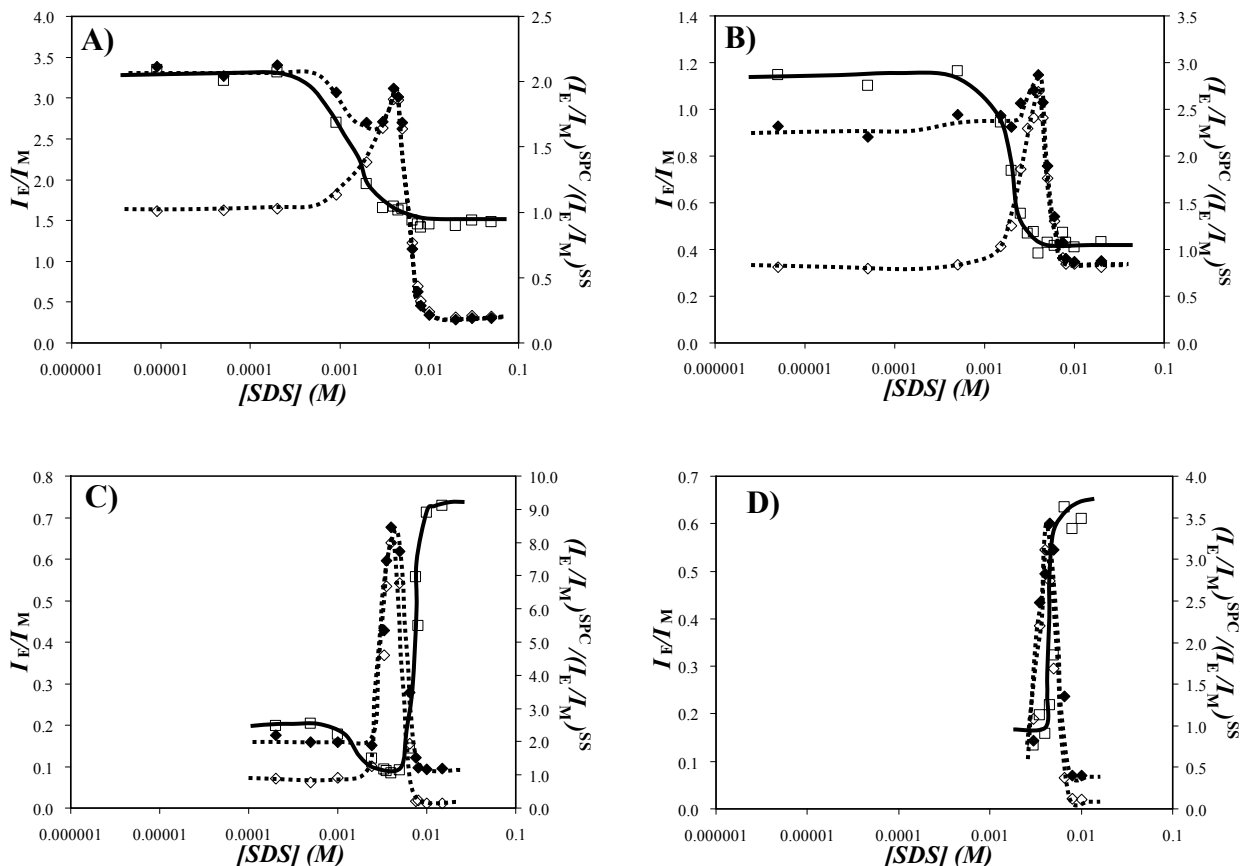


Figure 5.9: The $(I_E/I_M)^{SS}$ ratio (\diamond), $(I_E/I_M)^{SPC}$ ratio (\blacklozenge) and $(I_E/I_M)^{SPC}/(I_E/I_M)^{SS}$ (\square) as a function of SDS concentration for (A) PEO(2K)-Py₂, (B) PEO(5K)-Py₂, (C) PEO(10K)-Py₂ and (D) PEO(16.5K)-Py₂.

Theoretically, the I_E/I_M ratio determined by different fluorescence techniques must be the same, ie. the ratio obtained by time-resolved fluorescence $(I_E/I_M)^{TR}$ has to equal $(I_E/I_M)^{SS}$. The $(I_E/I_M)^{TR}$ ratio can be expressed by Equation 5.14³³

$$\left(\frac{I_E}{I_M}\right)^{TR} = K \frac{k_{rad}^{E0}}{k_{rad}^M} \left(\frac{I_E}{I_M}\right)^{SPC} = \left(\frac{I_E}{I_M}\right)^{SS} \quad (5.14)$$

where K is a constant that depends on the instrument, k_{rad}^{E0} is the radiative rate constant of the excimer, k_{rad}^M is the radiative rate constant of the excited pyrene monomer. At low SDS concentration, k_{rad}^{E0} represents the radiative rate constant of an excimer produced inside a pyrene aggregate whereas at high SDS concentration, k_{rad}^{E0} is the radiative rate constant of an excimer formed by the diffusive encounter between an excited and a ground-state pyrene monomers located in a same SDS micelle. The ratio $\psi = (I_E/I_M)^{SPC} / (I_E/I_M)^{SS}$ in Figure 5.9 represents the deviation between the I_E/I_M ratio obtained by steady-state and time-resolved fluorescence. According to Equation 5.14, ψ can be expressed by Equation 5.15.

$$\psi = \frac{\left(\frac{I_E}{I_M}\right)^{SPC}}{\left(\frac{I_E}{I_M}\right)^{SS}} = \frac{1}{K} \times \frac{k_{rad}^M}{k_{rad}^{E0}} \quad (5.15)$$

Figure 5.9A-C indicates that ψ takes a constant value at low and high SDS concentrations for PEO(2K)-Py₂, PEO(5K)-Py₂, and PEO(10K)-Py₂ (when the SDS concentration is less than 6 mM), respectively, and these values are listed in Table 5.1.

The value of k_{rad}^M of PEO(X)-Py₂ in aqueous solution and in SDS micelles has been found to equal $1.5 \times 10^{-6} \text{ s}^{-1}$ in water and $9.9 \times 10^{-5} \text{ s}^{-1}$ in 0.1 M SDS aqueous solution.³³ Based on the values listed in Table 5.1, k_{rad}^{E0} is found to be 1.48 ± 0.08 , 1.75 ± 0.10 , and 1.43 ± 0.12 times larger when a

pyrene excimer is formed by diffusion inside an SDS micelle than the excitation of a pyrene dimer in an aqueous solution of PEO(2K)-Py₂, PEO(5K)-Py₂, and PEO(10K)-Py₂, respectively.

Table 5.1: ψ obtained in the two plateau regions at low and high SDS concentrations for PEO(2K)-Py₂, PEO(5K)-Py₂, and PEO(10K)-Py₂. For PEO(10K)-Py₂, the results are only considered when [SDS] < 6 mM.

Samples	ψ	
	Low [SDS]	High [SDS]
PEO(2K)-Py ₂	2.06±0.04	0.93±0.04
PEO(5K)-Py ₂	2.84±0.07	1.08±0.05
PEO(10K)-Py ₂	2.41±0.18	1.12±0.04

The quantum yield of the pyrene excimer, ϕ_E , is obtained by Equation 5.16.

$$\phi_E = \tau_{E0} \times k_{rad}^{E0} \quad (5.16)$$

Since the lifetime of the pyrene excimer, τ_{E0} , for the PEO(X)-Py₂ samples was found to equal 45 ± 5 ns regardless of SDS concentration, ϕ_E of the pyrene dimer formed by PEO(X)-Py₂ in water was around 1.55 ± 0.06 times smaller than that of an excimer formed by diffusion inside an SDS micelle. The increase in quantum yield observed when the excimer is formed by diffusion is believed to be due to the self-quenching of pyrene excimer formed with two pre-associated ground-state pyrenes.³³ ϕ_E for the excimer generated by the pyrene aggregates of Py-HASE was found to be 4.5 times smaller than that of the excimer formed inside an SDS micelle.³³ Because an isolated Py-HASE molecule can have more than two pyrene pendants, the pyrene aggregate formed in aqueous solutions of Py-HASE might contain more pyrene groups than that formed by PEO(X)-Py₂ in water. Thus the

differences in ϕ_E for the pyrene aggregates generated by different Py-HMWSPs could be due to different numbers of pyrene molecules per pyrene aggregate.

For the PEO(10K)-Py₂ and PEO(16.5K)-Py₂ solutions with SDS concentration larger than 5 mM, the results significantly deviate from those obtained with the PEO(2K)-Py₂ and PEO(5K)-Py₂ constructs, as shown in Figure 5.9C and 5.9D. This observation can be attributed to the small amount of excimer formed by the long-chain PEO(X)-Py₂ constructs at high SDS concentrations. Under these conditions, f_{free} and f_{diff} were respectively underestimated and overestimated by the analysis, as the excited pyrene monomer that does not form excimer by diffusion is assumed to decay with a single rate constant τ_M^{-1} . As was determined in Chapter 2, while this assumption is certainly correct as a first approximation when strong excimer formation occurs, the biexponential decay of the excited pyrene interacting with the PEO backbone should be taken into account when little excimer is being formed. This would have required disposing of a PEO(10K)-Py₁ or PEO(16.5)-Py₁ sample, which unfortunately was not available at the time when these experiments were conducted. The $(I_E/I_M)^{\text{SPC}}$ ratio was found to be extremely sensitive to the value of f_{diff} when f_{diff} was very small. Therefore, the ratio ψ for PEO(10K)-Py₂ was only considered when the SDS concentration was smaller than 6 mM. The trends of the fractions shown in Figure 5.8 reflect the interactions taking place between PEO(X)-Py₂ and SDS at various SDS concentrations and can be used to propose the mechanisms that describe their interactions.

Interactions between SDS and PEO(X)-Py₂

It was established in Chapter 4 that in pure water without SDS, the shorter PEO(X)-Py₂ constructs form pyrene aggregates intramolecularly while most pyrene pendants attached onto the longer PEO chains are isolated. Upon addition of SDS, these molecules target the pyrene groups and pull them together to form mixed micelles, which results in an increase in $(I_E/I_M)^{\text{SS}}$. At this transition point, the I_1/I_3 ratio starts to decrease reflecting a change in the environment surrounding the pyrenes. For the short-chain samples, addition of SDS decomposes the pyrene aggregates, creates an

environment that solubilizes the pyrene groups, and allows them to form excimer by diffusion. This effect leads to a decrease in f_{E0} and an increase in f_{diff} in Figure 5.8. The rate constant $\langle k \rangle$ is more difficult to analyze as it depends on a combination of many factors that include hydrophobic interactions between pyrene pendants in the aqueous phase and whether excimer formation occurs intra- or intermolecularly in the water phase or in the hydrophobic domains created by SDS.

Increasing the SDS concentration past $[SDS]_p^{I_E/I_M}$ results in an increase in the number of pyrene pendants being incorporated into the mixed micelles, as indicated by the continuous decrease in the I_1/I_3 ratio in Figure 5.5. With all pyrene groups being solubilized inside the mixed micelles, I_1/I_3 plateaus for SDS concentrations larger than the CMC and takes the constant value of 1.43 ± 0.02 for all PEO(X)-Py₂ constructs. At all SDS concentrations, $(I_E/I_M)^{SS}$ took larger values for shorter PEO(X)-Py₂ constructs. This effect is certainly due to the higher local pyrene concentration obtained with the shorter PEO(X)-Py₂ samples. When the SDS concentration is larger than $[SDS]_p^{I_E/I_M}$, increasing amounts of SDS resulted in a decrease in both $\langle k \rangle$ and $(I_E/I_M)^{SS}$ due to a decrease in the local pyrene concentration. The pyrene groups distribute themselves into different hydrophobic junctions formed by the SDS molecules, isolating more pyrene end-groups and preventing them to form an excimer.

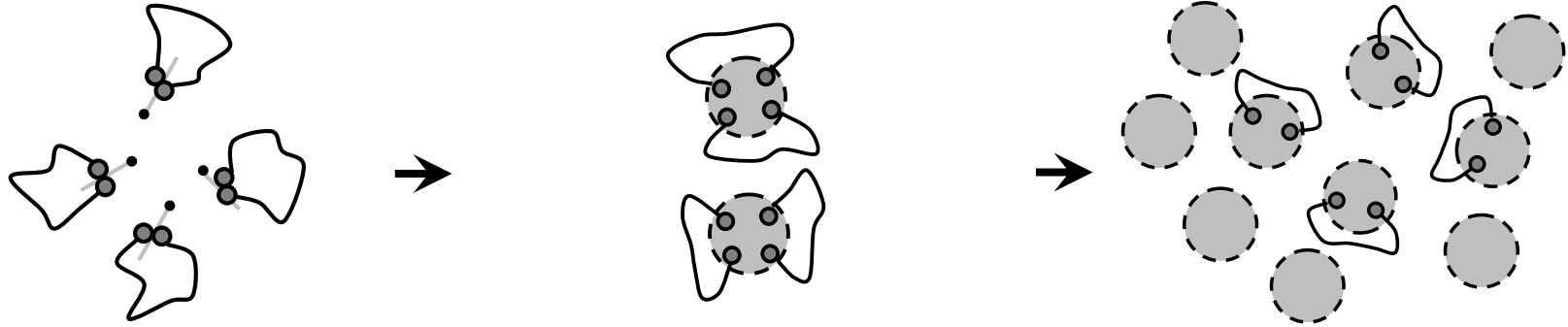
Addition of excess amounts of SDS results in the formation of free SDS micelles whose oily interior solvates the pyrene groups. Because the distance between pyrene end-groups is constrained by the PEO chain length, they cannot be isolated in different SDS micelles for short PEO(X)-Py₂ constructs and pyrene excimer is formed intramolecularly. In this concentration regime, f_{diff} is large and f_{E0} is small for PEO(2K)-Py₂ and PEO(5K)-Py₂. Interestingly, the same fluorescence behavior was found for the PEO(2K)-Py₂ and PEO(5K)-Py₂ samples for SDS concentration larger than the CMC, suggesting that intramolecular pyrene excimer formation is independent of polymer chain length. In the case of the longer PEO(10K)-Py₂ and PEO(16.5K)-Py₂ constructs, the pyrene end-groups can be located in different SDS micelles which results in a large f_{free} value in Figure 5.8.

Above the CMC, $\langle k \rangle$ is constant for all PEO(X)-Py₂ samples, suggesting that the intramolecular formation of pyrene excimer inside SDS micelles is independent of the PEO chain length.

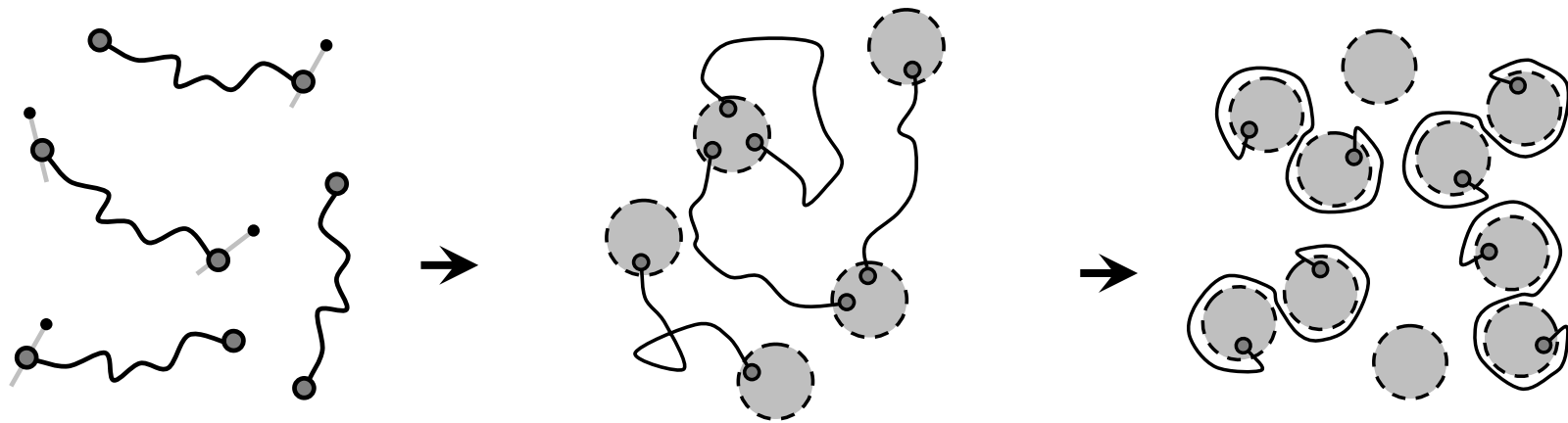
While the sequence of events is similar, with excimer formation being first promoted by intermolecular associations upon addition of SDS and then disfavored as the pyrene pendants are isolated in different micelles, the length of the PEO chain appear to have a major effect on the overall behavior of the PEO(X)-Py₂ constructs. On the one hand, short PEO chains do not allow one pyrene end-group to escape from the hydrophobic environment generated by either the other pyrene end-group in water or an SDS micelle. On the other hand, longer chains act as efficient spacers that hold the two pyrene units away from each other whether in water or in different SDS micelles.

The results that were obtained so far have been summarized schematically in Figure 5.10 to describe the interactions taking place between SDS and the PEO(X)-Py₂ samples. Figure 5.10 consists of two sequences of binding stages that apply for the short-chain samples, PEO(2K)-Py₂ and PEO(5K)-Py₂, on the one hand, and the long-chain samples, PEO(10K)-Py₂ and PEO(16.5K)-Py₂, on the other hand. At low SDS concentrations, SDS molecules target the pyrene pendants and bring them together to form mixed micelles, which results in an increase of the $(I_E/I_M)^{SS}$ ratio. Due to the stronger hydrophobic interactions between the pyrenes attached onto the short-chain samples and the shorter distance separating the pyrene end-groups, it is more difficult to separate them inside the different hydrophobic domains that are created in solution upon addition of SDS, which leads to a larger $(I_E/I_M)^{SS}$ observed than that of the longer chain samples. With excess amounts of SDS, free SDS micelles are formed and the pyrene end-groups of the shorter chain samples cannot be isolated into different SDS micelles. This effect results in intramolecular excimer formation inside a same SDS micelle. On the other hand, most pyrene end-groups attached onto the longer chain PEOs can be successfully separated and the PEO backbone can interact with the surface of the SDS micelles to decrease the electrostatic repulsion between two micelles and further insulate the hydrophobic domains of the micelles from the aqueous phase.

PEO(2K)-Py₂ and PEO(5K)-Py₂



PEO(10K)-Py₂ and PEO(16.5K)-Py₂



Increasing SDS concentration

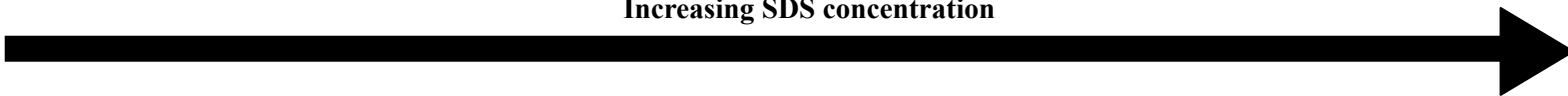


Figure 5.10: Schematic overview of the interactions between SDS and PEO(*X*)-Py₂ as a function of SDS concentration.

5.5 Conclusions

The interactions between SDS and a series of PEO(*X*)-Py₂ constructs were investigated in aqueous solution by ITC, potentiometry, conductimetry, and fluorescence measurements. ITC, EMF, and solution conductivity results showed that the binding between SDS and the PEO backbone takes place at higher polymer concentrations. No such interactions were detected at the low polymer concentrations used for the fluorescence experiments. The pyrene monomer and excimer decays of PEO(*X*)-Py₂ were globally fitted according to the MF analysis in the whole range of SDS concentrations. The fractions of the different excited pyrene species were calculated at different SDS concentrations. The molar fraction of aggregated pyrenes (f_{E0}) was found to decrease with increasing polymer chain length and SDS concentration, indicating that SDS molecules decompose the pyrene aggregates. For PEO(2K)-Py₂ and PEO(5K)-Py₂, the molar fraction of pyrenes forming excimer by diffusional encounter (f_{diff}) increased with SDS concentration and remained constant above the CMC of SDS in water, while f_{diff} of PEO(10K)-Py₂ and PEO(16.5K)-Py₂ peaked at 5 mM SDS before decreasing with increasing SDS amounts. The molar fractions of isolated pyrenes that do not form excimer (f_{free}) for PEO(2K)-Py₂, PEO(5K)-Py₂, and PEO(10K)-Py₂ are small at low SDS concentration and were found to increase with sample chain length. Unfortunately f_{free} could not be obtained for the PEO(16.5K)-Py₂ constructs at low SDS concentration. Increasing the SDS concentration past the CMC resulted in a significant increase of f_{free} for PEO(10K)-Py₂ and PEO(16.5K)-Py₂, as most pyrene groups became isolated in different SDS micelles. However the PEO(2K)-Py₂ and PEO(5K)-Py₂ samples were too short to allow SDS micelles to isolate the pyrene ends and pyrene excimer was still formed by intramolecular diffusion of the pyrene end-groups inside the SDS micelles. A scheme describing the interactions between SDS and the short and long PEO(*X*)-Py₂ constructs was proposed to rationalize the fluorescence results. This study has demonstrated the important role of the PEO chain length for the interaction of PEO-Hyd₂ constructs with SDS in water.

Chapter 6

Interactions between Hydrophobically Modified Alkali-Swellable Emulsion Polymers and Surfactant Probed by Fluorescence and Rheology

6.1 Overview

The interactions between a pyrene-labeled hydrophobically modified alkali-swellable emulsion (Py-HASE) polymer and the anionic surfactant sodium dodecyl sulfate (SDS) in aqueous solution were investigated with a fluorometer, a rheometer, and a combination of both instruments to probe the fluorescence of the polymer while the solution is being sheared. Different amounts of SDS were added to two Py-HASE solutions having concentrations of 8 g/L and 57 g/L. The pyrene monomer and excimer decays of the Py-HASE solutions were acquired and globally fitted with the fluorescence blob model (FBM) and the “model free” (MF) analysis. Both models yielded the same molar fractions of pyrenes that were isolated, aggregated, or forming excimer by diffusion. The average number of pyrenes per micelle, $\langle n \rangle$, was determined according to the FBM and found to equal 2.0 ± 0.1 at the SDS concentration where a maximum of the solution viscosity was observed. For a HASE concentration of 57 g/L, the solution viscosities at different SDS concentrations were measured from the Newtonian plateau regions and were found to peak at a SDS concentration of approximately 11 mM. The steady-state fluorescence spectra at SDS concentrations of 0.1, 6.0, 11.1, and 17 mM were acquired when the Py-HASE solution was sheared. Although a significant decrease in viscosity was observed for the solutions of Py-HASE with SDS under shear, no change in the fluorescence spectra was found when the shear rate was set to equal 0, 0.005, 0.05, 1, 10, and 500 s^{-1} . The overlap of the fluorescence spectra under conditions where the solution viscosity decreases dramatically suggests that the rearrangement of the hydrophobes from inter- to intramolecular associations resulting in

shear-thinning of the solution occurs on a time scale that is much faster than that over which the rheology experiments are being conducted. These results correlate the behavior of the pyrene hydrophobes of Py-HASE probed by fluorescence at the molecular level to the solution macroscopic behavior probed by rheology.

6.2 Introduction

Over the years, special attention has been paid to the interactions between hydrophobically modified water-soluble polymers (HMWSPs) and small molecular surfactants as the composition of their mixtures in aqueous solution can be adjusted to accurately control the viscosity of the resulting solution. Due to their peculiar rheological properties, aqueous solutions of HMWSP and surfactant mixtures are used in a number of important applications such as in cosmetics, paints, and enhanced oil recovery, to name but a few.¹⁻⁴

In semidilute aqueous solutions, the HMWSPs form both inter- and intramolecular polymeric aggregates due to hydrophobic interactions between the hydrophobic pendants.⁵ Adding a surfactant to a HMWSP aqueous solution substantially alters its rheological properties and two models have been proposed to rationalize this phenomenon. The first model assumes that the polymer network is altered by the interactions taking place between the HMWSP and the surfactant.⁶⁻¹¹ In the presence of a moderate amount of surfactant, a three-dimensional extended polymer network is created by physical crosslinking of the polymer chains through the formation of mixed micelles constituted of the hydrophobic pendants of the HMWSPs and surfactant molecules. Crosslinking of the polymer chains hinders their movement and the solution viscosity increases as a consequence. Addition of excess surfactant disrupts the polymeric network which results in a significant drop in solution viscosity due to the decreased connectivity between polymer chains. The second model uses the residence time (τ_{res}) of a hydrophobic group in an intermolecular micellar junction to describe the

changes in the rheological behavior of HMWSP solutions upon addition of a surfactant.¹²⁻¹⁴ In the case of telechelic hydrophobically modified ethoxylated urethane polymers (HEURs) which exhibit a single Maxwell relaxation time (τ_r), τ_{res} equals τ_r .^{12,13} Upon addition of a surfactant like sodium dodecyl sulfate (SDS), τ_{res} of the hydrophobe of a HEUR associative thickener was found to increase and peak at a certain SDS concentration.¹³ This result suggested that the hydrophobic groups stay longer inside the hydrophobic junctions leading to an increase in the solution viscosity.^{13,14} Further addition of surfactant shortens the relaxation time and the solution viscosity decreases accordingly.^{13,14} However, this model cannot be applied to determine τ_{res} for the transient networks formed by other HMWSPs such as the hydrophobically modified alkali-swelling emulsion polymers (HASEs) whose more complex rheological behavior is not described by the Maxwell model.¹⁵⁻¹⁷

The interactions between HASEs and various surfactants have been widely investigated by different experimental approaches, such as calorimetry,^{18,19} rheology,^{20,21} light scattering,²² surface tension,²³ and fluorescence.²³⁻²⁶ In the case of the fluorescence studies, the alkyl hydrophobic pendants typically used for HASEs were replaced by the chromophore pyrene.²³⁻²⁶ Pyrene is water-insoluble and the rheology of pyrene-labeled HASEs (Py-HASEs) was found to behave in a manner similar to that of HASEs bearing alkyl hydrophobes.²⁷ Pyrene is also a chromophore with several unique photophysical properties²⁸ which can be employed to study the behavior of Py-HASE in solution. First, its emission spectrum can be used to probe the polarity of its local environment.²⁹ Second, an excited pyrene can form an excimer by associating with a ground-state pyrene.³⁰ The pyrene excimer emits at different wavelengths compared to the excited pyrene monomer, which provides an easy means of detection for the association of pyrene pendants. Third, pyrenes form excimer by either diffusional encounter or direct excitation of ground-state pyrene aggregates.³¹ These two processes can be distinguished through the analysis of the excimer fluorescence decays. If the excimer is formed by diffusion between two pyrene groups, excimer formation is delayed and a

rise time is observed in the excimer decay. On the other hand, the formation of excimer by direct excitation of ground-state pyrene dimers is instantaneous and no rise time is detected in the excimer decay. For aqueous solutions of pyrene-labeled HMWSPs like Py-HASE, quantitative information about the molar fractions of the pyrene species present in solution, be they aggregated pyrenes, isolated pyrenes, or pyrenes forming excimer via diffusion, can be determined from the global analysis of the fluorescence decays of the pyrene monomer and excimer according to the Fluorescence Blob Model (FBM) and the Model Free analysis (MF), respectively.²³⁻²⁶ These parameters are extremely useful to describe the viscoelastic behavior of solutions of HMWSPs in general and Py-HASE in particular.²⁷

In this study, a Py-HASE sample with a 12 $\mu\text{mol/g}$ pyrene content (Py-HASE12), that is five times smaller than that of the Py-HASE sample investigated in Ref 32, was used as it was shown to undergo more intermolecular interactions in solution.²⁷ With no surfactant, the pyrene pendants of Py-HASE12 are aggregated in water and pyrene excimer is generated by direct excitation of ground-state pyrene aggregates. Addition of SDS to the Py-HASE12 solution induces the formation of mixed micelles at higher SDS concentration where pyrene pendants form excimer by diffusion and the rheological behavior of the solution is altered. This study used fluorescence to probe the interactions between Py-HASE12 and SDS at the molecular level and rheology to probe the solution behavior at the macroscopic level. The molar fractions of different pyrene species present in solution and the average numbers of pyrenes per SDS micelle were retrieved by global analysis of the pyrene monomer and excimer fluorescence decays, while the effect of shear rate on the solution viscosities was investigated by rheology as a function of SDS concentration. This study provided evidence that the change in the rheological behavior of the solution induced by the addition of SDS was due to the rearrangement of the hydrophobes that led to the disruption of the polymeric network. Additionally, τ_r was determined from the viscosity profiles obtained as a function of shear rate and exhibited a trend

similar to that of the solution zero-shear viscosity as a function of SDS concentration. Finally, coupling of the rheometer and fluorometer enabled the acquisition of the fluorescence spectra of Py-HASE12 and SDS solutions under shear. The overlap of the fluorescence spectra acquired at shear rates ranging from 0 to 500 s⁻¹ suggests that application of shear does not affect the fraction of aggregated pyrenes, but rather the nature of these aggregates that are formed intermolecularly at low shear and intramolecularly at high shear.

6.3 Experimental

Materials: Py-HASE12 was prepared by DOW Chemical Corp. using emulsion polymerization. The synthesis of Py-HASE12 has been described elsewhere.^{33,34} The chemical structure of the polymer is shown in Figure 6.1. It contained 12 μmol of pyrene per gram of polymer.^{27,35} The method of purification, the preparation of the aqueous polymer solution, and the determination of the polymer concentration in aqueous solution were conducted according to published procedures.^{23,27,35} SDS was purchased from EM Science and used as received.

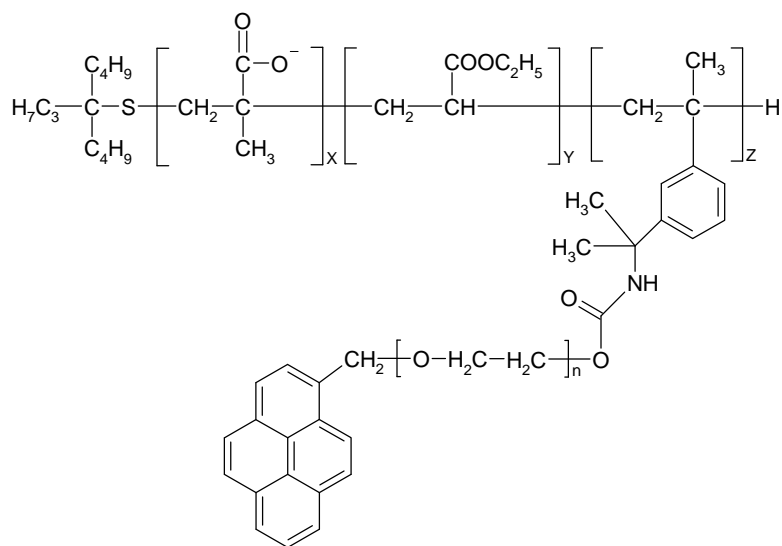


Figure 6.1: Chemical structure of Py-HASE12 with X:Y:Z = 40:59:0.2.

Steady-state fluorescence measurements: All steady-state fluorescence emission spectra were obtained using a Photon Technology International (PTI) fluorometer with a continuous Ushio UXL-75Xe xenon arc lamp as the light source and a PTI 814 photomultiplier detection system. To avoid the inner filter effect, all fluorescence spectra were acquired with a triangular cell purchased from Hellma using the front face geometry.³⁶ The Py-HASE12 solutions were excited at a wavelength of 344 nm. The fluorescence intensities of the pyrene monomer (I_M) and excimer (I_E) were determined by integrating the fluorescence spectra from 372 to 378 nm for the pyrene monomer and from 500 to 530 nm for the pyrene excimer. The I_1/I_3 ratio which reflects the polarity of the microenvironment where pyrene is located was determined by taking the ratio of the fluorescence intensity of the first (I_1) and third (I_3) peaks of the pyrene monomer at 374 and 385 nm, respectively.

Time-resolved fluorescence measurements: The fluorescence decay profiles were obtained by the time-correlated single-photon counting technique (TC-SPC) on an IBH time-resolved fluorometer using the front face geometry.³⁶ The excitation source was an IBH 340 nm LED used with a 500 kHz repetition rate. All fluorescence decays were acquired over 1024 channels ensuring a minimum of 20,000 counts at their maximum. All solutions were excited at 344 nm, and the emission wavelength of the pyrene monomer and excimer was set at 375 and 510 nm, respectively. To reduce potential scattered light, cutoff filters of 370 and 495 nm were used to obtain the fluorescence decays of the pyrene monomer and excimer, respectively. A time per channel of 2.04 ns/ch was used for the acquisition of the monomer and excimer decays of all solutions. For the analyses of the decays, reference decays of degassed solutions of PPO [2,5-diphenyloxazole] in cyclohexane ($\tau = 1.42$ ns) for the pyrene monomer and BBOT [2,5-bis(5-*tert*-butyl-2-benzoxazolyl)thiophene] in ethanol ($\tau = 1.47$ ns) for the pyrene excimer were used to obtain the instrument response function (IRF) via the MIMIC method.³⁷

Analysis of the fluorescence decays: Upon excitation, the excited pyrene species of Py-HASE in aqueous solution can be classified into four categories, namely Py_{free}^* , Py_{diff}^* , $E0^*$, and D^* . Py_{free}^* represents the excited pyrenes that emit with the natural lifetime τ_M and never form an excimer. This species can be detected in the monomer decay only. Py_{diff}^* refers to the excited pyrenes which form excimer via diffusional encounter with a ground-state pyrene. This process is dynamic and is probed in both the monomer and excimer decays. $E0^*$ represents the pyrene excimer that emits with a lifetime τ_E . D^* results from the direct excitation of poorly stacked pre-associated pyrene aggregates that emit with a longer lifetime τ_D . The sum of the concentrations of the two aggregated pyrene species [$E0^*$] and [D^*] yields [Py_{agg}^*], the overall concentration of excited aggregated pyrenes. The monomer and excimer decays were globally fitted according to the FBM^{31,38} with the mathematical expressions of the monomer and excimer given by Equations 6.1 and 6.2, respectively.

$$[M^*] = [Py_{diff}^*]_{(t=0)} \exp \left[- \left(A_2 + \frac{1}{\tau_M} \right) t - A_3 (1 - \exp(-A_4 t)) \right] + [Py_{free}^*]_{(t=0)} \exp(-t/\tau_M) \quad (6.1)$$

$$[E^*] = -[Py_{diff}^*]_{(t=0)} e^{-A_3} \sum_{i=0}^{\infty} \frac{A_3^i}{i!} \frac{A_2 + i A_4}{\frac{1}{\tau_M} - \frac{1}{\tau_{E0}} + A_2 + i A_4} \exp \left(- \left(\frac{1}{\tau_M} + A_2 + i A_4 \right) t \right) \\ + \left([E0^*]_{(t=0)} + [Py_{diff}^*]_{(t=0)} e^{-A_3} \sum_{i=0}^{\infty} \frac{A_3^i}{i!} \frac{A_2 + i A_4}{\frac{1}{\tau_M} - \frac{1}{\tau_{E0}} + A_2 + i A_4} \right) e^{-t/\tau_{E0}} \\ + [D^*]_{(t=0)} e^{-t/\tau_D} \quad (6.2)$$

The parameters A_2 , A_3 , and A_4 used in Equations 6.1 and 6.2 are given in Equation 6.3.

$$A_2 = \langle n \rangle \frac{k_{blob} k_{ex}[blob]}{k_{blob} + k_{ex}[blob]} \quad A_3 = \langle n \rangle \frac{k_{blob}^2}{(k_{blob} + k_{ex}[blob])^2}$$

$$A_4 = k_{blob} + k_{ex}[blob] \quad (6.3)$$

The parameters k_{blob} , $\langle n \rangle$, and $k_{ex}[blob]$ used in Equation 6.3 represent the rate constant of pyrene excimer formation inside a blob, the average number of pyrenes per blob, and the product of k_{ex} which is the rate constant describing the exchange of ground-state pyrenes between blobs and $[blob]$ which is the local blob concentration, respectively.

The monomer and excimer decays can also be fitted globally according to the MF analysis.^{24,39-41} The mathematical expressions used to fit the monomer and excimer fluorescence decays are given by Equations 6.4 and 6.5, respectively.

$$[Py^*]_{(t)} = [Py_{diff}^*]_{(t=0)} \times \sum_{i=1}^n a_i \times \exp(-t/\tau_i) + [Py_{free}^*]_{(t=0)} \times \exp(-t/\tau_M) \quad (6.4)$$

$$[E^*]_{(t)} = -[Py_{diff}^*]_{(t=0)} \times \sum_{i=1}^n a_i \frac{\frac{1}{\tau_i} - \frac{1}{\tau_M}}{\frac{1}{\tau_i} - \frac{1}{\tau_{E0}}} \exp(-t/\tau_i)$$

$$+ \left([E0^*]_{(t=0)} + [Py_{diff}^*]_{(t=0)} \times \sum_{i=1}^n a_i \frac{\frac{1}{\tau_i} - \frac{1}{\tau_M}}{\frac{1}{\tau_i} - \frac{1}{\tau_{E0}}} \right) \times \exp(-t/\tau_{E0})$$

$$+[D^*]_{(t=0)} \times \exp(-t / \tau_D) \quad (6.5)$$

Global analysis of the monomer and excimer decays using Equations 6.1 and 6.2 or 6.4 and 6.5 allows the determination of the fractions f_{Mdiff} , f_{Mfree} , f_{Ediff} , f_{EE0} , and f_{ED} whose expressions are given in Equations 6.6 – 6.10.

$$f_{Mdiff} = \frac{[Py_{diff}^*]_{(t=0)}}{[Py_{diff}^*]_{(t=0)} + [Py_{free}^*]_{(t=0)}} \quad (6.6)$$

$$f_{Mfree} = \frac{[Py_{free}^*]_{(t=0)}}{[Py_{diff}^*]_{(t=0)} + [Py_{free}^*]_{(t=0)}} \quad (6.7)$$

$$f_{Ediff} = \frac{[Py_{diff}^*]_{(t=0)}}{[Py_{diff}^*]_{(t=0)} + [E0^*]_{(t=0)} + [D^*]_{(t=0)}} \quad (6.8)$$

$$f_{EE0} = \frac{[E0^*]_{(t=0)}}{[Py_{diff}^*]_{(t=0)} + [E0^*]_{(t=0)} + [D^*]_{(t=0)}} \quad (6.9)$$

$$f_{ED} = \frac{[ES^*]_{(t=0)}}{[Py_{diff}^*]_{(t=0)} + [E0^*]_{(t=0)} + [D^*]_{(t=0)}} \quad (6.10)$$

The fractions obtained from Equations 6.6 – 6.10 can be used to calculate the overall contributions of aggregated pyrene, f_{agg} , diffusional pyrene, f_{diff} , and isolated pyrene, f_{free} in an aqueous Py-HASE solution according to Equations 6.11 – 6.15.

$$f_{diff} = \frac{[Py_{diff}^*]_{(t=0)}}{[Py_{diff}^*]_{(t=0)} + [Py_{free}^*]_{(t=0)} + [E0^*]_{(t=0)} + [D^*]_{(t=0)}} = \left(1 + \frac{f_{Mfree}}{f_{Mdiff}} + \frac{f_{EE0}}{f_{Ediff}} + \frac{f_{ED}}{f_{Ediff}} \right)^{-1} \quad (6.11)$$

$$f_{free} = \frac{[Py_{free}^*]_{(t=0)}}{[Py_{diff}^*]_{(t=0)} + [Py_{free}^*]_{(t=0)} + [E0^*]_{(t=0)} + [D^*]_{(t=0)}} = f_{diff} \times \frac{f_{Mfree}}{f_{Mdiff}} \quad (6.12)$$

$$f_{E0} = \frac{[E0^*]_{(t=0)}}{[Py_{diff}^*]_{(t=0)} + [Py_{free}^*]_{(t=0)} + [E0^*]_{(t=0)} + [D^*]_{(t=0)}} = f_{diff} \times \frac{f_{EE0}}{f_{Ediff}} \quad (6.13)$$

$$f_D = \frac{[D^*]_{(t=0)}}{[Py_{diff}^*]_{(t=0)} + [Py_{free}^*]_{(t=0)} + [E0^*]_{(t=0)} + [D^*]_{(t=0)}} = f_{diff} \times \frac{f_{ED}}{f_{Ediff}} \quad (6.14)$$

$$f_{agg} = f_{E0} + f_D \quad (6.15)$$

The natural lifetime of pyrene, τ_M , in aqueous solution and in SDS micelles was determined from the long decay time obtained by fitting the monomer fluorescence decays of Py-HASE12 at extremely low pyrene concentration ($[Py] = 2.5 \times 10^{-6}$ mol/L) without and with 0.1 M SDS and was found to equal 164 and 166 ns, respectively. Therefore, τ_M was fixed in all analysis by taking the average value of 165 ns. The analysis was carried out with the Marquardt-Levenberg algorithm⁴² to obtain the optimized pre-exponential factors and decay times. The fits were considered good if χ^2 was smaller than 1.30, and residuals and autocorrelation of the residuals were randomly distributed around zero.

Viscosity measurements: The viscosity of the 8 g/L Py-HASE12 aqueous solution was determined with an Ubbelohde viscometer at 25 ± 0.1 °C. The viscosity of the 57 g/L Py-HASE12 aqueous solution was measured at room temperature (23 ± 1 °C) with a stress-controlled Paar Physica DSR 4000 rheometer interfaced with a USD 200 tower. A parallel-plate geometry with a 25 mm diameter plate was used with a gap width of 1 mm for all samples. All data points were recorded within the sensitivity range of the instrument as specified by the manufacturer. The shear rate was varied from

0.0001 to 1000 s⁻¹.

Joint rheometer-fluorometer measurements: The setup combining the steady-state fluorometer and the rheometer is illustrated in Figure 6.2.³² The joint rheometer/fluorometer apparatus allows the simultaneous investigation of the Py-HASE12 solution by fluorescence and rheology. The rheometer was enclosed inside a light-proof box and the light signals corresponding to the excitation and emission of the fluorometer were delivered via fibre optic cables. A parallel-plate geometry was used with a gap width of 1 mm between the 25 mm diameter quartz plate at the top and the metal plate at the bottom. The fluorescence spectra of the solutions were acquired at fixed shear rates after the solution viscosity has reached a constant value at the target shear rate. The detailed description for the joint setup and the specifications of the fibre optic cables has been presented earlier.³²

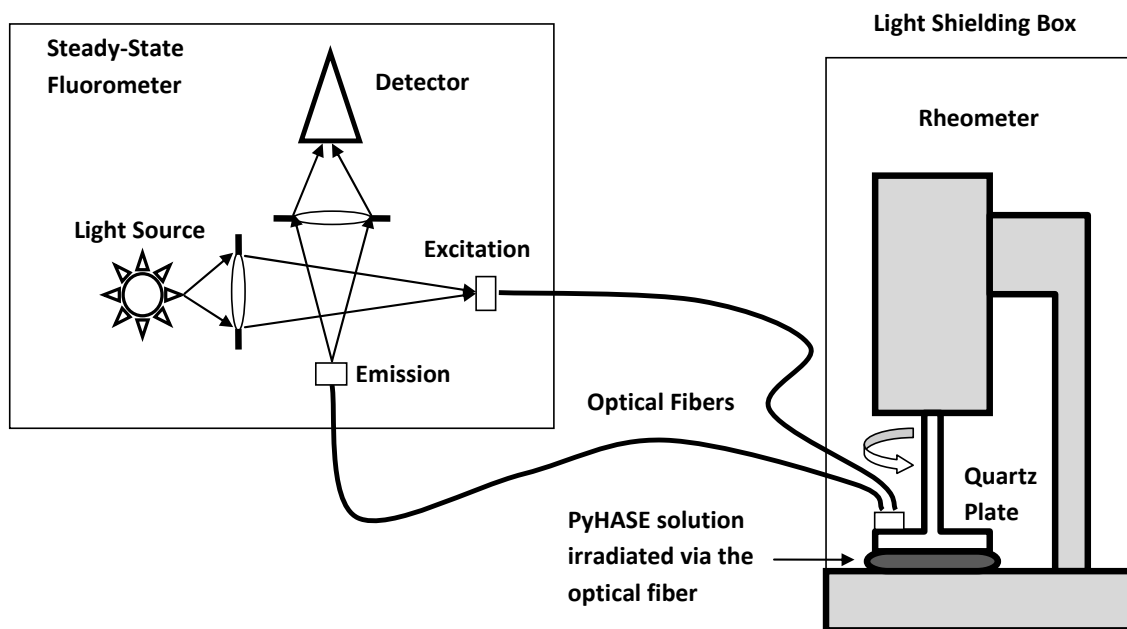


Figure 6.2: Experimental setup enabling the acquisition of fluorescence spectra of a Py-HASE solution under shear in the rheometer.

6.4 Results and Discussion

Two Py-HASE12 concentrations of 8 g/L and 57 g/L were used to investigate the interaction of SDS with the pyrene pendants of the polymer in 0.01 M Na₂CO₃ solution at pH 9. Under these conditions, the overlap concentration (C^*) of Py-HASE has been determined to equal 2.4 g/L.⁴³ Consequently, both concentrations are greater than C^* , indicating that the results obtained with these concentrations describe the behavior of the polymer solution in the semidilute regime.

Addition of SDS to the polymer solution altered the fluorescence spectrum of Py-HASE12, demonstrating that the SDS molecules interact with the pyrene groups. The fluorescence spectra of Py-HASE12 normalized at 374 nm are shown in Figure 6.3. The trends observed at both polymer concentrations are similar. For the 8 g/L Py-HASE12 concentration, Figures 6.3A and 6.3B indicate that the excimer intensity relative to that of the monomer increases for SDS concentrations increasing from 0 to 3.5 mM and decreases for SDS concentrations increasing from 3.5 mM to 1.6 mM. Similarly, the excimer intensity increases in Figure 6.3C for the 57 g/L Py-HASE12 concentration when the SDS concentration is raised from 0 to 10 mM but decreases in Figure 6.3D when the SDS concentration is further increased from 10 mM to 100 mM.

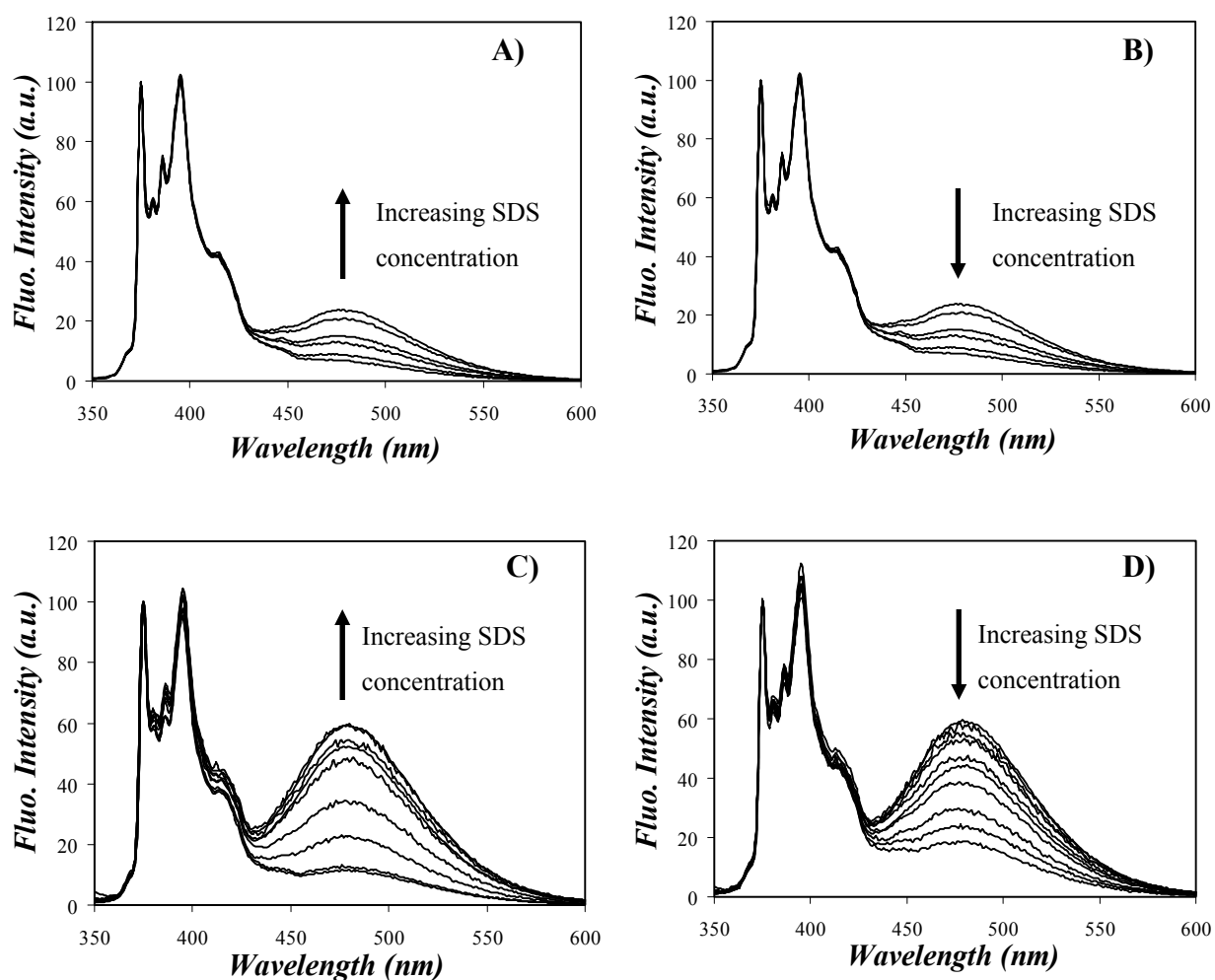


Figure 6.3: Fluorescence emission spectra of an 8 g/L Py-HASE12 solution (top) with SDS concentrations ranging from (A) 0 to 3.5 mM and (B) from 3.5 to 50 mM and a 57 g/L Py-HASE12 solution (bottom) with SDS concentrations ranging from (C) 0 to 10 mM and (D) from 10 to 100 mM. The solution is a 0.01 M Na_2CO_3 aqueous solution at pH 9. All spectra were normalized at 375 nm.

Figure 6.4 shows the I_E/I_M and I_1/I_3 ratios obtained for the two Py-HASE12 solutions as a function of SDS concentration. The intensity of the third peak (I_3) of the pyrene monomer emission in Figure 6.3 A-D increases with respect to the first peak (I_1) at intermediate SDS concentrations but remains constant at a lower or higher value for lower and higher SDS concentrations, respectively.

This behavior is captured in the top panel of Figure 6.4. The change in I_1/I_3 indicates that the pyrene pendants experience a more apolar environment as SDS is added to the Py-HASE12 solutions.²³

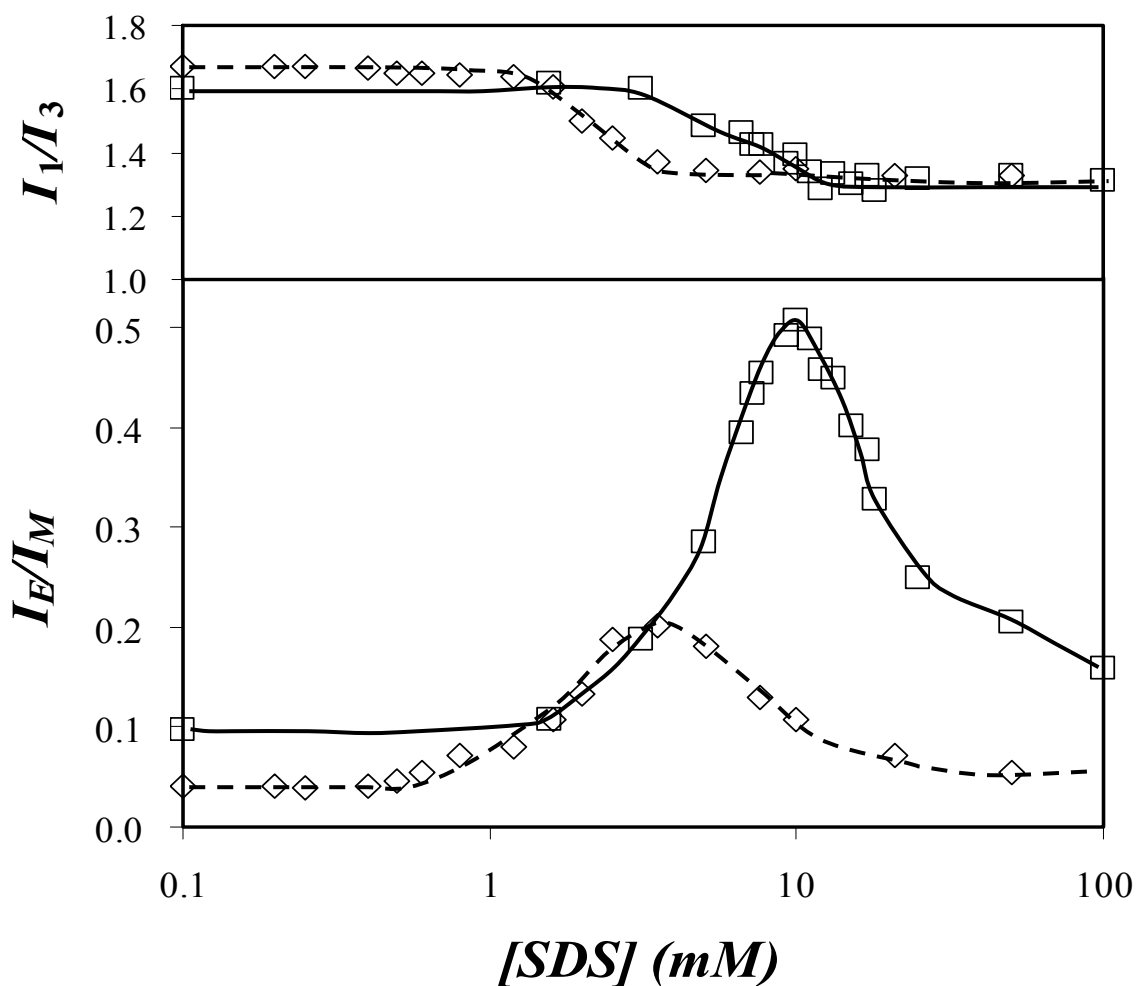


Figure 6.4: Plot of I_E/I_M (bottom panel) and I_1/I_3 (top panel) vs. SDS concentration for Py-HASE12 at 8 g/L (\diamond) and 57 g/L (\square). All samples were excited at 344 nm.

The I_E/I_M ratio describes qualitatively the efficiency of pyrene excimer formation and its behavior is shown in the bottom panel of Figure 6.4 as a function of SDS concentration. At low SDS

concentrations, most pyrene groups associate in solution and I_E/I_M remains constant suggesting that SDS does not interact with the pyrene aggregates certainly due to electrostatic repulsions between the SDS micelles/surfactants and the Py-HASE12 polymer coils. The low I_E/I_M ratio obtained in the plateau region corresponding to the low SDS concentration regime is due to the low fluorescence quantum yield of the pyrene excimer formed via the direct excitation of a pyrene aggregate.^{26,44,45} With more SDS added into the polymer solution, I_E/I_M increases as SDS targets the pyrene aggregates to form mixed micelles where the pyrene groups form excimer by diffusion with a higher fluorescence quantum yield – around 4.5 times larger than the excimer formed inside pyrene aggregates.²⁶ The hydrophobic alkyl chains of the SDS molecules interact with the pyrene aggregates, enabling the solvation of the pyrene moieties that form excimer more efficiently. After I_E/I_M peaks at the critical SDS concentrations of 3.5 mM and 10 mM for Py-HASE12 concentrations of, respectively, 8 g/L and 57 g/L, further addition of SDS results in a decrease of I_E/I_M due to the distribution of the pyrene pendants into different mixed micelles which hinders the diffusional encounters of pyrene groups located in different micelles. I_1/I_3 remains constant for SDS concentrations larger than the critical SDS concentration at the I_E/I_M peak ($[SDS]_p^{I_E/I_M}$) suggesting that the pyrene groups are located in the less polar environment provided by the hydrophobic domains of the mixed micelles. Therefore, the drop in I_E/I_M past $[SDS]_p^{I_E/I_M}$ can be attributed to the decrease in the average number of pyrenes per mixed micelle in this range of SDS concentration.²³ Figure 6.4 also shows that the profile of I_E/I_M versus SDS concentration obtained for the 57 g/L Py-HASE12 solution shifts to higher SDS concentration when compared with the profile obtained with the lower polymer concentration. These effects were also observed with a Py-HASE36 sample.²³ They are due to the increase in the number of pyrene groups present in a more concentrated Py-HASE solution, which requires more SDS to interact with the more numerous pyrene pendants.

The monomer and excimer fluorescence decays of Py-HASE12 were acquired at both polymer concentrations with different SDS concentrations. The decays were fitted globally with the FBM and MF analysis. The fits were good with χ^2 smaller than 1.30, and residuals and autocorrelation functions of the residuals randomly distributed around zero. The parameters including the decay times and pre-exponential factors retrieved from the analyses are listed in Table SI.6.1 of the Supporting Information (SI). According to these parameters, the molar fractions of aggregated pyrenes (f_{agg}), pyrenes forming excimer by diffusional encounter (f_{diff}), and isolated pyrenes that do not form excimer (f_{free}) were determined using Equations 6.6 – 6.15 according to procedures described in previous papers.³⁹⁻⁴¹ The fractions are listed in Table SI.6.2 and plotted as a function of SDS concentration in Figure 6.5. Both FBM and MF analyses yielded identical trends when the molar fractions f_{diff} , f_{free} , and f_{agg} were plotted as a function of SDS concentration demonstrating excellent agreement between the two analyses.

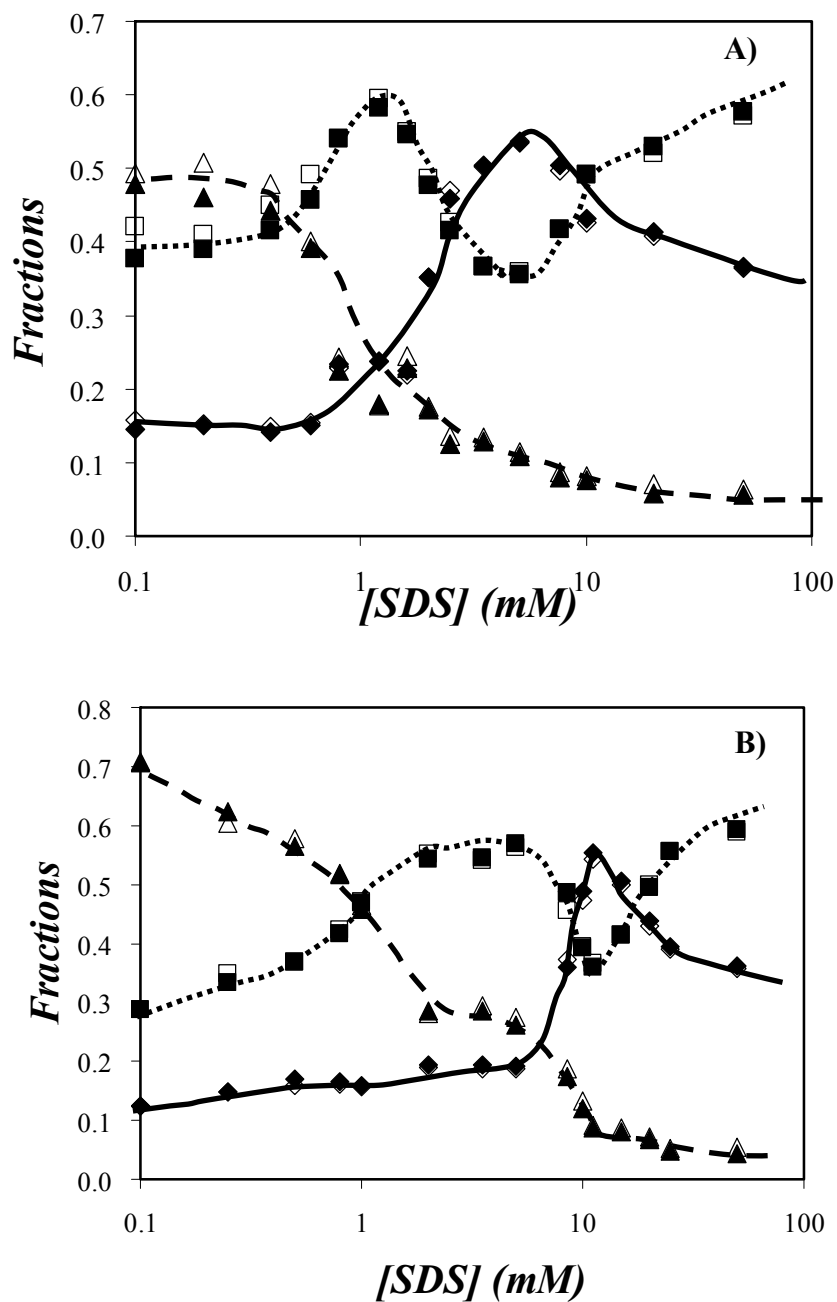


Figure 6.5: Fractions f_{diff} (\blacklozenge and \diamond), f_{free} (\blacksquare and \square), and f_{agg} (\blacktriangle and \triangle) as a function of SDS concentration for Py-HASE12 at polymer concentrations of (A) 8 and (B) 57 g/L. The filled and hollow symbols indicate that the pyrene monomer and excimer decays were globally fitted with the FBM or MF analysis, respectively.

At small SDS concentrations, Figure 6.5 shows that the most populated state of the pyrene pendants is that of the aggregated pyrenes and that the molar fraction f_{agg} increases from 0.50 to 0.71 with an increase in Py-HASE12 concentration from 8 to 57 g/L. With more SDS added to the solution, f_{agg} drops dramatically suggesting that SDS is targeting the pyrene aggregates. At high SDS concentrations, f_{agg} decreases to around 0.05 for both polymer solutions confirming the disappearance of the pyrene aggregates for large SDS concentrations. However, f_{agg} remains larger than zero at high SDS concentration suggesting that some residual pyrene aggregation is still present in the SDS micelles, as has been found previously.²³ Figure 6.5 also indicates that at low SDS concentrations, not all pyrene excimer is formed by direct excitation of the pyrene aggregates, and that some pyrene excimer is generated by the diffusive encounter between an excited and a ground-state pyrene. The fraction of pyrene forming excimer via diffusion, f_{diff} , is small at low SDS concentrations found to equal 0.14 and 0.13 for polymer concentrations of 8 and 57 g/L, respectively. With an increase in SDS concentration, f_{diff} increases and peaks at an SDS concentration ($[\text{SDS}]_p^{f_{\text{diff}}}$) where most pyrene groups are incorporated into mixed micelles and pyrene excimer is formed by diffusion. The molar fraction f_{diff} at $[\text{SDS}]_p^{f_{\text{diff}}}$ of 5.1 and 11.1 mM was found to equal 0.53 and 0.55 for the polymer concentrations of 8 and 57 g/L, respectively. The SDS concentration at $[\text{SDS}]_p^{f_{\text{diff}}}$ is very close to $[\text{SDS}]_p^{I_E/I_M}$ found to equal 3.5 and 10 mM at Py-HASE12 concentrations of 8 and 57 g/L. Increasing the SDS concentration past $[\text{SDS}]_p^{f_{\text{diff}}}$ results in a drop in f_{diff} as the pyrene pendants distribute themselves into different micelles in a process that decreases the I_E/I_M ratio. At very high SDS concentration, pyrene excimer is still formed by diffusion but with a reduced number of pyrene pendants.

Although pyrene is a hydrophobe that tends to aggregate in aqueous solution, a significant fraction of pyrenes that do not form excimer, f_{free} , is found at low SDS concentrations. The values for f_{free} without SDS equal 0.36 and 0.28 for the polymer concentrations of 8 and 57 g/L, respectively. The larger f_{free} value obtained at the lower Py-HASE12 concentration is expected as it reflects a decrease in intermolecular aggregation following a decrease in pyrene concentration. With a continuous increase in SDS concentration, the value of f_{free} first increases, then decreases, before increasing again past $[\text{SDS}]_p^{f_{\text{diff}}}$. This behavior can be rationalized as follows. At low SDS concentration, SDS targets the pyrene aggregates and expels pyrene moieties into the bulk solution where they act as isolated pyrenes.²³ With more SDS added to the solution, these free pyrene groups are “pulled back” into the mixed micelles which are generated between SDS molecules and the pyrene pendants. For SDS concentrations larger than $[\text{SDS}]_p^{f_{\text{diff}}}$, f_{free} increases because more pyrene groups are isolated in different SDS micelles. This rational has been corroborated by earlier surface tension experiments.²³

As stated earlier, the interactions between HMWSPs and surfactants result in solutions that exhibit particularly interesting viscoelastic properties.⁶⁻¹⁴ Such properties were observed for the Py-HASE12 solution having a concentration of 57 g/L whose zero-shear viscosity was found to increase dramatically upon SDS addition. Figure 6.6 shows the variation of the solution viscosity as a function of shear rate for a 57 g/L aqueous solution of Py-HASE12 with varying concentrations of SDS. In order to correlate the trends obtained from the rheological behavior of the polymer solutions and its associative behavior characterized by fluorescence, the SDS concentrations used for the rheological experiments covered the whole range of SDS concentrations used in the fluorescence experiments (see Figure 6.3C). A small Newtonian regime is observed for all samples at low shear rates where the viscosity remains constant with shear rate and is taken as the zero-shear viscosity, η_0 . Figure 6.6

demonstrates that the addition of SDS up to the concentration of 11.1 mM for the 57 g/L Py-HASE12 aqueous solution increases η_0 20-fold from 200 to 4,000 Pa.s. Further addition of SDS results in a dramatic decrease in η_0 to 30 Pa.s for an SDS concentration of 100 mM. Figure 6.6 also shows that when shear is applied to the solutions, the viscosity drops dramatically with increasing shear rate. This effect is referred to as shear thinning, which is a common effect for associating polymers and has been widely investigated before.^{12,15-17,20,21,27,46-48} Generally, shear thinning is due to a transition from intermolecular to intramolecular associations resulting from the “pull-out” and rearrangement of the hydrophobes. The results shown in Figure 6.6 have two implications: first, pyrene is an efficient hydrophobe that behaves similarly to other nonfluorescent hydrophobes such as the alkyl chains typically used in commercial HASEs; second, interactions between SDS and the pyrene groups result in a progressive change in the rheological behavior of the polymer solution. Figure 6.6 also demonstrates that shear thinning occurs at a lower onset shear rate for solutions having a higher viscosity, an observation which had been made earlier for solutions of Py-HASEs having different pyrene content.

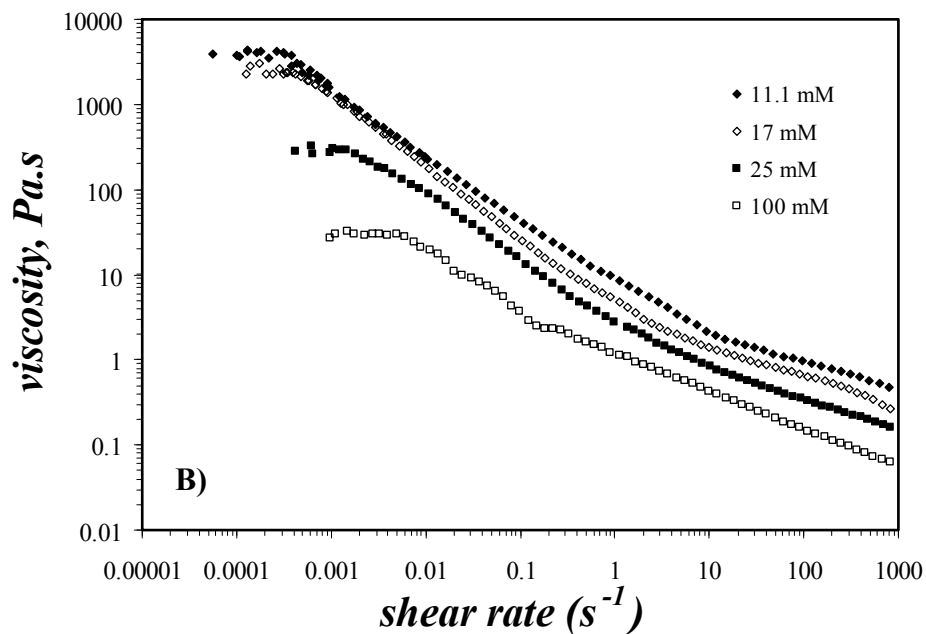
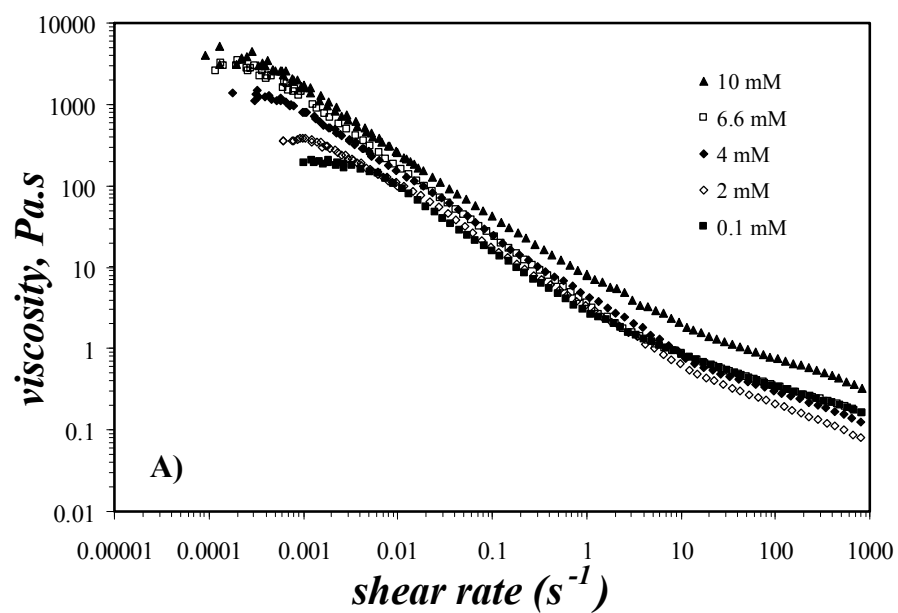


Figure 6.6: Steady-shear viscosity as a function of shear rate for Py-HASE12 at 57 g/L with SDS concentrations ranging from (A) 0.1 to 10 mM and (B) 11.1 to 100 mM.

To better correlate the results obtained by the fluorescence and viscosity measurements, the I_E/I_M ratios, the average number of pyrene pendants per mixed micelle, $\langle n \rangle$, retrieved from the global analysis of the monomer and excimer decays of the Py-HASE12 solutions using the FBM, and the zero-shear viscosity were plotted together in Figure 6.7 as a function of SDS concentration for the two polymer concentrations. At a Py-HASE12 concentration of 8 g/L, an Ubbelohde viscometer was used to measure η_0 since the solutions were much less viscous than the 57 g/L Py-HASE12 solutions. The viscosity profiles obtained for both polymer concentrations as a function of SDS concentration are typical of solutions where interactions between a surfactant and HMWSPs take place.⁶⁻¹¹ At low SDS concentrations, the associations between pyrene groups are most likely intrapolymeric in nature.²³ The addition of SDS enhances intermolecular pyrene excimer formation which reflects enhanced networking and results in an increase in solution viscosity. Beyond the SDS concentration where the viscosity peaks, the hydrophobes are separated between different micelles which reduces the networking ability of Py-HASE12. As a result, the viscosity drops progressively to even much lower values than those obtained for the Py-HASE12 solution without SDS, as shown in Figure 6.7 for both polymer concentrations. In Figure 6.7A, the error bars of η_0 acquired with the 8 g/L Py-HASE12 solution are not shown because they are smaller than the symbols.

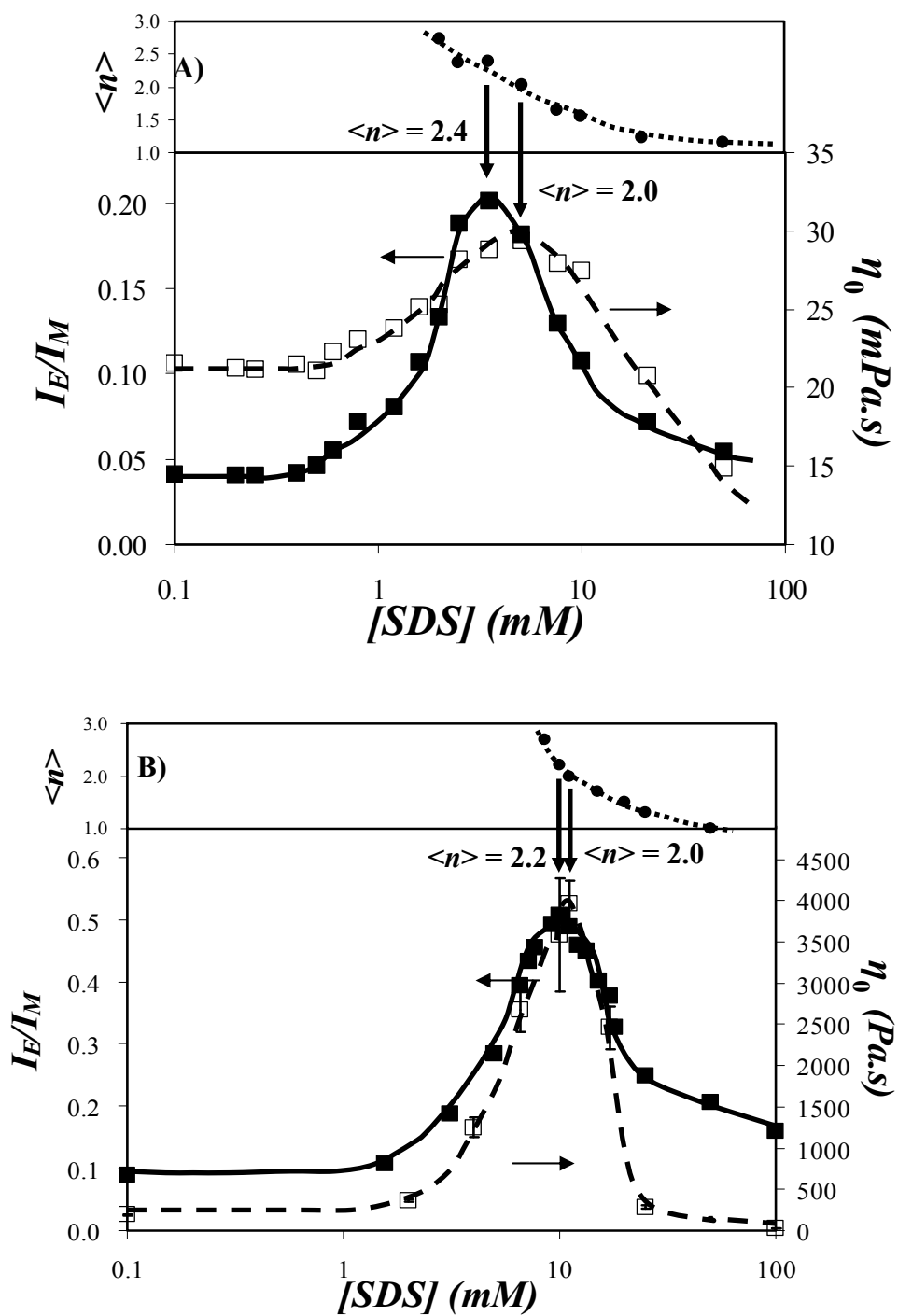


Figure 6.7: Values of $\langle n \rangle$ (top panel) and I_E/I_M and η (bottom panel) plotted as a function of SDS concentration for a Py-HASE12 concentration of (A) 8, and (B) 57 g/L.

For SDS concentration around $[\text{SDS}]_p^{I_E/I_M}$, the pyrene pendants are expected to be incorporated into SDS micelles where they distribute themselves randomly according to a Poisson distribution. Consequently, the parameter $\langle n \rangle$ retrieved from the analysis of the fluorescence decays with the FBM yields the average number of pyrenes per mixed micelles. It is plotted in Figure 6.7 as a function of SDS concentration. $\langle n \rangle$ decreases from a value of 2.8 to a value of 1.0 as the SDS concentration increases. Interestingly, $\langle n \rangle$ equals 2.0 ± 0.1 ⁴⁹ for those SDS concentrations where η_0 passes through a maximum for both polymer concentrations. Since the optimal networking ability of a HMWSP in the presence of surfactant micelles is attained when each mixed micelle contains 2 hydrophobes per micelle on average, the $\langle n \rangle$ value of 2.0 found at an SDS concentration where η_0 peaks in the present experiments and earlier one²³ represents a nice correlation between the results obtained by fluorescence and rheology. $\langle n \rangle$ appears to decrease towards unity at high SDS concentration.

The relaxation time (τ_r) of the polymeric network probed by rheology reflects the relaxation of individual polymer chains. Under shear, relaxation of the polymeric network results in a decrease in solution viscosity. τ_r of the 57 g/L Py-HASE12 solution at different SDS concentration was taken as the inverse of the shear rate obtained at the onset of shear-thinning. A plot of τ_r as a function of SDS concentration is presented in Figure 6.8. τ_r exhibits a trend that is similar to that obtained for the solution viscosity shown in Figure 6.7B. The data shown in Figure 6.8 indicate that τ_r increases with increasing SDS concentration until it passes through a maximum at an SDS concentration of 11.1 mM where all pyrene pendants are located in the hydrophobic domains formed by SDS. Further increase in SDS concentration results in a significant decrease in τ_r . Combining the data presented in Figures 6.5B, 6.7B and 6.8, these results suggest that when SDS is added into the Py-HASE12 solution, SDS molecules interact with the pyrene aggregates by replacing pyrene units that are ejected into the

solution where they enhance networking resulting in an increase in viscosity and τ_r . At higher SDS concentrations, the pyrenes are isolated in different hydrophobic junctions formed by SDS in a process that decreases the average number of hydrophobes per junction. While interactions between the pyrenyl pendants and the SDS molecules first promote intermolecular bridging of the polymeric network, a point is reached where further increase in $[SDS]$ disrupts the network and both viscosity and τ_r of the solution decrease.

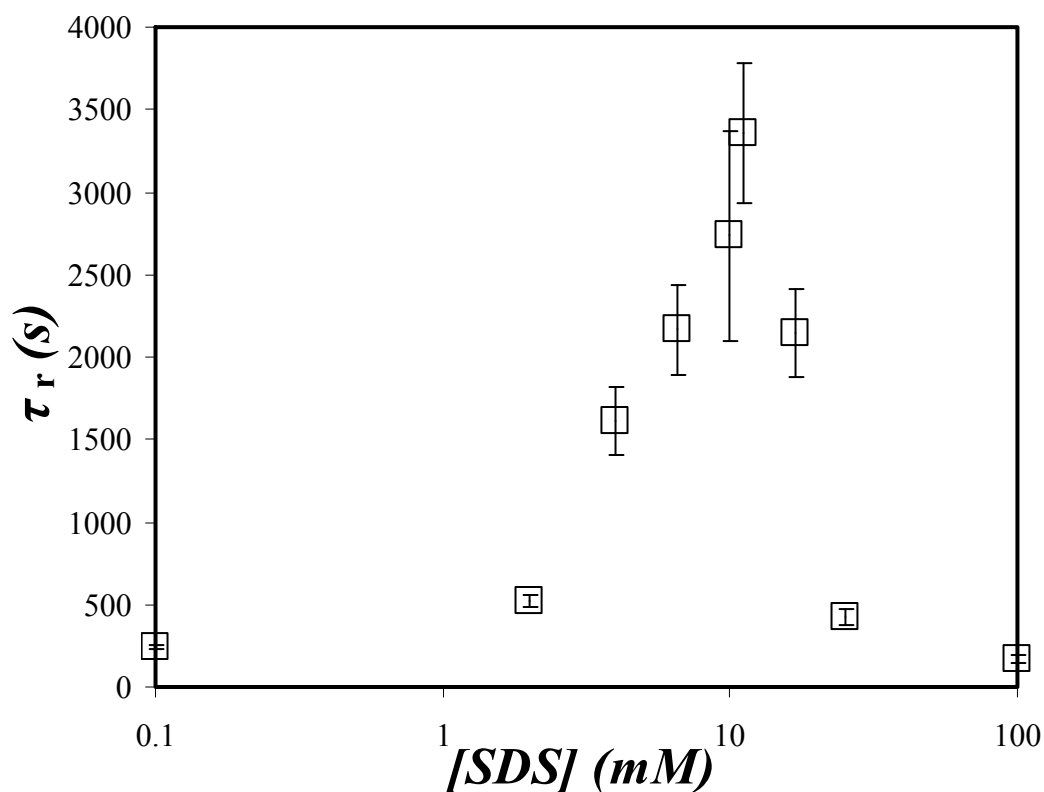


Figure 6.8: Plot of τ_r as a function of SDS concentration for the 57 g/L Py-HASE12 solution.

Since the shear thinning effect shown in Figure 6.6 results from a rearrangement of the configuration of the polymer chains in solution, the setup shown in Figure 6.2 was used to acquire the

fluorescence spectra of the polymer solution under shear in an effort to probe this rearrangement. The samples with a Py-HASE12 concentration of 57 g/L were used at SDS concentrations of 0.1, 6, 11.1, and 17 mM which cover the whole range of the SDS concentrations shown in Figure 6.7B. The steady-state emission spectra of the Py-HASE12 solutions were acquired for the SDS concentrations mentioned above using the joint setup at shear rates ranging from 0 to 500 s⁻¹. Figure 6.9 presents the fluorescence spectra obtained at a SDS concentration of 11.1 mM, which is the concentration where η_0 peaks ($[\text{SDS}]_p^{\eta_0}$) in Figure 6.7B and an optimal polymeric network is formed according to the $\langle n \rangle$ value of 2.0 ± 0.1 retrieved from the analysis of the fluorescence decays. For comparison purposes, the fluorescence spectrum of the solution was also acquired in the spectrofluorometer using a triangular quartz cell having the front face geometry to minimize the inner filter effect. All spectra were normalized at 375 nm. As demonstrated in Figure 6.9, the emission fluorescence spectra acquired at all shear rates with the setup shown in Figure 6.2 overlapped perfectly, even with the one acquired with the fluorescence cell. In this latter case, the acquisition of the fluorescence spectrum was carried out without optical fiber resulting in less light scattering being detected at 350 nm. Since the fluorescence spectra reflect the arrangement of the pyrene pendants in the solution, this lack of change in the fluorescence spectra is remarkable as it occurs over a range of shear rates where the solution viscosity decreases by over four orders of magnitude, from 4,000 Pa.s at $\dot{\gamma} = 0 \text{ s}^{-1}$ to 0.4 Pa.s at $\dot{\gamma} = 500 \text{ s}^{-1}$.

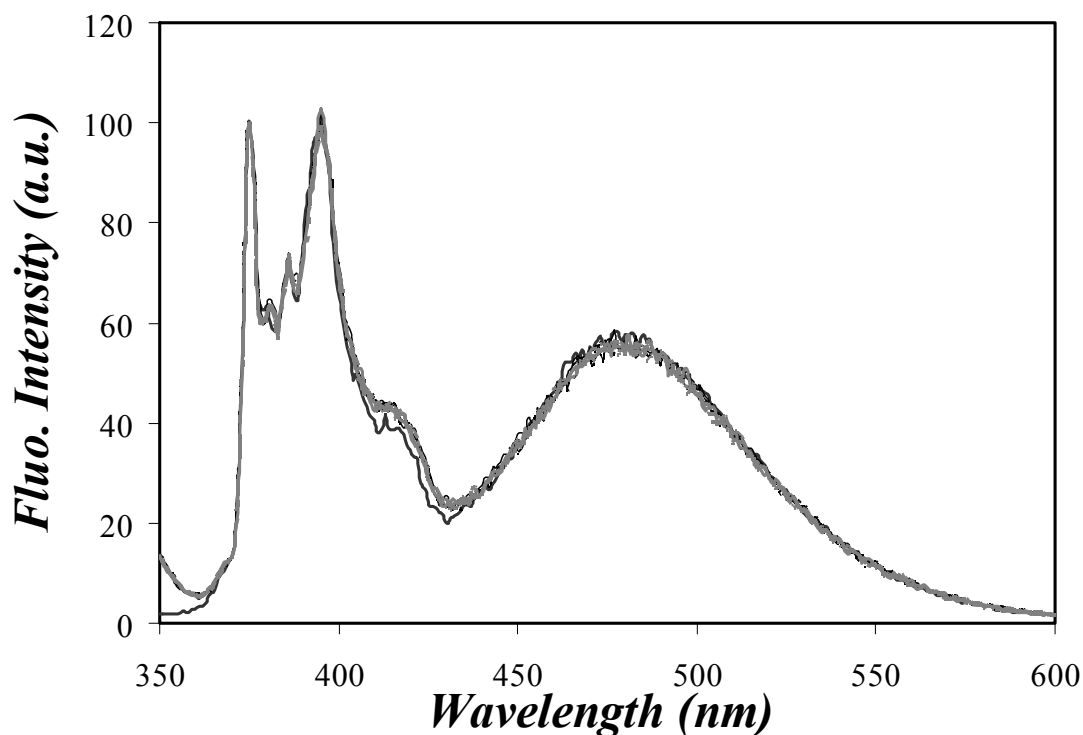


Figure 6.9: Fluorescence emission spectra normalized at 375 nm of 57 g/L Py-HASE12 solution with a SDS concentration of 11.1 mM acquired in a triangular fluorescence cell (—) and with shear rates of 0 (—), 0.005 (---), 0.05 (.....), 1 (—), 10 (— —) and 500 (.....) s^{-1} .

The ratios I_E/I_M and I_1/I_3 determined from the emission spectra of the Py-HASE12 solution at four SDS concentrations were plotted in Figure 6.10 as a function of shear rate. Again, although the viscosity at each SDS concentration dropped by several orders of magnitude with an increase in shear rate (see Figure 6.6), the I_E/I_M and I_1/I_3 ratios were all independent of shear rate. This result suggests that the overall arrangement of the pyrene pendants in the solution does not change and that the polarity of the local environment surrounding the pyrene groups remains constant when the solution is under shear. These results are similar to those obtained in other experiments carried out by this laboratory using the joint setup with the rheometer and the steady-state and time-resolved fluorimeters for solutions of Py-HASE65 at various polymer concentrations.⁴⁰ These experiments

also showed that f_{agg} remains constant at different shear rates despite a significant change in the macroscopic viscosity of the solution.

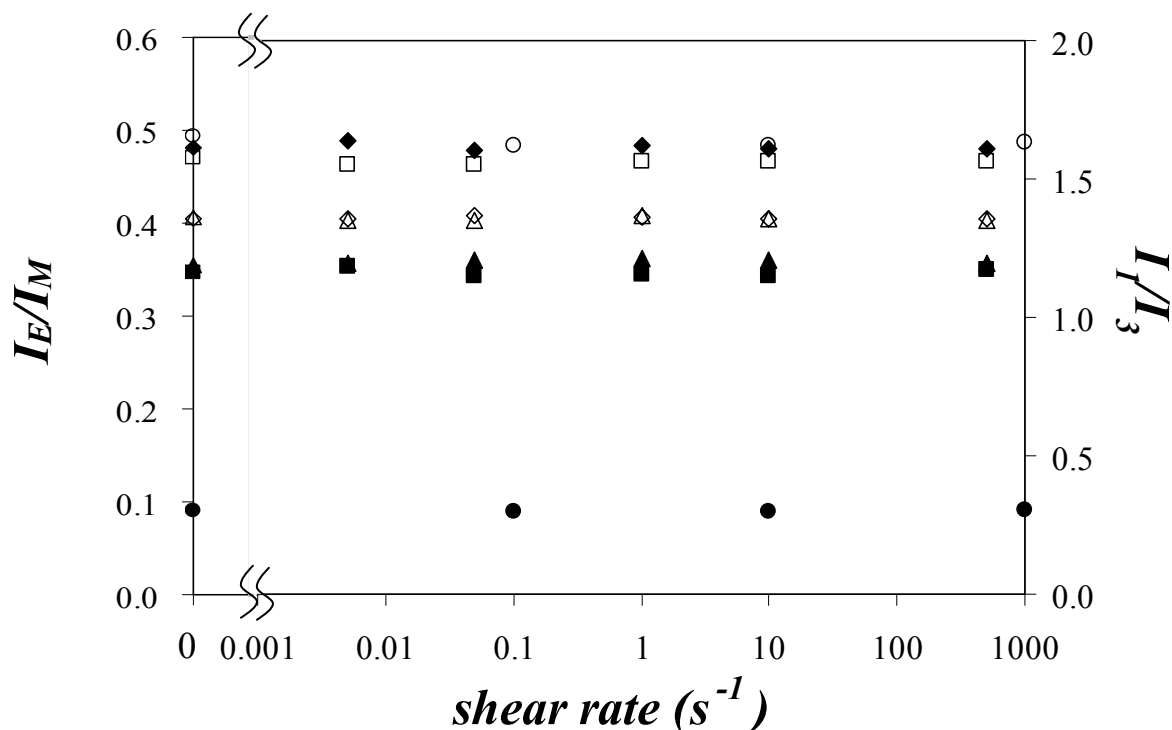


Figure 6.10: I_E/I_M (filled symbols) and I_1/I_3 (hollow symbols) of 57 g/L Py-HASE12 solution with SDS concentrations of 0.1 (circle), 6.0 (square), 11.1 (diamond) and 17 (triangle) mM.

The shear thinning effect is believed to result from a transition between inter- to intramolecular hydrophobic association and a similar phenomenon is expected to occur for the aqueous solutions of Py-HASE12 and SDS. An extremely low shear rate does not disrupt the polymer network and the hydrophobic aggregates are unaffected. Therefore the viscosity does not change and the sample exhibits the Newtonian plateau regime observed in Figure 6.6. At a higher shear rate, the polymeric network is extended due to the stretching of the polymer coils by shear. Under those

conditions, the physically crosslinked network is deformed until the hydrophobes are pulled out from the hydrophobic junctions. With more hydrophobes escaping from the junctions that bridge the polymer chains intermolecularly, the network collapses which is accompanied by a shear thinning effect. However, the hydrophobes which are pulled out from the aggregates are not isolated in solution. The rearrangement of the polymeric network triggered by the applied shear induces these hydrophobes to form intramolecular associations on a time scale that is too fast to be probed by our experimental setup. This process has been investigated by Winnik's group using HEURs which is known to form flower like micelles in aqueous solution.⁴⁶⁻⁴⁸ For HEURs, the shear thinning effect can be described as a "bridge-to-loop" transition.⁴⁸ At extremely high shear rates, the hydrophobes of the bridging chains are pulled out from the interpolymeric junctions but the overall number of micelles remains the same.^{46,47} These micelles whose hydrophobic cores are severed from the network do no longer contribute to the solution viscosity. Indeed, the results shown in Figure 6.10 suggest that this transition from inter- to intramolecular pyrene association does not affect the association between the hydrophobic pyrenes as the fluorescence spectra of the Py-HASE12 solutions remain unchanged. A schematic describing the change of the Py-HASE polymeric network with SDS under shear is shown in Figure 6.11. The polymeric network is decomposed under shear via the "pull-out" of pyrene pendants from intermolecular pyrene aggregates or mixed micelles followed by the rearrangement of the polymer coils under shear to enhance intramolecular pyrene interactions. However, this inter- to intramolecular transition does not affect the balance between free pyrene and aggregated pyrene species. Since the balance between isolated and excimer forming pyrenes remains the same under shear regardless of whether pyrene excimer formation occurs intra- or intermolecularly, the I_E/I_M ratio is unaffected. Furthermore, upon addition of SDS, the inter- to intramolecular transition does not affect the microenvironment that pyrene is probing. Therefore the I_1/I_3 ratio is also unaffected. Consequently, the fluorescence emission spectra remain unchanged under shear.

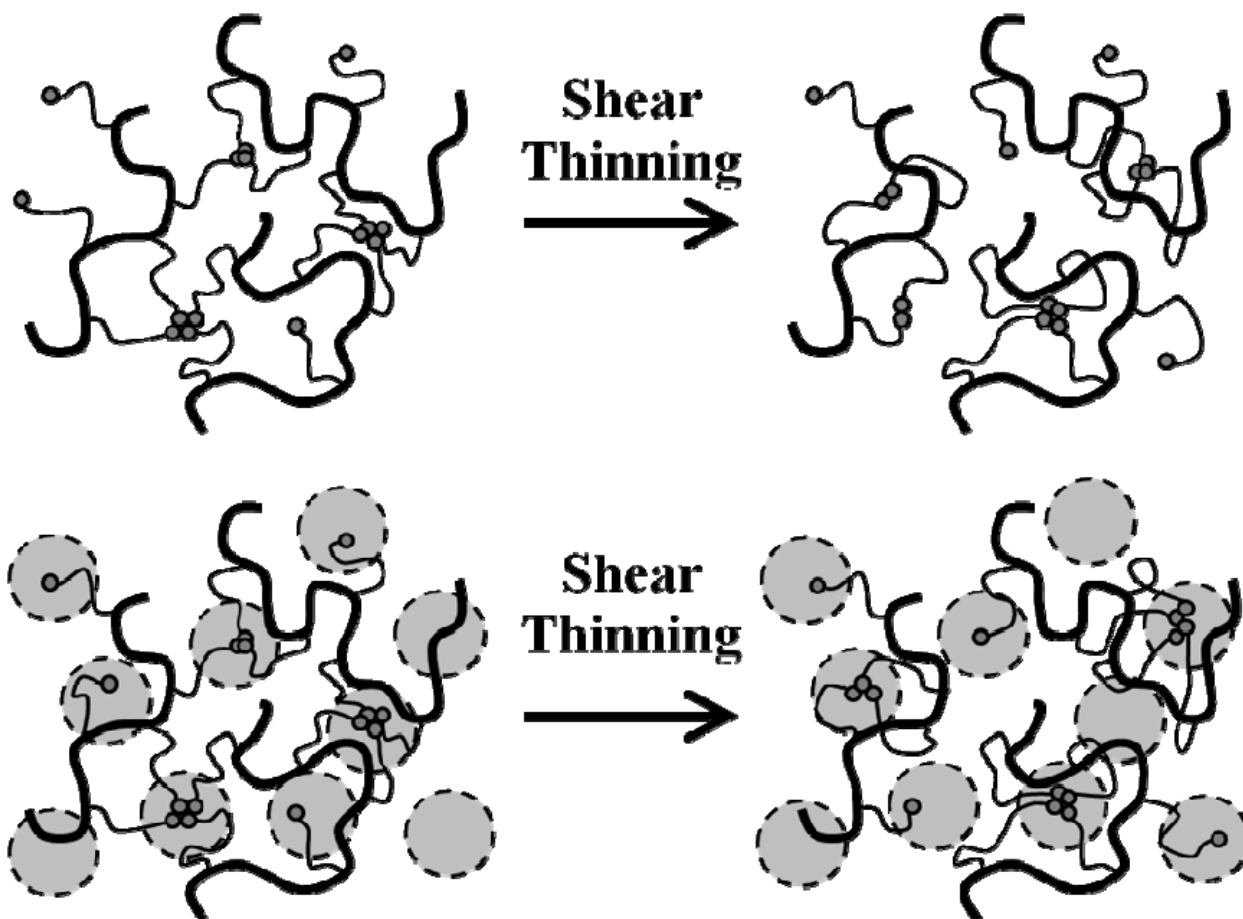


Figure 6.11: Proposed mechanism for the transition of inter- to intramolecular pyrene interaction of PyHASE solution with and without SDS under a shearing force.

6.5 Conclusions

The interactions between Py-HASE12 and the surfactant SDS were investigated at Py-HASE12 concentrations of 8 and 57 g/L in the semidilute regime. The FBM and the MF analyses were applied to globally fit the pyrene monomer and excimer fluorescence decays acquired over a wide range of SDS concentrations. The molar fractions representing the different excited pyrene species in solution, namely f_{diff} , f_{free} , and f_{agg} , were determined and the results obtained from the two

analyses were identical. At low SDS concentrations, no binding occurs between SDS and the pyrene pendants and most pyrene groups form aggregates. With more SDS being added, SDS targets and melts the pyrene aggregates to produce more isolated pyrenes. At higher SDS concentrations, SDS starts to form micelles and the pyrene aggregates are further decomposed until all pyrene pendants are incorporated into SDS micelles. This behavior results in an increase of the efficiency of pyrene excimer formation as well as the solution viscosity. With excess SDS, the pyrene pendants distribute themselves into different SDS micelles and more isolated pyrenes are generated severing interpolymeric associations. At this stage, both pyrene excimer formation and solution viscosity were found to decrease significantly.

For both Py-HASE12 concentrations, the average number of pyrenes per micelle, $\langle n \rangle$, was determined to equal 2.4 ± 0.1 and 2.2 ± 0.1 at the $[\text{SDS}]_p^{I_E/I_M}$,⁴⁹ suggesting that this $\langle n \rangle$ value represents the maximum pyrene loading capacity of the mixed micelles where most pyrene excimer is formed by diffusion and the least isolated pyrenes are present (see f_{free} in Figure 6.5). The viscosity of both Py-HASE12 solutions having a concentration of 8 g/L and 57 g/L was found to reach a maximum at an SDS concentration where $\langle n \rangle$ equals 2.0 ± 0.1 , as would be expected for the formation of an optimal polymeric network.

Adding SDS into the 57 g/L Py-HASE12 solution significantly increased the zero shear viscosity of the solution. As expected, shear thinning was observed at high shear rate for all solutions studied. However, no change in the fluorescence spectra was found as a function of shear rate despite the dramatic drop in the solution viscosity with increasing shear rate. The decrease in viscosity is attributed to the polymeric network experiencing a transition from inter- to intramolecular hydrophobic association as increasing shear is applied to the solution. A rationale was proposed to explain why this transition does not result in a change of I_E/I_M when shear is applied to the solution.

Chapter 7

Summary and Future Work

7.1 Summary of Thesis

Since 1977, different pyrene end-labeled poly(ethylene oxide) (PEO-Py₂) constructs have been used to investigate the internal dynamics of linear polymer chains in dilute solution,¹⁻⁵ the hydrophobic interactions between the pyrene end-groups in water,⁶⁻⁸ and the interactions taking place between hydrophobically modified PEO and the surfactant sodium dodecyl sulfate (SDS).⁹⁻¹² The reasons for the widespread attention paid to these chemically well-defined constructs are two-fold. First, the end-to-end cyclization (EEC) of a PEO chain in solution can be characterized via diffusion-controlled intramolecular pyrene excimer formation of PEO-Py₂. The process of EEC is similar to the loop formation of a polypeptide chain, which is viewed in some circles as being the most basic step in protein folding.¹³ Second, a PEO chain terminated at one end with a hydrophobe such as the PEO-Py₁ construct is the key structural component for two of the three commercially available associative thickeners (AT), namely the hydrophobically modified ethoxylated urethanes (HEUR) and the hydrophobically-modified alkali-swelling emulsion (HASE) polymers. These considerations resulted in an important effort conducted by the scientific community aiming at understanding the behavior of PEO-Py₂ constructs in organic solvents, where excimer formation reflects polymer chain dynamics, and in water, where excimer formation is related to the formation of hydrophobic pyrene aggregates and, most importantly, how the PEO chain length affects these properties. Despite their relatively large number,¹⁻¹² these earlier studies have been mostly qualitative in nature as they relied on the analysis of fluorescence spectra acquired by steady-state fluorescence.

This thesis used time-resolved fluorescence to characterize quantitatively and directly the behavior of a series of PEO(*X*)-Py₂ samples where *X* represents the number average molecular weight

(M_n) of the PEOs studied and equals 2, 5, 10, and 16.5 K. The first study described in this thesis investigated the EEC of the PEO(X)-Py₂ samples in various organic solvents with solvent viscosity (η) ranging from 0.32 to 1.92 mPa.s. Analysis of the steady-state fluorescence spectra showed that the I_E/I_M ratio scaled as $\eta^{-1.0} \times N_n^{-1.6}$ where N_n represents the number-average degree of polymerization. Analysis of the fluorescence decays according to Birks' scheme yielded the fraction of excited pyrene monomers (f_{free}) unable to form excimer, that increased with increasing η and N_n . This result suggested that excimer formation occurred in a subvolume of the polymer coil that was referred to as a *blob*. Beyond this volume, an excited pyrene monomer is likely to return to the ground state before encountering a ground-state pyrene to form an excimer. Interestingly, this apparent compartmentalization of the kinetics of excimer formation for pyrene end-labeled polymers is not considered by Birks' scheme, which might explain why Birks' scheme analysis of the fluorescence decays for the PEO(X)-Py₂ solutions never yielded a satisfying set of parameters to describe the kinetics of pyrene excimer formation. In contrast, analysis of the fluorescence decays with the fluorescence blob model (FBM) yielded an internally consistent set of parameters that described the kinetics of pyrene excimer formation of PEO(X)-Py₂ in organic solvents. Using a Gaussian end-to-end distance distribution for PEO and assuming that the fraction of chains that formed excimer by diffusion retrieved from the FBM analysis corresponded to those PEO chains whose ends were located in the same *blob*, the *blob* radius was determined and was found to increase linearly with increasing $(\tau_M/\eta)^{-1/2}$, as would be expected if the pyrenyl ends would undergo Brownian motion to probe a *blob*.

The second study of this thesis investigated the effect of unwanted fluorescent pyrene species on the fluorescence emitted by PEO(2K)-Py₂ and a pyrene end-labeled 4th generation dendritic hybrid referred to as Py₁₆-G4-PS. To conduct these experiments, known amounts of fluorescent pyrene impurities, namely PEO(2K)-Py₁ and 1-pyrenebutyric acid (PyBA), were added to solutions of

PEO(2K)-Py₂ in acetone and Py₁₆-G4-PS in THF, respectively. A “model free” (MF) analysis was applied to globally fit the pyrene monomer and excimer decays. The MF analysis yielded the following parameters: the average rate constant of excimer formation $\langle k \rangle$, which was found to be independent of the amounts of pyrene impurities added into the sample solution, because it only characterizes the rate of excimer formation; the $(I_E/I_M)^{SPC}$ ratio obtained by analysis of the fluorescence decays, which was proportional to the $(I_E/I_M)^{SS}$ ratio calculated from steady-state fluorescence spectra; the $(I_E/I_M)^{SPC}_{free=0}$ ratio, namely the $(I_E/I_M)^{SPC}$ ratio obtained when f_{free} was set to equal zero, which gives the theoretical value of the $(I_E/I_M)^{SPC}$ ratio for a spectroscopically pure sample. Among the most striking results of this study was the observation that the addition of 0.32 mol% of PyBA to a Py₁₆-G4-PS solution, equivalent to a 99.68% pure sample, decreased the $(I_E/I_M)^{SS}$ and $(I_E/I_M)^{SPC}$ ratios of the pure Py₁₆-G4-PS sample in THF by no less than 20%! This study demonstrated first, the extreme sensitivity of fluorescence to the presence of unwanted fluorescence impurities in the characterization of fluorescently labeled macromolecules and second, that our analysis protocol was capable of accounting quantitatively for this complication.

The hydrophobic interactions of the PEO(X)-Py₂ constructs in aqueous solution were investigated in the third study. The I_E/I_M ratio of the PEO(X)-Py₂ samples remained constant at low polymer concentration C_p , before increasing linearly with increasing C_p after an onset concentration, C^F of 4×10^{-5} M. Below C^F the I_E/I_M ratio remained constant, indicating that pyrene excimer was formed intramolecularly. The linear increase of the I_E/I_M ratio with increasing C_p above C^F suggested that intermolecular pyrene excimer formation occurred at high concentration. In aqueous solution, the I_E/I_M ratio of PEO(X)-Py₂ decreased significantly with increasing PEO chain length and was found to scale as $M_n^{-2.34 \pm 0.13}$ in agreement with the results reported by Char et al.⁸ The pyrene monomer and excimer fluorescence decays were fitted globally according to the sequential model (SM), which assumes that the pyrene excimer is formed in water via a sequential mechanism. Beyond a “capture

volume” centered around a hydrophobic pyrene in water, the pyrene pendants diffuse freely before being subject to some hydrophobic interactions inside the capture volume that leads to the rapid formation of a pyrene excimer. The molar fraction of aggregated pyrenes, f_{agg}^{SM} , of pyrenes diffusing inside the polymer coil, f_{diff}^{SM} , and of isolated pyrenes, f_{free}^{SM} , were obtained by analysis of the fluorescence decays. Based on these molar fractions, it was found that 97% of the pyrene groups were aggregated for PEO(2K)-Py₂ below C^F , while in the same polymer concentration range, only 10% of the pyrene pendants were aggregated for PEO(10K)-Py₂. Inside the capture volume, pyrene excimers are formed with a relatively larger rate constant of $7.3(\pm 0.5) \times 10^7 \text{ s}^{-1}$ which remains the same for all PEO(*X*)-Py₂ constructs at all C_p . By equating f_{E0} with the Gaussian probability of finding the ends of the PEO(*X*)-Py₂ samples within the capture radius, the radius of the capture volume (R_c) of a pyrene end-group was found to equal $2.2 \pm 0.2 \text{ nm}$ in good agreement with an earlier study based solely on steady-state fluorescence.⁷

In the fourth study, the interactions taking place between $1.25 \times 10^{-6} \text{ M}$ PEO(*X*)-Py₂ in water and SDS were investigated. At this highly diluted polymer concentration, the binding between the hydrophilic PEO backbone and SDS could not be detected by isothermal titration calorimetry, potentiometry using an SDS selective electrode, and conductance measurements. The decays acquired with PEO(*X*)-Py₂ at various SDS concentrations were fitted globally according to the MF analysis. The molar fractions of pyrenyl pendants that formed excimer by the direct excitation of pyrene aggregates, f_{agg} , that formed excimer via the diffusional encounter of an excited pyrene with a ground-state pyrene, f_{diff} , and that never formed excimer, f_{free} , were determined and used to propose the mechanism controlling the interactions between the PEO(*X*)-Py₂ constructs and SDS. $\langle k \rangle$ and the $(I_E/I_M)^{SPC}$ ratio were also calculated using the parameters retrieved from the MF analysis. Generally $(I_E/I_M)^{SPC}$ was found not to be equal to $(I_E/I_M)^{SS}$ at low SDS concentrations, due to the presence of

pyrene aggregates. The quantum yield of pyrene excimer formed by the pyrene aggregates of PEO(*X*)-Py₂ was found to be 1.55±0.06 times smaller than that of an excimer formed by diffusion inside an SDS micelle. When the SDS concentration was larger than 5 mM, the fractions obtained with PEO(10K)-Py₂ and PEO(16.5K)-Py₂ were not quantitative because f_{free} and f_{diff} were respectively underestimated and overestimated by the analysis. At SDS concentrations larger than the critical micelle concentration (CMC) of SDS in water, the I_E/I_M ratios obtained with the short-chain samples, PEO(2K)-Py₂ and PEO(5K)-Py₂, were identical and significantly larger than those obtained with the long-chain samples, PEO(10K)-Py₂ and PEO(16.5K)-Py₂. This observation can be rationalized by noting that intramolecular formation of pyrene excimer can occur inside a given micelle for the short-chain samples, but that it is prevented in the long-chain samples where most pyrene pendants are in separate micelles.

In the last study, the interactions between a hydrophobically modified alkali-swelling emulsion polymer labeled with pyrene (Py-HASE) and SDS were investigated using fluorescence, rheology, and a combination of fluorescence and rheological measurements, which were conducted simultaneously. The concentrations of Py-HASE used in this thesis were larger than the overlap concentration (C^*) of Py-HASE in water. The pyrene monomer and excimer decays were fitted globally according to the FBM and the MF analyses. The molar fractions f_{diff} , f_{free} , and f_{agg} were determined and the results obtained from the two models were identical. The average number of pyrenes per micelle, $\langle n \rangle$, was obtained from the FBM analysis and determined to equal 2.4±0.1 and 2.2±0.1 at the SDS concentrations where I_E/I_M peaked for the Py-HASE concentrations of 8 and 57 g/L, respectively, and $\langle n \rangle$ equaled 2.0±0.1 at the SDS concentrations where a maximum in solution viscosity was observed. The relaxation time (τ_r) of Py-HASE at different SDS concentrations was obtained from the break point in the plot of viscosity versus shear rate. τ_r was found to exhibit a trend as a function of SDS concentration which is similar to that observed with the zero-shear solution

viscosity. When the fluorescence spectra of the Py-HASE solutions were acquired while the solutions were sheared at different shear rates, the spectra overlapped despite the fact that the solution viscosity dropped by several orders of magnitude with shear rate increasing from 0 to 500 s⁻¹. This observation suggests that the decrease in viscosity with increasing shear rate is due to a rearrangement of the pyrene hydrophobes that favors intra- versus intermolecular associations either between pyrene pendants in water or mixed micelles but does not affect the balance between the different pyrene species forming excimer.

7.2 Future Work

Three important parameters can be used to characterize the complex properties of hydrophobically modified water-soluble polymers (HMWSPs) in solution. These parameters are the average number of hydrophobes per elastically active hydrophobic junction (N_{agg}), the fraction of associated hydrophobic pendants (f_{agg}), and the residence time of a hydrophobe in a hydrophobic aggregate (τ_{res}). In this thesis, f_{agg} of PEO(*X*)-Py₂ and Py-HASE was determined by global analysis of the pyrene monomer and excimer decays according to the various methods presented in Chapters 4-7. However, N_{agg} and τ_{res} of PEO(*X*)-Py₂ have not yet been measured. For a HMWSP bearing an alkyl hydrophobe, N_{agg} can be determined by loading a hydrophobic chromophore and quencher into the hydrophobic junctions, and applying the method originally proposed by Turro and Yekta¹⁴ to analyse the quenching of the excited chromophore.^{15,16} For a pyrene mono-labeled PEO having 53 ethylene oxide repeating units, N_{agg} was determined to equal 20±2 by monitoring the quenching of the pyrene excimer using the quencher dodecylpyridinium chloride (DPC).¹⁷ It would be interesting to apply this method to measure N_{agg} for the pyrene aggregates formed by PEO(*X*)-Py₂ and determine whether N_{agg} found for the singly and doubly labeled PEO constructs obey the rules that are typically observed for non-fluorescent HEUR polymers.

The relaxation time (τ_r) obtained with the 57 g/L Py-HASE solution in Chapter 7 reflects the relaxation of individual Py-HASE polymer chains. However, unlike the HEUR polymers whose solutions behave as Maxwell fluids where τ_{res} equals τ_r ,¹⁸ τ_{res} cannot be directly determined for the more complex HMWSPs like Py-HASE.¹⁹⁻²¹ Although the viscoelastic behavior Py-HASE is not maxwellian, the theory proposed by Green and Tobolsky²² to describe the relaxation process of transient networks can be modified to determine the largest relaxation time of Py-HASE solutions.²³ Therefore, τ_{res} of Py-HASE is related to τ_r and the number density of elastically active chains, ν , which can be obtained from the high frequency plateau modulus, G_0 .²¹ G_0 can be determined by oscillatory rheological measurements. Two rationales have been proposed to describe the maxima in zero-shear viscosity observed for solution mixtures of an AT and SDS. One rationale suggests that the viscosity profile as a function of SDS concentration is due to a change in ν ²⁴⁻²⁹ whereas the other invokes a change in τ_{res} .³⁰⁻³² The fluorescence and rheology measurements conducted in this study on the Py-HASE and SDS mixtures suggest that the change in viscosity reflects a change in ν . An important future study would investigate whether this conclusion is supported by oscillatory rheological measurements. These experiments would yield τ_{res} and ν and establish whether ν changes with the SDS concentration, as inferred by Chapter 6 of this thesis.

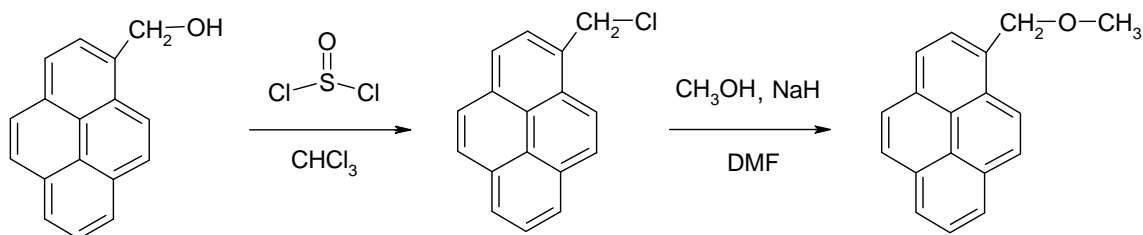
One unexpected result shown in Chapter 6 is the overlap of the Py-HASE fluorescence emission spectra acquired at various shear rates despite the significant decrease in solution viscosity observed with increasing shear rate. This observation was attributed to a transition from inter- to intramolecular hydrophobic association that does not affect the overall balance of the different excimer-forming pyrene species. In effect, using only pyrene as a label could not distinguish the different interactions taking place between the hydrophobes. A study that might better probe this transition would involve the mixture of two associative polymers having identical chemical structure but bearing different chromophores/hydrophobes such as anthracene and phenanthrene.

Intermolecular hydrophobic interaction would be detected by fluorescence resonance energy transfer (FRET) from an excited phenanthrene to a ground-state anthracene. Break-up of these interactions would result in stronger intramolecular associations, which can be detected by FRET as the solution is being sheared.

Appendix

Chapter 2 Supporting Information

Synthesis of 1-pyrenemethylmethyl ether (PyCH₂OMe): Synthesis of PyCH₂OMe was carried out according to Scheme SI.2.1.



Scheme SI.2.1: Synthesis of 1-pyrenemethyl methyl ether.

1-Pyrenemethanol (PyCH₂OH) was recrystallized three times from a 2:1 ethyl acetate:hexane mixture before use. In a round-bottom flask, the purified PyCH₂OH (0.5 g, 2.2 mmol) was dissolved into 10 mL of freshly distilled chloroform. The solution was kept under N₂ atmosphere. Thionyl chloride (0.48 mL, 6.6 mmol) was slowly added to the solution after the complete dissolution of PyCH₂OH. The mixture was stirred overnight at room temperature. Solvent and thionyl chloride evaporated during the night in the fumehood leaving dry 1-pyrenemethyl chloride (PyCH₂Cl) in the flask as a green powder. PyCH₂Cl was obtained with a yield of 96%.

A round-bottom flask was flamed three times under vacuum to remove any residual moisture and was kept under a nitrogen atmosphere. Freshly distilled methanol (0.50 mL, 12.5 mmol) was placed in the flask with 10 mL of freshly distilled DMF. Sodium hydride (0.4 g, 10 mmol) was added and the mixture was stirred at room temperature for 1 hour. PyCH₂Cl was dissolved in 5 mL of DMF and injected into the reaction flask through a syringe. The mixture was stirred in the dark overnight under nitrogen. DMF and unreacted methanol were removed at ca. 60 °C with a rotary evaporator. The resulting yellow powder was dissolved in 10 mL dichloromethane and washed three times with

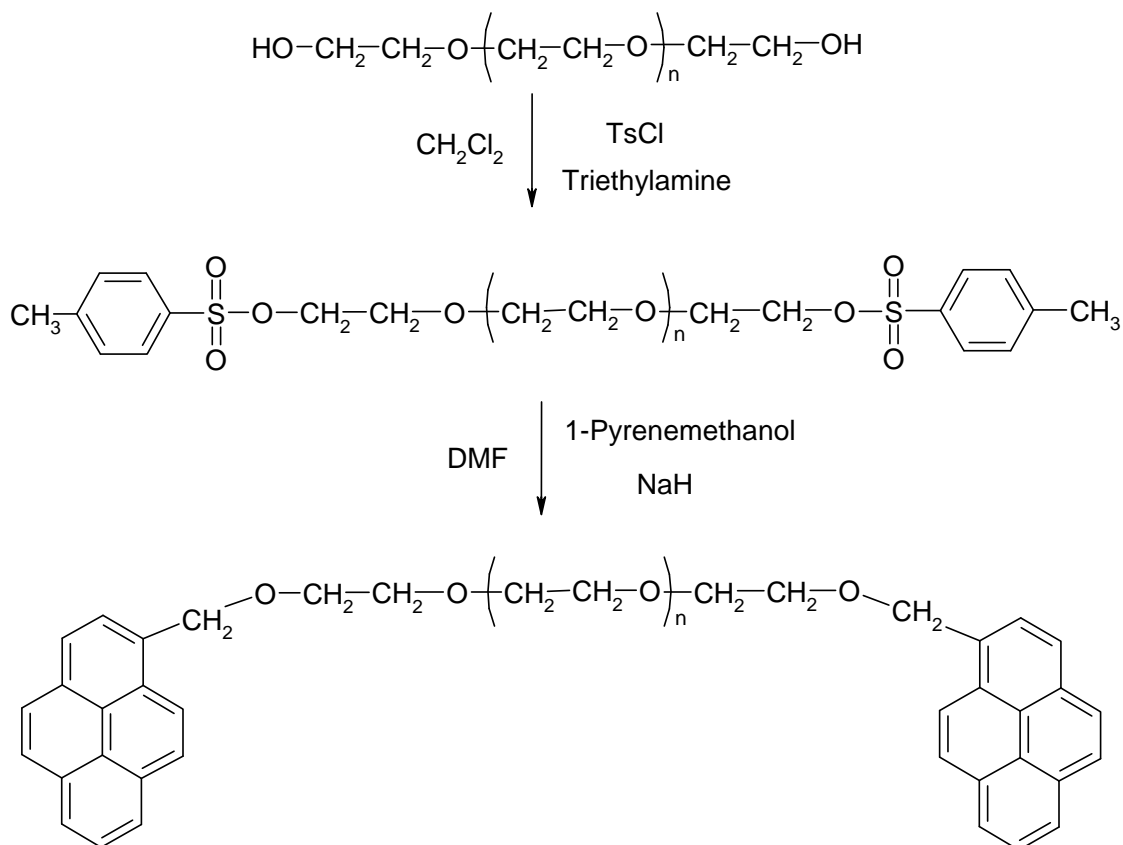
20 mL of water. The organic layer was collected and dried over MgSO_4 powder. Dichloromethane was evaporated and the residues were recrystallized five to six times from a 1:3 by volume ethyl acetate:hexane mixture. Yellow crystals of PyCH_2OMe were obtained with a yield of 35%.

PyCH_2OH . ^1H NMR (300 MHz, CDCl_3), δ (ppm): 1.86 (t, $\sim 1\text{H}$, -OH), 5.4 (d, $\sim 2\text{H}$, $-\text{CH}_2-$), 8.0-8.4 (m, $\sim 9\text{H}$, Pyrenyl H's).

PyCH_2Cl . ^1H NMR (300 MHz, CDCl_3), δ (ppm): 5.32 (s, $\sim 2\text{H}$, $-\text{CH}_2-$), 8.0-8.4 (m, $\sim 9\text{H}$, Pyrenyl H's).

PyCH_2OMe . ^1H NMR (300 MHz, CDCl_3), δ (ppm): 5.16 (s, $\sim 2\text{H}$, $-\text{CH}_2-\text{O}$), 3.5 (s, $\sim 3\text{H}$, $-\text{CH}_3$), 8.0-8.4 (m, $\sim 9\text{H}$, Pyrenyl H's). The molar absorption coefficients of PyCH_2OMe in THF and DMF were found to equal 43,000 and 39,000 $\text{M}^{-1}\text{cm}^{-1}$, respectively. PyCH_2OMe was found to yield a monoexponential decay in several organic solvents.

Preparation of the mono- and doubly-labeled poly(ethylene oxide): Scheme SI.2.2 describes the synthetic route that was followed to prepare the pyrene-labeled poly(ethylene oxide)s (PEO). First, the hydroxyl ends of the PEOs were reacted with *p*-toluenesulfonyl chloride (TsCl) to yield PEO-Ts. In a second step, the toluenesulfonyl moiety of PEO-Ts was displaced by an excess of sodium pyrenemethoxide to yield the PEOs bearing either a single pyrene when prepared with poly(ethylene oxide) methyl ether (PEO(2K)-Py₁) or two pyrenes when prepared with poly(ethylene oxide) (PEO(2K)-Py₂). The labeling procedure is described in detail for poly(ethylene oxide) methyl ether.



Scheme SI.2.2: Reaction scheme for the pyrene-labeling of poly(ethylene oxide).

Synthesis of PEO-Ts: The PEO-Ts was synthesized according to a published procedure.^{1,2} In a round-bottom flask, poly(ethylene oxide) methyl ether (2 g, 1 mmol) was dissolved into 15 mL of freshly distilled dichloromethane. The solution was kept under N₂ atmosphere. Triethylamine (7 mL, 5 mmol) was added to the solution after the dissolution of PEO was complete. The flask was immersed in an ice bath and the mixture was stirred for around 10 min. TsCl (0.572 g, 3 mmol) was added in small increments during the course of 10 minutes. After 3 hours, the ice bath was removed and the reaction was allowed to warm to room temperature and left to stir overnight under a nitrogen atmosphere. The following day, the mixture was concentrated to ca. 5 mL under vacuum and added dropwise to 50 mL of diethyl ether. The white precipitate (PEO-Ts) was filtered and dried in a vacuum oven at room temperature for 12 h. The dry PEO-Ts was ground into a powder, suspended in

20 mL toluene and stirred for 1 h. The impurities, including triethylamine hydrochloride and TsCl residues, were filtered off and the filtrate was rotary evaporated to ca. 5 mL and added dropwise to 50 mL of diethyl ether. The white precipitate was collected by filtration and dried for 2 days.

Unmodified poly(ethylene oxide) methyl ether. ^1H NMR (300 MHz, DMSO-*d*₆, Figure SI.2.1A), δ (ppm): 4.5 (t, ~1H, -OH), 3.2-3.7 (many small peaks, H from units close to the PEO ends), 3.5 (s, massive peak, H from backbone), 3.3 (m, H₂O), 3.2(~3H, -CH₃).

PEO-Ts. ^1H NMR (300 MHz, DMSO-*d*₆, Figure SI.2.1B), δ (ppm): 7.4 (d, ~2H, ArH), 7.7 (d, ~2H, ArH), 4.1 (t, ~2H, -CH₂-), 3.2-3.7 (many small peaks, H from units close to the PEO ends), 3.5 (s, massive peak, H from backbone), 3.3 (m, H₂O), 3.2(~3H, -CH₃).

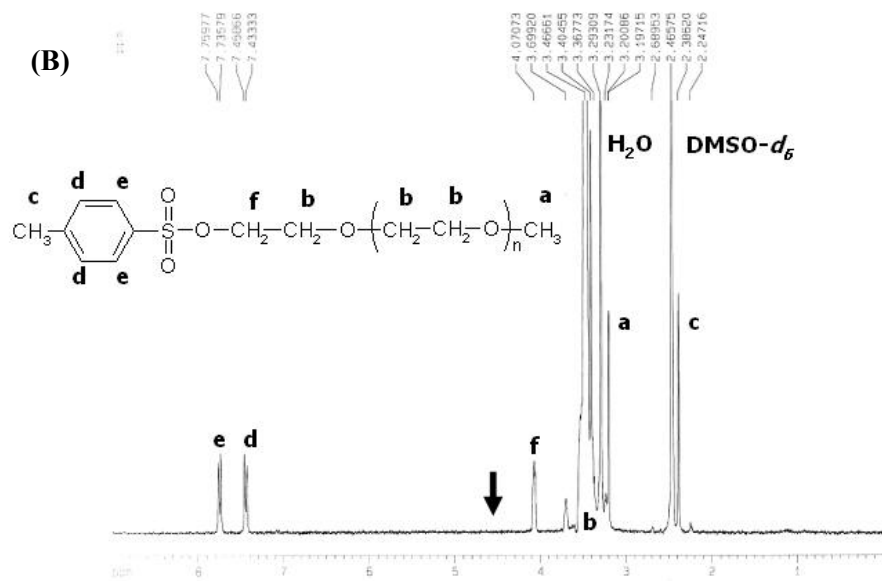
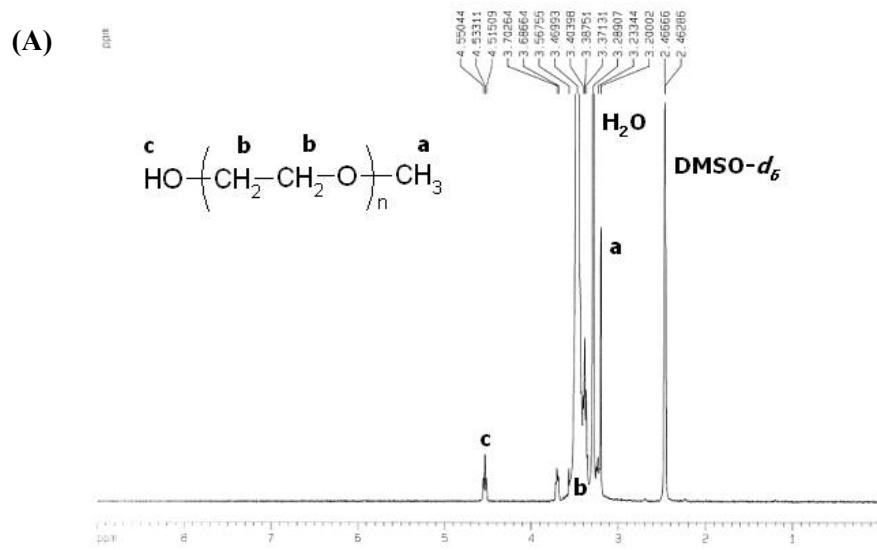
The ^1H NMR spectrum of PEO exhibits a triplet for the terminal hydroxyl groups at 4.56 (± 0.02) ppm in deuterated dimethyl sulfoxide (but not in other solvents) and this peak does not shift or broaden with the concentration of the PEO, water, or impurities and is well separated from the main peaks of the PEO backbone.¹ Therefore, DMSO-*d*₆ was used as the NMR solvent in this study to investigate the functionality of PEO. The disappearance in Figure SI.2.1B of the peak at 4.6 ppm observed in Figure SI.2.1A assigned to the hydroxyl proton of PEO suggests that within experimental error, all chains have reacted with a tosylate group. Furthermore, the peak at 4.1 ppm in Figure SI.2.1B representing the two protons of the last PEO unit next to the tosylate group indicates that the tosylate group was covalently attached to the PEO chain.

Synthesis of PEO(2K)-Py₁: After having been recrystallized three times from a 2-to-1 ethyl acetate-hexane mixture by volume, 1-pyrenemethanol (1.18 g, 5.1 mmol) was dissolved into 15 mL of freshly distilled DMF in a round-bottom flask. The flask was flamed beforehand three times under vacuum to completely remove any moisture and it was kept under a nitrogen atmosphere. Sodium hydride (0.17 g, 4.25 mmol) was added and the mixture was stirred in the dark at room temperature for 1 h resulting in a black solution. PEO-Ts was added to the reaction flask which was then placed in an oil bath at 60 °C, covered with aluminum foil to protect pyrene from light exposure, and stirred overnight under nitrogen. The oil bath was removed and the mixture was cooled to room temperature after

quenching the reaction with a drop of water. The solution was concentrated to 5 mL and precipitated into 50 mL diethyl ether, the yellow solid (PEO(2K)-Py₁) was collected from filtration and dried at room temperature under vacuum for 12 h.

To remove the sodium tosylate by-product, PEO(2K)-Py₁ was dissolved in 10 mL of dichloromethane and washed three times with 30 mL of water. The organic layer was collected and dried over MgSO₄ powder. The solution was concentrated to 5 mL and then precipitated in 50 mL diethyl ether. The precipitate was filtered and dried under vacuum at room temperature for 6 h. PEO(2K)-Py₁ was dissolved in methanol at room temperature and the solution was cooled and kept at 5 °C overnight, conditions under which the PEO crystallizes. The yellow precipitate of PEO(2K)-Py₁ was filtered, re-dissolved in methanol at room temperature and recrystallized by decreasing the temperature to 5 °C three more times to remove unreacted 1-pyrenemethanol and its derivatives. After the final precipitation, the solid was dried at room temperature under vacuum for 2 days. The disappearance of the peaks at 4.5 and 4.1 ppm in Figure SI.2.1C suggests that all PEO chains were successfully modified.

PEO(2K)-Py₁. ¹H NMR (300 MHz, DMSO-*d*₆, Figure SI.2.1C), δ (ppm): 8.0-8.4 (~9H, Pyrenyl H's), 5.2 (m, ~2H, Py-CH₂-O), 3.2-3.7 (many small peaks, H from units close to the PEO ends), 3.5 (s, massive peak, H from backbone), 3.3 (m, H₂O), 3.2(~3H, -CH₃).



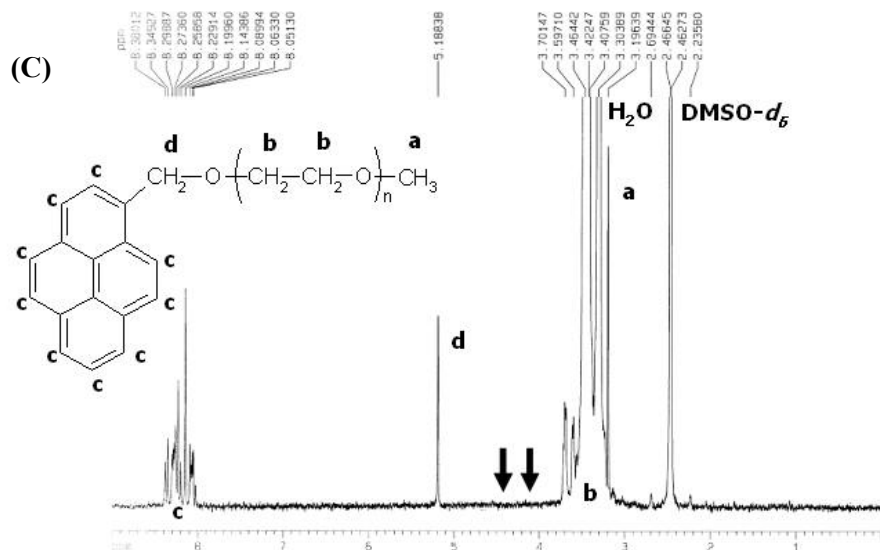


Figure SI.2.1: ^1H NMR spectra of (A) PEO, (B) PEO-Ts and (C) PEO(2K)-Py₁ in DMSO-*d*₆.

To investigate whether any residual 1-pyrenemethanol or its derivatives remained in the labeled PEO samples, the samples were passed through a GPC equipped with a fluorescence detector with the emission wavelength set at 375 nm to probe for the pyrene monomer (Figure SI.2.2). A main peak was detected in Trace A for an elution volume of 30.3 mL. It was attributed to the pyrene labeled PEO. Comparison of Trace A with Trace B with the peak obtained for 1-pyrenemethanol which eluted at 33.6 mL suggests that the sample was free from small molecule pyrene impurities.

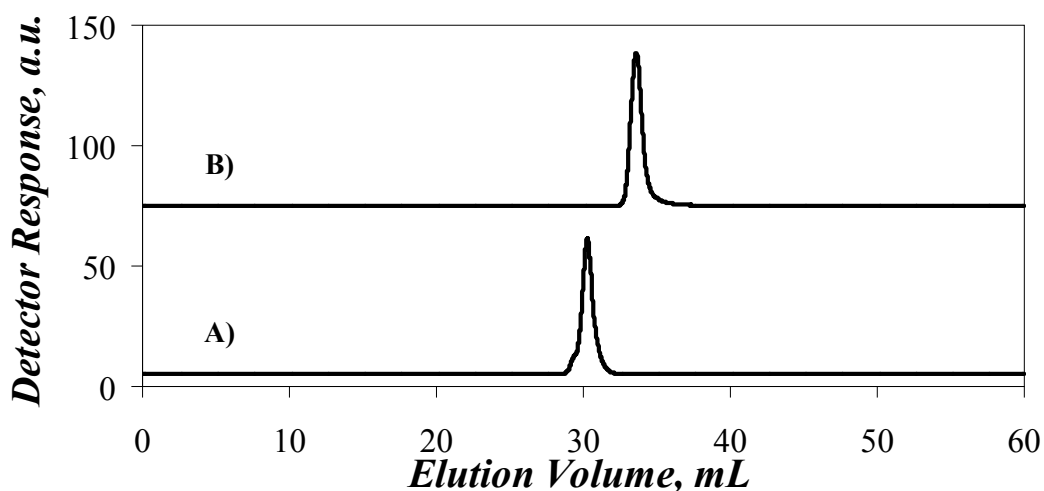


Figure SI.2.2: Gel permeation chromatography traces obtained with a fluorescence detector set at $\lambda_{\text{ex}} = 344 \text{ nm}$ and $\lambda_{\text{em}} = 375 \text{ nm}$ for (A) PEO(2K)-Py₁ and (B) 1-pyrenemethanol.

Theoretical adjustments made to Birks' scheme:

Birks' scheme predicts that the monomer and excimer decays can be fitted by Equations SI.2.1 and SI.2.2, respectively.

$$\begin{aligned}
 [Py^*] = & \frac{[Py_{diff}^*]_o}{\sqrt{(X - Y)^2 + 4k_{cy}k_{-cy}}} \left((X - \tau_2^{-1}) \times \exp(-t/\tau_1) - (X - \tau_1^{-1}) \times \exp(-t/\tau_2) \right) \\
 & + [Py_{free}^*]_o \exp(-t/\tau_M) + [Py_S^*]_o \exp(-t/\tau_S) \quad (SI.2.1)
 \end{aligned}$$

$$[E^*] = \frac{k_{cy}[Py_{diff}^*]_o}{\sqrt{(X - Y)^2 + 4k_{cy}k_{-cy}}} \left(-\exp(-t/\tau_1) + \exp(-t/\tau_2) \right) + [Py_S^*]_o \exp(-t/\tau_S) \quad (SI.2.2)$$

In his derivation, Birks used the parameters $X = k_{cy} + \tau_M^{-1}$ and $Y = k_{-cy} + \tau_E^{-1}$ as well as the decay times τ_1 and τ_2 whose expressions are given in Equations SI.2.3 and SI.2.4, respectively. Equations

SI.2.1 and SI.2.2 use the concentrations of pyrenes that form excimer by diffusion, $[Py_{diff}^*]_o$, do not form excimer because they are attached onto monolabeled chains, $[Py_{free}^*]_o$, and form poorly stacked excimers, $[Py_S^*]_o$, that emit with a short lifetime τ_S . The limit of τ_1^{-1} , τ_2^{-1} , and the monomer pre-exponential ratio $(X - \tau_2^{-1})/(\tau_1^{-1} - X)$ is given in, respectively, Equations SI.2.3, SI.2.4, and SI.2.5 when $|X - Y| \gg 4 \times k_{cy} k_{-cy}$ and $Y > X$. This condition is observed for the pyrene excimer when the chains are long and k_{cy} tends to zero.

$$\tau_1^{-1} = \frac{X + Y + \sqrt{(X - Y)^2 + 4k_{cy}k_{-cy}}}{2} \xrightarrow{|X-Y| \gg 4k_{cy}k_{-cy}} \left(\tau_E^{-1} + k_{-cy} + \frac{k_{cy}k_{-cy}}{Y - X} \right) \quad (\text{SI.2.3})$$

$$\tau_2^{-1} = \frac{X + Y - \sqrt{(X - Y)^2 + 4k_{cy}k_{-cy}}}{2} \xrightarrow{|X-Y| \gg 4k_{cy}k_{-cy}} \left(\tau_M^{-1} + k_{cy} - \frac{k_{cy}k_{-cy}}{Y - X} \right) \quad (\text{SI.2.4})$$

$$\frac{X - \tau_2^{-1}}{\tau_1^{-1} - X} \xrightarrow{|X-Y| \gg 4k_{cy}k_{-cy}} \frac{k_{cy}k_{-cy}}{(Y - X)^2} \quad (\text{SI.2.5})$$

The pre-exponential factor $X - \tau_2^{-1}$ of $\exp(-t/\tau_1)$ in Equation SI.2.1 tends to zero and $\exp(-t/\tau_2)$ decays as the pyrene monomer does since τ_2 tends to τ_M when k_{cy} tends to zero according to Equation SI.2.4.

Unfortunately, this ideal scenario breaks down if attaching pyrene to the polymer induces pyrene to decay in a non-exponential manner. As a matter of fact, the monomer of PEO(2K)-Py₁ was found to decay in a bi-exponential fashion, the shorter decay time being obtained with a smaller than 8% pre-exponential factor. Although small, this contribution affects the analysis of the fluorescence decays because as the chain length increases and k_{cy} tends to zero, the first term in Equation SI.2.1 is not allowed to decay as the experimentally found biexponential decay of the pyrene monomer of

PEO(2K)-Py₁, but rather as $\exp(-t/\tau_M)$. To account for this complication, Equations SI.2.1 and SI.2.2 were approximated by Equations SI.2.6 and SI.2.7 using the limit of Equations SI.2.3 and SI.2.4 when $|X - Y| \gg 4 \times k_{cy} k_{-cy}$.

$$\begin{aligned}
 [Py^*] = & \frac{[Py_{diff}^*]_o}{\sqrt{(X - Y)^2 + 4k_{cy}k_{-cy}}} \left[(X - \tau_M^{-1} - (\tau_2^{app})^{-1}) \times f_E(t) \times \exp(-t/\tau_1^{app}) \right. \\
 & \left. - (X - \tau_E^{-1} - (\tau_1^{app})^{-1}) \times f_M(t) \times \exp(-t/\tau_2^{app}) \right] \\
 & + [Py_{free}^*]_o f_M(t) + [Py_S^*]_o \exp(-t/\tau_S)
 \end{aligned} \tag{SI.2.6}$$

$$[E^*] = \frac{k_{cy} [Py_{diff}^*]_o}{\sqrt{(X - Y)^2 + 4k_{cy}k_{-cy}}} \left[-f_E(t) \times \exp(-t/\tau_1^{app}) + f_M(t) \times \exp(-t/\tau_2^{app}) \right] + [Py_S^*]_o \exp(-t/\tau_S) \tag{SI.2.7}$$

The expressions for the approximated decaytimes τ_1^{app} and τ_2^{app} are given in Equations SI.2.8 and SI.2.9, whereas Equations SI.2.10 and SI.2.11 give the expressions of $f_M(t)$ and $f_E(t)$, respectively.

$$(\tau_2^{app})^{-1} = k_{cy} + \frac{k_{cy}k_{-cy}}{X - Y} \tag{SI.2.8}$$

$$(\tau_1^{app})^{-1} = k_{-cy} - \frac{k_{cy}k_{-cy}}{X - Y} \tag{SI.2.9}$$

$$f_M(t) = \alpha \times \exp(-t/\tau_{M1}) + (1 - \alpha) \times \exp(-t/\tau_M) \quad \text{with } 0 < \alpha < 1 \tag{SI.2.10}$$

$$f_E(t) = \exp(-t/\tau_E) \tag{SI.2.11}$$

The parameters α , τ_{M1} , and τ_{M2} used in Equation SI.2.10 were determined by fitting the fluorescence decay of a PEO chain labeled at one end with pyrene in a given solvent with a biexponential function and their value was fixed in the analysis. As k_{cy} tends to zero, the first term in Equation SI.2.6 tends to $f_M(t)$ which takes the form given in Equation SI.2.10. Although Equations SI.2.6 and SI.2.7 were derived using the condition $|X - Y| \gg 4 \times k_{cy} k_{-cy}$, we found that with most sets of k_{cy} , k_{-cy} , and τ_E values retrieved in this study, the decay times τ_1 and τ_2 were well approximated by τ_1^{app} and τ_2^{app} , respectively.

Limitations of Birks' scheme analysis:

The main text of this study describes several limitations associated with the analysis of the fluorescence decays acquired with the PEO(X)-Py₂ solutions that are prepared with a long PEO chain and a high viscosity solvent. First, the excimer formation is strongly reduced, since k_{cy} decreases as $\eta^{-1.0} \times N_n^{-1.34}$ in Figure 2.5A. and longer acquisition times are required for the excimer fluorescence decays resulting in increased background noise (Figure 2.4). Second, the longer decay time τ_2 in Equations SI.2.1 and SI.2.2 increases with increasing N_n and η to the point where it becomes indistinguishable from τ_M , the lifetime of the pyrene monomer (see Equation SI.2.4). Although τ_M is determined independently with the monolabeled PEO(2K)-Py₁ sample and is fixed in the analysis, the reduced difference between τ_2 and τ_M makes the resolution of τ_2 from τ_M difficult. Third, the difficult resolution of τ_2 from τ_M is made harder still due to the increase in the parameter $f_{M\text{free}}$ (see Figure 2.5D). The two first limitations are well known in the field and, although not often advertised, are the main reasons why time-resolved fluorescence EEC experiments are usually restricted to the study of short polymers in low viscosity solvents.

To overcome these complications, several features were implemented in the analysis program. First, the monomer and excimer decays were fitted globally and the decay times τ_1 and τ_2 were kept the same in Equations SI.2.1 and SI.2.2 used to fit the monomer and excimer decays,

respectively. Second, the parameters k_{cy} , k_{-cy} , and τ_E were optimized directly in the analysis program which allowed the experimentalist to fix their value in the analysis if required. Fluorescence decays were simulated to test whether these improvements were sufficient to guarantee that, were k_{cy} scaling as $\eta^{-1.0} \times N_n^{-1.6}$ as found for the I_E/I_M ratio, our analysis program was robust enough to actually find this scaling relationship. Assuming that the data obtained for smaller PEO chains and lower viscosity solvents yielded the correct k_{cy} , k_{-cy} , and τ_E values, the quantities $X - \tau_2^{-1}$, $X - \tau_1^{-1}$, τ_1 , and τ_2 in Equations SI.2.1 and SI.2.2 were estimated by fixing the k_{-cy} and τ_E values to their average value found to equal $1.85 \times 10^6 \text{ s}^{-1}$ and 48 ns, respectively, and using the k_{cy} data obtained for PEO(2K)-Py₂ in the different solvents as a starting point to find the k_{cy} values of the other PEO(X)-Py₂ samples using the scaling relationship $k_{cy} \sim \eta^{-1.0} \times N_n^{-1.6}$. The values found for the contributions of the Py_S^* and Py_{free}^* species during the analysis of the experimental fluorescence decays were added to the simulated decays as well as the experimental background noise of the decays. For each solvent/PEO(X)-Py₂ pair, 20 fluorescence decays were simulated with different patterns of Poisson noise and analyzed with the same analysis program used to obtain the trends shown in Figures 2.5A-D. The data obtained from the 20 fits were averaged and their standard deviations were recorded. The trends obtained with the parameters k_{cy} , k_{-cy} , τ_E , and f_{Mfree} are shown in Figure SI.2.3A-D. Except for k_{-cy} which is retrieved with substantial error bars, the trends obtained with these parameters are fully consistent with the parameters that were used for the simulations. The rate constant k_{cy} scales as $\eta^{-1.0} \times N_n^{-1.6}$, and within experimental error, k_{-cy} and τ_E remain constant and equal to $1.85 \times 10^6 \text{ s}^{-1}$ and 48 ns, respectively. The fraction f_{Mfree} shows the exact same trend as the one found in Figure 2.5D with a clear break point. Fixing τ_E in the analysis yields the trends showed in Figures SI.2.4A-D which are the same trends as in Figures SI.2.3A-D but with hardly any scatter. Interestingly, poor fits were obtained when the experimental decays were fitted without allowing τ_E to float.

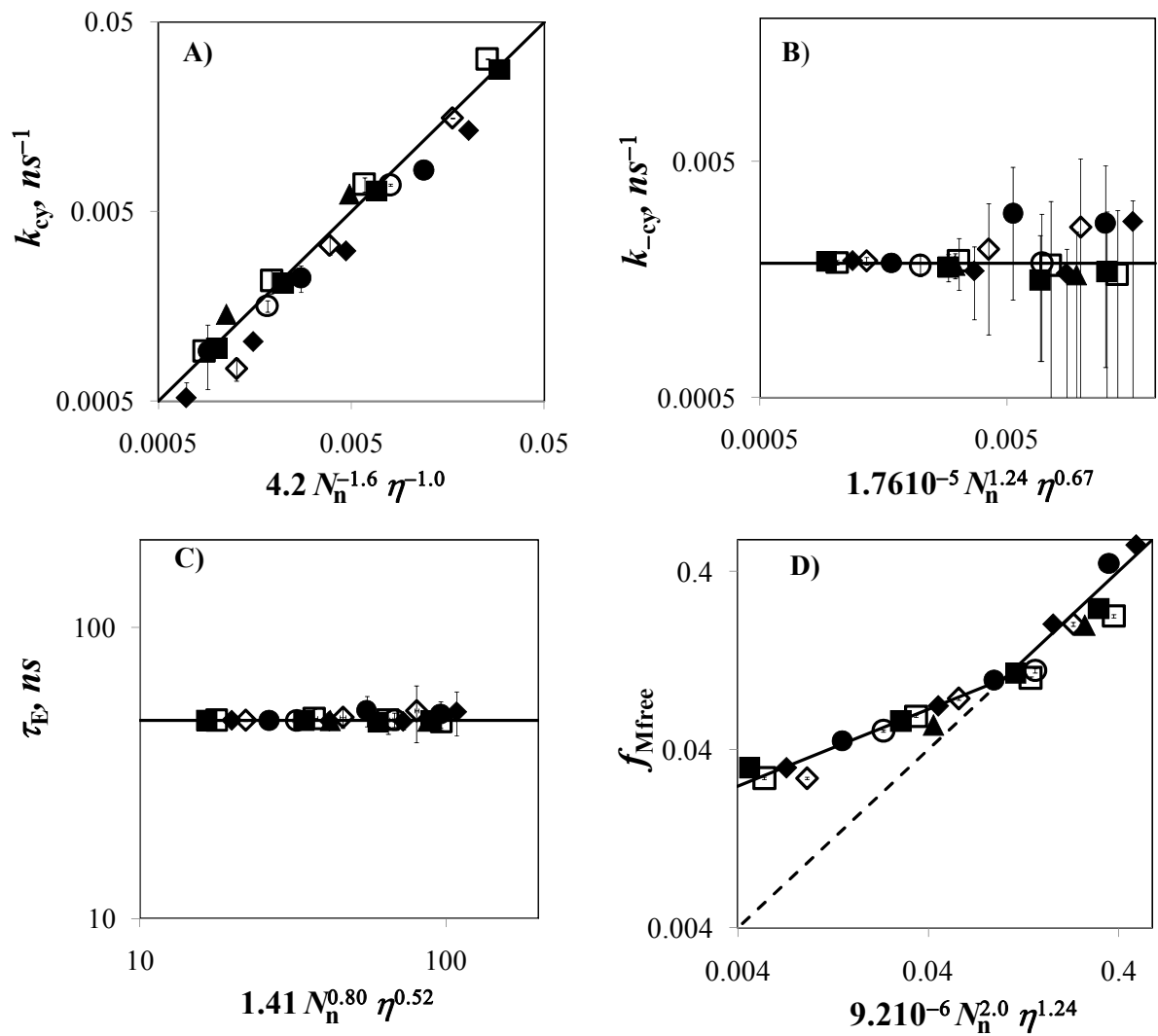


Figure SI.2.3: Scaling behavior of the parameters obtained from the simulation of 20 monomer and excimer fluorescence decays fitted with Equations SI.2.1 and SI.2.2, respectively. (■) acetone, (□) ACN, (◆) THF, (◇) toluene, (●) DMF, (○) dioxane, (▲) DMA.

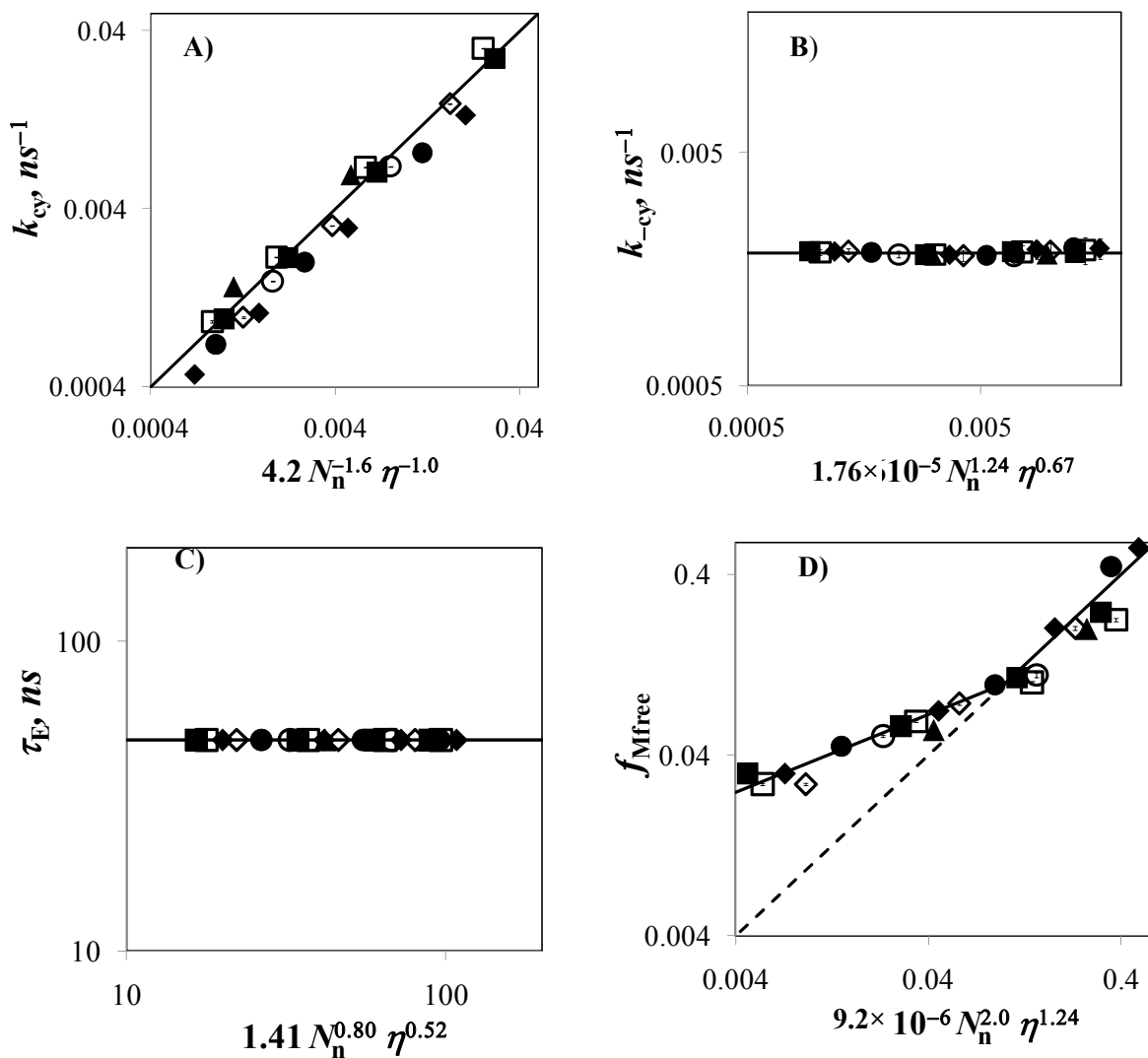


Figure SI.2.4: Scaling behavior of the parameters obtained from the global analysis of the pyrene monomer and excimer simulated fluorescence decays fitted with Equations SI.2.1 and SI.2.2, respectively. Symbols are the same as for Figure SI.2.3.

To confirm that the increase in f_{Mfree} is not due to τ_2 and τ_M being too close for proper resolution, f_{Mfree} was set to equal zero in the simulations. Analysis of the simulated decays yielded f_{Mfree} values equal to zero, further supporting that the increase observed for f_{Mfree} with increasing

viscosity is real. Together, the study with the simulated decays leads to the conclusion that the trends presented in Figures 2.5A-D are not a result of limitations of the analysis program.

If the analysis of the fluorescence decays is robust, the source for the inconsistencies observed in Figures 2.5A-D must be due to the data themselves. A short-lived component (Py_S^*) with a lifetime of ~ 3.5 ns has been found in the excimer decays (Figure 2.4). The analysis program found that its emission contributes little to the monomer decays, but to a much larger extent to the excimer decays acquired with long PEO chains and in high viscosity solvents. Its possible origin has been discussed earlier.^{3,4,5}

Nevertheless, the species Py_S^* should not affect the I_E/I_M ratios much, as it is so short-lived compared to the other fluorescing species present in solution (lifetimes of 48 ns and over 100 ns for the pyrene excimer and monomer, respectively). This statement is based on the fact that the fluorescence quantum yield of a compound is proportional to its lifetime. Another unaccounted for fluorescence emission might be due to pyrene-polymer interactions. Although 1-pyrenemethanol used to prepare the PEO(X)-Py₂ samples decayed with a single exponential (see Table SI.2.1), two exponentials were needed to fit the monomer decays of PEO(2K)-Py₁. The long decay time obtained with more than 92% of the pre-exponential weight in Table SI.2.1 was attributed to the lifetime of the pyrene monomer whereas the shorter decay time found to take values between 30 and 70 ns could be due to interactions between the pyrene label and the PEO backbone. Although small, the $\sim 5\%$ contribution of the short decaytime in the PEO(2K)-Py₁ decays was suspected to be sufficiently important to prevent the $(X - \tau_2^{-1})/(\tau_1^{-1} - X)$ ratio to tend to zero as it should when k_{cy} tends to zero (see Equation SI.2.5). This effect is clearly visible in Figure SI.2.5.

Whereas the ratio $(X - \tau_2^{-1})/(\tau_1^{-1} - X)$ is found to tend to zero when k_{cy} tends to zero for the simulations in Figure SI.2.5, the experimentally found $(X - \tau_2^{-1})/(\tau_1^{-1} - X)$ ratio plateaus at 0.09 ± 0.03 in Figure SI.2.5 for chains where $N \times \eta$ is greater than 80. As discussed in the Theory

section, this result is due to the fact that the first term in Equation SI.2.1 is expected to decay as $\exp(-t/\tau_M)$ when k_{cy} tends to zero, whereas experimentally, the monomer decays of the PEO(X)-Py₂ samples were found to tend to the non-exponential decay of the monolabeled PEO(2K)-Py₁ sample when k_{cy} tends to zero (see Figure 2.6B).

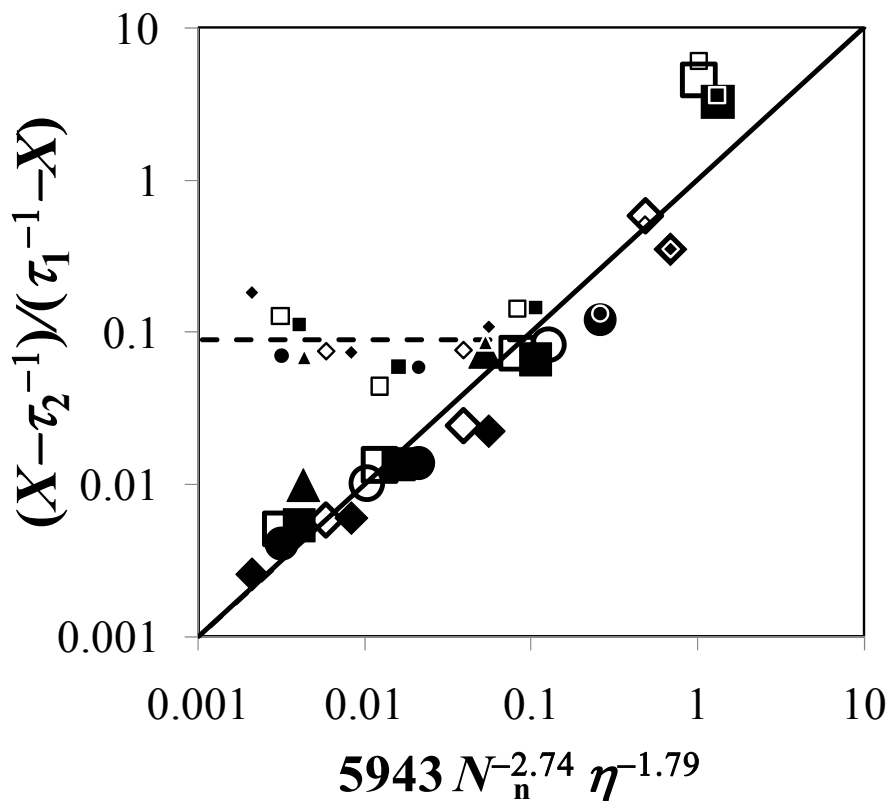


Figure SI.2.5: $(X - \tau_2^{-1})/(\tau_1^{-1} - X)$ ratio obtained from the analysis of the fluorescence decays of the PEO(X)-Py₂ samples (small symbols) and the simulated fluorescence decays (large symbols). The symbols are the same as those used in Figure SI.2.3.

The fact that a pyrene label does not decay monoexponentially when it is covalently attached to a PEO chain could be accounted for by using Equations SI.2.6 and SI.2.7. The monomer and excimer fluorescence decays were analyzed globally with Equations SI.2.6 and SI.2.7 and the excimer lifetime, τ_E , was set to equal 48 ns in all the analyses. The parameters retrieved from this analysis are

listed in Table SI.2.4. Good fits were obtained and the scaling behavior of the parameters k_{cy} , k_{-cy} , τ_E , and f_{Mfree} is shown in Figure SI.2.6A-D. The value of τ_E is also shown in Figure SI.2.6C, but it is fixed at 48 ns in the analysis. Since Equations SI.2.6 and SI.2.7 are obtained under conditions where $|X - Y| \gg 4k_{cy}k_{-cy}$, these conditions are not obeyed for the larger k_{cy} values obtained for PEO(2K)-Py₂ in acetonitrile, acetone, THF, and toluene. For these four samples, the k_{cy} , k_{-cy} , τ_E , and f_{Mfree} values obtained by fitting the monomer and excimer decays with Equations SI.2.1 and SI.2.2 have been used in Figures SI.2.6A-D where these values have been marked with an asterisk.

The use of $f_M(t)$ in Equations SI.2.6 and SI.2.7 yielded trends for k_{cy} and k_{-cy} with a more reasonable physical meaning. The rate constant k_{cy} in Figure SI.2.6A was found to decrease with increasing N_n and η scaling as $4.1 \times N_n^{-1.6} \times \eta^{-1}$, the exact same scaling relationship as the one found from fitting the simulated decays (see Figure 2.5A). The dissociation rate constant k_{-cy} remained more or less constant with N_n and η at $2.7 (\pm 1.1) \times 10^6 \text{ s}^{-1}$ taking values between 1.3 and $4.0 \times 10^6 \text{ s}^{-1}$ in all but one case. In particular the break points found in Figures 2.5A and 2.5B were absent in Figures SI.2.6A and much less pronounced in Figure SI.2.6B. Nevertheless and regardless of these improvements, f_{Mfree} in Figure SI.2.6D is found to increase with increasing N_n and η . The behavior of f_{Mfree} is inconsistent with Birks' scheme.

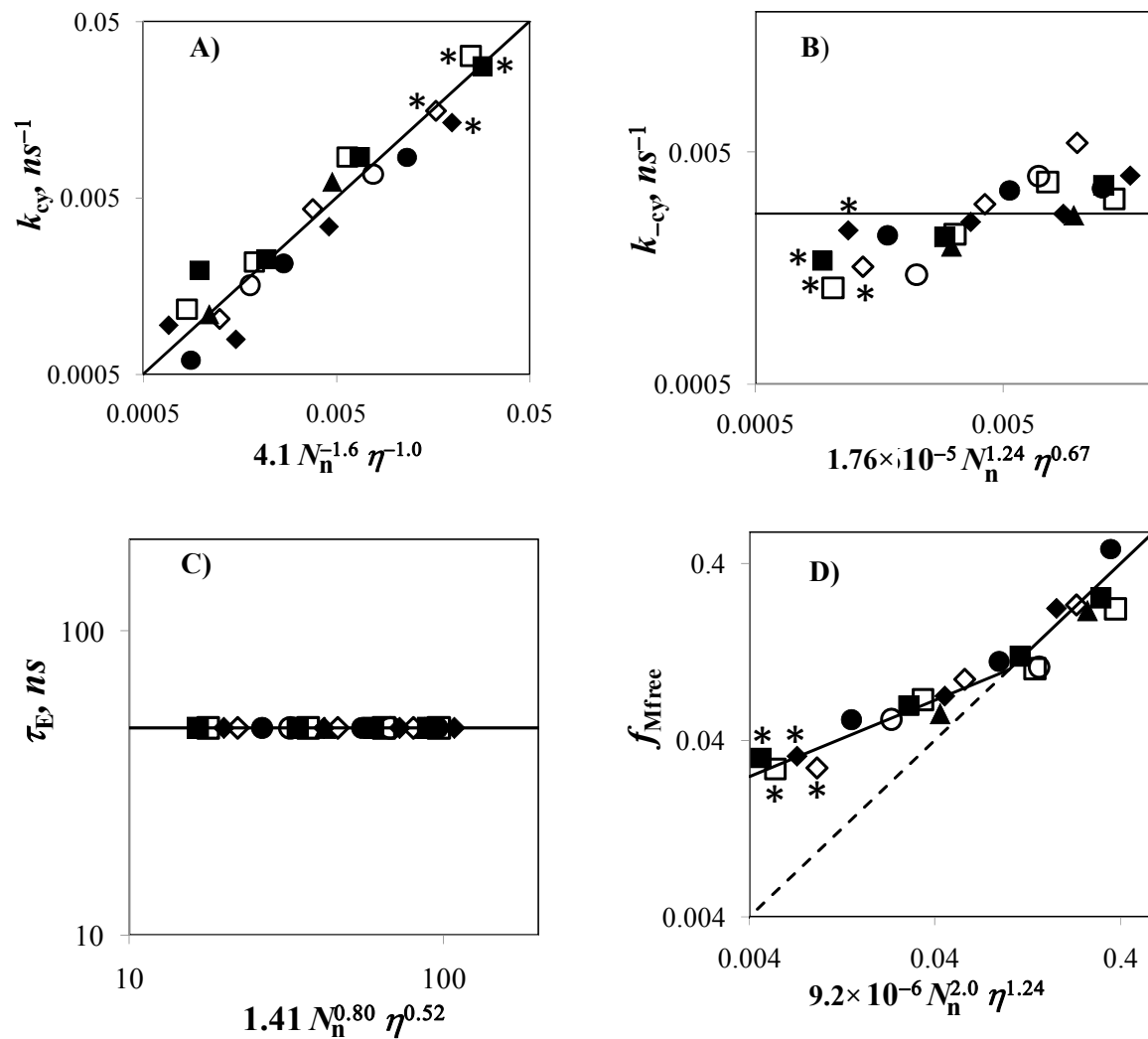


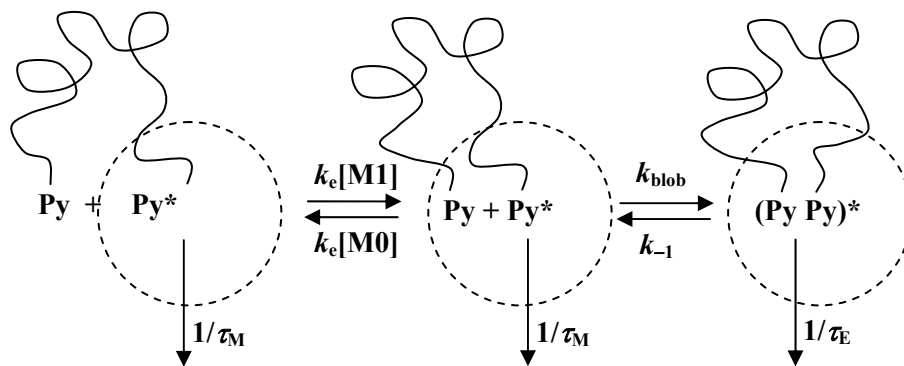
Figure SI.2.6: Scaling behavior of the parameters obtained from the global analysis of the pyrene monomer and excimer fluorescence decays of the PEO(X)-Py₂ samples fitted with Equations SI.2.6 and SI.2.7, respectively. Symbols are the same as for Figure SI.2.3. Asterisks indicate the decays that were fitted with Equations SI.2.1 and SI.2.2.

This study suggests that the Birks scheme analysis yields inconsistent results when fitting the monomer and excimer fluorescence decays acquired with PEO(X)-Py₂ samples in solvents where the product $N_n \times \eta$ is larger than 80 mPa.s. These conditions require that another type of analysis be applied to the fluorescence decays. To this end, we have introduced a Fluorescence Blob Model to

analyse the fluorescence decays.

Derivation of the Fluorescence Blob Model Equations

Scheme SI.2.3 depicts how excimer formation would proceed between an excited pyrene and a ground-state pyrene attached to the opposite ends of a chain within the framework of the Fluorescence Blob Model (FBM). The left panel in Scheme SI.2.3 represents an excited pyrene located in a *blob* that contains no ground-state pyrene. This excited pyrene will be referred to as P0*. The center panel of Scheme SI.2.3 describes a *blob* after P0* has diffused into a *blob* containing a ground-state pyrene M1 with an exchange rate constant k_e . The excited pyrene found in the center panel of Scheme SI.2.3 is referred to as P1*. The ground-state pyrene can diffuse out of the *blob* to give back P0*, or it can encounter the excited pyrene P1* to form an excimer with a rate constant k_{blob} . The process of excimer formation is described in the right panel of Scheme SI.2.3. The excimer can emit with a lifetime τ_E or dissociate back with a rate constant k_{-1} .



Scheme SI.2.3: End-to-end cyclization according to the Fluorescence Blob Model.

Assuming that k_{-1} is negligible in Scheme SI.2.3, a reasonable assumption in the case of pyrene excimer formation,⁶ the following differential equations can be derived to describe the time-dependent behavior of P0*, P1*, and E*.

$$\frac{d[P0^*]}{dt} = -\left(\frac{1}{\tau_M} + k_e[M1]\right) \times [P0^*] + k_e[M0] \times [P1^*] \quad (\text{SI.2.12})$$

$$\frac{d[P1^*]}{dt} = k_e[M1] \times [P0^*] - \left(\frac{1}{\tau_M} + k_e[M0] + k_{blob}\right) \times [P1^*] \quad (\text{SI.2.13})$$

$$\frac{d[E^*]}{dt} = k_{blob}[P1^*] - \frac{1}{\tau_E}[E^*] \quad (\text{SI.2.14})$$

A linear combination of Equations SI.2.12 and SI.2.13 yields Equation SI.2.15.

$$\frac{d^2[P0^*]}{dt^2} + \left[\frac{2}{\tau_M} + k_{blob} + k_e([M0] + [M1])\right] \times \frac{d[P0^*]}{dt} + \left[\left(\frac{1}{\tau_M} + k_{blob}\right) \times \left(\frac{1}{\tau_M} + k_e[M1]\right) + \frac{k_e[M0]}{\tau_M}\right] [P0^*] = 0 \quad (\text{SI.2.15})$$

Equation SI.2.15 is a second order differential equation which can be easily integrated to yield an expression of $[P0^*]$ as a function of time. It is given in Equation SI.2.16.

$$[P0^*]_{(t)} = A_1 \exp[-t \times (\tau_A^{-1} + \tau_M^{-1})] + A_2 \exp[-t \times (\tau_B^{-1} + \tau_M^{-1})] \quad (\text{SI.2.16})$$

In Equation SI.2.16, A_1 and A_2 are constants which will be determined later. The expressions of the decay times τ_A and τ_B are given in Equations SI.2.17 – 19.

$$\tau_A^{-1} = \frac{1}{2} \left(k_{blob} + k_e([M0] + [M1]) - \sqrt{\Delta} \right) \quad (\text{SI.2.17})$$

$$\tau_B^{-1} = \frac{1}{2} \left(k_{blob} + k_e([M0] + [M1]) + \sqrt{\Delta} \right) \quad (\text{SI.2.18})$$

$$\Delta = [k_{blob} + k_e([M0] - [M1])]^2 + 4k_e^2[M0][M1] \quad (\text{SI.2.19})$$

Equation SI.2.16 can be re-introduced into Equation SI.2.13 to determine the expression of $[P1^*]$ which is given in Equation SI.2.20.

$$[P1^*]_{(t)} = \frac{-A_1}{2k_e[M0]} \left[k_{blob} + k_e([M0] - [M1]) - \sqrt{\Delta} \right] \times \exp[-t \times (\tau_A^{-1} + \tau_M^{-1})] \\ - \frac{A_2}{2k_e[M0]} \left[k_{blob} + k_e([M0] - [M1]) + \sqrt{\Delta} \right] \times \exp[-t \times (\tau_B^{-1} + \tau_M^{-1})] \quad (SI.2.20)$$

Setting the initial conditions as $[P0^*]_{(t=0)} = [P0^*]_o$ and $[P1^*]_{(t=0)} = [P1^*]_o$ yields a set of two equations that can be used to find the expressions of A_1 and A_2 given in Equations SI.2.21 and SI.2.22.

$$A_1 = \frac{[P0^*]_o}{2\sqrt{\Delta}} (k_{blob} + k_e([M0] + [M1]) + \sqrt{\Delta}) \quad (SI.2.21)$$

$$A_2 = -\frac{[P0^*]_o}{2\sqrt{\Delta}} (k_{blob} + k_e([M0] + [M1]) - \sqrt{\Delta}) \quad (SI.2.22)$$

The expression for the overall pyrene monomer decay is then given in Equation SI.2.23 by summing the expressions for $[P0^*]_{(t)}$ and $[P1^*]_{(t)}$.

$$[Py^*]_{(t)} = \frac{[Py^*]_o}{4\sqrt{\Delta} \times k_e([M0] + [M1])} \left(\left[(k_e([M0] + [M1]) + \sqrt{\Delta})^2 - k_{blob}^2 \right] \times \exp[-t \times (\tau_A^{-1} + \tau_M^{-1})] \right. \\ \left. + \left[k_{blob}^2 - (k_e([M0] + [M1]) - \sqrt{\Delta})^2 \right] \times \exp[-t \times (\tau_B^{-1} + \tau_M^{-1})] \right) \quad (SI.2.23)$$

The expression of $[P1^*]_{(t)}$ given in Equation SI.2.20 can then be used to determine $[E^*]_{(t)}$ whose

expression is provided in Equation SI.2.24.

$$\begin{aligned}
[E^*]_{(t)} = & \frac{k_{blob}[Py^*]_o}{4\sqrt{\Delta}k_e([M0]+[M1])} \left[-\frac{(k_{blob} + k_e[M0])^2 - (k_e[M1] + \sqrt{\Delta})^2}{\tau_M^{-1} + \tau_A^{-1} + \tau_E^{-1}} \times \exp[-t \times (\tau_A^{-1} + \tau_M^{-1})] \right. \\
& \left. + \frac{(k_{blob} + k_e[M0])^2 - (k_e[M1] - \sqrt{\Delta})^2}{\tau_M^{-1} + \tau_B^{-1} + \tau_E^{-1}} \times \exp[-t \times (\tau_B^{-1} + \tau_M^{-1})] \right] \\
& + \left[[E^*]_o + \frac{k_{blob}[Py^*]_o}{4\sqrt{\Delta}k_e([M0]+[M1])} \left(\frac{(k_{blob} + k_e[M0])^2 - (k_e[M1] + \sqrt{\Delta})^2}{\tau_M^{-1} + \tau_A^{-1} + \tau_E^{-1}} \right. \right. \\
& \left. \left. - \frac{(k_{blob} + k_e[M0])^2 - (k_e[M1] - \sqrt{\Delta})^2}{\tau_M^{-1} + \tau_B^{-1} + \tau_E^{-1}} \right) \right] \times \exp[-t / \tau_E]
\end{aligned}
\tag{SI.2.24}$$

The following equalities were found to be useful in the derivation of Equations SI.2.23 and SI.2.24.

$$\frac{[P0^*]_o}{[M0]} = \frac{[P1^*]_o}{[M1]} = \frac{[P0^*]_o + [P1^*]_o}{[M0] + [M1]} = \frac{[Py^*]_o}{[M0] + [M1]}
\tag{SI.2.25}$$

Table SI.2.1. Lifetimes (in ns) of pyrene derivatives (τ_M) in different solvents and χ^2 of the fits.

Solvent	PEO(2K)-Py ₁					PyCH ₂ OMe		PyCH ₂ OH		PyMe		PyMe	
	τ_{M1}	a_{M1}	τ_{M2}	a_{M2}	χ^2	τ_M	χ^2	τ_M	χ^2	τ_M	χ^2	τ_M ^{a)}	
acetone	40	0.05	277	0.95	1.09	278	1.09	254	1.15	186	1.09	140	
ACN	53	0.06	265	0.94	1.05	264	1.18	247	1.00	185	1.16		
THF	59	0.03	258	0.97	1.03	259	1.17	241	1.12	188	1.10		
toluene	70	0.04	232	0.96	1.15	231	1.10	226	1.12	165	1.10		
DMF	70	0.06	220	0.94	1.07	218	1.12	202	1.11	154	1.18		
dioxane	59	0.05	230	0.95	1.16	231	1.19	211	1.12	170	1.16		166
DMA	49	0.03	212	0.97	1.14	211	1.06	189	1.15	156	1.06		
MeOH	30	0.08	291	0.92	1.14	292	1.14	282	1.17	210	1.12		210
EtOH	50	0.07	291	0.93	1.06	293	1.11	284	1.09	212	1.16		204

^{a)} Lifetimes from *J. Phys. Chem. B* **2009**, *113*, 618-626.

Table SI.2.2. Solvent viscosities and intrinsic viscosities for PEO(10K) at T = 25 °C.

Solvent	η , mPa.s	$[\eta]_{10K}$, L/g	$\pm[\eta]$, L/g
acetone	0.32	0.0226	0.0006
acetonitrile (ACN)	0.37	0.0219	0.0007
tetrahydrofuran (THF)	0.46	0.0215	0.0009
toluene	0.56	0.0224	0.0007
<i>N,N</i> -dimethylformamide (DMF)	0.79	0.0216	0.0010
dioxane	1.18	0.0227	0.0007
<i>N,N</i> -dimethylacetamide (DMA)	1.92	0.0218	0.0008

Table SI.2.3A: The lifetimes and pre-exponential factors obtained from the global analysis of the pyrene monomer and excimer decays with Equations 2.1 and 2.2. A short decay time (τ_s) is fixed to 3.5 ns. The monomer decay of PEO(2K)-Py₂ was considered mono-exponential, the lifetimes (τ_M) are listed in Table SI.2.1.

Solvent	M_n (g/mol)	τ_1 (ns)	τ_2 (ns)	a_{M1}	a_{M2}	f_{Mfree}	a_{MS}	a_{E1}	a_{E2}	a_{ES}	χ^2
acetone	2000	28.3	53.8	0.72	0.20	0.032	0.05	-1.16	1.19	0.05	1.17
	5000	41.0	94.0	0.10	0.70	0.058	0.15	-0.88	0.91	0.02	1.03
	10000	41.3	177.5	0.05	0.71	0.108	0.13	-0.40	0.45	0.26	1.12
	16500	40.3	187.0	0.06	0.52	0.249	0.13	-0.44	0.52	0.25	1.16
ACN	2000	26.2	50.5	0.78	0.13	0.027	0.06	-1.15	1.19	0.01	1.05
	5000	40.7	95.6	0.11	0.76	0.062	0.06	-0.90	0.93	0.03	1.09
	10000	40.1	187.2	0.04	0.82	0.107	0.03	-0.44	0.51	0.10	1.15
	16500	41.4	218.0	0.07	0.52	0.226	0.18	-0.08	0.11	0.22	1.05
THF	2000	38.0	71.5	0.24	0.68	0.032	0.04	-1.22	1.23	0.11	1.02
	5000	41.7	147.6	0.08	0.76	0.070	0.08	-0.60	0.64	0.07	1.14
	10000	40.9	218.1	0.05	0.66	0.190	0.10	-0.08	0.11	0.22	1.02
	16500	39.7	215.3	0.05	0.26	0.569	0.10	-0.10	0.14	0.27	1.11
toluene	2000	37.3	61.6	0.30	0.59	0.028	0.07	-1.47	1.49	0.05	1.09
	5000	40.5	128.4	0.06	0.78	0.078	0.05	-0.57	0.62	0.03	1.09
	10000	37.9	198.1	0.05	0.70	0.204	0.04	-0.13	0.17	0.22	1.11
DMF	2000	40.2	89.2	0.09	0.67	0.045	0.11	-0.86	0.88	0.10	1.01
	5000	40.3	159.7	0.05	0.84	0.098	0.02	-0.55	0.59	0.12	1.05
	10000	37.7	198.6	0.03	0.47	0.445	0.05	-0.08	0.13	0.25	1.14
dioxane	2000	43.7	96.6	0.06	0.74	0.051	0.14	-0.90	0.93	0.11	1.01
	5000	39.4	177.6	0.08	0.67	0.110	0.17	-0.32	0.46	0.01	1.04
	10000	33.9	213.9	0.05	0.00	0.848	0.12	-0.03	0.06	0.22	1.17
DMA	2000	42.0	99.3	0.07	0.81	0.055	0.06	-0.85	0.88	0.11	1.01
	5000	45.9	167.0	0.04	0.62	0.200	0.14	-0.47	0.54	0.21	1.12

Table SI.2.3B: The cyclization rate constant (k_{cy}), the dissociation rate constant (k_{-cy}), and the excimer lifetime (τ_E) obtained from the global analysis of the monomer and excimer fluorescence decays with Equations 2.1 and 2.2.

Solvent	M_n (g/mol)	k_{cy} (ns ⁻¹)	k_{-cy} (ns ⁻¹)	τ_E (ns)
acetone	2000	0.02793	0.00170	49
	5000	0.00859	0.00243	49
	10000	0.00293	0.00644	60
	16500	0.00359	0.00981	77
ACN	2000	0.03192	0.00128	47
	5000	0.00861	0.00252	49
	10000	0.00257	0.00604	56
	16500	0.00319	0.01206	101
THF	2000	0.01337	0.00226	48
	5000	0.00458	0.00570	60
	10000	0.00208	0.01220	92
	16500	0.00416	0.01399	128
toluene	2000	0.01551	0.00161	46
	5000	0.00472	0.00413	52
	10000	0.00224	0.01328	86
DMF	2000	0.00828	0.00228	48
	5000	0.00275	0.00657	58
	10000	0.00190	0.01489	98
dioxane	2000	0.00694	0.00162	49
	5000	0.00327	0.01085	80
	10000	0.00061	0.02539	214
DMA	2000	0.00621	0.00223	49
	5000	0.00206	0.00731	74

Table SI.2.4A: The lifetimes and pre-exponential factors obtained from the global analysis of the pyrene monomer and excimer decays with Equations SI.2.6 and SI.2.7. A short decay time (τ_s) is fixed to 3.5 ns. Asterisks (*) indicate the data were obtained with Equations 2.1 and 2.2. The biexponential decay of PEO(2K)-Py₁ was used for $f_M(t)$ with the decaytimes and pre-exponential factors being listed in Table SI.2.1.

Solvent	M_n (g/mol)	τ_1 (ns)	τ_2 (ns)	a_{M1}	a_{M2}	f_{Mfree}	a_{MS}	a_{E1}	a_{E2}	a_{ES}	χ^2
acetone	2000*	28.3	53.8	0.72	0.20	0.032	0.05	-1.16	1.19	0.05	1.17
	5000	40.5	94.6	0.10	0.74	0.063	0.10	-0.91	0.94	0.03	1.11
	10000	41.2	177.5	0.02	0.75	0.119	0.11	-0.42	0.48	0.27	1.14
	16500	40.3	187.4	0.01	0.54	0.256	0.19	-0.47	0.54	0.25	1.17
ACN	2000*	26.2	50.5	0.78	0.13	0.027	0.06	-1.15	1.19	0.01	1.05
	5000	40.4	96.1	0.11	0.82	0.068	0.01	-0.93	0.97	0.02	1.17
	10000	40.1	187.1	0.02	0.83	0.101	0.04	-0.45	0.54	0.25	1.14
	16500	41.4	218.0	0.00	0.54	0.221	0.22	-0.08	0.12	0.22	1.07
THF	2000*	38.0	71.5	0.24	0.68	0.032	0.04	-1.22	1.23	0.11	1.02
	5000	41.9	147.5	0.03	0.79	0.071	0.11	-0.63	0.68	0.07	1.17
	10000	42.3	219.7	0.00	0.59	0.223	0.18	-0.11	0.15	0.25	1.18
	16500	40.0	215.5	0.00	0.27	0.612	0.12	-0.11	0.15	0.26	1.09
toluene	2000*	37.3	61.6	0.30	0.59	0.028	0.07	-1.47	1.49	0.05	1.09
	5000	40.5	128.6	0.04	0.83	0.088	0.03	-0.59	0.65	0.03	1.13
	10000	37.6	197.3	0.01	0.68	0.234	0.08	-0.12	0.16	0.21	1.14
DMF	2000	40.2	89.6	0.11	0.72	0.052	0.11	-0.86	0.92	0.10	1.11
	5000	40.5	159.8	0.02	0.86	0.111	0.01	-0.58	0.62	0.12	1.06
	10000	41.0	201.7	0.00	0.43	0.482	0.08	-0.07	0.12	0.27	1.14
dioxane	2000	43.1	97.3	0.06	0.79	0.052	0.10	-0.89	0.96	0.11	1.07
	5000	39.8	177.6	0.01	0.69	0.114	0.19	-0.34	0.48	0.02	1.09
	10000	31.3	214.1	0.00	0.09	0.781	0.12	-0.03	0.06	0.22	1.19
DMA	2000	42.0	99.3	0.07	0.82	0.057	0.06	-0.86	0.93	0.12	1.03
	5000	46.4	166.8	0.00	0.65	0.216	0.13	-0.50	0.57	0.16	1.14

Table SI.2.4B: The cyclization rate constant (k_{cy}) and the dissociation rate constant (k_{-cy}) obtained from the global analysis of the monomer and excimer fluorescence decays with Equations SI.2.6 and SI.2.7. The excimer lifetime (τ_E) is fixed to 48 ns. Asterisks indicate the data were obtained with Equations SI.2.1 and SI.2.2.

Solvent	M_n (g/mol)	k_{cy} (ns ⁻¹)	k_{-cy} (ns ⁻¹)
acetone	2000*	0.02793	0.00170
	5000	0.00850	0.00215
	10000	0.00224	0.00305
	16500	0.00194	0.00359
ACN	2000*	0.03192	0.00128
	5000	0.00851	0.00221
	10000	0.00216	0.00370
	16500	0.00117	0.00313
THF	2000*	0.01337	0.00226
	5000	0.00344	0.00250
	10000	0.00079	0.00271
	16500	0.00095	0.00396
toluene	2000*	0.01551	0.00161
	5000	0.00431	0.00298
	10000	0.00103	0.00548
DMF	2000	0.00847	0.00219
	5000	0.00212	0.00341
	10000	0.00050	0.00348
dioxane	2000	0.00681	0.00148
	5000	0.00160	0.00394
	10000	0.00051	0.01088
DMA	2000	0.00614	0.00196
	5000	0.00109	0.00076

Table SI.2.5A: The lifetimes and molar fractions of pyrene forming and not forming excimer obtained from the global analysis of the pyrene monomer and excimer decays with Equations 2.3 and 2.4. A short decay time (τ_s) is fixed to 3.5 ns. The biexponential decay of PEO(2K)-Py₁ was used for $f_M(t)$ with the decaytimes and pre-exponential factors being listed in Table SI.2.1.

Solvent	M_n (g/mol)	τ_1 (ns)	τ_2 (ns)	f_{MP2}	f_{MP1}	f_{Mfree}	a_{MS}	χ^2
acetone	2000	29.2	51.0	0.055	0.906	0.038	0.02	1.16
	5000	52.8	96.8	0.134	0.800	0.066	0.04	1.01
	10000	73.6	181.3	0.319	0.571	0.110	0.04	1.07
	16500	62.9	200.4	0.444	0.325	0.230	0.05	1.02
ACN	2000	29.3	57.7	0.022	0.943	0.035	0.02	1.08
	5000	55.9	99.7	0.127	0.809	0.064	0.02	1.08
	10000	89.7	194.9	0.333	0.601	0.065	0.01	1.02
	16500	96.8	226.0	0.358	0.423	0.219	0.06	1.00
THF	2000	43.3	73.6	0.104	0.862	0.035	0.02	1.03
	5000	73.3	150.3	0.194	0.730	0.076	0.05	1.08
	10000	111.2	227.5	0.435	0.415	0.150	0.04	1.08
	16500	97.0	208.0	0.111	0.145	0.744	0.04	1.04
toluene	2000	44.5	64.4	0.052	0.916	0.032	0.02	1.10
	5000	50.8	130.1	0.310	0.607	0.082	0.02	1.08
	10000	65.8	201.2	0.572	0.248	0.180	0.02	1.06
DMF	2000	46.5	90.6	0.170	0.774	0.055	0.06	1.00
	5000	52.6	161.5	0.486	0.422	0.092	0.01	1.03
	10000	98.9	209.0	0.568	0.189	0.242	0.02	1.08
dioxane	2000	53.4	98.1	0.118	0.824	0.059	0.05	1.07
	5000	59.2	180.4	0.510	0.378	0.111	0.06	1.03
	10000	76.0	224.6	0.000	0.000	1.000	0.04	1.06
DMA	2000	48.3	100.5	0.205	0.740	0.055	0.02	1.01
	5000	83.1	169.0	0.566	0.223	0.212	0.06	1.10

Table SI.2.5B: The rate constants of pyrene excimer formation inside a blob (k_{blob}) and ground-state pyrenes moving inside and outside a blob ($k_{\text{ex}}[\text{M1}]$ and $k_{\text{ex}}[\text{M0}]$, respectively) obtained from the global analysis of the monomer and excimer fluorescence decays with Equations 2.3 and 2.4. The excimer lifetime (τ_{E}) is fixed to 48 ns.

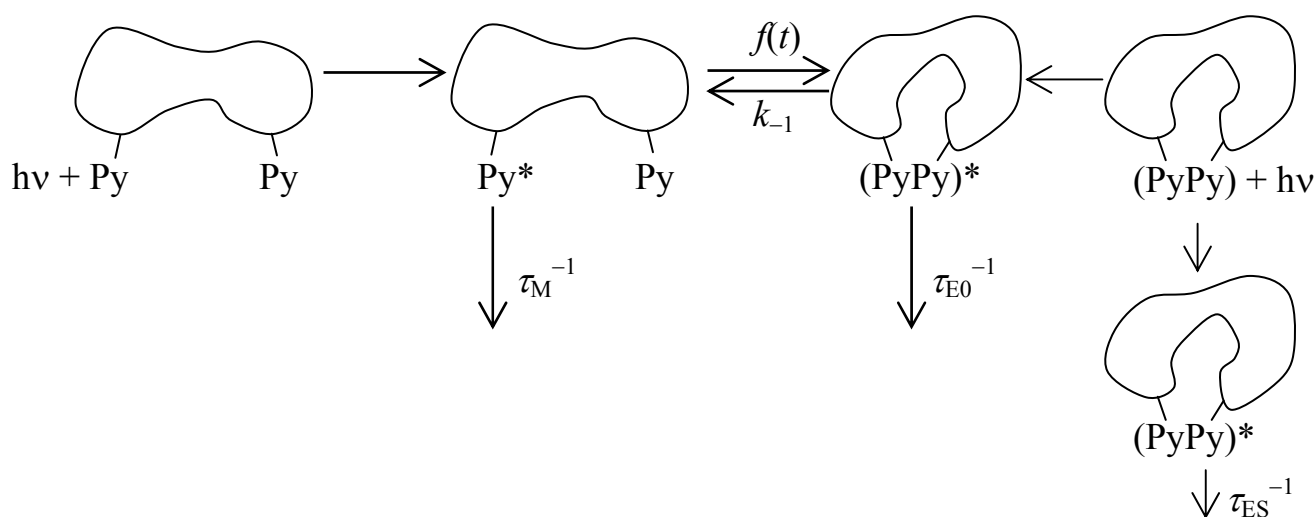
Solvent	M_n (g/mol)	f_{EP0}	f_{EP1}	f_{E0}	a_{ES}	k_{blob} (ns ⁻¹)	$k_{\text{ex}}[\text{M0}]$ (ns ⁻¹)	$k_{\text{ex}}[\text{M1}]$ (ns ⁻¹)
acetone	2000	0.056	0.917	0.027	0.06	0.0281	0.0011	0.0172
	5000	0.139	0.833	0.027	0.01	0.0095	0.0018	0.0105
	10000	0.352	0.631	0.017	0.24	0.0032	0.0030	0.0054
	16500	0.566	0.414	0.020	0.21	0.0036	0.0056	0.0041
ACN	2000	0.021	0.932	0.047	0.03	0.0299	0.0003	0.0140
	5000	0.132	0.841	0.027	0.01	0.0094	0.0015	0.0098
	10000	0.351	0.633	0.016	0.21	0.0029	0.0022	0.0040
	16500	0.451	0.533	0.016	0.21	0.0018	0.0027	0.0031
THF	2000	0.106	0.879	0.015	0.11	0.0144	0.0016	0.0130
	5000	0.206	0.776	0.017	0.04	0.0040	0.0018	0.0067
	10000	0.506	0.483	0.011	0.21	0.0012	0.0023	0.0022
	16500	0.422	0.553	0.026	0.26	0.0020	0.0023	0.0031
toluene	2000	0.052	0.926	0.022	0.05	0.0154	0.0008	0.0133
	5000	0.330	0.645	0.025	0.01	0.0063	0.0042	0.0083
	10000	0.689	0.298	0.013	0.21	0.0027	0.0062	0.0027
DMF	2000	0.178	0.805	0.018	0.09	0.0100	0.0024	0.0111
	5000	0.531	0.461	0.009	0.11	0.0044	0.0063	0.0055
	10000	0.745	0.248	0.007	0.24	0.0011	0.0035	0.0012
dioxane	2000	0.122	0.857	0.020	0.09	0.0076	0.0016	0.0110
	5000	0.561	0.416	0.023	0.01	0.0033	0.0060	0.0044
	10000	0.926	0.071	0.003	0.22	0.0014	0.0069	0.0005
DMA	2000	0.213	0.770	0.017	0.11	0.0077	0.0028	0.0102
	5000	0.711	0.280	0.009	0.20	0.0014	0.0019	0.0047

References

1. Dust, J. M.; Fang, Z.; Harris, J. M. *Macromolecules* **1990**, *23*, 3742.
2. Zhao, T.; Beckham, H. W. *Macromolecules* **2003**, *36*, 9859.
3. Piçarra, S.; Gomes, P. T.; Martinho, J. M. G. *Macromolecules* **2000**, *33*, 3947-3950.
4. Costa, T.; Seixas de Melo, J.; Burrows, H. D. *J. Phys. Chem. B* **2009**, *113*, 618-626.
5. Siu, H.; Duhamel, J. Pincus, J.; Sasaki, D. *Langmuir*, **2010**, *26*, 10985-10994.
6. Birks, J. B. *Photophysics of Aromatic Molecules*. Wiley: New York, 1970; p 301.

Chapter 3 Supporting Information

Scheme 3.2, describing the process of excimer formation between pyrene moieties covalently attached onto a macromolecule, can be re-arranged into Scheme SI.3.1 where excimer formation is described by a time-dependent rate constant $f(t)$ which is a function of the parameters f_{Pi} and k_{qi} defined in Scheme 3.2.¹⁻¹⁴ Since the pyrene moieties are covalently attached onto the macromolecule, an excimer formation event indicates that the macromolecule has re-arranged its conformation while the pyrene monomer remained excited and the function $f(t)$ reflects the time scale of the re-arrangement process.



Scheme SI.3.1: Generalization of the process of excimer formation between pyrenyl groups covalently attached onto a macromolecule. Processes on the right describe the direct excitation of pyrene dimers that form well- or poorly stacked pyrene excimers that emit with a lifetime τ_{E0} or τ_{ES} , respectively.

In the particular case where two pyrenyl pendants are covalently attached at two specific positions of a well-defined macromolecule such as the chain ends of a monodisperse polymer, $f(t)$ remains constant with time ($f(t) = k_1$)^{15,16} and the kinetics of excimer formation are well-described by

Birks' scheme where the pyrene monomer and excimer are expected to decay according to Equations SI.3.1 and SI.3.2.¹⁷

$$[Py^*] = \frac{[Py_{diff}^*]_{(t=0)}}{\sqrt{(X-Y)^2 + 4k_1k_{-1}}} \left((X - \tau_2^{-1}) \times \exp(-t/\tau_1) - (X - \tau_1^{-1}) \times \exp(-t/\tau_2) \right) + [Py_{free}^*]_{(t=0)} \exp(-t/\tau_M) \quad (SI.3.1)$$

$$[E^*] = \frac{k_1 [Py_{diff}^*]_{(t=0)}}{\sqrt{(X-Y)^2 + 4k_1k_{-1}}} \left(-\exp(-t/\tau_1) + \exp(-t/\tau_2) \right) + [E0^*]_{(t=0)} \exp(-t/\tau_{E0}) \quad (SI.3.2)$$

The parameters X and Y in Equations SI.3.1 and SI.3.2 equal $k_1 + \tau_M^{-1}$ and $k_{-1} + \tau_E^{-1}$, respectively.

The decay times τ_1 and τ_2 are given in Equations SI.3.3 and SI.3.4, respectively. The concentration

$[Py_{diff}^*]_{(t=0)}$ represents the initial concentrations of the pyrene species that form excimer by diffusion.

If the labeling reaction is not complete (as it normally is) and some macromolecules end up being monolabeled, or if some residual unattached pyrene remains in the sample, these pyrenyl moieties

emit as if they were free in solution and their initial concentration is given by $[Py_{free}^*]_{(t=0)}$.

$$\tau_1^{-1} = \frac{X + Y + \sqrt{(X-Y)^2 + 4k_1k_{-1}}}{2} \quad (SI.3.3)$$

$$\tau_2^{-1} = \frac{X + Y - \sqrt{(X-Y)^2 + 4k_1k_{-1}}}{2} \quad (SI.3.4)$$

In the more general cases where the pyrenyl labels are attached at non-specific positions of the macromolecule, or at more than two specific positions, a distribution of distances between every pair of pyrene labels ensues which yields a distribution of rate constants, resulting in the time-dependent rate constant referred to as $f(t)$ in Scheme 3.3.¹⁻¹⁴ Different solutions for $f(t)$ have been proposed depending on whether the Model Free (MF) and Fluorescence Blob Model (FBM) analyses are being applied.² MF analysis of the fluorescence decays of the pyrene monomer and excimer is conducted with Equations SI.3.5 and SI.3.6, respectively. In Equations SI.3.5 and SI.3.6, the pre-exponential factors a_i are normalized so that $\sum_{i=1}^n a_i = 1$.

$$[Py^*]_{(t)} = [Py_{diff}^*]_{(t=0)} \times \sum_{i=1}^n a_i \times \exp(-t/\tau_i) + [Py_{free}^*]_{(t=0)} \times \exp(-t/\tau_M) \quad (SI.3.5)$$

$$[E^*]_{(t)} = -[Py_{diff}^*]_{(t=0)} \times \sum_{i=1}^n a_i \frac{\frac{1}{\tau_i} - \frac{1}{\tau_M}}{\frac{1}{\tau_i} - \frac{1}{\tau_{E0}}} \exp(-t/\tau_i) + \left([E0^*]_{(t=0)} + [Py_{diff}^*]_{(t=0)} \times \sum_{i=1}^n a_i \frac{\frac{1}{\tau_i} - \frac{1}{\tau_M}}{\frac{1}{\tau_i} - \frac{1}{\tau_{E0}}} \right) \times \exp(-t/\tau_{E0}) + [ES^*]_{(t=0)} \times \exp(-t/\tau_{ES}) \quad (SI.3.6)$$

The species Py_{diff}^* and Py_{free}^* in Equations SI.3.5 and SI.3.6 have already been defined. Depending on the nature of the solvent or how crowded the labeled macromolecule is, ground-state pyrene dimers or aggregates are formed. These species are generated instantaneously by direct absorption of

a photon and they emit as an excimer $E0^*$ with a lifetime τ_{E0} of around 50 – 70 ns in organic solvents¹⁸ or a poorly stacked dimer ES^* with a short lifetime τ_S of around 2 – 4 ns,^{6,12,19,20} depending on solvent. Global analysis of the fluorescence decays of the pyrene monomer and excimer with the sets of Equations SI.3.1 and SI.3.2 or SI.3.5 and SI.3.6 yields the fraction f_{Mdiff} , f_{Mfree} , f_{Ediff} , f_{EE0} , and f_{EES} whose expressions are given in Equations SI.3.7 – SI.3.11.

$$f_{Mdiff} = \frac{[Py_{diff}^*]_{(t=0)}}{[Py_{diff}^*]_{(t=0)} + [Py_{free}^*]_{(t=0)}} \quad (SI.3.7)$$

$$f_{Mfree} = \frac{[Py_{free}^*]_{(t=0)}}{[Py_{diff}^*]_{(t=0)} + [Py_{free}^*]_{(t=0)}} \quad (SI.3.8)$$

$$f_{Ediff} = \frac{[Py_{diff}^*]_{(t=0)}}{[Py_{diff}^*]_{(t=0)} + [E0^*]_{(t=0)} + [ES^*]_{(t=0)}} \quad (SI.3.9)$$

$$f_{EE0} = \frac{[E0^*]_{(t=0)}}{[Py_{diff}^*]_{(t=0)} + [E0^*]_{(t=0)} + [ES^*]_{(t=0)}} \quad (SI.3.10)$$

$$f_{EES} = \frac{[ES^*]_{(t=0)}}{[Py_{diff}^*]_{(t=0)} + [E0^*]_{(t=0)} + [ES^*]_{(t=0)}} \quad (SI.3.11)$$

The indices “ M ” in Equations SI.3.7 and SI.3.8 and “ E ” in Equations SI.3.9 – SI.3.11 act as a reminder that these fractions describe the pyrene species Py_{diff}^* and Py_{free}^* that contribute to the monomer decays, and the pyrene species Py_{diff}^* , $E0^*$, and ES^* that contribute to the excimer decays, respectively. The fractions f_{diff} , f_{free} , f_{E0} , and f_{ES} that describe the overall population of pyrene species Py_{diff}^* , Py_{free}^* , $E0^*$, and ES^* are obtained by combining f_{Mdiff} , f_{Mfree} , f_{Ediff} , f_{EE0} , and f_{EES} according to Equations SI.3.12 – SI.3.15.

$$f_{diff} = \frac{[Py_{diff}^*]_{(t=0)}}{[Py_{diff}^*]_{(t=0)} + [Py_{free}^*]_{(t=0)} + [E0^*]_{(t=0)} + [ES^*]_{(t=0)}} = \left(1 + \frac{f_{Mfree}}{f_{Mdiff}} + \frac{f_{EE0}}{f_{Ediff}} + \frac{f_{EES}}{f_{Ediff}} \right)^{-1} \quad (SI.3.12)$$

$$f_{free} = \frac{[Py_{free}^*]_{(t=0)}}{[Py_{diff}^*]_{(t=0)} + [Py_{free}^*]_{(t=0)} + [E0^*]_{(t=0)} + [ES^*]_{(t=0)}} = f_{diff} \times \frac{f_{Mfree}}{f_{Mdiff}} \quad (SI.3.13)$$

$$f_{E0} = \frac{[E0^*]_{(t=0)}}{[Py_{diff}^*]_{(t=0)} + [Py_{free}^*]_{(t=0)} + [E0^*]_{(t=0)} + [ES^*]_{(t=0)}} = f_{diff} \times \frac{f_{EE0}}{f_{Ediff}} \quad (SI.3.14)$$

$$f_{ES} = \frac{[ES^*]_{(t=0)}}{[Py_{diff}^*]_{(t=0)} + [Py_{free}^*]_{(t=0)} + [E0^*]_{(t=0)} + [ES^*]_{(t=0)}} = f_{diff} \times \frac{f_{EES}}{f_{Ediff}} \quad (SI.3.15)$$

The fractions defined in Equations SI.3.12 – SI.3.15 can then be used to determine a measure of the fluorescence intensity of the monomer $(I_M)^{SPC}$ and excimer $(I_E)^{SPC}$ based on Equations SI.3.16 and SI.3.17 where the function $[Py^*]_{(t)}$ is given by Equation SI.3.1 or SI.3.5 whereas the function $[E^*]_{(t)}$ is given by Equation SI.3.2 or SI.3.6 depending on whether the Birks scheme or MF analysis is used.

$$(I_M)^{SPC} = \int_{t=0}^{\infty} [Py^*]_{(t)} dt \quad (SI.3.16)$$

$$(I_E)^{SPC} = \int_{t=0}^{\infty} [E^*]_{(t)} dt \quad (SI.3.17)$$

Taking the ratio of $(I_E)^{SPC}$ over $(I_M)^{SPC}$ yields the $(I_E/I_M)^{SPC}$ ratio whose expression is given in Equation SI.3.18 for the Birks scheme analysis and Equation SI.3.19 for the MF analysis.

$$\left(\frac{I_E}{I_M}\right)_{Birks}^{SPC} = \frac{k_1 \times f_{diff} \times (\tau_2 - \tau_1)}{f_{diff} \times ((X - \tau_2^{-1}) \times \tau_1 - (X - \tau_1^{-1}) \times \tau_2) + f_{free} \times \tau_M \times \sqrt{(X - Y)^2 + 4k_1 k_{-1}}}$$

(SI.3.18)

$$\left(\frac{I_E}{I_M}\right)_{MF}^{SPC} = \frac{-f_{diff} \times \sum_{i=1}^n a_i \frac{\frac{1}{\tau_i} - \frac{1}{\tau_M}}{\frac{1}{\tau_i} - \frac{1}{\tau_{E0}}} \times \tau_i + \left(f_{E0} + f_{diff} \times \sum_{i=1}^n a_i \frac{\frac{1}{\tau_i} - \frac{1}{\tau_M}}{\frac{1}{\tau_i} - \frac{1}{\tau_{E0}}} \right) \times \tau_{E0} + f_{ES} \times \tau_{ES}}{f_{diff} \times \sum_{i=1}^n a_i \times \tau_i + f_{free} \times \tau_M}$$

(SI.3.19)

Inspection of Equations SI.3.18 and SI.3.19 indicates that the ratios $(I_E / I_M)_{Birks}^{SPC}$ and $(I_E / I_M)_{MF}^{SPC}$ depend only on parameters that are retrieved from the analysis of the fluorescence decays and represent absolute quantities. An important aspect of Equations SI.3.18 and SI.3.19 is that they can be used to estimate how the presence of pyrene units emitting as Py_{free}^* affect the I_E/I_M ratio. This is done simply by setting $f_{free} = 0$ in Equations SI.3.18 and SI.3.19 yielding the ratio $(I_E / I_M)_{f_{free}=0}^{SPC}$, i.e. the value of the $(I_E/I_M)^{SPC}$ ratio if no Py_{free}^* species was present in solution.

The kinetics of excimer formation between pyrene groups covalently attached onto a macromolecule reflects the dynamics of the macromolecule. Whereas information about those dynamics is retrieved in a straightforward manner under the form of the rate constant k_1 when Birks' scheme applies, it is buried in the function $f(t)$ when the MF analysis is being used. Information about the dynamics of the macromolecule can still be obtained when dealing with the MF analysis by considering the average rate constant of excimer formation whose expression is given, either as a

function of the average lifetime in Equation SI.3.20²¹ or the average decay rate constant in Equation SI.3.21.¹⁸ Whereas the quantities $(I_E / I_M)_{f_{free}=0}^{SPC}$ and $\langle k \rangle$ are independent of the existence of Py_{free}^* , $(I_E / I_M)^{SPC}$ decreases steadily with increasing concentration of Py_{free}^* , as the fraction f_{free} in Equations SI.3.18 or SI.3.19 becomes larger.

$$\langle k \rangle = \left(\sum_{i=1}^n a_i \times \tau_i \right)^{-1} - \frac{1}{\tau_M} \quad (\text{SI.3.20})$$

$$\langle k \rangle = \sum_{i=1}^n \frac{a_i}{\tau_i} - \frac{1}{\tau_M} \quad (\text{SI.3.21})$$

References

1. Siu, H.; Duhamel, J. *Macromolecules* **2004**, *37*, 9287-9289.
2. Siu, H.; Duhamel, J. *J. Phys. Chem. B* **2005**, *109*, 1770-1780.
3. Siu, H.; Duhamel, J. *Macromolecules* **2005**, *38*, 7184-7186.
4. Siu, H.; Duhamel, J. *Macromolecules* **2006**, *39*, 1144-1155.
5. Siu, H.; Duhamel, J. *J. Phys. Chem. B* **2008**, *112*, 15301-15312.
6. Siu, H.; Duhamel, J.; Sasaki, D.; Pincus, J. L. *Langmuir* **2010**, *26*, 10985-10994.
7. Ingratta, M.; Duhamel, J. *Macromolecules* **2007**, *40*, 6647-6657.
8. Ingratta, M.; Duhamel, J. *J. Phys. Chem. B* **2008**, *112*, 9209-9218.
9. Ingratta, M.; Duhamel, J. *J. Phys. Chem. B* **2009**, *113*, 2284-2292.

10. Ingrassia, M.; Mathew, M.; Duhamel, J. *Can. J. Chem.* **2010**, *88*, 217-227.
11. Ingrassia, M.; Hollinger, J.; Duhamel, J. *J. Am. Chem. Soc.* **2008**, *130*, 9420-9428.
12. Chen, S.; Duhamel, J.; Winnik, M. A. *J. Phys. Chem. B* **2011**, *115*, 3289-3302.
13. Yip, J.; Duhamel, J.; Bahun, G.; Adronov, A. *J. Phys. Chem. B* **2010**, *114*, 10254-10265.
14. Keyes-Baig, C.; Duhamel, J.; Wettig, S. *Langmuir* **2011**, *27*, 3361-3371.
15. Wilemski, G.; Fixman, M. *J. Chem. Phys.* **1974**, *60*, 866-877.
16. Wilemski, G.; Fixman, M. *J. Chem. Phys.* **1974**, *60*, 878-890.
17. Winnik, M. A. *Acc. Chem. Res.* **1985**, *18*, 73-79.
18. Birks, J. B. *Photophysics of Aromatic Molecules*. Wiley: New York, 1970; p 301.
19. Costa, T.; Seixas de Melo, J.; Burrows, H. D. *J. Phys. Chem. B* **2009**, *113*, 618-626.
20. Piçarra, S.; Gomes, P. T.; Martinho, J. M. G. *Macromolecules* **2000**, *33*, 3947-3950.
21. Winnik, M. A.; Egan, L. S.; Tencer, M. Croucher, M. D. *Polymer* **1987**, *28*, 1553-1560.

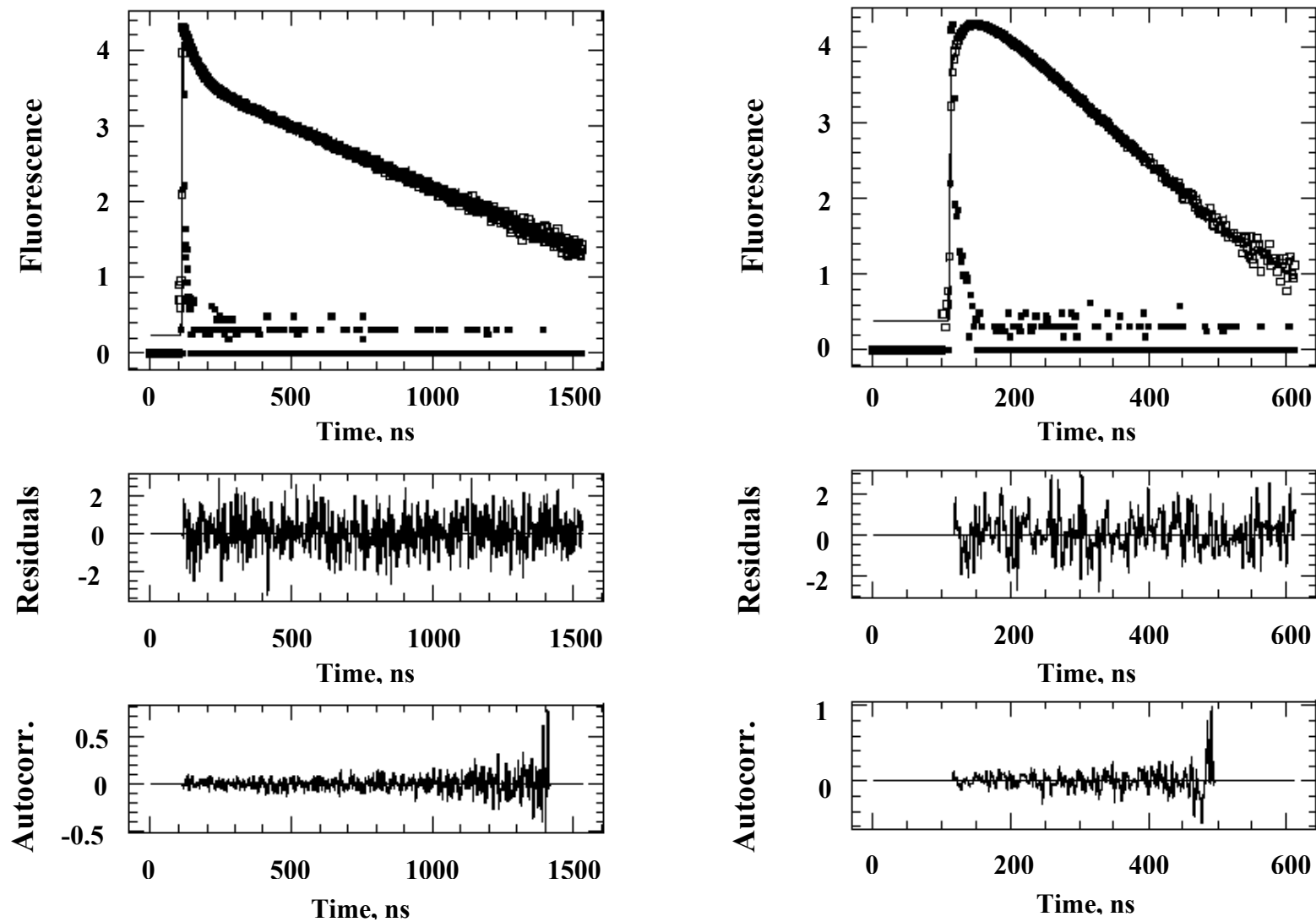


Figure SI.3.1: Fluorescence decays of the pyrene monomer (left; $\lambda_{\text{ex}} = 344$ nm, $\lambda_{\text{em}} = 375$ nm) and excimer (right; $\lambda_{\text{ex}} = 344$ nm, $\lambda_{\text{em}} = 510$ nm) of PEO(2K)-Py₂/PEO(2K)-Py₁ mixture ($\alpha = 0.25$) in acetone with a time per channel of 2.04 ns/ch. $\chi^2 = 1.05$.

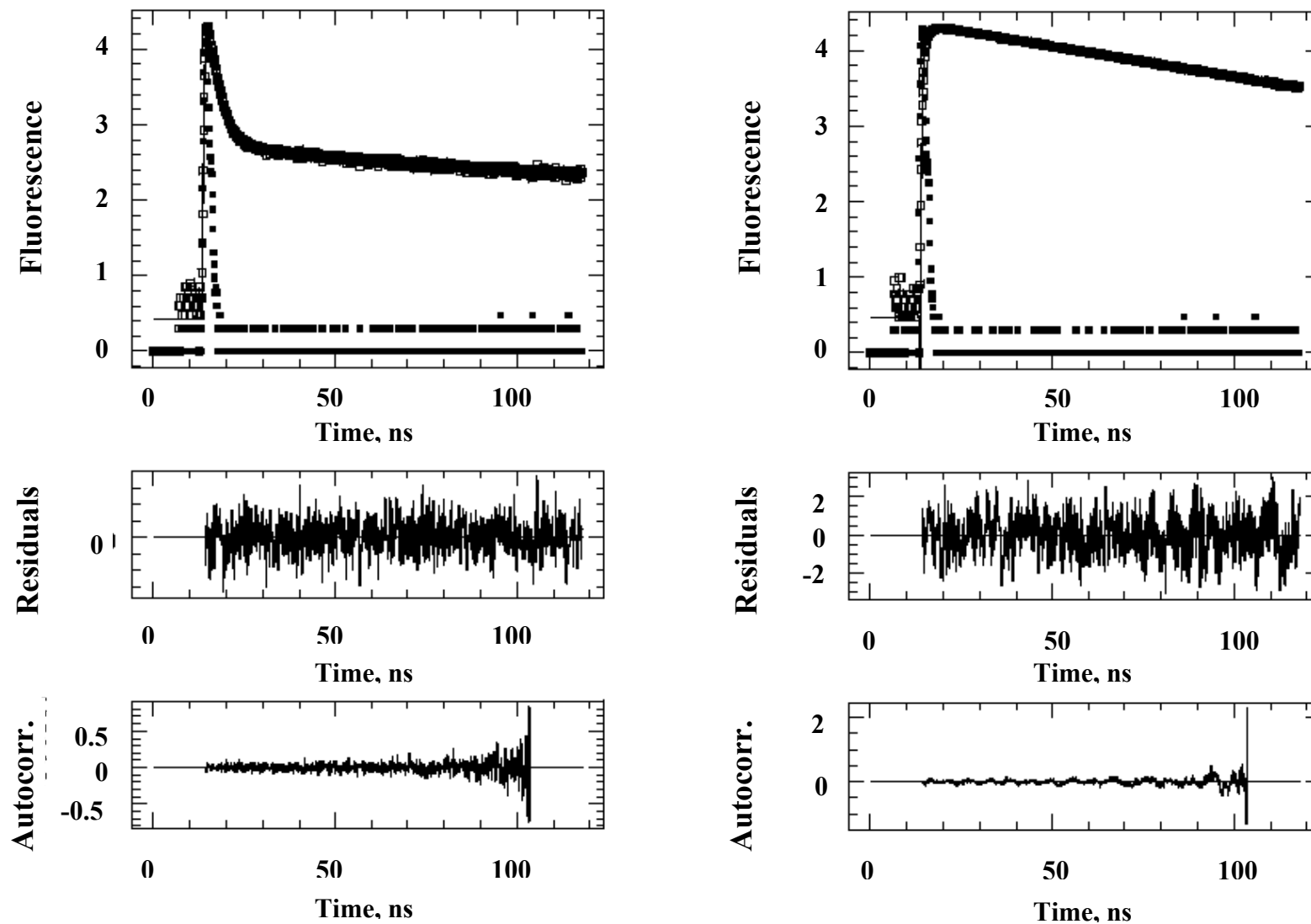


Figure SI.3.2: Fluorescence decays of the pyrene monomer (left; $\lambda_{\text{ex}} = 344 \text{ nm}$, $\lambda_{\text{em}} = 375 \text{ nm}$) and excimer (right; $\lambda_{\text{ex}} = 344 \text{ nm}$, $\lambda_{\text{em}} = 510 \text{ nm}$)

of the Py_{16} -G4-PS/PyBA mixture ($\alpha = 0.15$) in THF with a time per channel of 0.118 ns/ch. $\chi^2 = 1.14$.

Table SI.3.1: Decay times and pre-exponential factors obtained from the global analysis of the monomer and excimer decays of the PEO(2K)-Py₂/PEO(2K)-Py₁ mixtures in acetone with Equations SI.3.1 and SI.3.2. The fraction f_{Mdiff} equals $1 - f_{\text{Mfree}}$. τ_{M} is fixed to 265 ns in the analysis.

A) Monomer Decays:

Sample, $\alpha=$	τ_1 (ns)	a_1	τ_2 (ns)	a_2	τ_{M} (ns)	f_{Mfree}	χ^2
0	28.5	0.768	53.9	0.198	265	0.034	1.20
0.15	26.7	0.787	51.7	0.100	265	0.113	1.03
0.25	26.1	0.652	50.7	0.154	265	0.194	1.06
0.50	25.8	0.570	52.3	0.091	265	0.338	1.15
0.70	25.3	0.300	52.7	0.145	265	0.556	1.15
0.80	23.4	0.226	58.6	0.117	265	0.657	1.14

B) Excimer Decays:

Sample, $\alpha=$	a_{E1}	a_{E2}	τ_{E} (ns)	a_{E0}	k_1	k_{-1}
0	-1.16	1.16	49	0.041	0.028	0.0016
0.15	-1.08	1.08	49	0.044	0.032	0.0010
0.25	-1.14	1.14	47	0.044	0.031	0.0017
0.50	-1.03	1.03	49	0.035	0.032	0.0014
0.70	-1.05	1.05	46	0.042	0.030	0.0021
0.80	-0.76	0.76	48	0.028	0.030	0.0020

C) Molar fractions of all pyrene species:

Sample, $\alpha=$	f_{free}	f_{diff}	f_{E0}
0	0.033	0.928	0.040
0.15	0.108	0.852	0.039
0.25	0.187	0.777	0.036
0.50	0.330	0.646	0.023
0.70	0.545	0.436	0.020
0.80	0.650	0.340	0.010

Table SI.3.2: Decay times and pre-exponential factors obtained from the global analysis of the monomer and excimer decays of the PEO(2K)-Py₂/PEO(2K)-Py₁ mixtures in acetone with Equations SI.3.5 and SI.3.6. The parameters a_i with $i=1-2$ are those used in Equations SI.3.5 and SI.3.6 and their sum equals unity. The fraction f_{Mdiff} equals $1 - f_{\text{Mfree}}$. τ_{M} is fixed to 265 ns in the analysis.

A) Monomer Decays:

Sample, $\alpha=$	τ_1 (ns)	a_1	τ_2 (ns)	a_2	τ_{M} (ns)	f_{Mfree}	χ^2
0	27.9	0.755	51.3	0.245	265	0.034	1.20
0.15	26.6	0.881	50.3	0.119	265	0.112	1.11
0.25	24.9	0.725	45.8	0.275	265	0.194	1.05
0.50	25.8	0.863	52.3	0.137	265	0.338	1.16
0.70	26.9	0.795	59.3	0.205	265	0.553	1.19
0.80	28.3	0.877	116.6	0.123	265	0.650	1.17

B) Excimer Decays:

Sample, $\alpha=$	f_{Ediff}	τ_{E0} (ns)	f_{E0}
0	0.946	49.1	0.054
0.15	0.930	49.4	0.070
0.25	0.942	46.5	0.058
0.50	0.947	49.2	0.053
0.70	0.941	46.0	0.059
0.80	0.918	50.0	0.082

C) Molar fractions of all pyrene species:

Sample, $\alpha=$	f_{free}	f_{diff}	f_{E0}
0	0.032	0.916	0.052
0.15	0.105	0.832	0.063
0.25	0.185	0.768	0.047
0.50	0.326	0.638	0.036
0.70	0.538	0.435	0.027
0.80	0.630	0.339	0.030

Table SI.3.3: Decay times and pre-exponential factors obtained from the global analysis of the monomer and excimer decays of the Py₁₆-G4-PS/PyBA mixtures in THF. The parameters a_i with $i=1-3$ are those used in Equations SI.3.5 and SI.3.6 and their sum equals unity. The fraction f_{Mdiff} equals $1 - f_{\text{Mfree}}$. τ_{M} and τ_{ES} are fixed to, respectively, 210 ns and 4 ns in the analysis.

A) Monomer Decays:

Sample, $\alpha=$	τ_1 (ns)	a_1	τ_2 (ns)	a_2	τ_3 (ns)	a_3	τ_{M} (ns)	f_{Mfree}	χ^2
0	1.39	0.74	2.73	0.25	36	0.0072	210	0.0034	1.16
0.05	1.23	0.71	2.35	0.27	31	0.0078	210	0.0072	1.14
0.10	1.15	0.69	2.23	0.29	29	0.0081	210	0.0108	1.16
0.15	1.34	0.74	2.65	0.24	35	0.0077	210	0.0163	1.10
0.20	1.40	0.80	3.07	0.16	41	0.0071	210	0.0228	1.15
0.35	1.20	0.66	2.37	0.29	30	0.0081	210	0.0367	1.29
0.45	1.33	0.62	2.62	0.31	33	0.0085	210	0.0594	1.15
0.65	1.48	0.71	3.87	0.13	45	0.0112	210	0.1435	1.25
0.75	0.92	0.35	1.94	0.31	59	0.0190	210	0.3200	1.19

B) Excimer Decays:

Sample, $\alpha=$	f_{Ediff}	τ_{E0} (ns)	f_{EE0}	τ_{S} (ns)	f_{EES}
0	0.82	54.3	0.03	4	0.14
0.05	0.84	54.2	0.06	4	0.10
0.10	0.91	53.7	0.00	4	0.09
0.15	0.83	54.3	0.04	4	0.12
0.20	0.86	53.6	0.00	4	0.13
0.35	0.89	53.6	0.00	4	0.11
0.45	0.80	53.1	0.00	4	0.20
0.65	0.81	52.8	0.00	4	0.19
0.75	0.86	52.3	0.02	4	0.11

C) Molar fractions of all pyrene species:

Sample, $\alpha=$	f_{free}	f_{diff}	f_{E0}	f_{ES}
0	0.003	0.821	0.030	0.145
0.05	0.006	0.839	0.060	0.095
0.10	0.010	0.901	0.003	0.086
0.15	0.014	0.820	0.040	0.126
0.20	0.020	0.848	0.000	0.132
0.35	0.033	0.859	0.000	0.108
0.45	0.048	0.757	0.000	0.195
0.65	0.119	0.709	0.001	0.171
0.75	0.289	0.613	0.019	0.078

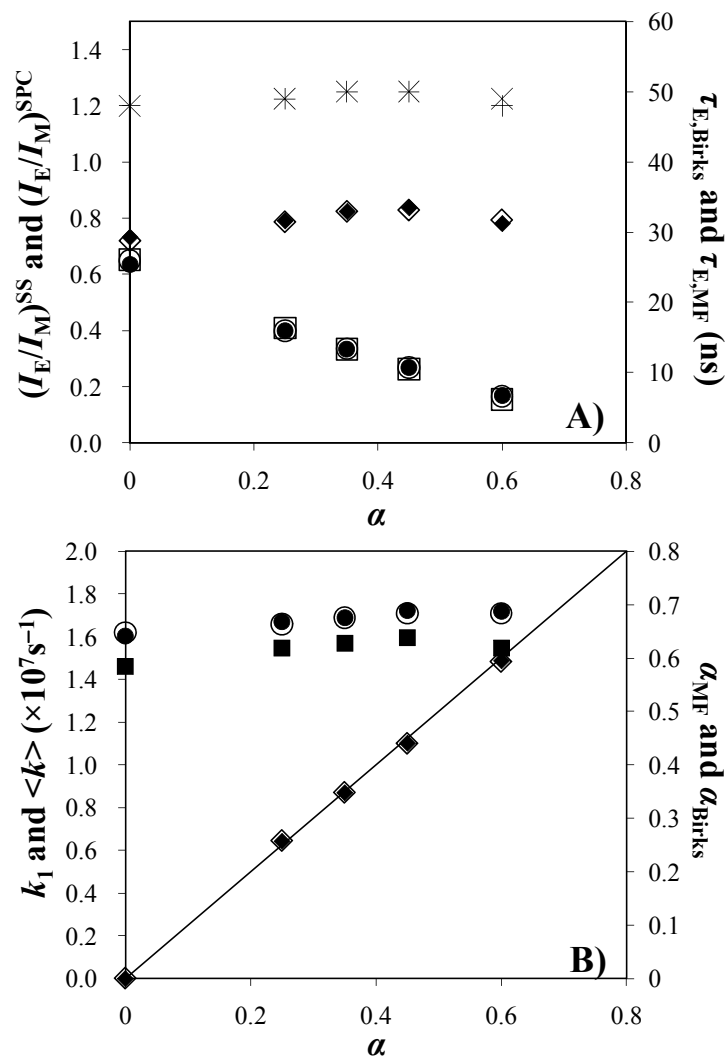


Figure SI.3.3: PEO(2K)-Py₂/PEO(2K)-Py₁ mixtures in toluene. A) Plot of $(I_E/I_M)^{SS}$ (\square), $(I_E/I_M)^{SPC}_{Birks}$ (\bullet), $(I_E/I_M)^{SPC}_{MF}$ (\circ), $(I_E/I_M)^{SPC}_{Birks,ffree=0}$ (\blacklozenge), $(I_E/I_M)^{SPC}_{MF,ffree=0}$ (\diamond), $\tau_{E,Birks}$ (+), and $\tau_{E,MF}$ (\times) as a function of the molar fraction α . B) Plot of k_1 (\bullet), $\langle k \rangle$ calculated with Equation SI.3.20 (\square), $\langle k \rangle$ calculated with Equation SI.3.21 (\circ), α_{MF} (\diamond), and α_{Birks} (\blacklozenge) as a function of α .

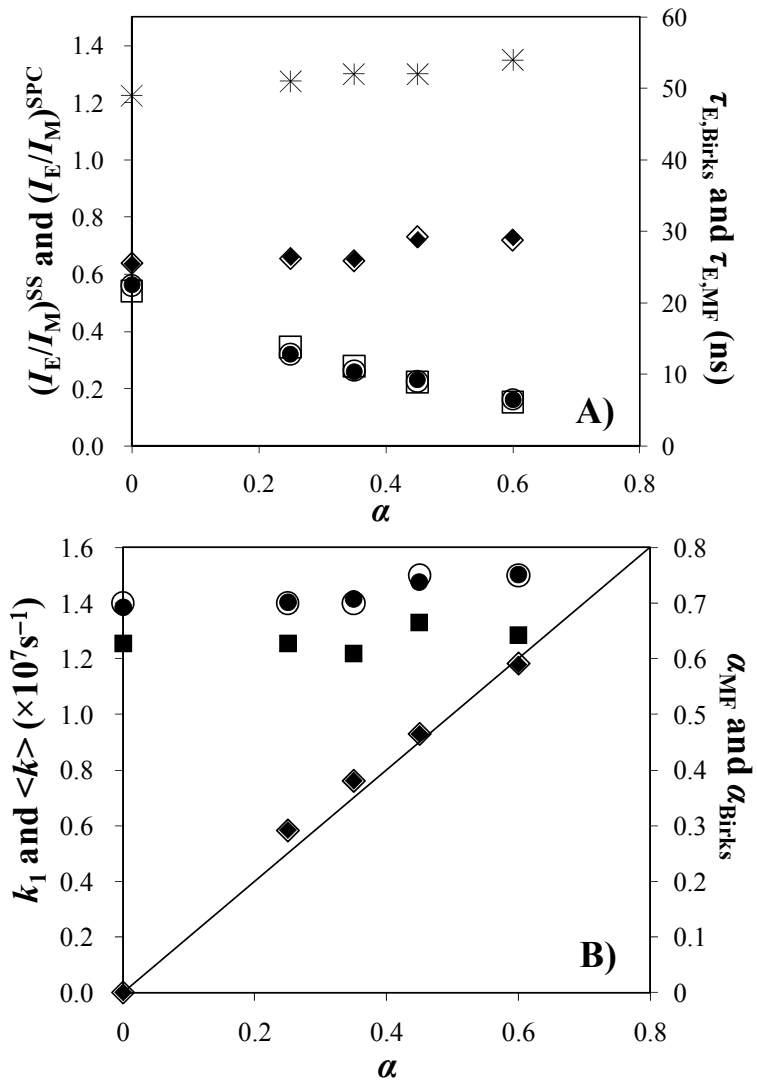


Figure SI.3.4: PEO(2K)-Py₂/PEO(2K)-Py₁ mixtures in tetrahydrofuran. A) Plot of $(I_E / I_M)^{SS}$ (\square), $(I_E / I_M)^{SPC}_{Birks}$ (\bullet), $(I_E / I_M)^{SPC}_{MF}$ (\circ), $(I_E / I_M)^{SPC}_{Birks,free=0}$ (\blacklozenge), $(I_E / I_M)^{SPC}_{MF,free=0}$ (\blacklozenge), $\tau_{E,Birks}$ ($+$), and $\tau_{E,MF}$ (\times) as a function of the molar fraction α . B) Plot of k_1 (\bullet), $\langle k \rangle$ calculated with Equation SI.3.20 (\square), $\langle k \rangle$ calculated with Equation SI.3.21 (\circ), α_{MF} (\blacklozenge), and α_{Birks} (\blacklozenge) as a function of α .

Table SI.3.4: Decay times and pre-exponential factors obtained from the global analysis of the monomer and excimer decays of the PEO(2K)-Py₂/PEO(2K)-Py₁ mixtures in toluene with Equations SI.3.1 and SI.3.2. The fraction f_{Mdiff} equals $1 - f_{\text{Mfree}}$. τ_{M} is fixed to 232 ns in the analysis.

A) Monomer Decays:

Sample, $\alpha=$	τ_1 (ns)	a_1	τ_2 (ns)	a_2	τ_{M} (ns)	f_{Mfree}	χ^2
0	35.5	0.367	63.1	0.604	232	0.029	1.03
0.25	37.6	0.369	61.3	0.455	232	0.176	1.09
0.35	37.9	0.370	61.4	0.391	232	0.239	1.13
0.45	37.5	0.342	61.2	0.349	232	0.310	1.15
0.60	35.4	0.244	63.5	0.308	232	0.448	1.07

B) Excimer Decays:

Sample, $\alpha=$	a_{E1}	a_{E2}	τ_{E} (ns)	a_{E0}	k_1	k_{-1}
0	-1.34	1.34	48	0.032	0.016	0.0022
0.25	-1.51	1.51	49	0.032	0.017	0.0016
0.35	-1.56	1.56	50	0.035	0.017	0.0015
0.45	-1.53	1.53	50	0.035	0.017	0.0016
0.60	-1.29	1.29	49	0.036	0.017	0.0023

C) Molar fractions of all pyrene species:

Sample, $\alpha=$	f_{free}	f_{diff}	f_{E0}
0	0.028	0.941	0.031
0.25	0.171	0.802	0.027
0.35	0.232	0.740	0.027
0.45	0.302	0.673	0.024
0.60	0.438	0.541	0.020

Table SI.3.5: Decay times and pre-exponential factors obtained from the global analysis of the monomer and excimer decays of the PEO(2K)-Py₂/PEO(2K)-Py₁ mixtures in toluene with Equations SI.3.5 and SI.3.6. The parameters a_i with $i=1-2$ are those used in Equations SI.3.5 and SI.3.6 and their sum equals unity. The fraction f_{Mdiff} equals $1 - f_{\text{Mfree}}$. τ_{M} is fixed to 232 ns in the analysis.

A) Monomer Decays:

Sample, $\alpha=$	τ_1 (ns)	a_1	τ_2 (ns)	a_2	τ_{M} (ns)	f_{Mfree}	χ^2
0	37.6	0.430	64.9	0.542	232	0.028	1.03
0.25	35.7	0.309	59.5	0.514	232	0.176	1.09
0.35	38.6	0.398	62.4	0.363	232	0.239	1.13
0.45	36.2	0.305	59.8	0.386	232	0.310	1.15
0.60	39.3	0.368	73.2	0.184	232	0.448	1.07

B) Excimer Decays:

Sample, $\alpha=$	f_{Ediff}	τ_{E0} (ns)	f_{EEO}
0	0.968	48	0.032
0.25	0.968	49	0.032
0.35	0.964	50	0.036
0.45	0.963	50	0.037
0.60	0.961	48	0.039

C) Molar fractions of all pyrene species:

Sample, $\alpha=$	f_{free}	f_{diff}	f_{E0}
0	0.027	0.942	0.031
0.25	0.171	0.802	0.027
0.35	0.232	0.740	0.028
0.45	0.302	0.672	0.026
0.60	0.438	0.540	0.022

Table SI.3.6: Decay times and pre-exponential factors obtained from the global analysis of the monomer and excimer decays of the PEO(2K)-Py₂/PEO(2K)-Py₁ mixtures in THF with Equations SI.3.1 and SI.3.2. The fraction f_{Mdiff} equals $1 - f_{\text{Mfree}}$. τ_{M} is fixed to 258 ns in the analysis.

A) Monomer Decays:

Sample, $\alpha=$	τ_1 (ns)	a_1	τ_2 (ns)	a_2	τ_{M} (ns)	f_{Mfree}	χ^2
0	37.3	0.275	72.7	0.694	258	0.032	1.07
0.25	38.3	0.278	72.6	0.522	258	0.200	1.08
0.35	37.8	0.277	73.1	0.460	258	0.263	1.01
0.45	37.9	0.260	72.6	0.409	258	0.331	1.10
0.60	37.2	0.245	72.7	0.309	258	0.446	1.10

B) Excimer Decays:

Sample, $\alpha=$	a_{E1}	a_{E2}	τ_{E} (ns)	a_{E0}	k_1	k_{-1}
0	-1.15	1.15	49	0.028	0.014	0.0025
0.25	-1.14	1.14	51	0.023	0.014	0.0024
0.35	-1.08	1.08	52	0.022	0.014	0.0026
0.45	-1.18	1.18	52	0.029	0.015	0.0025
0.60	-1.15	1.15	54	0.032	0.015	0.0027

C) Molar fractions of all pyrene species:

Sample, $\alpha=$	f_{free}	f_{diff}	f_{E0}
0	0.031	0.942	0.027
0.25	0.196	0.785	0.018
0.35	0.259	0.725	0.016
0.45	0.324	0.656	0.019
0.60	0.438	0.544	0.018

Table SI.3.7: Decay times and pre-exponential factors obtained from the global analysis of the monomer and excimer decays of the PEO(2K)-Py₂/PEO(2K)-Py₁ mixtures in THF with Equations SI.3.5 and SI.3.6. The parameters a_i with $i=1-2$ are those used in Equations SI.3.5 and SI.3.6 and their sum equals unity. The fraction f_{Mdiff} equals $1 - f_{\text{Mfree}}$. τ_{M} is fixed to 258 ns in the analysis.

A) Monomer Decays:

Sample, $\alpha=$	τ_1 (ns)	a_1	τ_2 (ns)	a_2	τ_{M} (ns)	f_{Mfree}	χ^2
0	41.6	0.383	73.4	0.587	258	0.031	1.04
0.25	40.7	0.323	74.6	0.476	258	0.200	1.08
0.35	38.3	0.286	77.5	0.451	258	0.263	1.01
0.45	42.4	0.345	75.0	0.324	258	0.331	1.08
0.60	41.7	0.324	85.0	0.231	258	0.445	1.07

B) Excimer Decays:

Sample, $\alpha=$	f_{Ediff}	τ_{E0} (ns)	f_{EEO}
0	0.973	49	0.027
0.25	0.976	51	0.024
0.35	0.977	52	0.023
0.45	0.969	52	0.031
0.60	0.965	54	0.035

C) Molar fractions of all pyrene species:

Sample, $\alpha=$	f_{free}	f_{diff}	f_{E0}
0	0.030	0.944	0.026
0.25	0.196	0.785	0.019
0.35	0.258	0.724	0.017
0.45	0.324	0.655	0.021
0.60	0.436	0.544	0.020

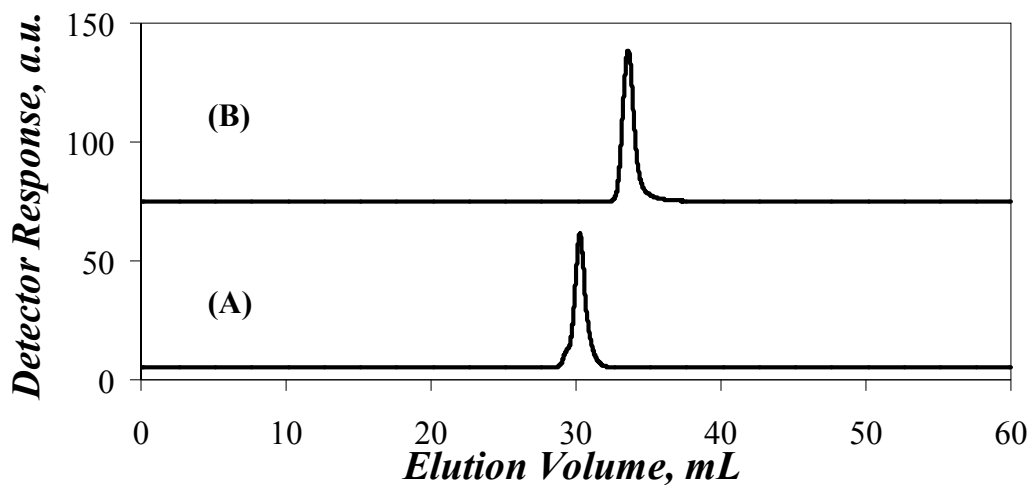


Figure SI.3.5: Gel permeation chromatography traces A) for the labeled PEO samples; B) for 1-pyrenemethanol monitored with a fluorescence detector set at $\lambda_{\text{ex}} = 344$ nm and $\lambda_{\text{em}} = 375$ nm.

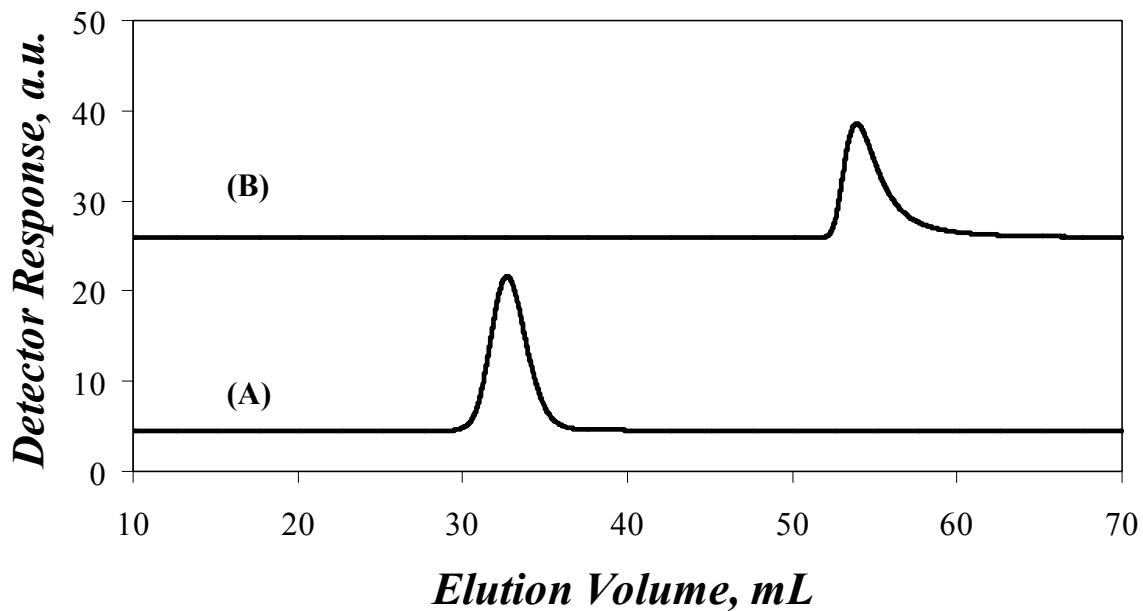


Figure SI.3.6: Gel permeation chromatography traces A) for the Py_{16} -G4-PS sample; B) for PBA monitored with a fluorescence detector set at $\lambda_{\text{ex}} = 344$ nm and $\lambda_{\text{em}} = 375$ nm.

Chapter 4 Supporting Information

Table SI.4.1: Parameters retrieved from the global SM analysis of the pyrene monomer and excimer fluorescence decays acquired with PEO(*X*)-Py₂ aqueous solution at different *C_P*. τ_{M} is fixed to 154 ns in the analysis.

(A) PEO(2K)-Py₂

<i>C_P</i> μM	<i>k</i> ₁₁ × 10 ⁷ s ⁻¹	<i>k</i> ₂ × 10 ⁷ s ⁻¹	<i>f</i> _{M1diff}	<i>f</i> _{Magg}	<i>f</i> _{Mfree}	τ_{E0} ns	<i>f</i> _{E1diff}	<i>f</i> _{Eagg}	<i>f</i> _{EE0}	χ^2
12.5	1.35	6.7	0.05	0.87	0.08	39	0.01	0.22	0.76	1.12
5.0	1.43	6.7	0.05	0.86	0.09	39	0.01	0.22	0.77	1.14
1.3	1.30	7.0	0.05	0.88	0.08	39	0.01	0.24	0.75	1.11

(B) PEO(5K)-Py₂ (*C_P* > *C^F*)

<i>C_P</i> μM	<i>k</i> ₁₁ × 10 ⁷ s ⁻¹	<i>k</i> ₁₂ × 10 ⁷ s ⁻¹	<i>k</i> ₂ × 10 ⁷ s ⁻¹	<i>f</i> _{M1diff}	<i>f</i> _{M2diff}	<i>f</i> _{Magg}	τ_{E0} ns	<i>f</i> _{E1diff}	<i>f</i> _{E2diff}	<i>f</i> _{EE0}	<i>f</i> _{Eagg}	χ^2
220	0.23	0.90	8.7	0.18	0.62	0.20	51	0.08	0.27	0.57	0.08	1.08
165	0.14	0.87	7.5	0.14	0.66	0.20	48	0.07	0.32	0.52	0.10	1.08
92	0.10	0.85	7.2	0.14	0.66	0.20	50	0.07	0.33	0.50	0.10	0.99
73	0.07	0.84	8.5	0.13	0.69	0.18	48	0.07	0.37	0.45	0.11	1.02
46	0.06	0.84	7.3	0.14	0.67	0.19	48	0.08	0.39	0.42	0.11	1.13

(C) PEO(5K)-Py₂ (*C_P* < *C^F*)

<i>C_P</i> μM	<i>k</i> ₁₁ × 10 ⁷ s ⁻¹	<i>k</i> ₂ × 10 ⁷ s ⁻¹	<i>f</i> _{M1diff}	<i>f</i> _{Magg}	<i>f</i> _{Mfree}	τ_{E0} ns	<i>f</i> _{E1diff}	<i>f</i> _{Eagg}	<i>f</i> _{EE0}	χ^2
18	0.83	6.9	0.69	0.21	0.10	46	0.44	0.13	0.42	1.18
9.2	0.84	6.8	0.68	0.21	0.10	48	0.42	0.13	0.45	1.11
3.7	0.83	7.1	0.67	0.22	0.11	49	0.42	0.14	0.44	1.18
1.3	0.83	6.8	0.70	0.20	0.10	48	0.42	0.12	0.45	1.18

(D) PEO(10K)-Py₂

C_P μM	k_{diff} $\times 10^7 \text{ s}^{-1}$	k_2 $\times 10^7 \text{ s}^{-1}$	f_{Mdiff}	f_{Magg}	f_{Mfree}	τ_{E0} ns	f_{Ediff}	f_{Eagg}	f_{EE0}	χ^2
1338	0.90	6.5	0.72	0.28	0.00	54	0.14	0.05	0.81	1.03
621	0.54	7.3	0.88	0.10	0.01	44	0.44	0.05	0.50	1.16
382	0.35	7.2	0.88	0.11	0.01	43	0.53	0.06	0.40	1.11
191	0.26	7.8	0.87	0.07	0.05	45	0.71	0.06	0.23	1.20
96	0.19	6.6	0.86	0.05	0.09	46	0.78	0.05	0.18	1.29
67	0.17	7.6	0.85	0.04	0.11	46	0.82	0.04	0.14	1.18
48	0.15	7.8	0.90	0.04	0.06	45	0.81	0.03	0.16	1.17
24	0.15	7.8	0.80	0.03	0.16	45	0.85	0.03	0.12	1.11
9.6	0.13	6.8	0.84	0.03	0.13	46	0.85	0.03	0.11	1.07
4.8	0.13	6.7	0.82	0.03	0.14	48	0.85	0.03	0.11	1.04
1.3	0.13	7.5	0.85	0.03	0.12	47	0.85	0.03	0.11	1.08

(E) PEO(16.5K)-Py₂

C_P μM	k_{diff} $\times 10^7 \text{ s}^{-1}$	k_2 $\times 10^7 \text{ s}^{-1}$	f_{Mdiff}	f_{Magg}	f_{Mfree}	τ_{E0} ns	f_{Ediff}	f_{Eagg}	f_{EE0}	χ^2
1000	0.47	6.5	0.87	0.10	0.02	45	0.51	0.06	0.44	1.05
500	0.30	7.8	0.87	0.08	0.04	44	0.60	0.06	0.34	1.06
300	0.22	7.5	0.85	0.06	0.09	48	0.73	0.05	0.22	1.12
100	0.14	7.4	0.90	0.03	0.07	45	0.82	0.02	0.15	1.12
80	0.10	7.9	0.96	0.02	0.01	47	0.85	0.02	0.13	1.14

Table SI.4.2: Molar fractions obtained from the global SM analysis of the pyrene monomer and excimer fluorescence decays acquired with PEO(*X*)-Py₂ aqueous solution at different C_P . τ_M is fixed to 154 ns in the analysis.

(A) PEO(2K)-Py₂ ($f_{diff2} = 0$)

C_P μM	f_{diff1}	f_{agg}	f_{E0}	f_{free}	f_{diff}^{SM}	f_{agg}^{SM}	f_{free}^{SM}
12.5	0.01	0.22	0.75	0.02	0.01	0.97	0.02
5.0	0.01	0.21	0.75	0.02	0.01	0.96	0.02
1.3	0.01	0.24	0.73	0.02	0.01	0.97	0.02

(B) PEO(5K)-Py₂ ($C_P > C^F, f_{free} = 0$)

C_P μM	f_{diff1}	f_{diff2}	f_{agg}	f_{E0}	f_{diff}^{SM}	f_{agg}^{SM}	f_{free}^{SM}
220	0.08	0.27	0.08	0.57	0.35	0.65	0.00
165	0.07	0.32	0.10	0.52	0.39	0.62	0.00
92	0.07	0.33	0.10	0.50	0.40	0.60	0.00
73	0.07	0.37	0.11	0.45	0.44	0.56	0.00
46	0.08	0.39	0.11	0.42	0.48	0.53	0.00

(C) PEO(5K)-Py₂ ($C_P < C^F, f_{diff2} = 0$)

C_P μM	f_{diff1}	f_{agg}	f_{E0}	f_{free}	f_{diff}^{SM}	f_{agg}^{SM}	f_{free}^{SM}
18	0.41	0.13	0.40	0.06	0.41	0.53	0.06
9.2	0.39	0.12	0.42	0.06	0.39	0.54	0.06
3.7	0.40	0.13	0.41	0.06	0.40	0.54	0.06
1.3	0.40	0.12	0.43	0.06	0.40	0.54	0.06

(D) PEO(10K)-Py₂

C_P μM	f_{diff}	f_{agg}	f_{E0}	f_{free}	f_{diff}^{SM}	f_{agg}^{SM}	f_{free}^{SM}
1338	0.14	0.05	0.81	0.00	0.14	0.86	0.00
621	0.44	0.05	0.50	0.01	0.44	0.55	0.01
382	0.53	0.06	0.40	0.01	0.53	0.46	0.01
191	0.68	0.06	0.22	0.04	0.68	0.27	0.04
96	0.71	0.04	0.16	0.08	0.71	0.20	0.08
67	0.74	0.04	0.13	0.09	0.74	0.16	0.09
48	0.76	0.03	0.15	0.05	0.76	0.18	0.05
24	0.72	0.03	0.10	0.15	0.72	0.13	0.15
9.6	0.76	0.03	0.10	0.12	0.76	0.13	0.12
4.8	0.74	0.03	0.10	0.13	0.74	0.13	0.13
1.3	0.76	0.03	0.10	0.11	0.76	0.13	0.11

(E) PEO(16.5K)-Py₂

C_P μM	f_{diff}	f_{agg}	f_{E0}	f_{free}	f_{diff}^{SM}	f_{agg}^{SM}	f_{free}^{SM}
1000	0.50	0.06	0.44	0.01	0.50	0.49	0.01
500	0.59	0.06	0.33	0.02	0.59	0.39	0.02
300	0.68	0.04	0.20	0.07	0.68	0.25	0.07
100	0.77	0.02	0.14	0.06	0.77	0.16	0.06
80	0.84	0.02	0.13	0.01	0.84	0.14	0.01

Chapter 5 Supporting Information

Table SI.5.1A: Parameters retrieved from the global MF analysis of the pyrene monomer and excimer fluorescence decays acquired with a 1.25×10^{-6} M PEO(2K)-Py₂ solution as a function of SDS concentration.

[SDS] mM	Monomer						Excimer			χ^2
	τ_1 ns	a_1	τ_2 ns	a_2	τ_M ns	f_{Mfree}	f_{Ediff}	τ_{E0} ns	f_{EE0}	
50.00	36.6	0.15	86.7	0.79	155	0.06	0.94	48	0.06	1.13
30.00	29.4	0.11	79.1	0.81	155	0.08	0.94	46	0.06	1.04
20.00	35.1	0.12	86.1	0.82	155	0.07	0.94	46	0.06	1.06
10.00	32.9	0.15	76.8	0.78	155	0.07	0.93	45	0.07	1.20
8.00	31.2	0.27	73.7	0.67	155	0.06	0.91	46	0.09	1.19
7.50	25.2	0.39	65.6	0.56	155	0.05	0.90	45	0.10	1.01
6.50	21.2	0.59	50.0	0.39	155	0.02	0.86	44	0.14	1.16
5.00	11.1	0.76	27.5	0.22	155	0.02	0.75	40	0.24	1.09
4.50	8.4	0.75	23.4	0.21	155	0.04	0.77	44	0.23	1.19
4.00	6.3	0.83	21.7	0.10	155	0.07	0.67	44	0.31	1.22
3.00	4.8	0.77	33.5	0.12	155	0.10	0.57	43	0.43	1.20
2.00	7.2	0.68	33.3	0.14	155	0.17	0.32	40	0.67	1.22
0.90	8.9	0.68	33.4	0.15	155	0.17	0.27	38	0.73	1.14
0.20	8.4	0.61	37.1	0.19	155	0.20	0.22	42	0.78	1.29
0.05	8.1	0.62	35.8	0.20	155	0.18	0.25	41	0.75	1.10
0.01	8.2	0.60	32.4	0.22	155	0.17	0.23	38	0.77	1.22

Table SI.5.1B: Parameters retrieved from the global MF analysis of the pyrene monomer and excimer fluorescence decays acquired with a 1.25×10^{-6} M PEO(5K)-Py₂ solution as a function of SDS concentration.

[SDS] mM	Monomer						Excimer				χ^2
	τ_1 ns	a_1	τ_2 ns	a_2	τ_M ns	f_{Mfree}	f_{Ediff}	τ_{E0} ns	f_{EE0}		
20.00	24.3	0.13	77.8	0.77	155	0.10	0.94	50	0.06	1.09	
10.00	27.2	0.15	78.5	0.76	155	0.09	0.95	49	0.05	1.08	
8.00	27.5	0.16	78.5	0.75	155	0.08	0.94	49	0.06	1.13	
7.50	23.7	0.19	73.7	0.73	155	0.08	0.93	50	0.07	1.10	
6.00	23.7	0.26	64.3	0.66	155	0.07	0.91	47	0.09	1.20	
5.00	18.8	0.31	49.6	0.62	155	0.07	0.90	46	0.09	1.04	
4.80	18.3	0.34	45.1	0.58	155	0.08	0.89	46	0.11	1.04	
4.50	14.6	0.40	38.8	0.52	155	0.08	0.87	44	0.13	1.12	
4.00	12.4	0.52	37.3	0.38	155	0.10	0.82	43	0.18	1.22	
3.50	11.7	0.56	45.8	0.32	155	0.12	0.75	42	0.25	1.26	
2.50	10.8	0.41	58.1	0.48	155	0.11	0.71	48	0.30	1.24	
2.00	9.9	0.30	63.9	0.60	155	0.10	0.60	43	0.40	1.24	
1.50	10.5	0.23	65.1	0.67	155	0.10	0.53	42	0.47	1.19	
0.50	28.2	0.19	71.9	0.71	155	0.10	0.51	50	0.48	1.07	
0.05	28.8	0.19	71.3	0.72	155	0.10	0.54	48	0.46	1.06	
0.01	31.7	0.21	72.0	0.69	155	0.10	0.53	49	0.47	1.09	

Table SI.5.1C: Parameters retrieved from the global MF analysis of the pyrene monomer and excimer fluorescence decays acquired with a 1.25×10^{-6} M PEO(10K)-Py₂ solution as a function of SDS concentration.

[SDS] mM	Monomer						Excimer				χ^2
	τ_1 ns	a_1	τ_2 ns	a_2	τ_M ns	f_{Mfree}	f_{Ediff}	τ_{E0} ns	f_{EE0}		
15.0	38.7	0.11	117.3	0.12	165	0.77	0.77	71	0.23	1.03	
10.0	40.0	0.12	122.3	0.12	165	0.76	0.77	70	0.23	1.03	
8.0	39.4	0.11	116.7	0.12	165	0.75	0.76	73	0.24	0.99	
7.5	36.2	0.14	118.7	0.10	165	0.76	0.74	78	0.26	1.10	
7.0	30.4	0.25	82.5	0.27	155	0.48	0.88	67	0.12	1.25	
6.5	25.0	0.23	81.4	0.37	155	0.39	0.89	60	0.11	1.16	
5.8	23.9	0.32	66.4	0.48	155	0.20	0.91	49	0.10	1.09	
5.0	18.9	0.29	56.4	0.58	155	0.13	0.90	50	0.10	1.14	
4.0	48.9	0.44	21.3	0.41	155	0.15	0.87	47	0.13	1.23	
3.5	21.7	0.53	56.9	0.28	155	0.20	0.86	45	0.14	1.26	
3.3	28.0	0.54	95.5	0.20	155	0.26	0.80	45	0.20	1.11	
2.4	16.3	0.14	123.8	0.65	155	0.21	0.84	42	0.16	1.26	
1.0	28.5	0.12	127.6	0.74	155	0.15	0.81	45	0.19	1.02	
0.5	15.0	0.02	117.9	0.87	155	0.11	0.82	46	0.18	1.08	
0.2	22.2	0.04	110.4	0.82	155	0.14	0.81	42	0.19	1.17	

Table SI.5.1D: Parameters retrieved from the global MF analysis of the pyrene monomer and excimer fluorescence decays acquired with a 1.25×10^{-6} M PEO(16.5K)-Py₂ solution as a function of SDS concentration.

[SDS] mM	Monomer						Excimer				χ^2
	τ_1 ns	a_1	τ_2 ns	a_2	τ_M ns	f_{Mfree}	f_{Ediff}	τ_{E0} ns	f_{EE0}		
10.0	33.5	0.08	157.5	0.09	165	0.82	0.78	88	0.22	1.05	
8.0	34.6	0.08	157.7	0.10	165	0.82	0.77	88	0.23	1.06	
7.5	26.8	0.14	93.6	0.37	165	0.49	0.80	44	0.20	1.04	
6.5	30.5	0.19	83.2	0.42	165	0.39	0.91	59	0.09	1.12	
5.8	31.0	0.17	60.1	0.61	155	0.22	0.91	50	0.09	1.01	
5.0	22.8	0.22	59.7	0.66	155	0.12	0.91	51	0.09	0.96	
4.5	25.7	0.30	50.5	0.55	155	0.15	0.90	49	0.10	1.19	
4.0	25.6	0.47	68.3	0.31	155	0.22	0.81	45	0.19	1.21	
3.5	22.6	0.34	51.9	0.37	155	0.29	0.87	49	0.13	1.18	
3.2	24.7	0.31	97.6	0.23	155	0.46	0.81	45	0.19	1.14	
3.0	26.2	0.19	113.1	0.29	155	0.52	0.77	45	0.23	1.21	

Table SI.5.2A: Fractions of all pyrene species and average rate constant of excimer formation determined by the global analysis of the decays acquired with a 1.25×10^{-6} M PEO(2K)-Py₂ solution as a function of SDS concentration.

[SDS] mM	f_{diff}	f_{free}	f_{E0}	$\langle k \rangle$ $\times 10^7 \text{ s}^{-1}$
50.00	0.88	0.06	0.06	0.76
30.00	0.87	0.08	0.05	0.86
20.00	0.89	0.05	0.06	0.73
10.00	0.87	0.07	0.06	0.93
8.00	0.86	0.05	0.09	1.24
7.50	0.86	0.05	0.10	1.88
6.50	0.84	0.02	0.14	3.00
5.00	0.74	0.02	0.24	7.17
4.50	0.75	0.03	0.22	9.57
4.00	0.65	0.05	0.30	14.1
3.00	0.54	0.06	0.40	17.9
2.00	0.30	0.06	0.63	11.3
0.90	0.26	0.05	0.69	9.17
0.20	0.21	0.05	0.74	9.00
0.05	0.24	0.05	0.71	9.35
0.01	0.22	0.05	0.73	9.11

Table SI.5.2B: Fractions of all pyrene species and average rate constant of excimer formation determined by the global analysis of the decays acquired with a 1.25×10^{-6} M PEO(5K)-Py₂ solution as a function of SDS concentration.

[SDS] mM	f_{diff}	f_{free}	f_{E0}	$\langle k \rangle$ $\times 10^7 \text{ s}^{-1}$
20.00	0.86	0.09	0.05	1.04
10.00	0.86	0.09	0.05	1.02
8.00	0.86	0.08	0.06	1.05
7.50	0.86	0.08	0.06	1.30
6.00	0.85	0.07	0.08	1.67
5.00	0.84	0.07	0.09	2.48
4.80	0.82	0.07	0.10	2.79
4.50	0.81	0.07	0.12	3.80
4.00	0.75	0.08	0.17	5.13
3.50	0.68	0.09	0.22	5.59
2.50	0.65	0.08	0.27	4.56
2.00	0.56	0.06	0.37	3.80
1.50	0.50	0.05	0.45	2.93
0.50	0.49	0.05	0.46	1.21
0.05	0.51	0.05	0.44	1.18
0.01	0.50	0.05	0.45	1.16

Table SI.5.2C: Fractions of all pyrene species and average rate constant of excimer formation determined by the global analysis of the decays acquired with a 1.25×10^{-6} M PEO(10K)-Py₂ solution as a function of SDS concentration.

[SDS] mM	f_{diff}	f_{free}	f_{E0}	$\langle k \rangle$ $\times 10^7 \text{ s}^{-1}$
15.0	0.22	0.72	0.07	1.05
10.0	0.22	0.71	0.07	0.99
8.0	0.23	0.71	0.07	1.03
7.5	0.22	0.70	0.08	1.29
7.0	0.48	0.45	0.07	1.57
6.5	0.57	0.36	0.07	1.65
5.8	0.74	0.18	0.08	1.94
5.0	0.79	0.12	0.09	2.32
4.0	0.74	0.14	0.11	2.69
3.5	0.71	0.17	0.12	2.98
3.3	0.62	0.22	0.16	2.24
2.4	0.69	0.18	0.13	1.11
1.0	0.71	0.12	0.17	0.52
0.5	0.74	0.09	0.16	0.32
0.2	0.71	0.12	0.17	0.44

Table SI.5.2D: Fractions of all pyrene species and average rate constant of excimer formation determined by the global analysis of the decays acquired with a 1.25×10^{-6} M PEO(16.5K)-Py₂ solution as a function of SDS concentration.

[SDS] mM	f_{diff}	f_{free}	f_{E0}	$\langle k \rangle$ $\times 10^7 \text{ s}^{-1}$
10.0	0.17	0.78	0.05	1.08
8.0	0.17	0.78	0.05	1.01
7.5	0.45	0.44	0.11	1.14
6.5	0.57	0.37	0.06	1.21
5.8	0.72	0.21	0.07	1.35
5.0	0.81	0.11	0.08	1.71
4.5	0.78	0.14	0.09	2.00
4.0	0.66	0.19	0.15	2.29
3.5	0.64	0.26	0.09	2.46
3.2	0.48	0.41	0.11	3.13
3.0	0.42	0.46	0.13	1.39

Chapter 6 Supporting Information

Table SI.6.1A: Parameters retrieved from the global MF analysis of the pyrene monomer and excimer fluorescence decays acquired with an 8 g/L Py-HASE12 in 0.01 M Na₂CO₃, pH 9 solution.

[SDS] mM	Monomer						Excimer							χ^2
	τ_1 ns	a_1	τ_2 ns	a_2	τ_M ns	f_{Mfree}	f_{Ediff}	τ_{E0} ns	f_{EE0}	τ_{ED} ns	f_{ED}	τ_{ES} ns	f_{ES}	
50.0	35.4	0.16	99.0	0.23	165	0.61	0.54	61	0.09	-	-	3.5	0.36	1.14
20.0	35.3	0.19	95.6	0.25	165	0.56	0.60	57	0.10	-	-	3.5	0.29	1.11
10.0	31.2	0.23	87.8	0.24	165	0.54	0.63	56	0.12	-	-	3.5	0.24	1.11
7.6	33.1	0.24	84.4	0.30	165	0.46	0.70	55	0.12	-	-	3.5	0.17	1.14
5.1	32.7	0.29	80.6	0.31	165	0.40	0.82	53	0.16	92	0.01	-	-	1.15
3.5	29.0	0.30	70.2	0.28	165	0.42	0.79	52	0.20	150	0.01	-	-	1.04
2.5	22.7	0.24	56.6	0.29	165	0.47	0.77	48	0.17	107	0.05	-	-	1.04
2.0	22.2	0.25	58.9	0.17	165	0.58	0.67	47	0.30	114	0.02	-	-	1.15
1.6	17.1	0.18	73.8	0.11	165	0.71	0.47	45	0.49	155	0.03	-	-	1.12
1.2	15.1	0.10	45.0	0.18	165	0.72	0.57	41	0.38	127	0.05	-	-	1.14
0.8	18.6	0.18	86.7	0.11	165	0.70	0.48	46	0.49	162	0.02	-	-	1.06
0.6	18.8	0.12	70.7	0.12	165	0.76	0.28	47	0.64	141	0.08	-	-	1.07
0.4	14.7	0.10	71.7	0.14	165	0.75	0.24	49	0.64	143	0.12	-	-	1.13
0.2	15.9	0.10	84.0	0.17	165	0.73	0.23	50	0.66	145	0.10	-	-	1.09
0.1	16.3	0.11	85.4	0.16	165	0.73	0.24	49	0.65	143	0.11	-	-	0.96

Table SI.6.1B: Parameters retrieved from the global FBM analysis of the pyrene monomer and excimer fluorescence decays acquired with an 8 g/L Py-HASE12 in 0.01 M Na₂CO₃, pH 9 solution.

[SDS] mM	Monomer						Excimer							χ^2
	k_{ex} $\times 10^7 \text{ s}^{-1}$	f_{Mdiff}	k_{blob} $\times 10^7 \text{ s}^{-1}$	$\langle n \rangle$	τ_{M} ns	f_{Mfree}	f_{Ediff}	τ_{E0} ns	f_{EE0}	τ_{ED} ns	f_{ED}	τ_{ES} ns	f_{ES}	
50.0	0.55	0.39	1.1	1.16	165	0.61	0.53	61	0.08	-	-	3.5	0.39	1.15
20.0	0.64	0.44	1.0	1.23	165	0.56	0.62	56	0.09	-	-	3.5	0.29	1.14
10.0	0.46	0.47	1.1	1.55	165	0.53	0.63	57	0.11	-	-	3.5	0.26	1.10
7.6	0.54	0.55	0.9	1.64	165	0.45	0.70	54	0.11	-	-	3.5	0.18	1.11
5.1	0.49	0.60	0.8	2.03	165	0.40	0.83	52	0.12	88	0.04	-	-	1.15
3.5	0.53	0.58	0.8	2.39	165	0.42	0.80	51	0.19	158	0.01	-	-	1.05
2.5	0.89	0.52	1.0	2.37	165	0.47	0.78	48	0.15	103	0.06	-	-	1.04
2.0	0.46	0.42	1.0	2.74	165	0.57	0.67	47	0.29	105	0.03	-	-	1.15
1.6	0.53	0.29	2.6	1.59	165	0.71	0.49	45	0.47	151	0.03	-	-	1.12
1.2	1.35	0.29	1.8	1.89	165	0.71	0.57	43	0.39	131	0.04	-	-	1.13
0.8	0.40	0.30	2.4	1.43	165	0.70	0.51	45	0.46	155	0.02	-	-	1.06
0.6	0.86	0.25	2.7	1.25	165	0.75	0.28	48	0.64	142	0.08	-	-	1.06
0.4	1.16	0.26	4.2	0.89	165	0.74	0.24	49	0.64	144	0.12	-	-	1.13
0.2	0.86	0.28	3.8	0.81	165	0.72	0.25	50	0.64	143	0.11	-	-	0.96
0.1	0.98	0.28	4.4	0.75	165	0.72	0.23	51	0.66	146	0.10	-	-	1.09

Table SI.6.1C: Parameters retrieved from the global MF analysis of the pyrene monomer and excimer fluorescence decays acquired with a 57 g/L Py-HASE12 in 0.01 M Na₂CO₃, pH 9 solution.

[SDS] mM	Monomer						Excimer							χ^2
	τ_1 ns	a_1	τ_2 ns	a_2	τ_M ns	f_{Mfree}	f_{Ediff}	τ_{E0} ns	f_{EE0}	τ_{ED} ns	f_{ED}	τ_{ES} ns	f_{ES}	
50.0	35.2	0.14	93.7	0.23	165	0.62	0.55	60	0.08	-	-	3.5	0.36	1.16
25.0	35.1	0.13	87.0	0.29	165	0.59	0.63	54	0.08	-	-	3.5	0.29	1.09
20.0	35.3	0.24	93.6	0.22	165	0.54	0.59	54	0.10	-	-	3.5	0.32	1.04
15.0	32.4	0.24	84.8	0.31	165	0.45	0.70	56	0.12	-	-	3.5	0.18	1.19
11.1	29.5	0.36	82.5	0.24	165	0.40	0.80	55	0.13	-	-	3.5	0.07	1.09
10.0	25.5	0.33	72.7	0.21	165	0.45	0.72	48	0.20	-	-	3.5	0.07	1.11
8.5	22.3	0.26	59.9	0.16	165	0.55	0.67	48	0.31	117	0.03	-	-	1.15
5.0	22.0	0.13	85.4	0.12	165	0.75	0.41	43	0.55	139	0.05	-	-	1.10
3.5	18.4	0.13	82.1	0.13	165	0.74	0.39	44	0.56	145	0.05	-	-	1.08
2.0	19.2	0.13	75.0	0.12	165	0.74	0.40	43	0.55	145	0.05	-	-	0.98
1.0	25.8	0.11	88.1	0.14	165	0.75	0.25	49	0.60	135	0.15	-	-	1.10
0.8	25.3	0.12	95.9	0.16	165	0.72	0.24	48	0.61	135	0.15	-	-	1.18
0.5	34.9	0.13	113.6	0.17	165	0.70	0.22	48	0.64	135	0.14	-	-	1.03
0.3	16.5	0.11	91.9	0.19	165	0.70	0.20	50	0.67	141	0.13	-	-	1.04
0.1	15.4	0.11	90.2	0.19	165	0.70	0.15	51	0.71	141	0.14	-	-	1.01

Table SI.6.1D: Parameters retrieved from the global FBM analysis of the pyrene monomer and excimer fluorescence decays acquired with a 57 g/L Py-HASE12 in 0.01 M Na₂CO₃, pH 9 solution.

[SDS] mM	Monomer						Excimer							χ^2
	k_{ex} $\times 10^7 \text{ s}^{-1}$	f_{Mdiff}	k_{blob} $\times 10^7 \text{ s}^{-1}$	$\langle n \rangle$	τ_{M} ns	f_{Mfree}	f_{Ediff}	τ_{E0} ns	f_{EE0}	τ_{ED} ns	f_{ED}	τ_{ES} ns	f_{ES}	
50.0	0.84	0.38	0.9	1.0	165	0.62	0.55	59	0.07	-	-	3.5	0.38	1.21
25.0	0.85	0.42	0.9	1.3	165	0.58	0.63	54	0.08	-	-	3.5	0.29	1.10
20.0	0.32	0.47	0.9	1.5	165	0.53	0.59	54	0.09	-	-	3.5	0.32	1.04
15.0	0.57	0.55	0.9	1.7	165	0.45	0.69	56	0.11	-	-	3.5	0.20	1.19
11.1	0.33	0.61	1.0	2.0	165	0.40	0.81	55	0.13	-	-	3.5	0.07	1.06
10.0	0.44	0.55	1.1	2.2	165	0.45	0.72	48	0.18	-	-	3.5	0.10	1.10
8.5	0.44	0.42	1.1	2.7	165	0.57	0.67	48	0.29	107	0.03	-	-	1.15
5.0	0.50	0.25	1.9	1.3	165	0.75	0.42	43	0.53	136	0.05	-	-	1.11
3.5	0.61	0.26	2.6	1.2	165	0.74	0.40	45	0.55	142	0.05	-	-	1.08
2.0	0.66	0.26	2.3	1.3	165	0.74	0.41	44	0.54	143	0.05	-	-	0.99
1.0	0.29	0.25	0.9	1.5	165	0.75	0.26	45	0.60	133	0.14	-	-	1.11
0.8	0.39	0.28	1.4	1.1	165	0.72	0.24	46	0.61	133	0.15	-	-	1.18
0.5	0.28	0.32	1.2	1.0	165	0.68	0.23	48	0.63	135	0.14	-	-	1.03
0.3	0.85	0.31	4.3	0.8	165	0.70	0.19	50	0.67	141	0.14	-	-	1.04
0.1	0.90	0.30	4.0	0.7	165	0.70	0.15	51	0.71	143	0.14	-	-	1.01

Table SI.6.2A: Fractions of all pyrene species determined by the global analysis of the decays acquired with an 8 g/L Py-HASE12 in 0.01 M Na₂CO₃, pH 9 solution.

[SDS] mM	MF					FBM				
	f_{diff}	f_{free}	f_{E0}	f_{D}	f_{agg}	f_{diff}	f_{free}	f_{E0}	f_{D}	f_{agg}
50.0	0.36	0.57	0.06	-	0.06	0.37	0.58	0.06	-	0.06
20.0	0.41	0.52	0.07	-	0.07	0.41	0.53	0.06	-	0.06
10.0	0.42	0.49	0.08	-	0.08	0.43	0.49	0.08	-	0.08
7.6	0.50	0.42	0.09	-	0.09	0.50	0.42	0.08	-	0.08
5.1	0.53	0.35	0.10	0.01	0.11	0.53	0.36	0.08	0.03	0.11
3.5	0.50	0.36	0.13	0.00	0.13	0.50	0.37	0.12	0.01	0.13
2.5	0.45	0.41	0.10	0.03	0.13	0.46	0.41	0.09	0.03	0.13
2.0	0.35	0.48	0.16	0.01	0.17	0.35	0.48	0.15	0.02	0.17
1.6	0.22	0.54	0.23	0.01	0.24	0.22	0.55	0.21	0.01	0.23
1.2	0.23	0.59	0.15	0.02	0.17	0.24	0.58	0.16	0.02	0.18
0.8	0.23	0.53	0.23	0.01	0.24	0.23	0.54	0.21	0.01	0.23
0.6	0.15	0.47	0.34	0.04	0.38	0.15	0.46	0.35	0.04	0.39
0.4	0.14	0.42	0.37	0.07	0.44	0.14	0.41	0.37	0.07	0.44
0.2	0.14	0.38	0.41	0.07	0.47	0.15	0.39	0.39	0.07	0.46
0.1	0.15	0.39	0.39	0.07	0.46	0.14	0.38	0.41	0.07	0.48

Table SI.6.2B: Fractions of all pyrene species determined by the global analysis of the decays acquired with a 57 g/L Py-HASE12 in 0.01 M Na₂CO₃, pH 9 solution.

[SDS] mM	MF					FBM				
	f_{diff}	f_{free}	f_{E0}	f_{D}	f_{agg}	f_{diff}	f_{free}	f_{E0}	f_{D}	f_{agg}
50.0	0.36	0.59	0.05	-	0.05	0.36	0.59	0.04	-	0.04
25.0	0.39	0.56	0.05	-	0.05	0.39	0.56	0.05	-	0.05
20.0	0.43	0.50	0.07	-	0.07	0.44	0.49	0.07	-	0.07
15.0	0.50	0.41	0.08	-	0.08	0.51	0.41	0.08	-	0.08
11.1	0.54	0.37	0.09	-	0.09	0.55	0.36	0.09	-	0.09
10.0	0.47	0.39	0.13	-	0.13	0.49	0.39	0.12	-	0.12
8.5	0.37	0.45	0.17	0.01	0.18	0.35	0.48	0.15	0.02	0.17
5.0	0.18	0.55	0.24	0.02	0.27	0.19	0.56	0.23	0.02	0.26
3.5	0.18	0.53	0.26	0.02	0.29	0.19	0.53	0.26	0.02	0.28
2.0	0.19	0.54	0.25	0.02	0.27	0.19	0.53	0.26	0.02	0.28
1.0	0.14	0.43	0.34	0.08	0.42	0.15	0.43	0.34	0.08	0.42
0.8	0.15	0.38	0.38	0.09	0.47	0.15	0.38	0.38	0.09	0.47
0.5	0.14	0.33	0.43	0.10	0.52	0.15	0.33	0.42	0.09	0.51
0.3	0.13	0.32	0.46	0.09	0.55	0.13	0.30	0.47	0.10	0.56
0.1	0.11	0.26	0.53	0.10	0.63	0.11	0.26	0.53	0.10	0.63

References

Chapter 1

1. *Polymers in Aqueous Media: Performance through Association*, Glass, J. E., Ed. Advances in Chemistry Series 223; American Chemical Society: Washington, DC, 1989.
2. *Hydrophilic Polymers: Performance with Environmental Acceptance*, Glass, J. E., Ed. Advances in Chemistry Series 248; American Chemical Society: Washington, DC, 1996.
3. *Associative Polymers in Aqueous Media*, Glass, J. E., Ed. Advances in Chemistry Series 765; American Chemical Society: Washington, DC, 2000.
4. *Polymers as Rheology Modifiers*, Schulz, D.N.; Glass, J.E., Ed. ACS Symposium Series 462; American Chemical Society: Washington, DC, 1991.
5. Kwak, J. C. *Polymer-Surfactant Systems*; Surfactant Science Series 77; Marcel Decker; New York, 1998.
6. Winnik, M. A.; Yekta, A. *Curr. Opin. Colloid Interface Sci.* **1997**, *2*, 424-436.
7. El-Sherbiny, S.; Xiao, H. *Ind. Eng. Chem. Res.* **2005**, *44*, 9875-9883.
8. Abdala, A. A.; Olesen, K.; Khan, S. A. *J. Rheol.* **2003**, *47*, 497-511.
9. Cantor, C.R.; Schimmel, P.R. *Biophysical Chemistry Part I The Conformation of Biological Macromolecules*; W.H. Freeman and Company: New York, 1980, pp 279-288.
10. Tripathi, A.; Tam, K. C.; McKinley, G. H. *Macromolecules* **2006**, *39*, 1981-1999.
11. Volpert, E.; Selb, J.; Candau, F. *Macromolecules* **1996**, *29*, 1452-1463.
12. Maestro, A.; González, C.; Gutiérrez, J. M. *J. Rheol.* **2002**, *46*, 127-143.
13. Kim, M.; Sim, J. -H.; Sohn, D. *Macromolecules*, **2003**, *36*, 9986-9993.
14. Tam, K. C.; Jenkins, R.D.; Winnik, M. A.; Bassett, D. R. *Macromolecules* **1998**, *31*, 4149-4159.
15. Dai, S.; Tam, K. C.; Jenkins, R. D.; Bassett, D. R. *Macromolecules* **2000**, *33*, 7021-7028.
16. Yoshimitsu, U.; Macdonald, P. M. *Macromolecules* **1996**, *29*, 63-69.

17. Dai, S.; Tam, K. C.; Jenkins, R. D. *J. Phys. Chem. B* **2001**, *105*, 10189-10196.
18. Dai, S.; Tam, K. C.; Wyn-Jones, E.; Jenkins, R. D. *J. Phys. Chem. B* **2004**, *108*, 4979-4988.
19. Yekta, A.; Xu, B.; Duhamel, J.; Adiwidjaja, H.; Winnik, M. A. *Macromolecules* **1995**, *28*, 956-966.
20. Yekta, A.; Duhamel, J.; Adiwidjaja, H.; Brochard, P.; Winnik, M. A. *Langmuir* **1992**, *9*, 881-883.
21. Tanaka, F.; Edwards, S. F. *J. Non-Newtonian Fluid Mech.* **1992**, *43*, 247-271.
22. Yekta, A.; Duhamel, J.; Adiwidjaja, H.; Brochard, P.; Winnik, M. A. *Langmuir* **1993**, *9*, 881-883.
23. Xu, B.; Yekta, A.; Winnik, M. A.; Sadeghy-Dalivand, K.; James, D. F.; Jenkins, R. D.; Bassett, D. R. *Langmuir* **1997**, *13*, 6903-6911.
24. Xu, B.; Li, L.; Yekta, A.; Masoumi, Z.; Kanagalingam, S.; Winnik, M. A.; Zhang, K. W.; Macdonald, P. M.; Menchen, S. *Langmuir* **1997**, *13*, 2447-2456.
25. Annable, T.; Buscall, R.; Ettelaie, R.; Whittlestone, D. *J. Rheol.* **1993**, *37*, 695-726.
26. Annable, T.; Buscall, R.; Ettelaie, R. *Colloids Surf. A* **1996**, *112*, 97-116.
27. Ma, S. X.; Cooper, S. L. *Macromolecules* **2001**, *34*, 3294-3301.
28. Annable, T.; Buscall, R.; Ettelaie, R.; Shepherd, P.; Whittlestone, D. *Langmuir* **1994**, *10*, 1060-1070.
29. Prazeres, T. V. J.; Duhamel, J.; Olesen, K.; Shay, G. *J. Phys. Chem. B* **2005**, *109*, 17406-17416.
30. Tirtaatmadja, V.; Tam, K. C.; Jenkins, R. D. *Macromolecules* **1997**, *30*, 1426-1433.
31. Tirtaatmadja, V.; Tam, K. C.; Jenkins, R. D. *Macromolecules* **1997**, *30*, 3271-3282.
32. English, R. J.; Gulati, H. S.; Jenkins, R. D.; Khan, S. A. *J. Rheol.* **1997**, *41*, 427-444.
33. Zhao, G.; Chen, S. B. *J. Colloid. Interface Sci.* **2007**, *316*, 858-866.
34. Turro, N. J.; Yekta, A. *J. Am. Chem. Soc.* **1978**, *100*, 5951-5952.

35. *Interactions of Surfactants with Polymers and Proteins*, Goddard, E. O.; Ananthapadamanabham, K. P., Eds. CRC Press: Boca Raton, FL, 1993.
36. Thuresson, K.; Lindman, B.; Nyström, B. *J. Phys. Chem. B* **1997**, *101*, 6450-6459.
37. Nilsson, S.; Thuresson, K.; Hansson, P.; Lindman, B. *J. Phys. Chem. B* **1998**, *102*, 7099-7105.
38. Hu, Y.-Z.; Zhao, C.-L.; Winnik, M. A.; Sundararajan, P. R. *Langmuir* **1990**, *6*, 880-883.
39. Rufier, C.; Collet, A.; Viguier, M.; Oberdisse, J.; Mora, S. *Macromolecules* **2009**, *42*, 5226-5235.
40. Zhang, K.; Xu, B.; Winnik, M. A.; Macdonald, P. M. *J. Phys. Chem.* **1996**, *100*, 9834-9841.
41. Siu, H.; Duhamel, J. *Macromolecules* **2006**, *39*, 1144-1155.
42. Jiménez-Regalado, E.; Selb, J.; Candau, F. *Langmuir* **2000**, *16*, 8611-8621.
43. Dai, S.; Tam, K. C. *J. Phys. Chem. B* **2001**, *105*, 10759-10763.
44. Wang, G.; Olofsson, G. *J. Phys. Chem. B* **1998**, *102*, 9276-9283.
45. Bernazzani, L.; Borsacchi, S.; Catalano, D.; Gianni, P.; Mollica, V.; Vitelli, M.; Asaro, F.; Feruglio, L. *J. Phys. Chem. B* **2004**, *108*, 8960-8969.
46. Cooke, D. J.; Blondel, J. A. K.; Lu, J. R.; Thomas, R. K.; Wang, Y.; Han, B.; Yan, H.; Penfold, J. *Langmuir* **1998**, *14*, 1990-1995.
47. Cabane, B. *J. Phys. Chem.* **1977**, *81*, 1639-1645.
48. Brown, W.; Fundin, J.; Miguel, G. M. *Macromolecules* **1992**, *25*, 7192-7198.
49. Chari, K.; Kowalczyk, J.; Lal, J. *J. Phys. Chem. B* **2004**, *108*, 2857-2861.
50. Bernazzani, L.; Borsacchi, S.; Catalano, D.; Gianni, P.; Mollica, V.; Vitelli, M.; Asaro, F.; Feruglio, L. *J. Phys. Chem. B* **2004**, *108*, 8960-8969.
51. Cabane, B. *J. Phys. Chem.* **1977**, *81*, 1639-1645.
52. Gao, Z.; Wasylshen, R. E.; Kwak, J. C. T. *J. Phys. Chem.* **1991**, *95*, 462-467.
53. Rodenhiser, A. P.; Kwak, J. C. T. *Colloids Surf. A* **1999**, *150*, 191-206.

54. Lakowicz, J. R. *Principles of Fluorescence Spectroscopy*; Kluwer Academic/Plenum Publishers: New York, 1999.
55. Nakajima, A. *J. Lumin.* **1976**, *11*, 429-432.
56. Kalyanasundaram, K.; Thomas, J. K. *J. Am. Chem. Soc.* **1977**, *99*, 2039-2044.
57. Dong, D. C.; Winnik, M. A. *Can. J. Chem.* **1984**, *62*, 2560-2565.
58. Winnik, F. M. *Chem. Rev.* **1993**, *93*, 587-614.
59. Duhamel, J. *Molecular Interfacial Phenomena of Polymer and Biopolymers*; Chen, P., Ed.; Woodhead: New York, 2005.
60. Birks, J. B. *Photophysics of Aromatic Molecules*; Wiley: New York, 1970; pp 301.
61. Anghel, D. F.; Alderson, V.; Winnik, F. M.; Mizusaki, M.; Morishima, Y. *Polymer* **1998**, *39*, 3035-3044.
62. Zachariasse, K. A.; Vaz, W. L. C.; Sotomayor, C.; Kühnle, W. *Biochim. Biophys. Acta* **1982**, *688*, 323-332.
63. Winnik, M. A. *Acc. Chem. Res.* **1985**, *18*, 73-79.
64. Duhamel, J. *Acc. Chem. Res.* **2006**, *39*, 953-960.
65. Duhamel, J.; Kanagalingam, S.; O'Brien, T.; Ingratta, M. *J. Am. Chem. Soc.* **2003**, *125*, 12810-12822.
66. Picarra, S.; Duhamel, J.; Fedorov, A.; Martinho, J. M. G. *J. Phys. Chem. B* **2004**, *108*, 12009-12015.
67. Siu, H.; Duhamel, J. *J. Phys. Chem. B* **2005**, *109*, 1770-1780.
68. Siu, H.; Duhamel, J. *Macromolecules* **2004**, *37*, 9287-9289.
69. Siu, H.; Duhamel, J. *Macromolecules* **2005**, *38*, 7184-7186.
70. Prazeres, T. J. V.; Beingessner, R.; Duhamel, J.; Olesen, K.; Shay, G.; Bassett, D. R. *Macromolecules* **2001**, *34*, 7876-7884.

71. Char, K.; Frank, C. W.; Gast, A. P.; Tang, W. T. *Macromolecules* **1987**, *20*, 1833-1838.
72. Winnik, F. M. *Macromolecules* **1987**, *20*, 2745-2750.
73. Berlman, I. B. *Handbook of Fluorescence Spectra of Aromatic Molecules*; Academic Press Inc. 1965; p 173.
74. Eaton, D. F.; Smart, B. E. *J. Am. Chem. Soc.* **1990**, *112*, 2821-2823.
75. Ingratta, M.; Hollinger, J.; Duhamel, J. *J. Am. Chem. Soc.* **2008**, *130*, 9420-9428.
76. Reis e Sousa, A. T.; Castanheira, E. M. S.; Fedorov, A.; Martinho, J. M. G. *J. Phys. Chem. A* **1998**, *102*, 6406-6411.
77. Wilemski, G.; Fixman, M. *J. Chem. Phys.* **1974**, *60*, 866-877.
78. Wilemski, G.; Fixman, M. *J. Chem. Phys.* **1974**, *60*, 878-890.
79. Zachariasse, K.; Kühnle, W. *Z. Phys. Chem. Neue Fol.* **1976**, *101*, 267-276.
80. Cuniberti, C.; Perico, A. *Eur. Polym. J.* **1977**, *13*, 369-374.
81. Winnik, M. A.; Redpath, T.; Richards, D. H. *Macromolecules* **1980**, *13*, 328-335.
82. Kane, M. A.; Baker, G. A.; Pandey, S.; Maziarz III, E. P.; Hoth, D. C.; Bright, F. V. *J. Phys. Chem. B* **2000**, *104*, 8585-8591.
83. Kim, S. D.; Torkelson, J. M. *Macromolecules* **2002**, *35*, 5943-5952.
84. Boileau, S.; Méchin, F.; Martinho, J. M. G.; Winnik, M. A. *Macromolecules* **1989**, *22*, 215-220.
85. Piçarra, S.; Gomes, P. T.; Martinho, J. M. G. *Macromolecules* **2000**, *33*, 3947-3950.
86. Yip, J.; Duhamel, J.; Qiu, X. P.; Winnik, F. M. *Macromolecules* **2011**, *44*, 5363-5372.
87. Zachariasse, K. A.; Maçanita, A. L.; Kühnle, W. *J. Phys. Chem. B* **1990**, *103*, 9356-9365.
88. Maçanita, A. L.; Zachariasse, K. A. *J. Phys. Chem. A* **2011**, *115*, 3183-3195.
89. Zachariasse, K. A.; Duveneck, G.; Busse, R. *J. Am. Chem. Soc.* **1984**, *106*, 1045-1051.
90. Kanaya, T.; Goshiki, K.; Yamamoto, M.; Nishijima, Y. *J. Am. Chem. Soc.* **1982**, *104*, 3580-3587.

91. Anghel, D. F.; Toca-Herrera, J. L.; Winnik, F. M.; Rettig, W.; Klitzing, R. *Langmuir* **2002**, *18*, 5600-5606.
92. Seixas de Melo, J.; Costa, T.; da G. Miguel, M.; Lindman, B.; Schillen, K. *J. Phys. Chem. B* **2003**, *107*, 12605-12621.
93. Deo, P.; Deo, N.; Somasundaran, P.; Jockusch, S.; Turro, N. J. *J. Phys. Chem. B* **2005**, *109*, 20714-20718.
94. Kanagalingam, S.; Ngan, C. F.; Duhamel, J. *Macromolecules* **2002**, *35*, 8560-8570.
95. Kanagalingam, S.; Spartalis, J.; Cao, T.-C.; Duhamel, J. *Macromolecules* **2002**, *35*, 8571-8577.
96. Siu, H.; Duhamel, J. *J. Phys. Chem. B* **2008**, *112*, 15301-15312.
97. Winnik, M. A.; Bystryak, S. M.; Liu, Z. *Macromolecules* **1998**, *31*, 6855-6864.
98. Nishikawa, K.; Yekta, A.; Pham, H. H.; Winnik, M. A. *Langmuir* **1998**, *14*, 7119-7129.
99. Char, K.; Frank, C. W.; Gast, A. P. *Macromolecules* **1989**, *22*, 3177-3180.
100. Duhamel, J.; Yekta, A.; Hu, Y. Z.; Winnik, M. A. *Macromolecules* **1992**, *25*, 7024-7030.
101. Costa, T.; Seixas de Melo, J.; Burrows, H. D. *J. Phys. Chem. B* **2009**, *113*, 618-626.
102. Chen, S.; Duhamel, J.; Winnik, M. A. *J. Phys. Chem. B* **2011**, *115*, 3289-3302.
103. Birks, J. B.; Dyson, D. J.; Munro, I. H. *Proc. Roy. Soc. A* **1963**, *275*, 575-588.
104. Lee, S.; Duhamel, J. *Macromolecules* **1998**, *31*, 9193-9200.
105. Mathew, H.; Siu, H.; Duhamel, J. *Macromolecules* **1999**, *32*, 7100-7108.
106. Cuniberti, C.; Perico, A. *Prog. Polym. Sci.* **1984**, *10*, 271-316.
107. Yip, J.; Duhamel, J.; Bahun, G.; Adronov, A. *J. Phys. Chem. B* **2010**, *114*, 10254-10265.
108. Keyes-Baig, C.; Duhamel, J.; Wettig, S. *Langmuir* **2011**, *27*, 3361-3371.
109. Chen, S.; Duhamel, J.; Bahun, G. J.; Adronov, A. *J. Phys. Chem. B* **2011**, *115*, 9921-9929.
110. Duhamel, J. submitted to *Polymers*, **2012**, *4*, 211-239.

Chapter 2

1. Jacobson, H.; Stockmayer, W. H. *J. Chem. Phys.* **18**, 1600-1607 (1950); doi:10.1063/1.1747547.
2. Wilemski, G.; Fixman, M. *J. Chem. Phys.* **1974**, *60*, 866-877.
3. Wilemski, G.; Fixman, M. *J. Chem. Phys.* **1974**, *60*, 878-890.
4. Eaton, W.A.; Muñoz, V.; Hagen, S. J.; Jas, G. S.; Lapidus, L. J.; Henry, E. R.; Hofrichter, J. *Annu. Rev. Biophys. Biomol. Struct.* **2000**, *29*, 327-359.
5. Hagen, S. J.; Hofrichter, J.; Szabo, A.; Eaton, W. A. *Proc. Natl. Acad. Sci.* **1996**, *93*, 11615-11617.
6. McGimpsey, W. G.; Chen, L.; Carraway, R.; Samaniego, W. N. *J. Phys. Chem. A* **1999**, *103*, 6082-6090.
7. Möglich, A.; Krieger, F.; Kiefhaber, T. *J. Mol. Biol.* **2005**, *345*, 153-162.
8. Fierz, B.; Satzger, H.; Root, C.; Gich, P.; Zinth, W.; Kiefhaber, T. *Proc. Natl. Acad. Sci.* **2007**, *104*, 2163-2168.
9. Möglich, A.; Joder, K.; Kiefhaber, T. *Proc. Natl. Acad. Sci.* **2006**, *103*, 12394-12399.
10. Hudgins, R. R.; Huang, F.; Gramlich, G.; Nau, W. M. *J. Am. Chem. Soc.* **2002**, *124*, 556-564.
11. Huang, F.; Hudgins, R. R.; Nau, W. M. *J. Am. Chem. Soc.* **2004**, *126*, 16665-16675.
12. Roccatano, D.; Sahoo, H.; Zacharias, M.; Nau, W. M. *J. Phys. Chem. B* **2007**, *111*, 2639-2646.
13. Bieri, O.; Wirz, J.; Hellrung, B.; Schutkowski, M.; Drewello, M.; Kiefhaber, T. *Proc. Natl. Acad. Sci.* **1999**, *96*, 9597-9601.
14. Krieger, F.; Fierz, B.; Bieri, O.; Drewello, M.; Kiefhaber, T. *J. Mol. Biol.* **2003**, *332*, 265-274.
15. Lapidus, L. J.; Eaton, W. A.; Hofrichter, J. *Proc. Natl. Acad. Sci.* **2000**, *97*, 7220-7225.
16. Neuweiler, H.; Löllmann, M.; Doose, S.; Sauer, M. *J. Mol. Biol.* **2007**, *365*, 856-869.
17. Winnik, M. A. *Acc. Chem. Res.* **1985**, *18*, 73-79.

18. Svirskaya, P.; Danhelka, J.; Redpath, A. E. C.; Winnik, M. A. *Polymer* **1983**, *24*, 319-322.
19. Boileau, S.; Méchin, F.; Martinho, J. M. G.; Winnik, M. A. *Macromolecules* **1989**, *22*, 215-220.
20. Ghigginio, K. P.; Snare, M. J.; Thistlethwaite, P. J. *Eur. Polym. J.* **1985**, *21*, 265-272.
21. Cheung, S.-T.; Winnik, M. A.; Redpath, A. E. C. *Makromol. Chem.* **1982**, *183*, 1815-1824.
22. Slomkowski, S.; Winnik, M. A. *Macromolecules* **1986**, *19*, 500-501.
23. Kim, S. D.; Torkelson, J. M. *Macromolecules* **2002**, *35*, 5943-5952.
24. Gardinier, W. E.; Bright, F. V. *J. Phys. Chem. B* **2005**, *109*, 14824-14829.
25. Duhamel, J.; Khayakin, Y.; Hu, Y. Z.; Winnik, M. A.; Boileau, S.; Méchin, F. *Eur. Polymer. J.* **1994**, *30*, 129-134.
26. Lee, S.; Winnik, M. A. *Macromolecules* **1997**, *30*, 2633-2641.
27. Lee, S.; Duhamel, J. *Macromolecules* **1998**, *31*, 9193-9200.
28. Farinha, J. P. S.; Piçarra, S.; Miesel, K.; Martinho, J. M. G. *J. Phys. Chem. B* **2001**, *105*, 10536-10545.
29. Piçarra, S.; Gomes, P. T.; Martinho, J. M. G. *Macromolecules* **2000**, *33*, 3947-3950.
30. Costa, T.; Seixas de Melo, J.; Burrows, H. D. *J. Phys. Chem. B* **2009**, *113*, 618-626.
31. Ingratta, M.; Hollinger, J.; Duhamel, J. *J. Am. Chem. Soc.* **2008**, *130*, 9420-9428.
32. Cuniberti, C.; Perico, A. *Eur. Polym. J.* **1977**, *13*, 369-374.
33. Cuniberti, C.; Perico, A. *Prog. Polym. Sci.* **1984**, *10*, 271-316.
34. Winnik, M. A.; Basu, S. N.; Lee, C. K.; Saunders, D. S. *J. Am. Chem. Soc.* **1976**, *98*, 2928-2935.
35. Horie, K.; Schnabel, W.; Mita, I.; Ushiki, H. *Macromolecules* **1981**, *14*, 1422-1428.
36. Lee, S.; Winnik, M. A. *Can. J. Chem.* **1993**, *71*, 1216-1224.
37. Lee, S.; Winnik, M. A. *Can. J. Chem.* **1994**, *72*, 1587-1595.
38. Birks, J. B. *Photophysics of Aromatic Molecules*. Wiley: New York, 1970; p 301.

39. Siu, H.; Duhamel, J. Pincus, J.; Sasaki, D. *Langmuir*, **2010**, *26*, 10985-10994.
40. Mathew, H.; Siu, H.; Duhamel, J. *Macromolecules* **1999**, *32*, 7100-7108.
41. Duhamel, J. *Acc. Chem. Res.* **2006**, *39*, 953-960.
42. Press, W. H.; Flannery, B. P.; Teukolsky, S. A.; Vetterling, W. T. *Numerical Recipes. The Art of Scientific Computing (Fortran Version)*; Cambridge University Press: Cambridge, 1992.
43. Nakajima, A. *J. Lumin.* **1976**, *11*, 429-432.
44. Kalyanasundaram, K.; Thomas, J. K. *J. Am. Chem. Soc.* **1977**, *99*, 2039-2044.
45. Lianos, P.; Georghiou, S. *Photochem. Photobiol.* **1979**, *30*, 355-362.
46. Dong, D. C.; Winnik, M. A. *Photochem. Photobiol.* **1982**, *35*, 17-21.
47. Dong, D. C.; Winnik, M. A. *Can. J. Chem.* **1984**, *62*, 2560-2565.
48. Zachariass, K. A.; Vaz, W. L. C.; Sotomayor, C.; Kühnle, W. *Biochim. Biophys. Acta* **1982**, *688*, 323-332.
49. Ingratta, M.; Mathew, M.; Duhamel, J. *Can. J. Chem.* **2010**, *88*, 217-227.
50. Yip, J.; Duhamel, J.; Qiu, X. P.; Winnik, F. M. *Macromolecules* **2011**, *44*, 5363-5372.
51. Pattanayek, S. K.; Juvekar, V. A. *Macromolecules* **2002**, *35*, 9574-9585.
52. Bandrup, J. ; Immergut, E. H. ; Grulke, E. A. *Polymer Handbook*, 4th ed.; John Wiley & Sons: NY, 1999, p VII 675-683.

Chapter 3

1. Lakowicz, J. R. *Principles of Fluorescence Spectroscopy* 3rd Ed. Springer, Singapore, 2006.
2. Yekta, A.; Aikawa, M.; Turro, N. J. *Chem. Phys. Lett.* **1979**, *63*, 543-548.
3. Turro, N. J.; Yekta, A. *J. Am. Chem. Soc.* **1978**, *100*, 5951-5952.
4. Tachiya, M. *Chem. Phys. Lett.* **1975**, *33*, 289-292.
5. Duhamel, J. *Acc. Chem. Res.* **2006**, *39*, 953-960.
6. Hannemann, F.; Bera, A. K.; Fischer, B.; Lisurek, M.; Teuchner, K.; Bernhardt, R. *Biochemistry* **2002**, *41*, 11008-11016.
7. Soulages, J. L.; Arrese, E. L. *Biochemistry* **2000**, *39*, 10574-10580.
8. Birks, J. B. *Photophysics of Aromatic Molecules*. Wiley: New York, 1970; p 301.
9. Winnik, F. M. *Chem. Rev.* **1993**, *93*, 587 – 614.
10. Winnik, F. M.; Regismond, S. T. A. *Colloids Surf. A: Physicochem. Eng. Asp.* **1996**, *118*, 1-39.
11. Duhamel, J. *Molecular Interfacial Phenomena of Polymers and Biopolymers*; Chen, P., Ed.; Woodhead: New York, 2005; pp 214 – 248.
12. Winnik, M. A. *Acc. Chem. Res.* **1985**, *18*, 73-79.
13. Svirskaya, P.; Danhelka, J.; Redpath, A. E. C.; Winnik, M. A. *Polymer* **1983**, *24*, 319-322.
14. Boileau, S.; Méchin, F.; Martinho, J. M. G.; Winnik, M. A. *Macromolecules* **1989**, *22*, 215-220.
15. Ghiggino, K. P.; Snare, M. J.; Thistlethwaite, P. J. *Eur. Polym. J.* **1985**, *21*, 265-272.
16. Cheung, S.-T.; Winnik, M. A.; Redpath, A. E. C. *Makromol. Chem.* **1982**, *183*, 1815-1824.
17. Kim, S. D.; Torkelson, J. M. *Macromolecules* **2002**, *35*, 5943-5952.
18. Gardinier, W. E.; Bright, F. V. *J. Phys. Chem. B* **2005**, *109*, 14824-14829.
19. Duhamel, J.; Khayakin, Y.; Hu, Y. Z.; Winnik, M. A.; Boileau, S.; Méchin, F. *Eur. Polymer. J.* **1994**, *30*, 129-134.
20. Lee, S.; Winnik, M. A. *Macromolecules* **1997**, *30*, 2633-2641.

21. Lee, S.; Duhamel, J. *Macromolecules* **1998**, *31*, 9193-9200.
22. Farinha, J. P. S.; Piçarra, S.; Miesel, K.; Martinho, J. M. G. *J. Phys. Chem. B* **2001**, *105*, 10536-10545.
23. Piçarra, S.; Gomes, P. T.; Martinho, J. M. G. *Macromolecules* **2000**, *33*, 3947-3950.
24. Costa, T.; Seixas de Melo, J.; Burrows, H. D. *J. Phys. Chem. B* **2009**, *113*, 618-626.
25. Cuniberti, C.; Perico, A. *Eur. Polym. J.* **1977**, *13*, 369-374.
26. Cuniberti, C.; Perico, A. *Prog. Polym. Sci.* **1984**, *10*, 271-316.
27. Lee, S.; Winnik, M. A. *Can. J. Chem.* **1993**, *71*, 1216-1224.
28. Lee, S.; Winnik, M. A. *Can. J. Chem.* **1994**, *72*, 1587-1595.
29. Ahn, T.-S.; Nantalaksakul, A.; Dasari, R. R.; Al-Kaysi, R. O.; Müller, A. M.; Thayumanavan, S.; Bardeen, C. J. *J. Phys. Chem. B* **2006**, *110*, 24331-24339.
30. Gu, T.; Whitesell, J. K.; Fox, M. A. *J. Phys. Chem. B* **2006**, *110*, 25149-25152.
31. Cicchi, S.; Fabbrizzi, P.; Ghini, G.; Brandi, A.; Foggi, P.; Marcelli, A.; Righini, R.; Botta, C. *Chem. Eur. J.* **2009**, *15*, 754-764.
32. Baker, L. A.; Crooks, R. M. *Macromolecules* **2000**, *33*, 9034-9039.
33. Wang, B.-B.; Zhang, X.; Yang, L.; Jia, X.-R.; Ji, Y.; Li, W.-S.; Wei, Y. *Polym. Bull.* **2006**, *56*, 63-74.
34. Modrakowski, C.; Flores, S. C.; Beinhoff, M.; Schlüter, A. D. *Synthesis* **2001**, *14*, 2143-2155.
35. Brauge, L.; Vériot, G.; Franc, G.; Deloncle, R.; Caminade, A.-M.; Majoral, J.-P. *Tetrahedron* **2006**, *62*, 11891-11899.
36. Brauge, L.; Caminade, A.-M.; Majoral, J.-P.; Słomkowski, S.; Wolszczak, M. *Macromolecules* **2001**, *34*, 5599-5606.
37. Stewart, G. M.; Fox, M. A. *J. Am. Chem. Soc.* **1996**, *118*, 4354-4360.
38. Wilken, R.; Adams, J. *Macromol. Rapid Commun.* **1997**, *18*, 659-665.

39. Wang, B.-B.; Zhang, X.; Jia, X.-R.; Li, Z.-C.; Ji, Y.; Yang, L.; Wei, Y. *J. Am. Chem. Soc.* **2004**, *126*, 15180-15194.
40. Zachariasse, K. A.; Duveneck, G.; Busse, R. *J. Am. Chem. Soc.* **1984**, *106*, 1045-1051.
41. Zachariasse, K. A.; Duveneck, G. *J. Am. Chem. Soc.* **1987**, *109*, 3790-3792.
42. Maçanita, A. L.; Zachariasse, K. A. *J. Phys. Chem. A* **2011**, *115*, 3183-3195.
43. Andriessen, R.; Boens, N.; Ameloot, M.; De Schryver, F. C. *J. Phys. Chem.* **1991**, *95*, 2047-2058.
44. Andriessen, R.; Ameloot, M.; Boens, N.; De Schryver, F. C. *J. Phys. Chem.* **1992**, *96*, 314-326.
45. Boens, N.; Ameloot, M. *Int. J. Quantum Chem.* **2006**, *106*, 300-315.
46. Siu, H.; Duhamel, J. *Macromolecules* **2004**, *37*, 9287-9289.
47. Siu, H.; Duhamel, J. *J. Phys. Chem. B* **2005**, *109*, 1770-1780.
48. Siu, H.; Duhamel, J. *Macromolecules* **2005**, *38*, 7184-7186.
49. Siu, H.; Duhamel, J. *Macromolecules* **2006**, *39*, 1144-1155.
50. Siu, H.; Duhamel, J. *J. Phys. Chem. B* **2008**, *112*, 15301-15312.
51. Siu, H.; Duhamel, J.; Sasaki, D.; Pincus, J. L. *Langmuir* **2010**, *26*, 10985-10994.
52. Ingrassia, M.; Duhamel, J. *Macromolecules* **2007**, *40*, 6647-6657.
53. Ingrassia, M.; Duhamel, J. *J. Phys. Chem. B* **2008**, *112*, 9209-9218.
54. Ingrassia, M.; Duhamel, J. *J. Phys. Chem. B* **2009**, *113*, 2284-2292.
55. Ingrassia, M.; Mathew, M.; Duhamel, J. *Can. J. Chem.* **2010**, *88*, 217-227.
56. Ingrassia, M.; Hollinger, J.; Duhamel, J. *J. Am. Chem. Soc.* **2008**, *130*, 9420-9428.
57. Chen, S.; Duhamel, J.; Winnik, M. A. *J. Phys. Chem. B* **2011**, *115*, 3289-3302.
58. Yip, J.; Duhamel, J.; Bahun, G.; Adronov, A. *J. Phys. Chem. B* **2010**, *114*, 10254-10265.
59. Keyes-Baig, C.; Duhamel, J.; Wettig, S. *Langmuir* **2011**, *27*, 3361-3371.
60. Bahun, G. J.; Adronov, A. *J. Polym. Sci. A: Polym. Chem.* **2010**, *48*, 1016-1028.

61. James, D. R.; Demmer, D. R.; Verall, R. E.; Steer, R. P. *Rev. Sci. Instrum.* **1983**, *54*, 1121-1130.
62. Piçarra, S.; Gomes, P. T.; Martinho, J. M. G. *Macromolecules* **2000**, *33*, 3947-3950.
63. Press, W. H.; Flannery, B. P.; Teukolsky, S. A.; Vetterling, W. T. *Numerical Recipes. The Art of Scientific Computing (Fortran Version)*; Cambridge University Press: Cambridge, 1992.

Chapter 4

1. Winnik, M. A.; Yekta, A. *Curr. Opin. Colloid Interface Sci.* **1997**, *2*, 424-436.
2. Wetzel, W. H.; Chen, M.; Glass, J. E. In *Hydrophilic Polymers: Performance with Environmental Acceptability*; Glass, J. E., Ed.: Advances in Chemistry series 248; American Chemical Society: Washington, DC, 1996. pp 163-180.
3. Lundberg, D.; Glass, E.; Eley, R. R. *J. Rheol.* **1991**, *35*, 1255-1274.
4. Rao, B.; Umera, Y.; Dyke, L.; McDonald, P. M. *Macromolecules* **1995**, *28*, 531-538.
5. Yekta, A.; Xu, B.; Duhamel, J.; Adiwidjaja, H.; Winnik, M. A. *Macromolecules* **1995**, *28*, 956-966.
6. Beaudoin, E.; Borisov, O.; Lapp, A.; Billon, L.; Hiorns, R. C.; François, J. *Macromolecules* **2002**, *35*, 7436-7447.
7. Alami, E.; Almgren, M.; Brown, W. *Macromolecules* **1996**, *29*, 5026-5035.
8. Alami, E.; Almgren, M.; Brown, W.; François, J. *Macromolecules* **1996**, *29*, 2229-2243.
9. Annable, T.; Buscall, R.; Ettelaie, R.; Whittlestone, D. *J. Rheol.* **1993**, *37*, 695-726.
10. Tam, K. C.; Jenkins, R.D.; Winnik, M. A.; Bassett, D. R. *Macromolecules* **1998**, *31*, 4149-4159.
11. Xu, B.; Yekta, A.; Winnik, M. A.; Sadeghy-Dalivand, K.; James, D. F.; Jenkins, R. D.; Bassett, D. R. *Langmuir* **1997**, *13*, 6903-6911.
12. Xu, B.; Li, L.; Yekta, A.; Masoumi, Z.; Kanagalingam, S.; Winnik, M. A.; Zhang, K. W.; Macdonald, P. M.; Menchen, S. *Langmuir* **1997**, *13*, 2447-2456.
13. Anwari, F. M.; Schwab, F. G. In *Polymers in Aqueous Media. Performance Through Association*; Glass, J. E., Ed.; Advances in Chemistry series 223; American Chemical Society: Washington, DC, 1989. pp 527-542.
14. François, J. *Prog. Org. Coatings* **1994**, *24*, 67-79.
15. Maechling-Strasser, C.; Clouet, F.; François, J. *Polymer* **1993**, *33*, 1021-1025.

16. Seixas de Melo, J.; Costa, T.; Miguel, M. D.; Lindman, B.; Schillén, K. *J. Phys. Chem. B* **2003**, *107*, 12605-12621.
17. Pokhrel, M. R.; Bossmann, S. H. *J. Phys. Chem. B* **2000**, *104*, 2215-2223.
18. Costa, T.; Seixas de Melo, J.; Castro, C. S.; Gago, S.; Pillinger, M.; Gonçalves, I. S. *J. Phys. Chem. B* **2010**, *114*, 12439-12447.
19. Deo, P.; Deo, N.; Somasundaran, P.; Jockusch, S.; Turro, N. J. *J. Phys. Chem. B* **2005**, *109*, 20714-20718.
20. Siu, H.; Duhamel, J. *Macromolecules* **2006**, *39*, 1144-1155.
21. Siu, H.; Duhamel, J. *J. Phys. Chem. B* **2005**, *109*, 1770-1780.
22. Siu, H.; Duhamel, J. *Macromolecules* **2004**, *37*, 9287-9289.
23. Siu, H.; Duhamel, J. *Macromolecules* **2005**, *38*, 7184-7186.
24. Prazeres, T. J. V.; Beingessner, R.; Duhamel, J.; Olesen, K.; Shay, G.; Bassett, D. R. *Macromolecules* **2001**, *34*, 7876-7884.
25. Relógio, P.; Martinho, J. M. G.; Farinha J. P. S. *Macromolecules* **2005**, *38*, 10799-10811.
26. Kanagalingam, S.; Ngan, C. F.; Duhamel, J. *Macromolecules* **2002**, *35*, 8560-8570.
27. Siu, H.; Duhamel, J. *J. Phys. Chem. B* **2008**, *112*, 15301-15312.
28. Barros, T. C.; Adronov, A.; Winnik, F. M.; Bohne, C. *Langmuir* **1997**, *13*, 6089-6094.
29. Yip, J.; Duhamel, J.; Qiu, X.; Winnik, F. M. *Can. J. Chem.* **2011**, *89*, 163-172.
30. Winnik, F. M. *Macromolecules* **1990**, *23*, 233-242.
31. Winnik, M. A.; Bystryak, S. M.; Liu, Z.; Siddiqui, J. *Macromolecules* **1998**, *31*, 6855-6864.
32. Winnik, F. M.; Winnik, M. A.; Tazuke, S.; Ober, C. K. *Macromolecules* **1987**, *20*, 38-44.
33. Winnik, F. M.; Regismond, S. T. A.; Goddard, E. D. *Langmuir* **1997**, *13*, 111-114.
34. Hu, Y. Z.; Zhao, C. L.; Winnik, M. A.; Sundararajan, P. R. *Langmuir* **1990**, *6*, 880-883.
35. Costa, T.; Seixas de Melo, J.; Burrows, H. D. *J. Phys. Chem. B* **2009**, *113*, 618-626.

36. Siu, H.; Prazeres, T. J. V.; Duhamel, J.; Olesen, K.; Shay, G. *Macromolecules* **2005**, *38*, 2865-2875.
37. Richey, B.; Kirk, A. B.; Eisenhart, E. K.; Fitwater, S.; Hook, J. J. *Coat. Tech.* **1991**, *63*, 31-40.
38. Lee, S.; Winnik, M. A. *Macromolecules* **1997**, *30*, 2633-2641.
39. Lee, S.; Duhamel, J. *Macromolecules* **1998**, *31*, 9193-9200.
40. Duhamel, J.; Yekta, A.; Hu, Y. Z.; Winnik M. A. *Macromolecules* **1992**, *25*, 7024-7030.
41. Cheung, S.-T.; Winnik, M. A.; Redpath, A. E. C. *Makromol. Chem.* **1982**, *183*, 1815-1824.
42. Char, K.; Gast, A. P.; Frank, C. W. *Langmuir* **1988**, *4*, 989-998.
43. Oyama, H. T.; Tang, W. T.; Frank, C. W. *Macromolecules* **1987**, *20*, 474-480.
44. Char, K.; Frank, C. W.; Gast, A. P.; Tang, W. T. *Macromolecules* **1987**, *20*, 1833-1838.
45. Char, K.; Frank, C. W.; Gast, A. P. *Macromolecules* **1989**, *22*, 3177-3180.
46. Wilemski, G.; Fixman, M. *J. Chem. Phys.* **1974**, *60*, 866-877.
47. Wilemski, G.; Fixman, M. *J. Chem. Phys.* **1974**, *60*, 878-890.
48. Chen, S.; Duhamel, D.; Winnik, M. A. *J. Phys. Chem. B* **2011**, *115*, 3289-3302.
49. Lakowicz, J. R. *Principles of Fluorescence Spectroscopy*; Plenum Press: New York, 1983; p 45.
50. James, D. R.; Demmer, D. R.; Verall, R. E.; Steer, R. P. *Rev. Sci. Instrum.* **1983**, *54*, 1121-1130.
51. Press, W. H.; Flannery, B. P.; Teukolsky, S. A.; Vetterling, W. T. *Numerical Recipes. The Art of Scientific Computing (Fortran Version)*; Cambridge University Press: Cambridge, 1992.
52. Kim, S. D.; Torkelson, J. M. *Macromolecules* **2002**, *35*, 5943-5952.
53. Birks, J. B. *Photophysics of Aromatic Molecules*; Wiley: New York, 1970. p 351.
54. Eckert, A. R.; Hsiao, J.-S.; Webber, S. E. *J. Phys. Chem.* **1994**, *98*, 12025-12031.
55. Torkelson, J. M.; Gilbert, S. R. *Macromolecules* **1987**, *20*, 1860-1865.
56. Bandrup, J. ; Immergut, E. H. ; Grulke, E. A. *Polymer Handbook*, 4th ed.; John Wiley & Sons: NY, 1999, pp VII 675-683.

57. Chen, S.; Duhamel, J.; Bahun, G. J.; Adronov, A. *J. Phys. Chem. B* **2011**, *115*, 9921-9929.
58. *CRC Handbook of Chemistry and Physics*, 84th ed.; CRC Press: Boca Raton, FL., 2003.
59. Bieri, O.; Wirz, J.; Hellrung, B.; Schutkowski, M.; Drewello, M.; Kiefhaber, T. *Proc. Natl. Acad. Sci. U.S.A.* **1999**, *96*, 9597-9601.
60. Krieger, F.; Fierz, B.; Bieri, O.; Drewello, M.; Kiefhaber, T. *J. Mol. Biol.* **2003**, *332*, 265-274.
61. Lapidus, L. J.; Eaton, W. A.; Hofrichter, J. *Proc. Natl. Acad. Sci. U.S.A.* **2000**, *97*, 7220-7225.
62. Neuweiler, H.; Löllmann, M.; Doose, S.; Sauer, M. *J. Mol. Biol.* **2007**, *365*, 856-869.
63. Winnik, M. A. *Acc. Chem. Res.* **1985**, *18*, 73-79.
64. Svirskaya, P.; Danhelka, J.; Redpath, A. E. C.; Winnik, M. A. *Polymer* **1983**, *24*, 319-322.
65. Boileau, S.; Méchin, F.; Martinho, J. M. G.; Winnik, M. A. *Macromolecules* **1989**, *22*, 215-220.
66. Ghiggino, K. P.; Snare, M. J.; Thistlethwaite, P. J. *Eur. Polym. J.* **1985**, *21*, 265-272.
67. Horie, K.; Schnabel, W.; Mita, I.; Ushiki, H. *Macromolecules* **1981**, *14*, 1422-1428.
68. Anghel, D. F.; Toca-Herrera, J. L.; Winnik, F. M.; Rettig, W.; v. Kliting, R. *Langmuir* **2002**, *18*, 5600-5606.
69. Winnik, F. M.; Regismond, S. T. A.; Goddard, E. D. *Langmuir* **1997**, *13*, 111-114.
70. Pattanayek, S. K.; Juvekar, V. A. *Macromolecules* **2002**, *35*, 9574-9585.

Chapter 5

1. Glass, J. E., Ed.; *Polymers in Aqueous Media: Performance through Association*; Advances in Chemistry Series 223; American Chemical Society: Washington, DC, 1989.
2. Schulze, D. N.; Glass, J. E., Ed.; *Polymers as Rheology Modifiers*; ACS Symposium Series 462; American Chemical Society: Washington, DC, 1991.
3. Kwak, J. C. T., Ed.; *Polymer-Surfactant Systems*; Surfactant Science Series 77; Marcel Dekker: New York, 1998.
4. Goddard, E. O.; Ananthapadamanabham, K. P., Ed.; *Interactions of Surfactants with Polymers and Proteins*; CRC Press: Boca Raton, FL, 1993.
5. Rufier, C.; Collet, A.; Viguier, M.; Oberdisse, J.; Mora, S. *Macromolecules* **2011**, *44*, 7451-7459.
6. Hu, Y.-Z.; Zhao, C.-L.; Winnik, M. A.; Sundararajan, P. R. *Langmuir* **1990**, *6*, 880-883.
7. Annable, T.; Buscall, R.; Ettelaie, R.; Shepherd, P.; Whittlestone, D. *Langmuir* **1994**, *10*, 1060-1070.
8. Binana-Limbele, W.; Clouet, F.; François, J. *Colloid Polym. Sci.* **1993**, *271*, 748-758.
9. Dai, S.; Tam, K. C.; Wyn-Jones, E.; Jenkins, R. D. *J. Phys. Chem. B* **2004**, *108*, 4979-4988.
10. Abrahmsen-Alami, S.; Stilbs, P. *J. Phys. Chem.* **1994**, *98*, 6359-6367.
11. Zhang, K.; Xu, B.; Winnik, M. A.; Macdonald, P. M. *J. Phys. Chem.* **1996**, *100*, 9834-9841.
12. Rufier, C.; Collet, A.; Viguier, M.; Oberdisse, J.; Mora, S. *Macromolecules* **2008**, *41*, 5854-5862.
13. Dai, S.; Tam, K. C. *J. Phys. Chem. B* **2001**, *105*, 10759-10763.
14. Olofsson, G.; Wang, G. *Pure Appl. Chem.* **1994**, *66*, 527-532.
15. Wang, G.; Olofsson, G. *J. Phys. Chem. B* **1998**, *102*, 9276-9283.

16. Bernazzani, L.; Borsacchi, S.; Catalano, D.; Gianni, P.; Mollica, V.; Vitelli, M.; Asaro, F.; Feruglio, L. *J. Phys. Chem. B* **2004**, *108*, 8960-8969.
17. Cooke, D. J.; Blondel, J. A. K.; Lu, J. R.; Thomas, R. K.; Wang, Y.; Han, B.; Yan, H.; Penfold, J. *Langmuir* **1998**, *14*, 1990-1995.
18. Cabane, B. *J. Phys. Chem.* **1977**, *81*, 1639-1645.
19. Chari, K.; Kowalczyk, J.; Lal, J. *J. Phys. Chem. B* **2004**, *108*, 2857-2861.
20. Brown, W.; Fundin, J.; Miguel, G. M. *Macromolecules* **1992**, *25*, 7192-7198.
21. Gao, Z.; Wasylshen, R. E.; Kwak, J. C. T. *J. Phys. Chem.* **1991**, *95*, 462-467.
22. Kim, J. H.; Domach, M. M.; Tilton, R. D. *J. Phys. Chem. B* **1999**, *103*, 10582-10590.
23. Zana, R.; Lianos, P.; Lang, J. *J. Phys. Chem.* **1985**, *89*, 41-44.
24. Turro, N. J.; Baretz, B. H.; Kuo, P. L. *Macromolecules* **1984**, *17*, 1321-1324.
25. Wang, Y.; Lu, D.; Yan, H.; Thomas, R. K. *J. Phys. Chem.* **1997**, *101*, 3953-3956.
26. Mészáros, R.; Varga, I.; Gilányi, T. *J. Phys. Chem. B* **2005**, *109*, 13538-13544.
27. François, J.; Dayantis, J.; Sabbadin, J. *Eur. Polym. J.* **1985**, *21*, 165-174.
28. Dai, S.; Tam, K. C.; Jenkins, R. D. *J. Phys. Chem. B* **2001**, *105*, 10189-10196.
29. Rufier, C.; Collet, A.; Viguier, M.; Oberdisse, J.; Mora, S. *Macromolecules* **2009**, *42*, 5226-5235.
30. Siu, H.; Duhamel, J. *Macromolecules* **2006**, *39*, 1144-1155.
31. Siu, H.; Duhamel, J. *J. Phys. Chem. B* **2005**, *109*, 1770-1780.
32. Siu, H.; Duhamel, J. *Macromolecules* **2004**, *37*, 9287-9289.
33. Siu, H.; Duhamel, J. *Macromolecules* **2005**, *38*, 7184-7186.
34. Anghel, D. F.; Toca-Herrera, J. L.; Winnik, F. M.; Rettig, W.; v. Kliting, R. *Langmuir* **2002**, *18*, 5600-5606.
35. Winnik, F. M.; Regismond, S. T. A.; Goddard, E. D. *Langmuir* **1997**, *13*, 111-114.

36. Quina, F.; Abuin, E.; Lissi, E. *Macromolecules* **1990**, *23*, 5173-5175.
37. Maltesh, C.; Somasundaran, P. *Langmuir* **1992**, *8*, 1926-1930.
38. Winnik, F. M.; Ringsdorf, H.; Venzmer, J. *Langmuir* **1991**, *7*, 912-917.
39. Winnik, M. A.; Bystriak, S. M.; Siddiqui, J. *Macromolecules* **1999**, *32*, 624-632.
40. Winnik, F. M.; Winnik, M. A.; Tazuke, S. *J. Phys. Chem.* **1987**, *91*, 594-597.
41. Haldar, B.; Chakrabarty, A.; Mallick, A.; Mandal, M. C.; Das, P.; Chattopadhyay, N. *Langmuir* **2006**, *22*, 3514-3520.
42. Haldar, B.; Mallick, A.; Chattopadhyay, N. *J. Mol. Liq.* **2004**, *115*, 113-120.
43. Char, K.; Frank, C. W.; Gast, A. P.; Tang, W. T. *Macromolecules* **1987**, *20*, 1833-1838.
44. Kalyanasundaram, K.; Thomas, J. K. *J. Am. Chem. Soc.* **1977**, *99*, 2039-2044.
45. Birks, J. B. *Photophysics of Aromatic Molecules*; Wiley: New York, 1970. pp 351.
46. Duhamel, J. *Acc. Chem. Res.* **2006**, *39*, 953-960.
47. Chen, S.; Duhamel, D.; Winnik, M. A. *J. Phys. Chem. B* **2011**, *115*, 3289-3302.
48. James, D. R.; Demmer, D. R.; Verall, R. E.; Steer, R. P. *Rev. Sci. Instrum.* **1983**, *54*, 1121-1130.
49. Yip, J.; Duhamel, J.; Bahun, G.; Adronov, A. *J. Phys. Chem. B* **2010**, *114*, 10254-10265.
50. Keyes-Baig, C.; Duhamel, J.; Wettig, S. *Langmuir* **2011**, *27*, 3361-3371.
51. Chen, S.; Duhamel, J.; Bahun, G.; Adronov, A. *J. Phys. Chem. B* **2011**, *115*, 9921-9925.
52. Press, W. H.; Flannery, B. P.; Teukolsky, S. A.; Vetterling, W. T. *Numerical Recipes. The Art of Scientific Computing (Fortran Version)*; Cambridge University Press: Cambridge, 1992.
53. Chapter 4 in this thesis.
54. Chapter 7 in this thesis.
55. Costa, T.; Seixas de Melo, J.; Burrows, H. D. *J. Phys. Chem. B* **2009**, *113*, 618-626.

Chapter 6

1. Glass, J. E., Ed.; *Polymers in Aqueous Media: Performance through Association*; Advances in Chemistry Series 223; American Chemical Society: Washington, DC, 1989.
2. Schulze, D. N.; Glass, J. E., Ed.; *Polymers as Rheology Modifiers*; ACS Symposium Series 462; American Chemical Society: Washington, DC, 1991.
3. Kwak, J. C. T., Ed.; *Polymer-Surfactant Systems*; Surfactant Science Series 77; Marcel Dekker: New York, 1998.
4. Goddard, E. O.; Ananthapadamanabham, K. P., Ed.; *Interactions of Surfactants with Polymers and Proteins*; CRC Press: Boca Raton, FL, 1993.
5. Winnik, M. A.; Yekta, A. *Curr. Opin. Colloid Interface Sci.* **1997**, *2*, 424-436.
6. Magny, B.; Iliopoulos, I.; Zana, R.; Audebert, R. *Langmuir* **1994**, *10*, 3180-3187.
7. Thuresson, K.; Lindman, B.; Nyström, B. *J. Phys. Chem. B* **1997**, *101*, 6450-6459.
8. Nilsson, S.; Thuresson, K.; Hansson, P.; Lindman, B. *J. Phys. Chem. B* **1998**, *102*, 7099-7105.
9. Patruyo, L. G.; Müller, A. J.; Sáez, A.E. *Polymer* **2002**, *43*, 6481-6493.
10. Panmai, S.; Prud'homme, R. K.; Peiffer, D. G.; Jockusch, S.; Turro, N. J. *Langmuir* **2002**, *18*, 3860-3864.
11. Panmai, S.; Prud'homme, R. K.; Peiffer, D. G. *Colloids Surf. A, Physicochem. Eng. Aspects* **1999**, *147*, 3-15.
12. Annable, T.; Buscall, R.; Ettelaie, R.; Whittlestone, D. *J. Rheol.* **1993**, *37*, 695-726.
13. Annable, T.; Buscall, R.; Ettelaie, R.; Shepherd, P.; Whittlestone, D. *Langmuir* **1994**, *10*, 1060-1070.
14. Jiménez-Regalado, E.; Selb, J.; Candau, F. *Langmuir* **2000**, *16*, 8611-8621.
15. Tirtaatmadja, V.; Tam, K. C.; Jenkins, R. D. *Macromolecules* **1997**, *30*, 1426-1433.
16. Tirtaatmadja, V.; Tam, K. C.; Jenkins, R. D. *Macromolecules* **1997**, *30*, 3271-3282.

17. English, R. J.; Gulati, H. S.; Jenkins, R. D.; Khan, S. A. *J. Rheol.* **1997**, *41*, 427-444.
18. Seng, W. P.; Tam, K. C.; Jenkins, R. D.; Bassett, D. R. *Langmuir* **2000**, *16*, 2151-2156.
19. Seng, W. P.; Tam, K. C.; Jenkins, R. D.; Bassett, D. R. *Macromolecules* **2000**, *33*, 1727-1733.
20. Seng, W. P.; Tam, K. C.; Jenkins, R. D. *Colloids Surf. A Physicochem. Eng. Aspects* **1999**, *154*, 365-382.
21. Tarng, M. R.; Kaczmarek, J. P.; Lundberg, D. J.; Glass, J. E. In *Hydrophilic Polymers: Performance with Environmental Acceptability*; Glass, J. E., Ed.: Advances in Chemistry series 248; American Chemical Society: Washington, DC, 1996. pp 305-341.
22. Islam, M. F.; Jenkins, R. D.; Bassett, D. R.; Lau, W.; Ou-Yang, H. D. *Macromolecules* **2000**, *33*, 2480-2485.
23. Siu, H.; Duhamel, J. *Macromolecules* **2006**, *39*, 1144-1155.
24. Siu, H.; Duhamel, J. *J. Phys. Chem. B* **2005**, *109*, 1770-1780.
25. Siu, H.; Duhamel, J. *Macromolecules* **2004**, *37*, 9287-9289.
26. Siu, H.; Duhamel, J. *Macromolecules* **2005**, *38*, 7184-7186.
27. Prazeres, T. V. J.; Duhamel, J.; Olesen, K.; Shay, G. *J. Phys. Chem. B* **2005**, *109*, 17406-17416.
28. Duhamel, J. In *Molecular Interfacial Phenomena of Polymers and Biopolymers*; Chen, P., Ed.; Woodhead: New York, 2005. pp 214-248.
29. Kalyanasundaram, K.; Thomas, J. K. *J. Am. Chem. Soc.* **1977**, *99*, 2039-2044.
30. Birks, J. B. *Photophysics of Aromatic Molecules*; Wiley: New York, 1970. p 351.
31. Duhamel, J. *Acc. Chem. Res.* **2006**, *39*, 953-960.
32. Siu, H. *Characterization of the Self-Assembly of Pyrene-Labelled Macromolecules in Water* Ph.D. Thesis, University of Waterloo, 2010.
33. Jenkins, R. D.; DeLong, L. M.; Bassett, D. R. In *Hydrophilic Polymers. Performance with Environmental Acceptability*, Glass, J. E., Ed.: Advances in Chemistry series 248; American

Chemical Society: Washington, DC, 1996. pp 425-447.

34. Shay, G.D.; Kravitz, F.K.; Brizgys, P.V. *Polymers as Rheology Modifiers*, Schulz, D.N.; Glass, J.E., Ed.: ACS Symposium Series 462; American Chemical Society: Washington, DC, 1991. pp 121-141.
35. Prazeres, T. J. V.; Beingessner, R.; Duhamel, J.; Olesen, K.; Shay, G.; Bassett, D. R. *Macromolecules* **2001**, *34*, 7876-7884.
36. Lakowicz, J. R. *Principles of Fluorescence Spectroscopy*; Plenum Press: New York, 1983; p 45.
37. James, D. R.; Demmer, D. R.; Verall, R. E.; Steer, R. P. *Rev. Sci. Instrum.* **1983**, *54*, 1121-1130.
38. Mathew, A. K.; Siu, H.; Duhamel, J. *Macromolecules* **1999**, *32*, 7100-7108.
39. Yip, J.; Duhamel, J.; Bahun, G.; Adronov, A. *J. Phys. Chem. B* **2010**, *114*, 10254-10265.
40. Keyes-Baig, C.; Duhamel, J.; Wettig, S. *Langmuir* **2011**, *27*, 3361-3371.
41. Chen, S.; Duhamel, J.; Bahun, G.; Adronov, A. *J. Phys. Chem. B* **2011**, *115*, 9921-9929.
42. Press, W. H.; Flannery, B. P.; Teukolsky, S. A.; Vetterling, W. T. *Numerical Recipes. The Art of Scientific Computing (Fortran Version)*; Cambridge University Press: Cambridge, 1992.
43. Regalado, E. J.; Selb, J.; Candau, F. *Macromolecules* **1999**, *32*, 8580-8588.
44. Anghel, D. F.; Toca-Herrera, J. L.; Winnik, F. M.; Rettig, W.; v. Kliting, R. *Langmuir* **2002**, *18*, 5600-5606.
45. Winnik, F. M.; Regismond, S. T. A.; Goddard, E. D. *Langmuir* **1997**, *13*, 111-114.
46. Xu, B.; Yekta, A.; Li, L.; Masoumi, Z.; Winnik, M. A. *Colloids Surf. A Physicochem. Eng. Aspects* **1996**, *112*, 239-250.
47. Yekta, A.; Xu, B.; Duhamel, J.; Adiwidjaja, H.; Winnik, M. A. *Macromolecules* **1995**, *28*, 956-966.
48. Tam, K. C.; Jenkins, R.D.; Winnik, M. A.; Bassett, D. R. *Macromolecules* **1998**, *31*, 4149-4159.

49. The error on $\langle n \rangle$ was obtained by the method of the propagation of uncertainty. At high SDS concentration where all pyrene pendants are incorporated into SDS micelles, a plot of $\langle n \rangle$ as a function of $1/\ln([SDS])$ yielded a straight line that could be fitted according to the following equations:

$$\text{For } [\text{Py-HASE12}] = 8 \text{ g/L: } \quad \langle n \rangle = (2.39 \pm 0.13) \times \frac{1}{\ln([SDS])} + (0.50 \pm 0.07)$$

$$\text{For } [\text{Py-HASE12}] = 57 \text{ g/L: } \quad \langle n \rangle = (6.62 \pm 0.25) \times \frac{1}{\ln([SDS])} + (-0.72 \pm 0.09)$$

Using these equations, the error on $\langle n \rangle$ at the solution viscosity maximum was determined to equal 2.0 ± 0.1 for both polymer concentrations. At the SDS concentration of $[SDS]_p^{E/I_M}$, $\langle n \rangle$ was found to equal 2.4 ± 0.1 and 2.2 ± 0.1 for the 8 and 57 g/L Py-HASE12 concentrations, respectively.

Chapter 7

1. Cuniberti, C.; Perico, A. *Eur. Polym. J.* **1977**, *13*, 369-374.
2. Lee, S.; Winnik, M. A. *Macromolecules* **1997**, *30*, 2633-2641.
3. Cheung, S.-T.; Winnik, M. A.; Redpath, A. E. C. *Makromol. Chem.* **1982**, *183*, 1815-1824.
4. Ghiggino, K. P.; Snare, M. J.; Thistlethwaite, P. J. *Eur. Polym. J.* **1985**, *21*, 265-272.
5. Costa, T.; Seixas de Melo, J.; Burrows, H. D. *J. Phys. Chem. B* **2009**, *113*, 618-626.
6. Lee, S.; Duhamel, J. *Macromolecules* **1998**, *31*, 9193-9200.
7. Char, K.; Frank, C. W.; Gast, A. P. *Macromolecules* **1989**, *22*, 3177-3180.
8. Char, K.; Frank, C. W.; Gast, A. P.; Tang, W. T. *Macromolecules* **1987**, *20*, 1833-1838.
9. Hu, Y.-Z.; Zhao, C.-L.; Winnik, M. A.; Sundararajan, P. R. *Langmuir* **1990**, *6*, 880-883.
10. Quina, F.; Abuin, E.; Lissi, E. *Macromolecules* **1990**, *23*, 5173-5175.
11. Maltesh, C.; Somasundaran, P. *Langmuir* **1992**, *8*, 1926-1930.
12. Haldar, B.; Chakrabarty, A.; Mallick, A.; Mandal, M. C.; Das, P.; Chattopadhyay, N. *Langmuir* **2006**, *22*, 3514-3520.
13. Neuweiler, H.; Lollmann, M.; Doose, S.; Sauer, M. *J. Mol. Biol.* **2007**, *365*, 856-869.
14. Turro, N. J.; Yekta, A. *J. Am. Chem. Soc.* **1978**, *100*, 5951-5952.
15. Yekta, A.; Xu, B.; Duhamel, J.; Adiwidjaja, H.; Winnik, M. A. *Macromolecules* **1995**, *28*, 956-966.
16. Araujo, E.; Rharbi, Y.; Huang, X.; Winnik, M. A.; Bassett, D. R.; Jenkins, R. D. *Langmuir* **2000**, *16*, 8664-8671.
17. Siu, H.; Prazeres, T. J. V.; Duhamel, J.; Olesen, K.; Shay, G. *Macromolecules* **2005**, *38*, 2865-2875.
18. Annable, T.; Buscall, R.; Ettelaie, R.; Whittlestone, D. *J. Rheol.* **1993**, *37*, 695-726.
19. Tirtaatmadja, V.; Tam, K. C.; Jenkins, R. D. *Macromolecules* **1997**, *30*, 1426-1433.

20. Tirtaatmadja, V.; Tam, K. C.; Jenkins, R. D. *Macromolecules* **1997**, *30*, 3271-3282.
21. English, R. J.; Gulati, H. S.; Jenkins, R. D.; Khan, S. A. *J. Rheol.* **1997**, *41*, 427-444.
22. Green, M. S.; Tobolsky, A. V. *J. Chem. Phys.* **1946**, *14*, 80-92.
23. Prazeres, T. V. J.; Duhamel, J.; Olesen, K.; Shay, G. *J. Phys. Chem. B* **2005**, *109*, 17406-17416.
24. Magny, B.; Iliopoulos, I.; Zana, R.; Audebert, R. *Langmuir* **1994**, *10*, 3180-3187.
25. Thuresson, K.; Lindman, B.; Nyström, B. *J. Phys. Chem. B* **1997**, *101*, 6450-6459.
26. Nilsson, S.; Thuresson, K.; Hansson, P.; Lindman, B. *J. Phys. Chem. B* **1998**, *102*, 7099-7105.
27. Patruyo, L. G.; Müller, A. J.; Sáez, A.E. *Polymer* **2002**, *43*, 6481-6493.
28. Panmai, S.; Prud'homme, R. K.; Peiffer, D. G.; Jockusch, S.; Turro, N. J. *Langmuir* **2002**, *18*, 3860-3864.
29. Panmai, S.; Prud'homme, R. K.; Peiffer, D. G. *Colloids Surf. A, Physicochem. Eng. Aspects* **1999**, *147*, 3-15.
30. Annable, T.; Buscall, R.; Ettelaie, R.; Whittlestone, D. *J. Rheol.* **1993**, *37*, 695-726.
31. Annable, T.; Buscall, R.; Ettelaie, R.; Shepherd, P.; Whittlestone, D. *Langmuir* **1994**, *10*, 1060-1070.
32. Jiménez-Regalado, E.; Selb, J.; Candau, F. *Langmuir* **2000**, *16*, 8611-8621.